CONDUCTIVITY AND NUCLEAR MAGNETIC RESONANCE STUDIES ON POLYMER ELECTROLYTES BASED ON POLY (ETHYLENE OXIDE)

Anthony Stephen Tomlin

A Thesis Submitted for the Degree of PhD
at the
University of St Andrews

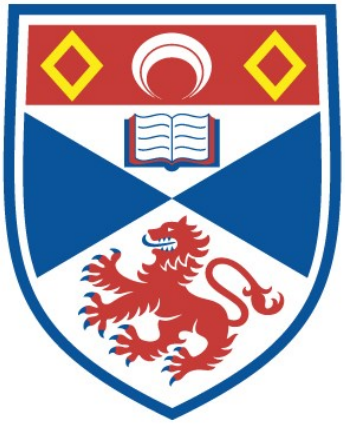

1988

CONDUCTIVITY AND NUCLEAR MAGNETIC RESONANCE STUDIES ON POLYMER ELECTROLYTES BASED ON POLY(ETHYLENE OXIDE)

A Thesis

presented for the degree of

DOCTOR OF PHILOSOPHY

in the Faculty of Science of the

University of St. Andrews

by

Anthony Stephen Tomlin, B.Sc.

United College of

St. Salvator and St. Leonard,

St. Andrews.

November 1987

ProQuest LLC.
789 East Eisenhower Parkway
P.O. Box 1346
Ann Arbor, MI 48106 – 1346

In submitting this thesis to the University of St. Andrews I understand that I am giving permission for it to be made available for use in accordance with the regulations of the University Library for the time being in force, subject to any copyright vested in the work not being affected thereby. I also understand that the title and abstract will be published, and that a copy of the work may be made and supplied to any *bona fide* library or research worker.

DECLARATION

I Anthony Stephen Tomlin hereby certify that this thesis has been composed by myself, that it is a record of my own work, and that it has not been accepted in partial or complete fulfilment of any other degree or professional qualification.

Signed ..... Date 7/2/88

I was admitted to the Faculty of Science of the University of St. Andrews under Ordinance General No 12 on 1st. October, 1984.

Signed ..... Date 7/2/88

CERTIFICATE

I hereby certify that the candidate has fulfilled the conditions of the Resolution and Regulations appropriate to the degree of Ph. D.

Signature of Supervisor ..... Date .....

ACKNOWLEDGEMENTS

Special thanks are given to my supervisor, Professor James MacCallum, from whom I have learned so much during my Ph. D. period. I am grateful for his constructive comments, good humour and perhaps most importantly in my view, encouragement on his part for me to construct and impliment my own ideas. Thanks are also given to Dr. Colin Vincent. From his knowledge of polymer electrolytes, electrochemistry and his systematic approach to any problem, I learned many things. At a later stage in my studies I was seconded to the Physics department of the University where Dr. David Tunstall kindly introduced me to Nuclear Magnetic Resonance. I thank him profusely for his help, encouragement and guidance, as my eyes were slowly opened to the power and elegance of this spectroscopic technique.

Other colleagues who must receive thanks for their help during this time are Dr. Fiona Gray, James Evans and Derick Higgins, as well as two members of the technical staff of the chemistry department, Milanja Smith and Colin Smith. A special mention is given to Mrs Mary Lang for her gentle encouragement and good humour at all times during my studies.

Sincere thanks are due to my parents for the sacrifices they have made and support they have given throughout my university studies. In many respects this is their thesis as much as it is mine.

Contents

To *my parents*, with all my love,

To *Lance*, my pal,

To *Leasil*, the love of my life.

ABSTRACT

The thesis details studies relating to polymer electrolytes; the solid ionic conductors formed by the dissolution of salts in suitable high molecular weight polymers.

An outline of polymer electrolyte study is presented with respect to current understanding of the phase behaviour, morphology and conductance behaviour of the electrolyte materials. (In particular, those based upon the linear homopolymer poly(ethylene oxide), PEO.)

An electrochemical study has been undertaken (298 K) involving a low molecular weight PEO analogue, PEO(400)e ≡ $CH_3CO_2(CH_2CH_2O)_nCO\ CH_3$ (n = 8 - 9), containing $LiCF_3SO_3$ or $LiClO_4$. The study has shown that at low to medium salt concentrations in polyether media ion - ion interactions are important and are realised as ion association. The conductance vs. concentration behaviour has been modelled according to an equilibrium between single, ion pair and triple ion species where the concentration of simple (single) ions are small and decreasing, and above a total salt concentration of about 0.01 mol kg^{-1}, the majority of the current is carried by triple ion species of the form $Li_2X^+\ LiX_2^-$ (X = $CF_3SO_3^-$, ClO_4^-).

Equilibrium constant data were obtained for single and triple ion formation (from neutral ion pairs). Determination of triple ion formation constants vs. temperature has shown that the triple ion formation process for $LiCF_3SO_3$ in PEO(400)e is an exothermic process, $\Delta H^{\ominus}$ negative, whereas for $LiClO_4$ $\Delta H^{\ominus} \simeq 0$ $kJmol^{-1}$.

Using nuclear magnetic resonance (nmr), diffusion coefficients have been obtained for the oligomer chain in PEO(400)e and PEO(400)e.$LiCF_3SO_3$ solutions. The chain diffusion coefficients have been shown to give good agreement with those for salt diffusion, determined from conductance measurements via the Nernst - Einstein relation.

An in - depth nmr investigation of the PEO.$LiCF_3SO_3$ system (high molecular weight PEO) has shown that there is partition of lithium environments, probably within the salt rich crystalline phase (EO/Li $\simeq$ 3.5/1). Significant numbers of lithium nuclei are not observed with the nmr technique because they occupy enviroments of low symmetry. This was reinforced by other nmr measurements which suggested cation - anion proximity in the crystalline phase.

A mixed salt system has been studied, PEO.$LiCF_3SO_3$.NaI, and it has been shown that the mixing of salts gave materials with superior conductivities to the relevant single salt systems (PEO.$LiCF_3SO_3$ and PEO.NaI) of the same overall salt content. Nmr has shown that the mixed salt effect was due to a larger amorphous (conducting) polymer phase and more potential charge carriers for the mixed salt in comparison to the

single salt materials. A marked effect upon lithium motion was observed for PEO.$LiCF_3SO_3$.NaI system in comparison to PEO.$LiCF_3SO_3$ and it has been proposed that this was due to the observed lithium species becoming mobile at notably lower temperatures for the mixed salt system.

Chapter 1

1 INTRODUCTION

'Polymer electrolytes' are defined as solid ionic conductors formed by the dissolution of salts in suitable high molecular weight polymers.

Such materials possess good ionic conductivity at reasonable temperatures ($\propto 4 \times 10^{-3}$ Ω^{-1} cm^{-1}, $\geq$ 350 K) and show considerable promise as electrolytic components in high energy density batteries and other devices[1,2]. In such a role, they are expected to have several advantages over what are considered to be conventional electrolyte materials[3] :

(1) An improved electrochemical stability window compared to electrolytes based on low molar mass organic solvents, such as $LiClO_4$ in propylene carbonate, which are subject to oxidation / reduction reactions at the electrode.

(2) Ease of processing, by virtue of their plastic properties, allowing the design of optimum electrode - electrolyte configurations for a given application.

(3) Accommodation of electrode volume changes i.e intercalating electrode materials like TiS_2 and V_6O_{13} expand as they include ions, causing stress cracking in brittle electrolytes. Plastic flow of a polymer electrolyte reduces stress and maintains battery performance.

(4) High energy density batteries (> 100 Wh / kg.) in a thin film flexible configuration. (Batteries based upon low molar mass organic solvents usually have energy densities of about 40 Wh / kg.[4])

The first reports on ionically conducting polymer electrolyte materials formed by the dissolution of alkali metal salts of the type (M^+X^-) in the linear homopolymer poly(ethylene oxide) were presented by Wright *et al*[5] in 1973. It was not until 1978 however that Armand and co - workers[6] suggested the potential of such materials as practical solid electrolytes for high energy density batteries. In the nine years that have followed Armand's initial remarks there has been considerable activity in this new field and although other polymers have been considered (including poly(propylene oxide)[7], poly(ethylene - imine)[8] and poly(thia alkanes)[9]) those polymeric electrolytes based on poly(ethylene oxide) have received the most attention.

This introduction details the current understanding of those polymer electrolytes formed by the dissolution of various simple salts in poly(ethylene oxide). Attention is given to the morphology, phase behaviour, and ionic conductance of the resultant poly(ethylene oxide) - based materials, as well as a qualitative outline of the theories used in modelling the conductance behaviour.

1.1 Poly(ethylene oxide)

Poly(ethylene oxide), usually designated PEO, is a simple linear homopolymer of repeat unit $-(CH_2-CH_2-O)-$ which is obtained from the ring - opening polymerization of ethylene oxide using a calcium amide catalyst[10] i.e :

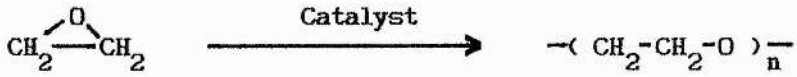

ethylene oxide — poly(ethylene oxide)

giving molecular weights up to 5×10^6 ($\simeq 10^5$ monomer units). The polymer is linear, stereoregular, and semi - crystalline, with about eighty to ninety per cent of the material in the form of lamellae arranged as spherulites[11]. Pristine PEO adopts a helical configuration with seven monomer units and a thread of 1.93 nm. per unit quadratic cell corresponding to two turns of the helix (Fig. 1.1)[12].

The glass transition temperature, Tg, of the amorphous phase is about 213 K, depending on molecular weight and sample preparation, while the melting temperature for the lamellar crystallites, Tm, is usually around 333 K (although the true thermodynamic melting temperature has been calculated to be 349 K for a perfect crystal)[13].

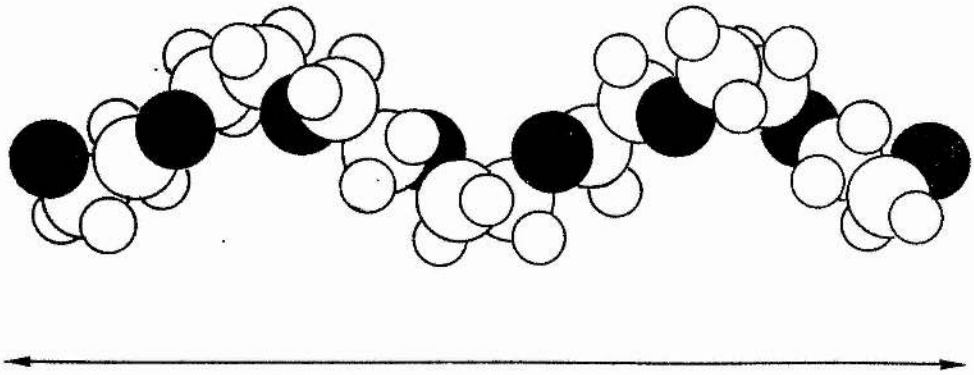

1.93 nm

— Oxygen — Carbon — Hydrogen

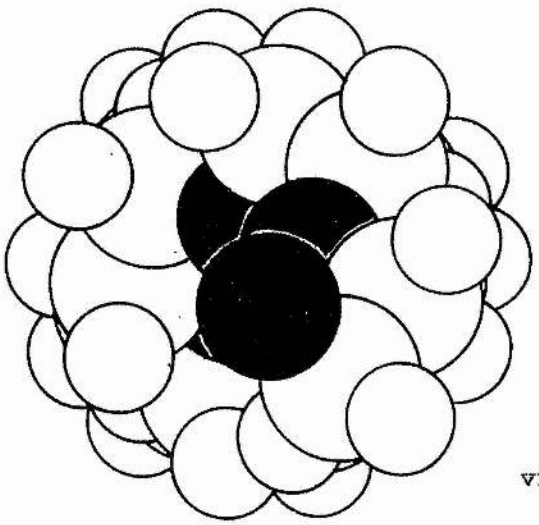

view down the helix

Fig. 1.1. The helical structure of PEO. (From reference 12.)

1.2 Formation of a polymer electrolyte

A salt dissolves in a solvent only if the energy and entropy changes associated with the transfer of its constituent ions from the crystal lattice to their equilibrium positions in the host medium produce an overall reduction in the free energy of the system[14]. Lattice energy must therefore be compensated for by ion - solvent interactions. In a polymer electrolyte, the 'solvent' is the macromolecular array of Lewis bases determined by the repeat unit of the host polymer i.e the oxygen atoms of a polyether, the sulphur atoms of a polysulphide, or the nitrogen atoms of a polyimine.

In polymer media, the loss of translational entropy of the solvent caused by ion solvation is much smaller than for low molecular weight solvents hence the entropy of solution is always likely to be positive (and so favourable) in such systems. In contrast, the enthalpy changes accompanying solvation do not always compensate the lattice energy of the salt, as demonstated by Shriver *et al*[15] and Chabagno[16]. In both studies the existence of an upper limit for the lattice energy was found (of around 850 $kJ\,mol^{-1}$ for lithium derivatives) above which PEO - salt adducts did not form (see Table. 1.1).

Anion :	F^-	Cl^-	Br^-	I^-	SCN^-	ClO_4^-	$CF_3SO_3^-$	BPh_4^-
Cation								
Li^+	1036	853	807	757	807	723	< 725	< 700
	-	+	+	+	+	+	+	+
Na^+	923	785	747	704	682	648	< 650	< 630
	-	-	+	+	+	+	+	+
K^+	821	715	682	644	616	602	< 605	< 630
	-	-	-	+	+	+	+	+
Rb^+	785	689	660	630	619	582	< 585	< 600
	-	-	-	+	+	+	+	+
Cs^+	740	659	631	604	568	542	< 550	< 550
	-	-	-	+	+	+	+	+

\+ existence of a crystalline adduct.

\- crystalline adduct does not exist.

Table 1.1. Complex formation between various monvalent metal salts and PEO (from ref. 16.). Numeric values given are the salt lattice energies in kJ mol^{-1}.

The main reason for this effect concerns the aprotic nature of the solvent. Whereas solvation of the cation is envisaged as occurring mainly via electrostatic interactions between the positive ion and the lone pairs on the ether oxygens of the polymer chain, anions have been shown to exhibit no specific solvation effects in aprotic solvents i.e the hydrogen bonding interactions which stabilise anions in protic media can no longer occur. Further, this anion destabilisation, directly related to the charge density and basicity of the ion, has been found to follow the general order[17] :

$$CH_3COO^- > Cl^- > Br^- > I^- > SCN^- > ClO_4^- > BF_4^-$$

hence it is to be expected that the most suitable anions for polymer electrolytes based upon dipolar aprotic repeat units, like the ether oxygen unit in PEO, will be the large 'soft' ions such as BF_4^- and ClO_4^-. Such ions have low ion - dipole stabilization energies, but ion - solvent and ion - cation interactions due to anion polarizability are relatively large.

1.3 Morphology

The dissolution of a suitable salt in PEO may give rise to a semi - crystalline material featuring the co - existence of several phases; the relative amounts of which are dependent on temperature, salt identity, and salt content :

(1) A crystalline adduct; usually of ether oxygen to salt ratio $\leq$ 4 / 1 , melting at elevated temperature i.e $\simeq$ 440 K for PEO.$LiCF_3SO_3$.

(2) Pure crystalline poly(ethylene oxide); which has not taken part in the dissolution process.

(3) Amorphous material; the amount of which is mainly dependent on temperature and the relative amounts of (1) and (2).

The above points are most easily summarised in a phase diagram, which has been determined for several PEO - based electrolyte materials including those containing the following salts : $LiCF_3SO_3$, $LiClO_4$, $LiAsF_6$, $LiBH_4$, NaI and NH_4SCN[13,18,19]. Fig. 1.2. shows two of the more well known phase diagrams obtained by a variety of techniques for PEO.NaI and PEO.$LiClO_4$ electrolytes. Phases written as PEO$_n$MX indicate the mole ratio of ether oxygen units, EO, to salt, MX, and is the accepted notation i.e PEO_3NaI represents a phase with EO / Na^+ = 3 / 1. The overall salt content of a given sample, summed over all phases, is also represented in this way but it is usually clear if the phase or overall stoichiometry is being discussed. The examples are given in order to illustrate the differences which can be conferred upon the phase properties of the electrolyte simply by changing the salt. In the case of PEO.$LiClO_4$, the diagram is one of the more complex for PEO - based electrolytes, featuring more than one adduct and a series of eutectic compositions. In contrast, the PEO.NaI phase diagram[13] is one of the simplest and will form

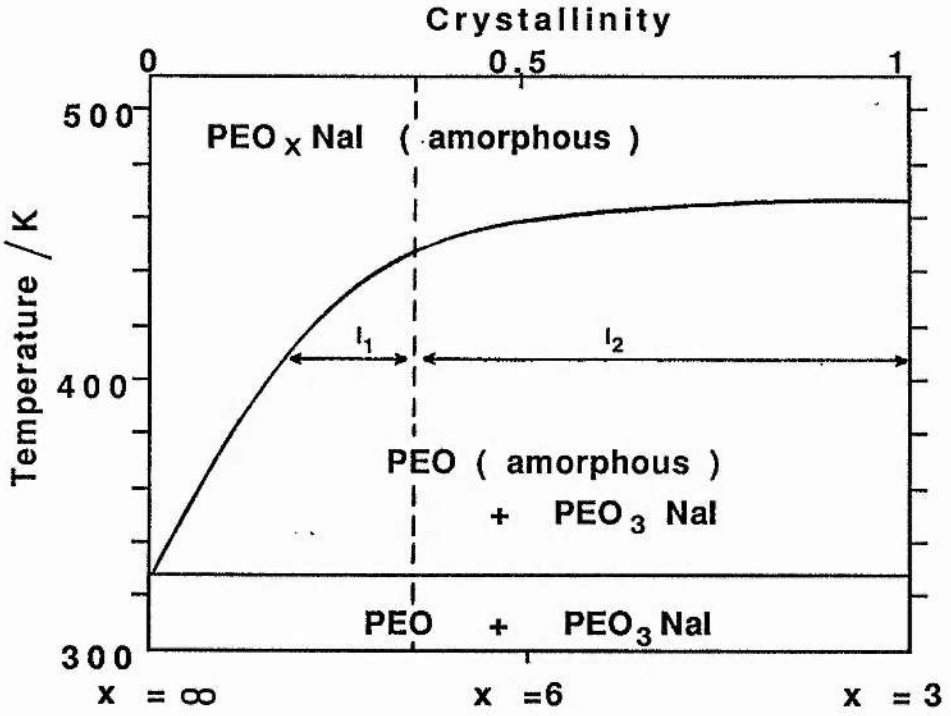

Fig. 1.2(a). $PEO_X NaI$ phase diagram.

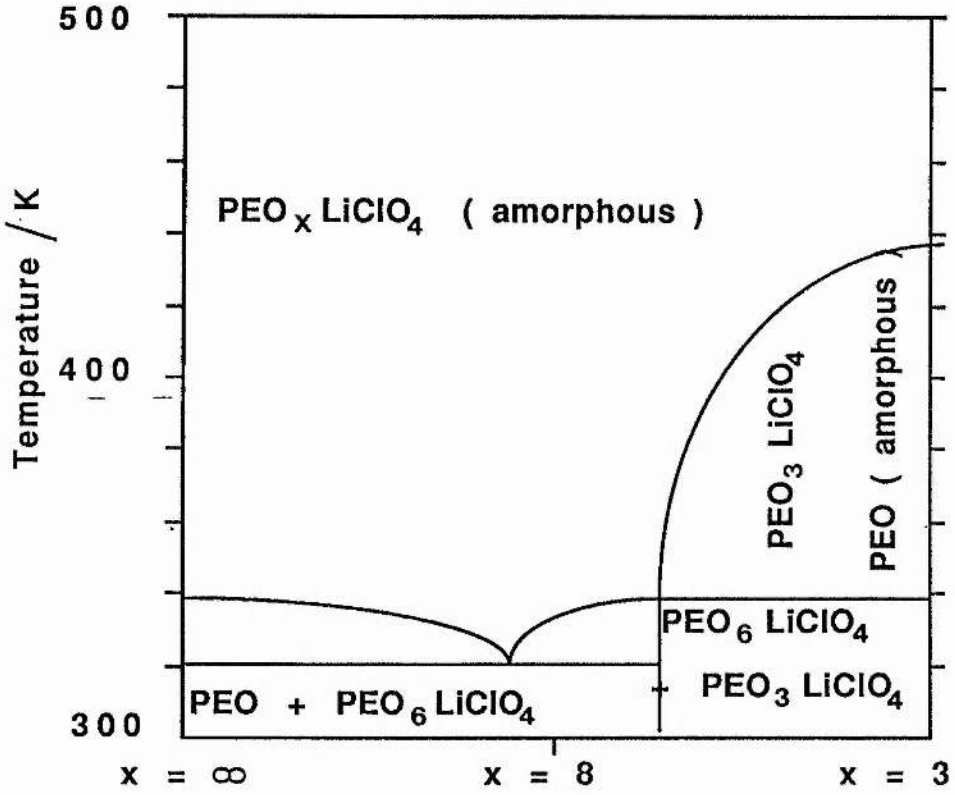

Fig. 1.2(b) $PEO_X LiClO_4$ phase diagram.

the basis of a general outline on the temperature dependent phase behaviour of the electrolyte systems.

In the latter case, below ≃ 333 K, the phase diagram predicts the co - existence between pure crystalline PEO and the salt - containing adduct, PEO_3NaI (usually referred to as the crystalline complex), the relative amounts dependent on the overall salt mole fraction. (The diagram obviously does not take into account residual amorphous material present in this temperature regime.) With increasing temperature comes the melting point of the PEO crystallites at ≃ 333 K to leave crystalline complex co - existent with a newly aquired amorphous PEO phase. There then begins a temperature dependent dissolution of the crystalline complex where the fraction, C, remaining at this and higher temperatures is given conveniently by the relationship[13] :

$$C = l_1 / (l_1 + l_2)$$

where l_1 and l_2 are represented on the figure. At an even higher temperature comes the point of total dissolution of the crystalline complex into the PEO phase, yielding a single amorphous phase with stoichiometry (i.e EO / Na^+ ratio) equal to the overall electrolyte stoichiometry.

1.4 Conductance

Polymer electrolytes have generated intense research effort on a worldwide scale simply because they are good ionic conductors with several potential applications and they represent a new area of solid - state electrochemistry. With this in mind, knowledge of the conductance behaviour of is of prime importance in their characterisation :

(1) To determine the magnitude of the conductance under a given set of conditions i.e temperature, pressure, salt content/type etc.

(2) The nature of the conducting species.

(3) The role of the polymer in the conduction process.

(4) To present a satisfactory microscopic model to describe the formation of, and ionic transport properties within, polymer electrolytes.

1.4.1 Location of the conducting phase

Initial postulates as to the conducting phase and mechanism centered on Armand's idea[1] of cation hopping along the oxygen - lined inner tube of a PEO helix in the crystalline phase, shown schematically in Fig. 1.3. The model was obviously influenced by inorganic considerations based upon framework conductors such as ß - alumina[20], and early x-ray - based

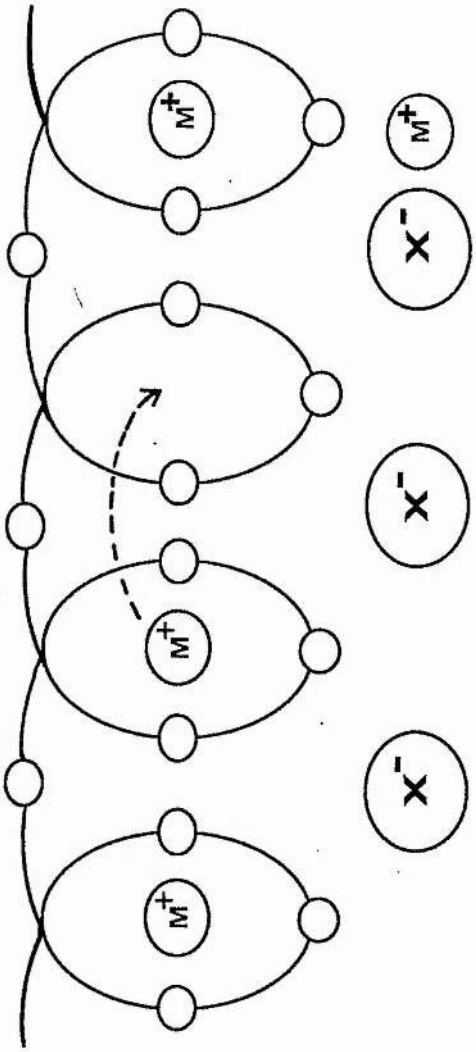

Fig.1.3. Armands idea of cation hopping within the PEO helix in the crystalline adduct.

evidence[21] of cations residing within PEO helices in the crystalline complex, the anions in some external, unspecified position.

A key advance in the understanding of polymer electrolytes was made however when it was recognised that the significant ionic conductivity in these materials was due to ionic motion in the amorphous phase and that crystalline phases were essentially non - contributary. This was due, in part, to several studies including that of Dupon *et al*[15] who showed that the strongly ion - paired $NaBH_4$ species did not notably impede the mobility of $NaBF_4$ in the same sample, as would have been expected if the alkali ion carrier (Na^+) encountered blocking alkali metal ion while moving down the PEO helix. Further, electrolytic materials based upon poly(propylene oxide), PPO*, which are known to be totally amorphous at all temperatures, showed almost comparable ionic conductivities to PEO electrolytes[1]. Final evidence, and perhaps the most convincing, came from the Berthier group using the nuclear magnetic resonance (nmr) technique in tandem with differential scanning calorimetry (DSC)[13,22,23]. For PEO - based electrolytes containing NaI, $LiCF_3SO_3$ or $LiClO_4$, nmr identified mobile ionic species as being in the amorphous polymer fraction, the concentration of which could be roughly related to that predicted by DSC and to the measured ionic conductivity of the system.

* PPO $\equiv -(CH(CH_3)CH_2O)_n-$

1.4.2 Transport numbers

The conductivity, σ, of any material can be written as :

$$\sigma = \sum_i n_i z_i \mu_i \qquad (1.1)$$

where n_i is the number of charge carriers of type i, q_i the charge on each, and μ_i is the mobility. In most solid electrolytes the expression is greatly clarified by the existence of only one charge carrying type i.e Na^+ in β - alumina[24], which carries all the current. It soon became clear that in many polymer electrolytes this was not the case; cationic transport numbers, t_+, measured by a variety of techniques, were less than one (and usually $t_+ < ½$). This result means that the following expressions must be written for the conducting species[14] :

$$t_+ = \Sigma i_+ / (\Sigma i_+ + \Sigma i_-) \qquad (1.2)$$

and

$$t_- = \Sigma i_- / (\Sigma i_+ + \Sigma i_-) \qquad (1.3)$$

where the total current $i = (\Sigma i_+ + \Sigma i_-)$ and the sums of the partial currents refer to all of the mobile charged species in the electrolyte. The transport scenario is further complicated by the fact that the conducting species, either cationic or anionic, have not been firmly identified in polymer electrolytes i.e single ions have been supposed but other species, such as triple ions[25,26] (+-+ or -+-), cannot be discounted.

With these possible complications to the ionic transport picture in mind only some examples are given. For $PEO.LiClO_4$ electrolytes at high salt content (EO / Li ≃ 8 / 1 - 12 / 1) and at temperatures of around 400 K, a number of techniques[27,28,29] (mainly electrochemical) give a t_+(Li) value of about 0.25 to 0.30. In $PEO.LiCF_3SO_3$ electrolytes at similar temperatures t_+(Li) varies from 0.2 to 0.45 depending on experimental technique[30,31]. The temperature and concentration dependence of transport numbers in these systems is obviously another matter and there appears to be no firm agreement on either at the present time. An interesting study on the system $PEO_8LiCF_3SO_3$ by Bhattacharja *et al*[31] using nuclear magnetic resonance yielded the data shown in Fig. 1.4. Here cationic transport numbers were found to increase with temperature in the totally amorphous electrolyte.

1.4.3 The temperature dependence of conductance.

Armand' and Chabagno'[6] studied the temperature dependence of conductance for a range of poly(ethylene oxide) - based electrolyte systems and classified the conductance behaviour of a given system according to one of three types (shown schematically in Fig. 1.5.) :

Type (I) : Non - Arrhenius behaviour over the entire temperature range of study (usually ≃ (298 - 410) K) i.e $PEO_{4.5}LiClO_4$

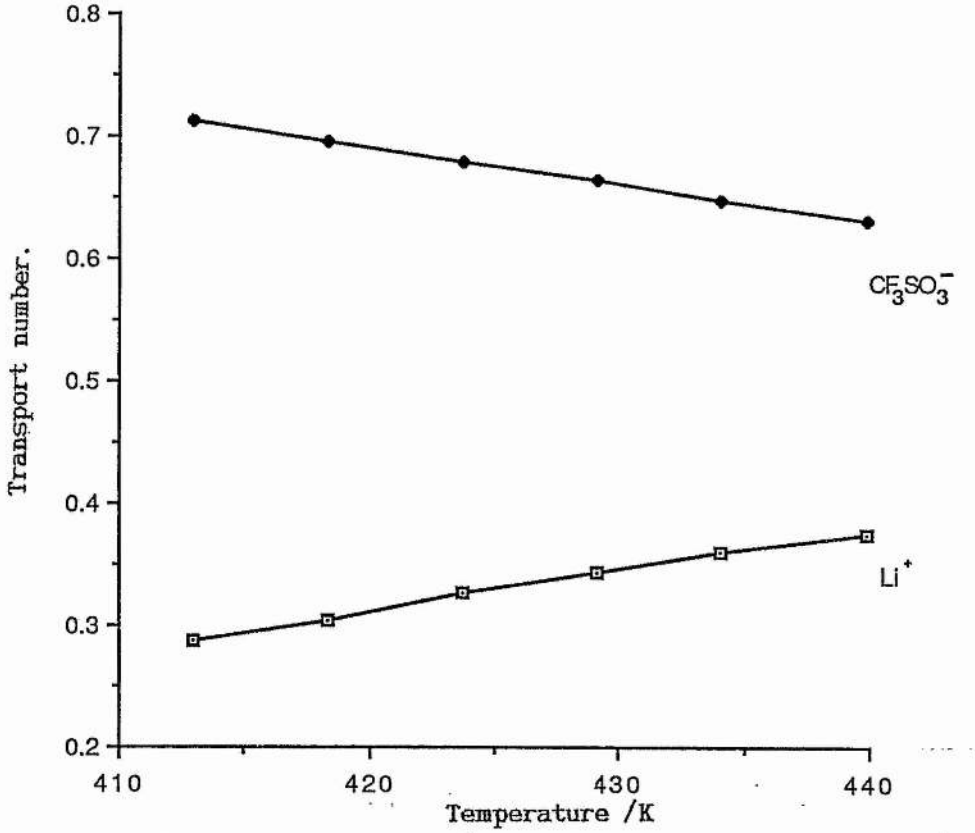

Fig. 1.4. Anionic and cationic transport numbers in $PEO_8LiCF_3SO_3$ determined by nuclear magnetic resonance.

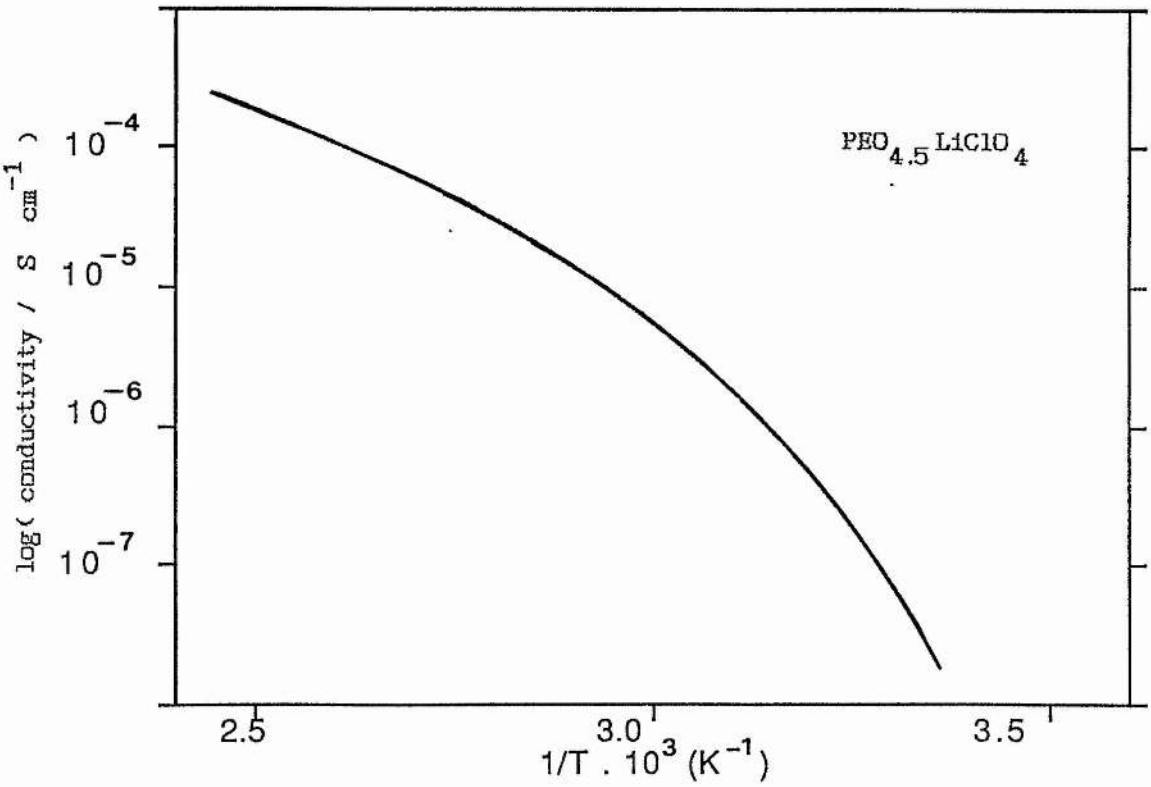

Fig. 1.5(a). Type I conductance behaviour.

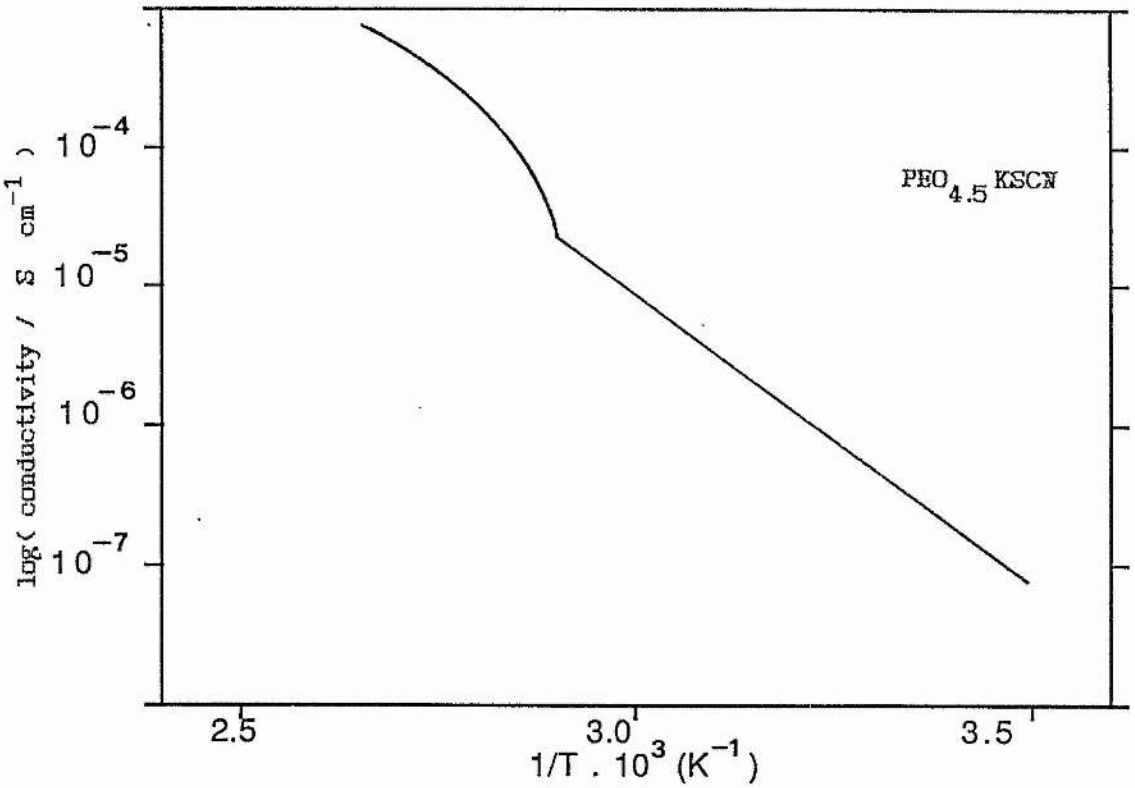

Fig. 1.5(**b**). Type II conductance behaviour.

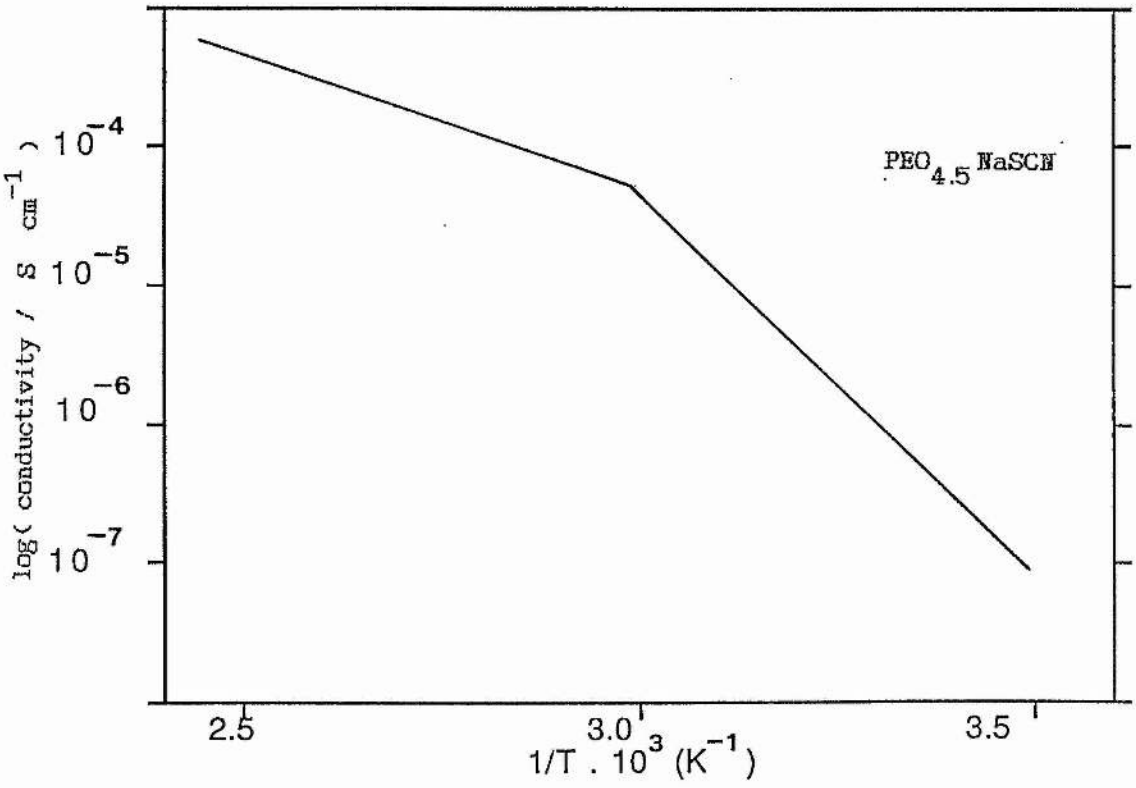

Fig. 1.5(**c**). Type III conductance behaviour.

Type (II) : Arrhenius behaviour below the melting temperature of the pure PEO crystallites (≃ 333 K) but non - Arrhenius above i.e $PEO_{4.5}KSCN$

Type (III): Arrhenius behaviour at all temperatures but with a smaller apparent activation term (Ea) above 333 K than below i.e $PEO_{4.5}NaSCN$.

Here, 'Arrhenius behaviour' means a linear plot of ln(σ) vs. 1/T according to the familiar law[34] :

$$\sigma = \sigma_o.\exp(-Ea / RT) \qquad (1.4)$$

where σ_o is a constant, R the gas constant (8.314 J $K^{-1}mol^{-1}$), and Ea the activation energy for the transport process.

1.4.4 Non - Arrhenius behaviour; the Vogel - Tamman - Fulcher equation.

In addition to the *type (I)* and *type (II)* behaviour noted above for PEO.MX systems, non - Arrhenius behaviour of conductance with temperature is a feature common to many totally amorphous electrolytes with a PEO base, such as the comb - branched electrolytes[33], cross - linked materials[34] and low mol. wt. PEO oligomer systems[25], all featuring the ether oxygen unit as the solvating moiety. (PPO - based electrolytes must also be included here, they are totally amorphous and show non - Arrhenius behaviour[7]).

In most cases, where the conductance does not follow the Arrhenius form, the Vogel - Tamman - Fulcher (VTF) equation[1,35] has been used to linearise the data i.e :

$$\sigma = A\,T^{-\frac{1}{2}} \exp(-E / R(T - T_o)) \qquad (1.5)$$

where $\ln(\sigma T^{\frac{1}{2}})$ vs. $1 / (T - T_o)$ yields a linear plot, A and E are constants and T_o is a reference temperature. This empirical equation was originally used to describe the viscosity of supercooled liquids. At a later stage Cohen and Turnbull[36] arrived at the same formalism, using free volume ideas, where the basic assumption for the model was that diffusion was not an activated process but occurred as a result of the redistribution of free volume within the liquid. (The 'E' term in the VTF equation now becomes a function of expansivity, not energy.) The molecules are assumed confined within cages except when a hole is opened which is large enough for the diffusing species to jump into. In the free volume model the T_o term is the 'equilibrium glass transition temperature' at which free volume tends to zero. It is not to be confused with the thermodynamic glass transition temperature, Tg, at which an endotherm may be observed in DSC for example; the following approximate relationship is found :

$$T_o \simeq Tg - 50\ K$$

The relevance here is that Cheradame's group[4] have used both free volume *and* Arrhenius considerations in interpreting results for cross - linked network electrolytes based upon poly(ethylene glycol), $-\!\!\leftarrow CH_2\ CH_2\ O \rightarrow\!\!-_n$, $n \leq 25$, containing salts such as $NaBH_4$ and $LiClO_4$.

Other ideas for modelling the conductance behaviour have been based on configurational entropy ideas, as proposed by Adam and Gibbs[37] to explain the general transport properties of pure (no solute) amorphous polymer phases. As in the free volume picture, the associated theory arrives at the same formalism as the VTF equation but is based upon 'group co - operative' rearrangements of the polymer chain to give transport. The configurational entropy model was originally applied to polymer electrolyte systems by Papke *et al*[38], and has since been favoured by several authors. The E term (see the VTF form above) in this model is relatable to an energy (unlike the free volume model) i.e :

$$E = \Delta\mu\ S_c^*\ T_o\ /\ kB \qquad (1.6)$$

where $\Delta\mu$ is the free energy barrier impeding the basic configurational rearrangement, S_c^* the minimum entropy required for the rearrangement, T_o where the configurational entropy goes to zero (again an equilibrium glass transition temperature $\simeq$ Tg - 50 K), k and B are constants.

Although both models have been used in polymer electrolyte study, it is recognised that there are several conceptual drawbacks in their application : Firstly, they are not microscopic, and describe only polymer motion, not that of the ionic species. Secondly, they are static pictures based upon thermodynamic arguments and as such do not introduce the dynamic ideas necessary to give actual rates and mechanisms of transport.

1.4.5 Dynamic Bond Percolation Theory

In recognition of the above factors Ratner[35] has recently introduced the 'Dynamic Bond Percolation Model', the only detailed microscopic model developed specifically for describing the transport properties in polymer electrolytes. The model develops well known percolation theories[36], based on a set of sites at which the moving species (ions) can reside, and describes allowed motions with a set of master equations :

$$\dot{P}_i = \sum_j \{ P_j W_{ji} - P_i W_{ij} \} \qquad (1.7)$$

where $\dot{P}_i$ is the probability of finding the charge carrier at site i at time t, and $W_{ji} = W_{j \to i}$ is the rate at which the carrier hops from site j to site i (the site hopping is regarded as to nearest - neighbour sites). The static model defines a 'bond' as a pathway between hopping sites, which can be open, i.e available for a hop, or closed, unavailable (this is not to be confused with a chemical bond). The model

also defines f as the fraction of bonds available for a hop (they are 'open') and when this fraction is above a threshold value it allows a series of uninterrupted open bonds on the lattice and diffusive transport can take place.

The transition to the dynamic case, and relevance to polymer electrolytes, comes with the additional requirement that which bonds are open or closed changes with a characteristic rate λ, the renewal rate. Physically, the polymer has now been introduced, the renewal event describing motion of a polymer segment which, for example, either permits a cation to change co - ordinating ligands or frees a previously blocked pathway for ions to move. Finally, W, the hopping rate, is postulated as depending on the molecular mechanism involved in the transport i.e cations are envisaged as interacting specifically with the polymer chain at ether oxygen co - ordinating sites while anions may jump between 'void' sites. The model is at an admittedly early stage of development and requires experimental input in the form of estimates for the f, λ and W parameters but it does represent a beginning towards a dedicated polymer electrolyte theory.

1.5 Overview

The study of polymer electrolyte systems is still at a comparitively early stage, with a need to refine and inter - relate both physical and theoretical aspects of their study. In the broadest sense, the macroscopic evaluation of these systems i.e phase behaviour, conductance characterisation, and development of phenomenological models, has given way in recent years to microscopic investigations, which have come with the need to gain information on the following aspects :

(1) The state of the salt in these systems i.e the degree of dissociation and identity of the conducting species, which has direct dependence upon ion - ion and ion - solvent interactions.

(2) 'Microscopic' phase behaviour. Does a simple case exist of partition between phases with mobile amorphous and non - mobile crystalline regions or are phase boundaries more subtle?

(3) The dynamics of all species ; ionic and polymer. This includes both local effects, such as a polymer chain motion correlation time for the liquid - like behaviour believed to exist in the amorphous phase, and true diffusion effects, pertinent to the transport of ions.

In addition to an improved physical description, a developing theory like Dynamic Bond Percolation would then benifit by having a better estimation of the f, λ and W parameters.

With this in mind, work was undertaken to investigate some aspects of the above considerations: Chapter 2 addresses current ideas on the state of the salt and nature of the conducting species in polymer electrolytes. The results of an electrochemical study on a low molecular weight PEO - analogue system are presented, serving as a model system for the high molecular weight case. Chapter 3 introduces nuclear magnetic resonance and the results of studies on the low molecular weight model system. Chapters 4 and 5 continue the nmr theme, detailing studies on systems considered to be conventional polymer electrolytes; high molecular weight poly(ethylene oxide) containing dissolved salt.

Chapter 2

2 CONDUCTANCE STUDIES ON LOW MOLECULAR WEIGHT PEO ANALOGUE - INORGANIC SALT SYSTEMS.

2.1 Introduction.

Two of the main questions still concerning the study of polyether electrolyte systems are that of the microscopic transport mechanism for the conducting species and the nature of the conducting species. Indeed, a serious problem with the current theories of polymer electrolytes concerns the strength of the interactions between the salt and the polymer host in comparison to that of the interionic forces. This leads to the question of exactly how the salt exists in these polyether media. Is salt dissociation complete with cations situated within a four co-ordinate ether oxygen cage, the anions in some external unspecified position, or is the dissociation incomplete with the presence of species more complex than simple single ions?

Intuitively one would consider that ion - ion interactions must be of major importance in media with relatively low dielectric constant. If we consider that the dielectric constant, ϵ, of PEO - type materials is no more than seven[39], and is generally assumed to have a value of five, then such systems are well outside the range adopted by Parker[40] to define "dipolar aprotic electrolytic solvents" i.e dimethylformamide has $\epsilon = 36.7$. The implication here is that ion-ion interactions, manifest as ion association, may be an important factor in polyether electrolyte systems.

The importance of ion pairing has been pointed out previously by a number of workers[41,42], and direct spectroscopic evidence has been obtained in several instances: Ratner[43,44] identified $Li^+BH_4^-$ and $Na^+BH_4^-$ ion pairs in $PEO.MBH_4$ (infra - red and Raman spectroscopy), Teeters and Frech[45] suggested strong cation - anion interactions in PPO_7NaSCN solutions (Raman spectroscopy) and Chadwick[46] determined Rubidium - Iodine contact pairs in PEO_8RbI (Exafs).

In the main such studies have identified the presence of neutral species (ion pairs) which are obviously non-conducting. In this chapter we attempt to establish the state of the electrolyte in polyether media and thus to suggest the nature of the *conducting* species.

Much useful information on ion - ion interactions can often be derived by measuring conductance as a function of concentration at relatively low salt content. This approach has been used reliably over many decades to address problems in various media and benefits a tested theoretical base[47]. There are however problems associated with obtaining reliable results when using polymers with the molecular weight (mol.wt.) commonly selected for forming polymer electrolytes (> 200,000). Ionic impurities, mainly from catalyt residues, are very difficult to remove and therefore one would expect a large error to be introduced into the supposed ionic concentration for a low salt content experiment. Further, the removal of phase heterogeneity to ensure a uniform distribution of salt can only be achieved for many systems by working at high temperatures where the dimensions of the electrolyte are no longer stable.

For these reasons it was decided to study conductance in a low mol.wt. analogue of PEO which is a liquid at room temperature and thus negates the above problems.

As has been mentioned, it is now widely accepted that the amorphous regions in polyether electrolytes are responsible for the observed high ionic conductivity. Above Tg the local structure and segmental dynamics of the amorphous regions are liquid - like and the only important difference between the conductance behaviour of high and low mol.wt. materials is likely to be in the overall conformational motion of the different lengths of the polymer chain (as demonstrated by the pronounced rise in viscosity with mol.wt.). It is not considered that this variation has any significant influence on the state of the electrolyte in polyether media, and it is suggested that the results presented here may be extrapolated to high mol.wt. analogues.

2.2 Experimental.

2.2.1 Preparation of salts, solute and solutions.

Salts:

$LiCF_3SO_3$ (3M's Ltd.) was dried in the manner selected by most authors, heating under vacuum at 425 K for forty-eight hours. Upon cooling, the salt was stored in a vacuum dessicator over phosphorus pentoxide (P_2O_5) before use.

$LiClO_4$ (Aldrich Chemicals Ltd.) is known to retain water of crystallisation as a solid[48]. This was removed by heating and melting under vacuum at 300°C for forty - eight hours. The dried salt was then cooled and stored as for $LiCF_3SO_3$.

Solvent:

The short chain polyethylene glycol, $HO-(CH_2-CH_2-O)_n-H$ (n = 8 - 9, average mol.wt. 400), obtained from Aldrich Chemicals Ltd., was found to dissolve salts such as $LiCF_3SO_3$, $LiClO_4$, and NaI readily. However, the glycol as received was not considered to be a practicable solvent in this investigation:

(a) The relatively high viscosity of the solvent, probably due to hydroxyl end - group hydrogen bonding interactions, made the preparation, handling, and conductance measurement of electrolyte solutions awkward (by mol.wt. ≃ 600 these materials are waxes).

(b) Proton nmr (Bruker, model WP80) indicated that salt dissolution was accompanied by strong specific interaction between the added salt and the hydroxyl end - groups, and that salt - chain interaction was not apparent (to ± 1 Hz.). This is shown in Fig. 2.1. where the addition of $LiCF_3SO_3$ is observed to strongly affect the hydroxyl but not the chain resonance $-(CH_2CH_2O)-$. In contrast, the addition of salts such as NaSCN to glymes of the form :

$$CH_3-O-(CH_2-CH_2-O)_n-CH_3$$

has been shown to result in a peak frequency shift and peak splitting of the chain resonance[43].

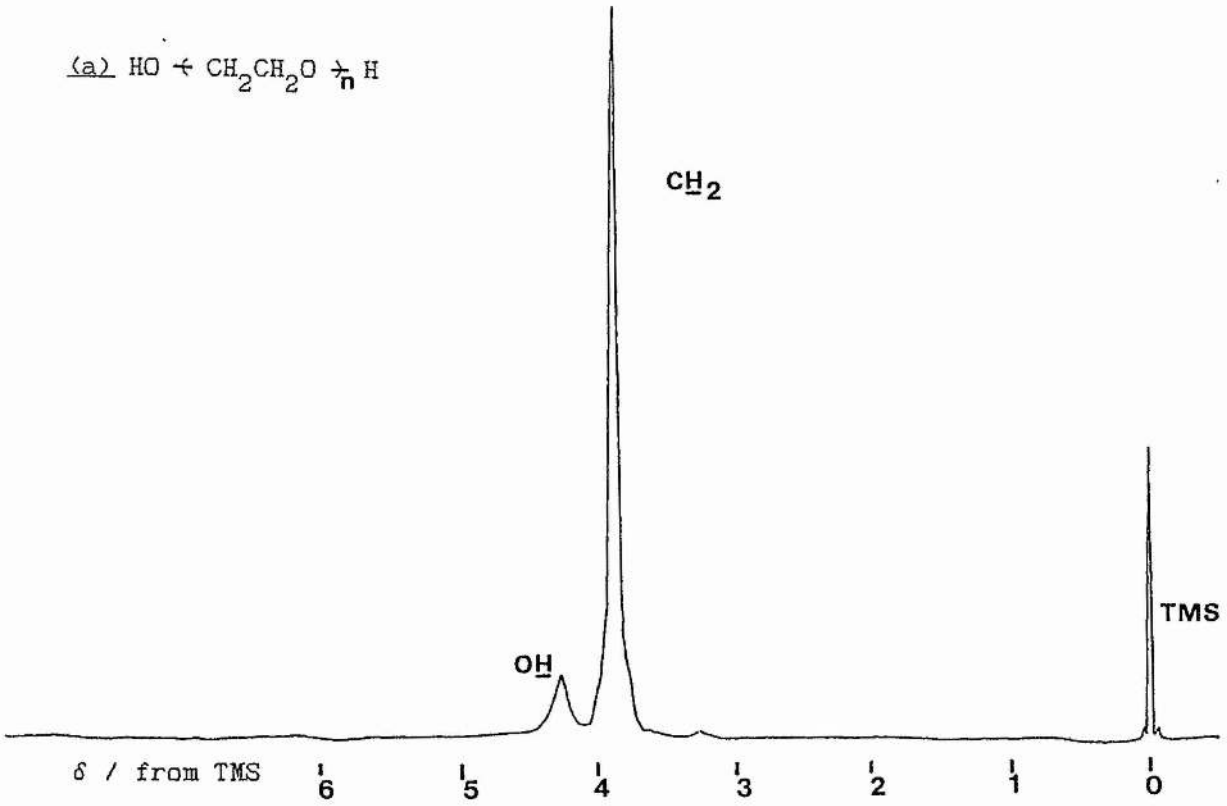

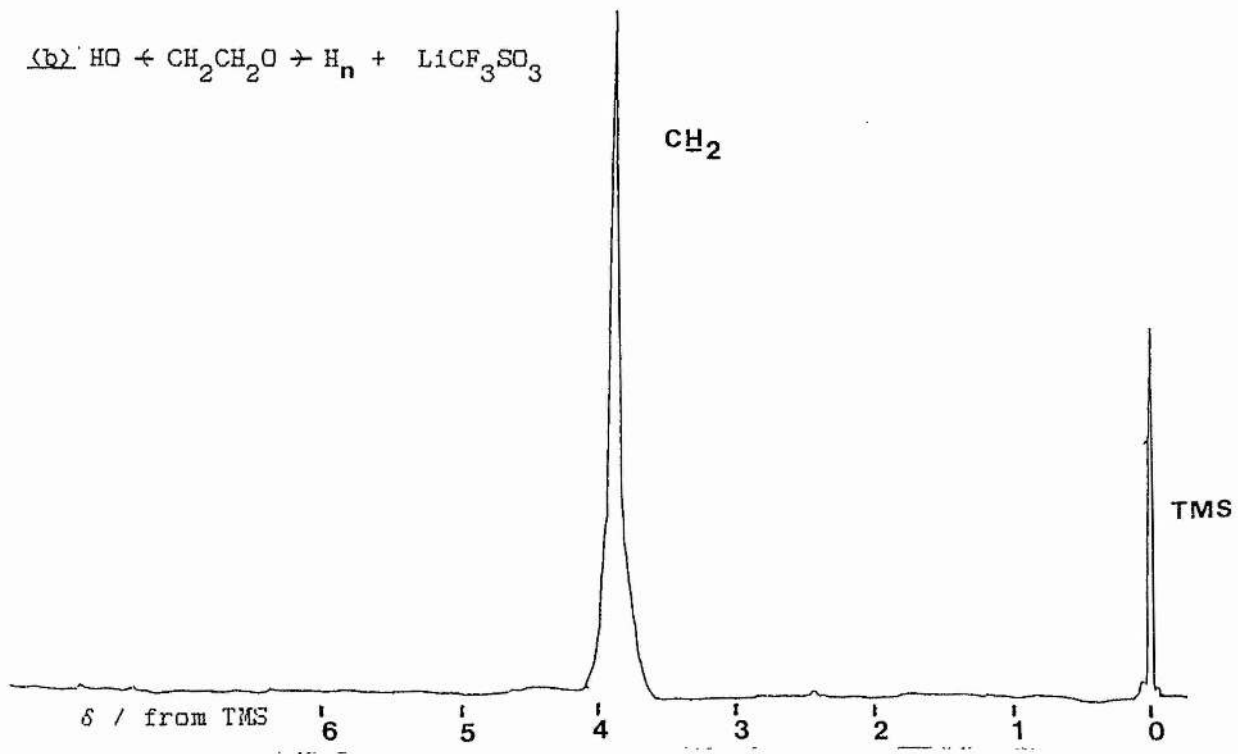

Fig. 2.1. Nmr spectra (80 MHz, $CHCl_3$ solution) for (a) PEO(400) and (b) $PEO(400)_4LiCF_3SO_3$. (PEO(400) = HO ← CH_2CH_2O → H, n = 8 – 9).

* TMS = tetramethylsilane, $(CH_3)_4Si$

Endo - acetylation of poly(ethylene glycol).

For the above reasons , terminal hydroxyls were removed by endo-acetylating the glycol according to the method of Shigehara *et al*[50]. The method involves esterification of the terminal hydroxyl groups by reaction with a two - fold excess of acetic anhydride i.e

$$2(CH_3CO)_2O$$

$$HO\text{-}(CH_2CH_2O)_n\text{-}H \longrightarrow CH_3CO_2\text{-}(CH_2CH_2O)_n\text{-}CO\,CH_3 + 2\,CH_3CO_2H$$

PEO(400) PEO(400)e

Here, sufficient anhydride (Analar grade, BDH Chemicals Ltd.) was added directly to PEO(400) in a round - bottomed flask and the mixture stirred at 345 K for eight hours under a stream of dry nitrogen gas. Excess anhydride and eliminated acid were then removed; initially by rotary evaporation and then finally by passing the mixture through a basic alumina column (Merck Grade 1, dried under vacuum, 425 K for two days) which was eluted with chloroform. The chloroform was removed by rotary evaporation and the remaining material held under vacuum at 355 K for twenty - four hours before storing in a vacuum dessicator over P_2O_5 until further use.

That the end - capping procedure was successful was confirmed by infra red (Perkin Elmer, model 1330) and nmr spectroscopy. Fig. 2.2. shows the infra red spectra of PEO(400) and PEO(400)e respectively where the various modes are assigned according to the literature values for PEO[51] and polyethylene glycol[52]. End - capping is accompanied by the removal of the strong hydroxyl stretching mode centered at about 3300 cm^{-1}, Fig. 2.2.(a), and the appearance of the carbonyl stretch at 1735 cm^{-1}, Fig. 2.2.(b). (Structure in the 3400 - 3700 cm^{-1} region of the latter is likely to be due to combination and / or overtone bands from lower frequency modes.)

Fig. 2.3. shows the proton nmr spectra for PEO(400)e and PEO(400)e_4 $LiCF_3SO_3$. In Fig. 2.3.(a) there is no hydroxyl absorbtion (as the case of the glycol, Fig. 2.1.(a).) and new structure has appeared in the spectrum. The assignments given are consistent with the formula $CH_3CO_2 \leftarrow CH_2CH_2O \rightarrow_n CO\ CH_3$ (n = 8 - 9, mol.wt. ≃ 486). More significantly, Fig. 2.3.(b) shows an affect upon the main chain resonance with the addition of salt, the peak shifted about 6 Hz. to higher frequency and split. In a qualitative sense this paramagnetic shift can be viewed a result of electrostatic interaction between positive species, or positively polarised species, and the ether oxygens. Such an interaction has been shown to withdraw electron density from the oligomer chain and deshield the chain protons, giving absorbtion at higher frequencies[49,53].

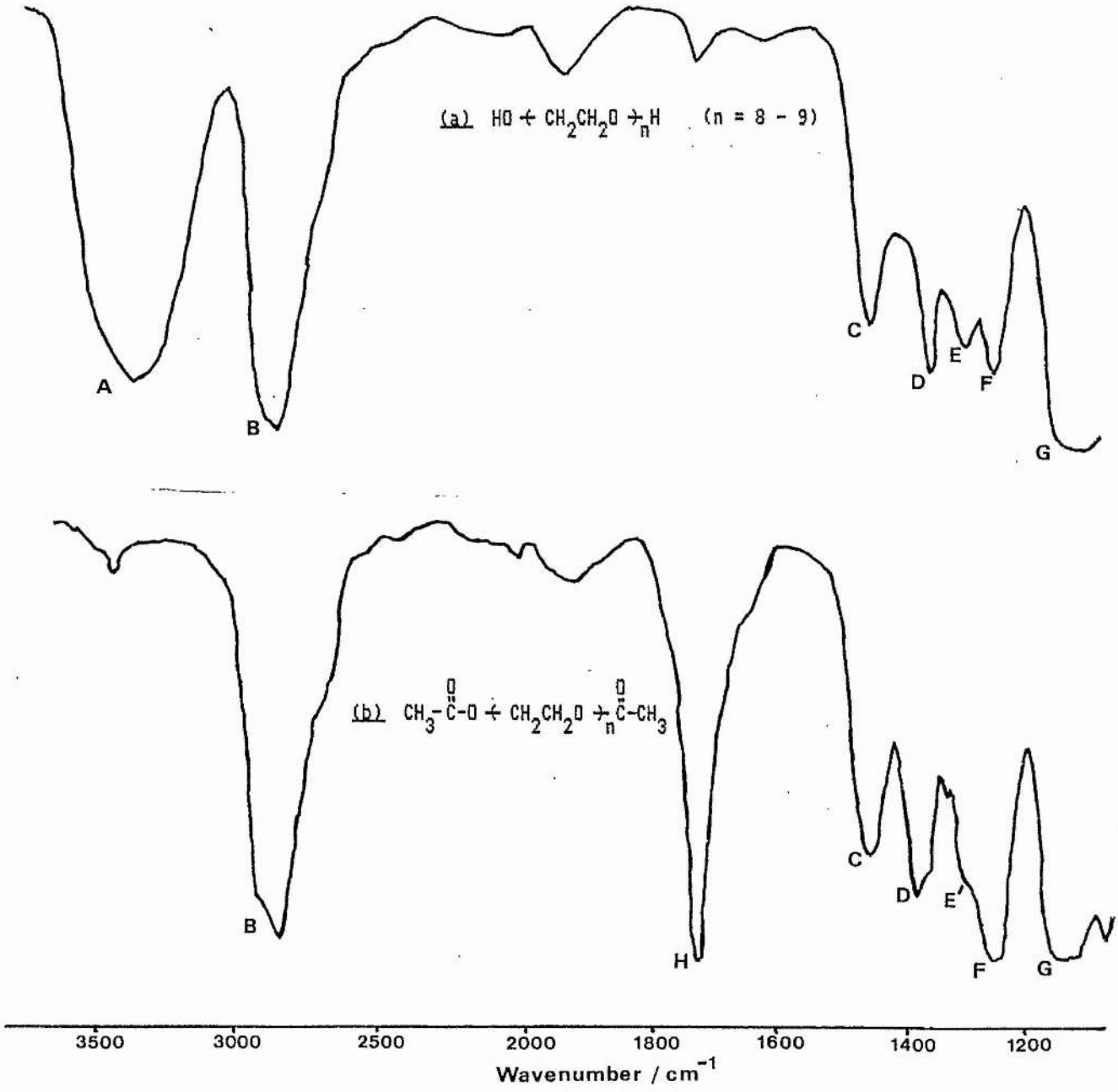

KEY:

Label	Assignment	Label	Assignment
A	(O-H) stretch	E	(CH_2) torsion
B	(CH_2) stretch	F	(CH_2) torsion
C	(CH_2) bending	G	(C-O-C) stretch
D	(CH_2) wagging / (CH_2) stretch	H	(C=O) stretch

Fig. 2.2. The infra - red spectra of (a) PEO(400) and (b) PEO(400)e.

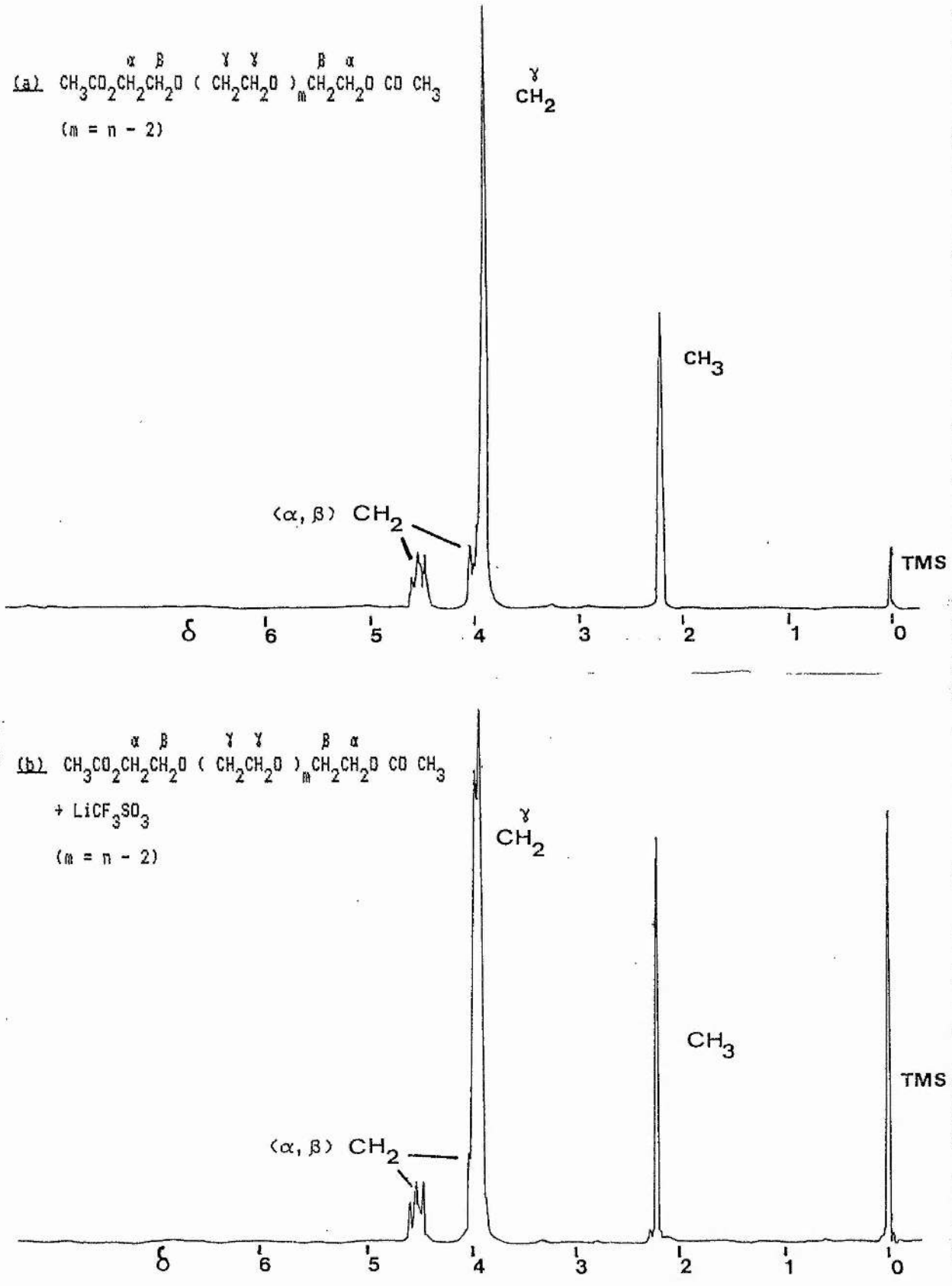

Fig. 2.3. Nmr spectra (80 MHz, $CHCl_3$ solution) for (a) PEO(400)e and (b) PEO(400)e$_4$$LiCF_3SO_3$. (PEO(400)e = CH_3CO_2(CH_2CH_2O)$_n$CO CH_3, n = 8 - 9).

Polymer Dialysis.

The endo - acetylated material, as prepared, showed residual conductivity of (0.08 - 0.20)μScm^{-1}, depending on batch. By the nature of their synthesis, one would expect PEO - type materials to contain residual ionic impurities from sources such as initiators and catalysts[54]. This was confirmed by atomic absorbtion analysis, which showed Ca^{+2} and Na^{+} to be the main contaminants at about 4.0 $\times 10^{-3}$ mol kg^{-1} and 1.5 $\times 10^{-3}$ mol kg^{-1} respectively. Rogue species at these concentrations would be expected to have a serious effect on the measured conductance in a low concentration experiment such as this (0.002 - 0.080 mol Kg^{-1}), and it was decided to remove them by the membrane dialysis technique[55].

Dialysis is used to separate large and small species and depends on the fact that a semi - permeable membrane allows the smaller species to pass through but not the large ones. In practice, the material to be dialysed is placed in a dialysis sac immersed in a large volume of solvent. The small species (ions in this case) pass through the membrane into the external solvent until an equilibrium is reached. The material can be virtually freed from contaminants by repeatedly changing the external solvent.

Cellophane tubing (Visking division, Union Carbide Chemical Co.) is the most commonly used material for dialysis, with a cut - off point down to about mol. wt. = 1000, below which molecules or ions can pass through. Since PEO(400)e has mol. wt. ≃ 486 and would pass through the membrane with the contaminants, the tubing was chemically modified to a cut - off point of ≃ 200 according to the method of Craig *et al*[56]. This involved washing the membrane with 10% acetic anhydride in dry pyridine then 0.01N acetic acid in distilled water. A dialysis sac of about 250 cm^3 volume, containing contaminated PEO(400)e in distilled water (about 1 / 4 by volume), was dialysed against distilled water, changing the external solution five times over an eight hour period. The dialysed mixture was then subject to rotary evaporation, to remove bulk water, then dried by passing through a column of freshly prepared alumina, eluting with chloroform. Removal of the chloroform gave a material with no, or very low, levels of ionic contaminants, as evidenced by atomic absorbtion analysis ($[Ca^{+2}]$, $[Na^{+}]$ ≃ 0) and a residual conductivity below the lower limit of the conductivity bridge measurement (≤ 10^{-8} Scm^{-1}).

Solutions.

Stock solutions of about 0.1 mol kg^{-1} were prepared by addition of the required weight of salt to PEO(400)e. Gentle shaking at room temperature effected dissolution. Solutions of the required concentration for experiment were obtained by dilution of a known weight of stock solution with that of PEO(400)e. (The molal scale was used here

for reasons of accuracy, with weights measured to four decimal places on a calibrated Stanton Instruments precision balance.)

2.2.2 Conductance Measurements:

Conductance values were obtained using a Philips PW9509 digital conductivity bridge (Pye Unicam Ltd.) with calibrated immersion cells (Orion Ltd.). A schematic of the bridge and cell components is shown in Fig. 2.4.

The conductivity bridge was based upon the familiar Wheatstone bridge[57] where an alternating current is applied across the two arms of a circuit containing four resistances. Symbolic assignments are as follows:

r(Cell) ; is the resistance of the solution to be measured.

R ; is a calibrated resistance box.

r_1 and r_2 ; are known resistances.

S ; an alternating current source.

D ; an ammeter.

F ; a variable capacitor (≃ 0.001 μF)to eliminate the effects of cell and lead capacitance. These effects were also reduced by working at lower frequency, 80 Hz. in this case[58].

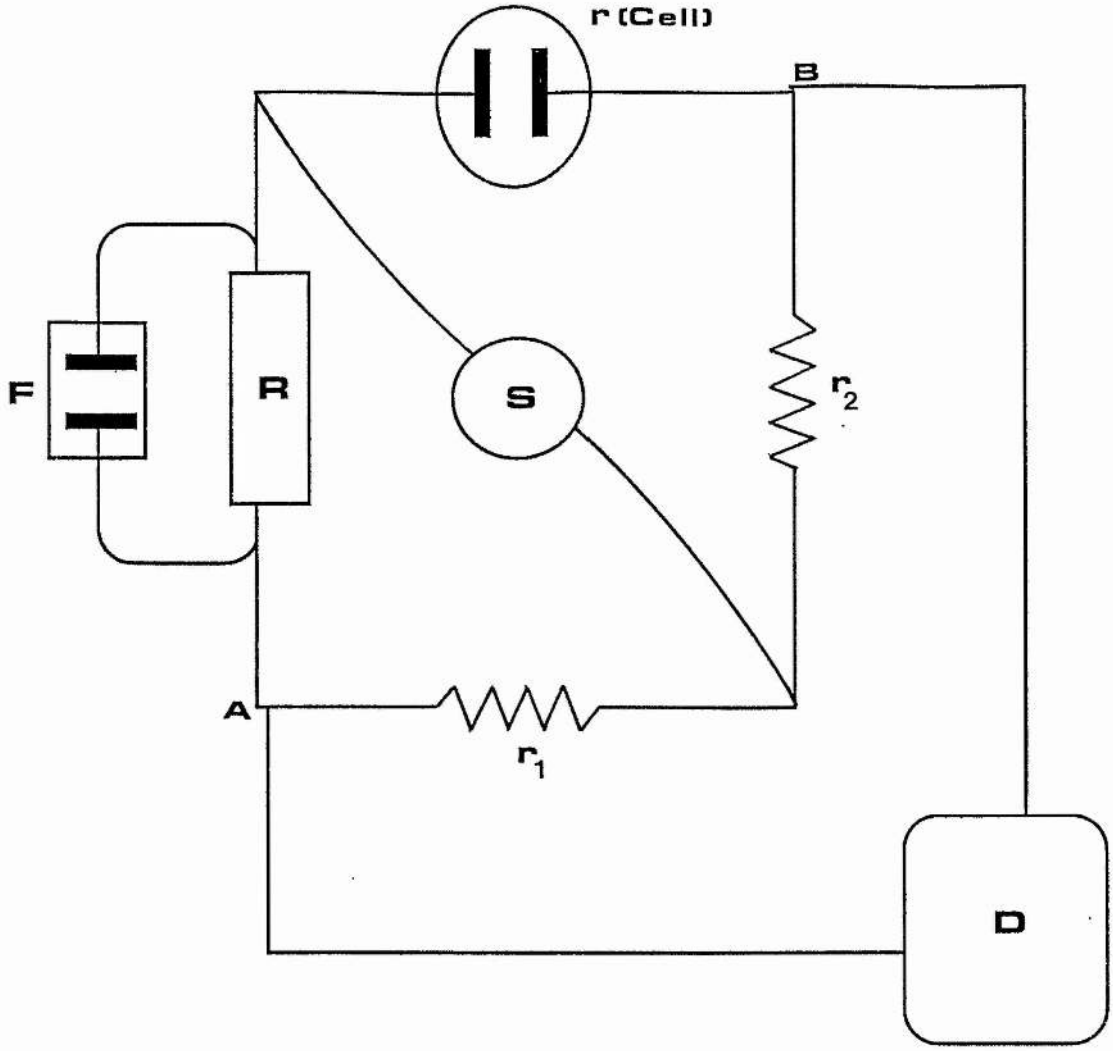

Fig. 2.4. A schematic representation of the bridge and cell components used in conductance determination. (Symbolic assignments are given in the text.)

Obtaining a conductance value for the solution under test relies upon balancing the bridge by adjusting resistances until no current flows through D. At this null point for the current A and B are at the same instantaneous potential and so the fall in potential through R and r_1 is the same as through r(Cell) and r_2. Thus :

$$R / r_1 = r(Cell) / r_2 \qquad (2.1)$$

and[57]

$$\text{Conductance}(\sigma) = \text{Cell constant} / r(Cell) \quad . \ \Omega^{-1}cm^{-1} \qquad (2.2)$$

Ω^{-1} is known as the Siemen, S, and the conductance is expressed as Siemens per centimetre, Scm^{-1}.

Three immersion cells were used in this work in order to speed up data acquisition by measuring conductance values for three solutions at any one time in parallel. Cells consisted of two platinized platinum electrodes held within a glass former to prevent mechanical damage to the electrodes, altering the cell constant and hence the measured conductance. The electrodes were connected via co - axial cable to the meter input.

To measure the conductance of an unknown solution, it is necessary to calibrate conductance cells against a standard of known conductivity to give the cell constant, a parameter dependent on electrode area and separation. This was achieved by using a standard 0.01 mol dm^{-3} KCl solution, which has a known conductivity at 298 K^{se}, 12.88 mS cm^{-1}. The bridge measures the solution resistance, r(Cell), hence:

$$\text{Cell Constant}(\ cm^{-1}\ ) \quad = \quad r(\text{Cell}) \times \text{conductivity} \qquad . \Omega \times \Omega^{-1}cm^{-1}$$

Values obtained at 298 K were all 1.00 ± 0.02 cm^{-1} for the three cells used. Cell constants were checked periodically and any necessary corrections made.

Solutions for conductance measurement, usually about 5g. of material, were contained within glass tubes of appropriate size into which the immersion cells were introduced. The tubes were then flushed with dry nitrogen and sealed with parafilm coated in vaseline before locating in a Grant Instruments LE8 low temperature ethanol bath with, thermostat control to ± 0.02 K.

Time was allowed for proper electrode coating by the relatively viscous solutions (≃ ½ hour) and measurements were taken when meter readings had stabilized. Variable temperature experiments involved data aquisition on a cooling cycle of about 30 min. K^{-1}.

2.3 RESULTS AND DISCUSSION.

2.3.1 Conductance as a function of concentration at 298 K.

At concentrations above about 0.5 molkg^{-1} (i.e above a Li/EO ratio of 1/50), it is well established[18] that the specific conductance (σ) of salts such as $LiCF_3SO_3$, $LiClO_4$, and $LiAsF_6$ in high mol.wt. PEO rises with increasing electrolyte concentration to form a relatively flat maximum at a Li / EO ratio of about 1 / 12, and thereafter falls quite rapidly as the concentration is increased still further. Such behaviour at high salt concentration is unexceptional and well known in conventional aprotic electrolyte solutions, based on, for example, propylene carbonate[59]. The explanation generally accepted for the fall in the conductance after the maximum is that it is due to the significant rise in solution viscosity (hence decrease in carrier mobilty) with electrolyte concentration, a phenonemon exaggerated in polymer solvents where the electrolyte can act as a form of transient crosslinking agent. Such maxima were found for the solutions studied here but are not considered further since the observed conductance response at and beyond the maximun reflects the first order effect of changing viscosity upon the carrier mobility. In contrast, it has been shown by several authors, including

Hall[25], and Ingram[60], that below about 0.1 mol dm^{-3} oligomer electrolyte solutions of the type used here show essentially no viscosity changes with concentration. With this in mind, the conductance response in the concentration range of this study, (0.002 - 0.08)mol kg^{-1}, can be interpreted in terms of carrier number and type and not as due to viscosity effects.

The conductance behaviour of $LiClO_4$ and $LiCF_3SO_3$ solutions at lower values of concentration is shown in Fig. 2.5., which is a plot of the molal conductance Λ / $Scm^{-1}mol^{-1}kg$ versus concentration. Both sets of data are similar in profile with a sharp decrease in Λ at lower concentrations, a conduction minimum at about 0.025 mol kg^{-1}, and then an increasing Λ above this value.

Measurements of molal conductances at low to medium concentrations generally reveal two classes of behaviour[32]:

(1) Strong Electrolyte Behaviour; is shown where molal conductances depend only weakly on the solute concentration i.e KCl in water, where the electrolyte is considered to be completely dissociated. The molal conductance is found to remain relatively close to Λ_o, the molal conductance at infinite dilution, since the only influence of increasing the concentration is the effect of the ionic atmospheres on the mean ionic velocity. This factor would normally give rise to a reduction of no more than ten per cent for a 0.01 $molkg^{-1}$ solution.

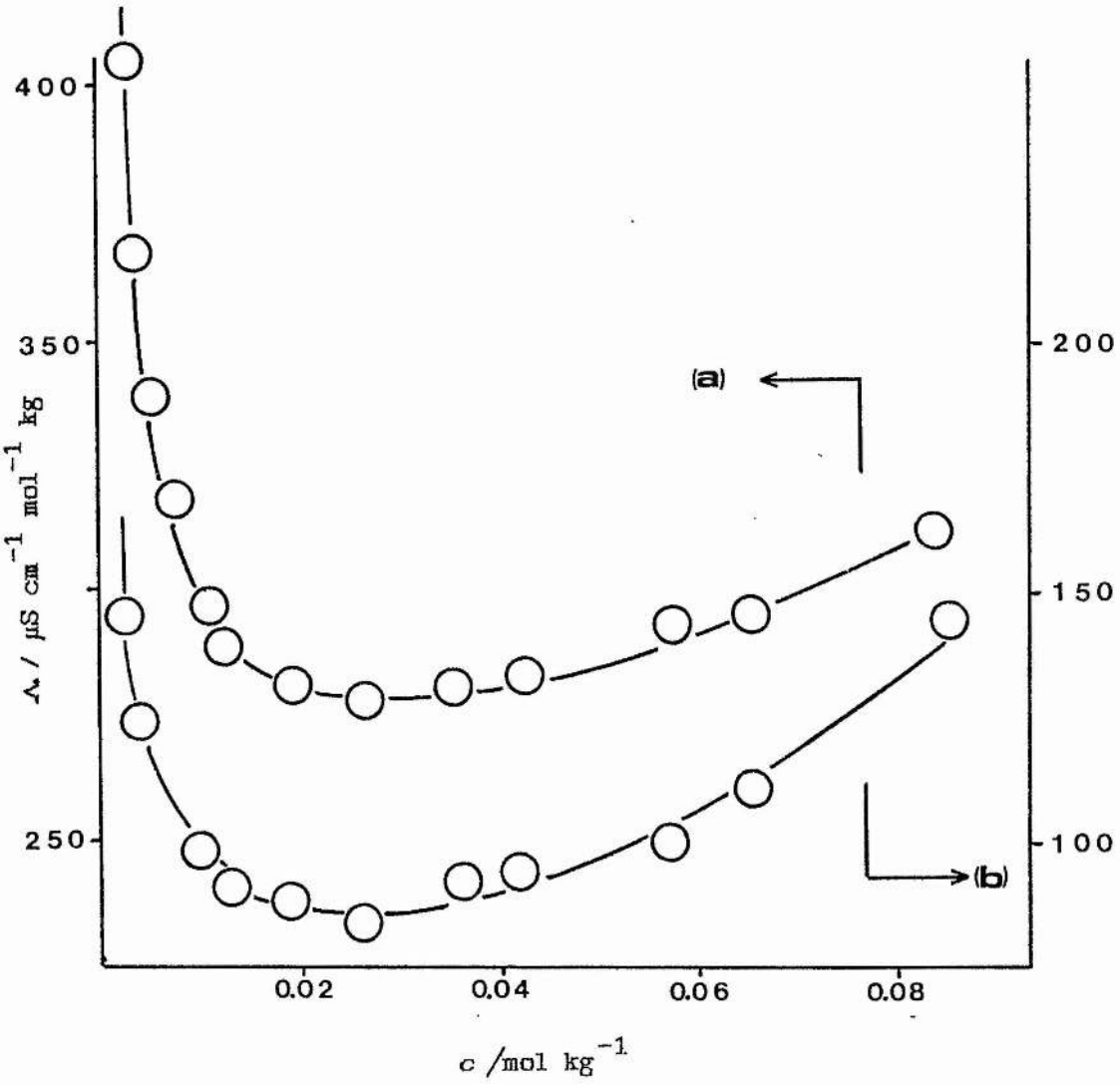

Fig. 2.5. Molal conductance as a function of concentration for (a) $LiClO_4$ and (b) $LiCF_3SO_3$ in PEO(400)e at 298 K.

(2) Weak Electrolyte Behaviour; features a steep monotonic fall in the molal conductance with concentration i.e KI in acetone[61], and is due to an incompletely dissociated electrolyte, which is usually interpreted as an equilibrium $MA \rightleftharpoons M^{+} + A^{-}$, where a decreasing degree of dissociation with concentration reduces the number of charge carriers and hence the conductance.

Conduction minima do not occur in either of the above cases.

Although the initial behaviour observed here at lower concentrations is consistent with the weak electrolyte case, it does not explain the overall behaviour, featuring a conduction minimum and increasing Λ with higher concentration. This type of behaviour is similar to that noted for solutions of very low dielectric constant where ionic association into larger groupings such as triplets, quadruplets, and higher aggregates is thought to occur as the concentration of the electrolyte is increased. Formation of triple ion clusters was postulated as long ago as 1933 by Fuoss and Kraus[62] to explain comparable conductance minima in dioxane - water solutions of tetraisoamylammonium nitrate. More recently, similar behaviour has been reported by Petrucci and co - workers for $LiClO_4$ and $LiAsF_6$ in tetrahydrofuran, 1,2 - dimethoxymethane, and 1,3 - dioxolane[63,64,65].

2.3.1.1 Theory and equations for triple ion formation.

The thermodynamics of higher association have been the subject of many treatments and that it is to be expected in low dielectric constant media can readily be shown by simple arguement. If the parameter $b = e^2/\mathring{a}\epsilon kT$ (where $\mathring{a}$ is separation between ionic centres and ϵ is the dielectric constant of the medium) is defined as a measure of the ratio of the electrostatic potential energy of two ions in contact to the average thermal energy of a solvent molecule[62], then in round numbers at 298 K, $b = 100/\epsilon$ for $\mathring{a} = 5.60$ Å. In water ($\epsilon \simeq 78.5$), formamide ($\epsilon \simeq 109.5$), or in other solvents of high dielectric constant, b is about one or two; that is, a pair of ions in contact represents a configuration which is not very stable thermally. At $\epsilon \simeq 20$, $b \simeq 5$ and the dissociation energy of a pair is about 12.5 $kJmol^{-1}$; therefore considerable association to pairs would be expected in such solvents. Now an ion pair, while electrically neutral, still possesses a dipole field, and as a dipole is attracted by either anions or cations. The potential energy of a cation for example, in contact with the anion of a pair, would have the usual Coulomb value of $e^2 / 2\mathring{a}\epsilon$ and so configurations of three ions would be expected to become thermally stable below $\epsilon = 20$ i.e well within the range of a polyether host.

In the concentration range of this study, (0.002 - 0.08) mol kg^{-1}, it is assumed that the majority of the electrolyte is present as non - conducting ion pairs, LiX (X = $CF_3SO_3^-$, ClO_4^-), and that some of these dissociate according to the dynamic equilibria:

$$\underset{(1-\alpha_s)c}{LiX} \rightleftharpoons \underset{\alpha_s c}{Li^+} + \underset{\alpha_s c}{X^-} \qquad (2.3)$$

and

$$\underset{(1-3\alpha_t)c}{LiX} \rightleftharpoons \underset{\alpha_t c}{{}^1/_3Li_2X^+} + \underset{\alpha_t c}{{}^1/_3LiX_2^-} \qquad (2.4)$$

Following Fuoss and Accascina[66], the relevant equations are now stated as :

$$Li^+ + X^- \overset{K_s}{\rightleftharpoons} LiX \qquad (2.5)$$

and

$$LiX + Li^+ \overset{K_t^1}{\rightleftharpoons} Li_2X^+ \qquad (2.6)$$

$$LiX + X^- \overset{K_t^2}{\rightleftharpoons} LiX_2^- \qquad (2.7)$$

Where K_s and K_t are the respective single and triple ion equilibrium constants.

To simplify the algebra it is assumed that $K_t^1 \simeq K_t^2$ and define α_s and α_t as the fraction of solute existing as simple ions and triple ion complexes respectively. Hence from equations (2.3) - (2.7) :

$$K_s = (1 - \alpha_s)/\alpha_s^2 c \qquad (2.8)$$

solving for α_s

$$K_s \alpha_s^2 c + \alpha_s - 1 = 0 \qquad (2.9)$$

equation (2.9) is quadratic i.e of the type :

$$ax^2 + bx + c = 0$$

with solutions

$$x = \{ -b \pm (b^2 - 4ac)^{1/2}) / 2a$$

in this work $x = \alpha_s$ in equation (2.9) and

$$\alpha_s = (-1 + (1 + 4K_s c)^{1/2})/2K_s c \qquad (2.10)$$

using (2.3) - (2.7) to obtain K_t

$$K_t = \alpha_t / \alpha_s c (1 - \alpha_s - 3\alpha_t) \qquad (2.11)$$

solving for α_t

$$\alpha_t = (K_t \alpha_s c (1 - \alpha_s)) / (1 + 3K_t \alpha_s c) \qquad (2.12)$$

In the absence of ion atmosphere retardation, the conductance of the system can be considered to be due to the separate contributions from the various ionic types, in this case singles and triples i.e

$$\Lambda = \alpha_s \Lambda_o^s + \alpha_t \Lambda_o^t \qquad (2.13)$$

Where $\alpha_s \Lambda_o^s$ and $\alpha_t \Lambda_o^t$ are the respective single and triple ion terms. Λ_o^s is the limiting molal conductance of the free ions and Λ_o^t represents that of the hypothetical electrolyte $Li_2X^+ LiX_2^-$. When α_s and α_t are small (because the ionic concentration is by hypothesis small), equation (2.13) simplifies to

$$\Lambda = \Lambda_o^s / K_s^{½} c^{½} + \Lambda_o^t K_t c^{½} / K_s^{½} \qquad (2.14)$$

which is of the form

$$\Lambda = Ac^{-½} + Bc^{½} \qquad (2.15)$$

If the salt concentration is very small then $\Lambda = Ac^{-1/2}$ and a plot of log Λ vs. log c should approach linearity with slope equal to -½. There is ample experimental evidence to support this conclusion[67,68,69,70]. As concentration increases, the $Bc^{1/2}$ term begins to be significant; since Λ is thus the sum of two functions, one of which decreases with concentration, one which increases, we therefore expect Λ as a function of concentration to go through a minimum. This is what is observed here.

A convenient form for comparing (2.15) with experimental data is obtained by multiplication with $c^{1/2}$ to give :

$$\Lambda c^{\frac{1}{2}} = A + Bc \qquad (2.16)$$

according to which the observed quantity $\Lambda c^{\frac{1}{2}}$ is linear in concentration with slope B ($= \Lambda_o^t K_t / K_s^{\frac{1}{2}}$) and intercept A ($= \Lambda_o^s / K_s^{\frac{1}{2}}$). Such plots are shown in Fig. 2.6. for the two salts studied in the present investigation and are seen to be essentially linear. The curvature at low concentrations for $LiClO_4$ solutions is likely to arise from failure to include mobility corrections[64].

2.3.1.2 Evaluation of K_s and K_t.

Having obtained the A and B terms from the data (by least squares analysis) it is still nec essary to know the limiting molal conductance of the salt (Λ_o^s) and the hypothetical electrolyte $Li_2X^+LiX_2^-$ (Λ_o^t). In many conductimetric studies, it is usually possible to obtain the former by combining values for the limiting conductances of electrolytes which do not associate. Such a procedure is not possible however for solvents with lower values of dielectric constant, such as in this study, where ionic association occurs. Rather, use may be made of Waldens rule[92] (derivable from Stokes' law) which states that, for a given salt with change of solvent:

$$(\Lambda_o \eta)_{\text{solvent1}} = (\Lambda_o \eta)_{\text{solvent 2}} \qquad (2.17)$$

where η is the viscosity of the pure solvent. This relation may be applied with reasonable confidence in aprotic solvents and serves the purpose here.

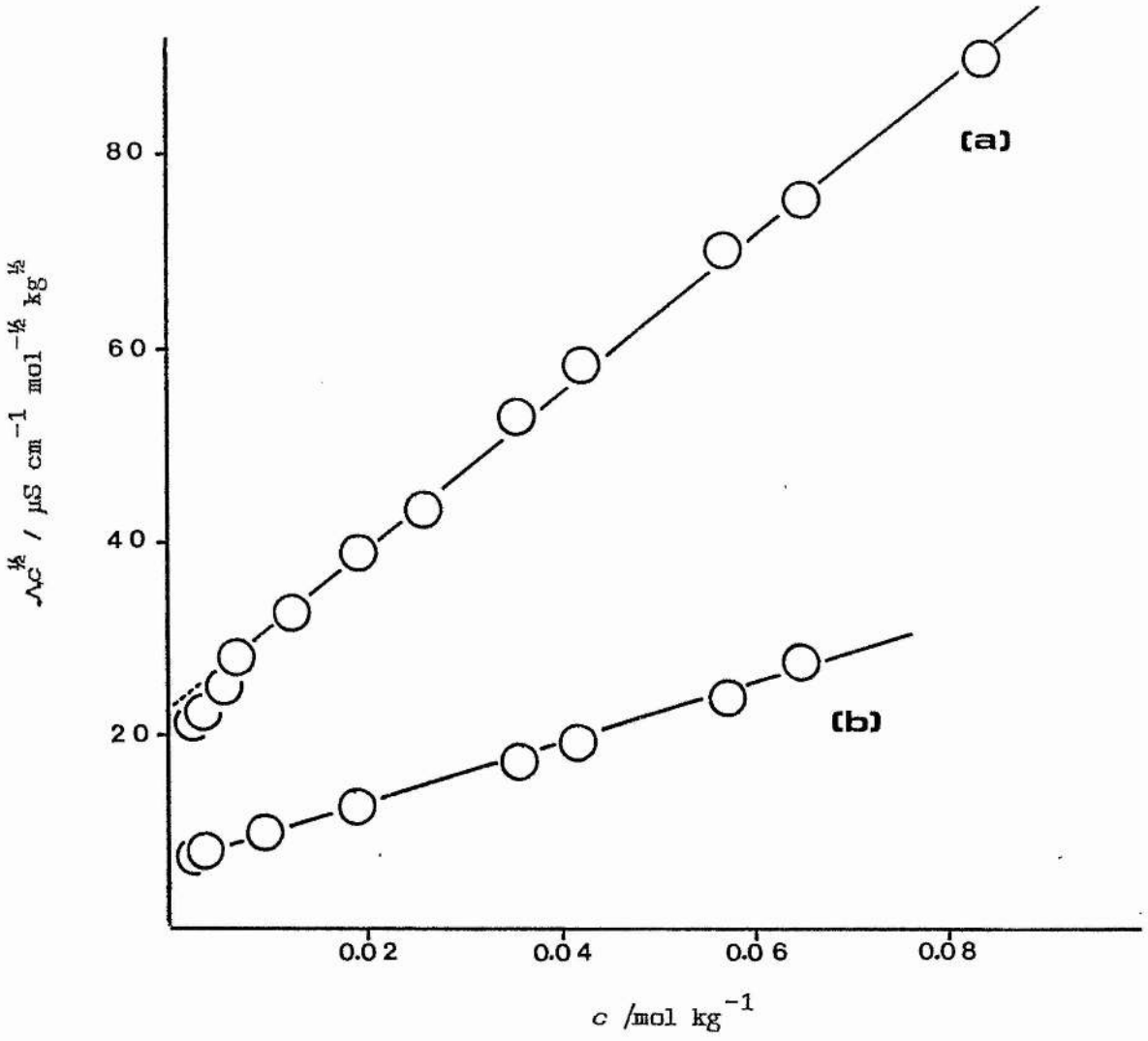

Fig. 2.6. Plot of $\Lambda c^{½}$ vs. c for (a) $LiClO_4$ and (b) $LiCF_3SO_3$ in PEO(400)e at 298 K.

Limiting molal conductance and viscosity data are available for $LiClO_4$ in several solvents[64,71,72] and are shown in Table 2.1.

Solvent	Λ_o (Scm^2mol^{-1})	$10^3\,\eta$ (P)	$\Lambda_o\eta$ ($Scm^2P\ mol^{-1}$)
†1,2 - DME	149[64]	4.13[71]	0.615
1,3 - DXL	104[64]	5.89[71]	0.612
N,N - DMF	77.4[72]	7.96[72]	0.616

Table 2.1. Walden product data for $LiClO_4$ at 298 K.

†1,2 - DME = 1,2 - Dimethoxyethane, 1,3 - DXL = 1,3 - Dioxolane, *N,N* - DMF = *N,N* - Dimethylformamide.

The data were used to calculate a Walden product for each solvent and thus obtain a mean value of $\Lambda_o\eta$ = 0.614 Scm^2Pmol^{-1}. The viscosity and density of PEO(400)e at 298 K are known[73] to be η = 45.9 cP and ρ = 1.121 g cm^{-3} hence, applying equation (2.17) :

$$\Lambda_o(LiClO_4)_{PEO(400)e} = (\Lambda_o\eta)_{mean} / \eta_{PEO(400)e} \qquad (2.18)$$

$$= 1.338 \quad Scm^2mol^{-1}$$

or, multiplying by $\rho_{PEO(400)e}$

$$= 1.50 \times 10^{-3} \quad Scm^{-1}molkg^{-1}$$

There are insufficient data available to allow a similar calculation to be made for $LiCF_3SO_3$ but an estimate may be made by noting that:

$$\Lambda_o(LiClO_4) = \lambda_o(Li^+) + \lambda_o(ClO_4^-) \quad (2.19)$$

and

$$\Lambda_o(LiCF_3SO_3) = \lambda_o(Li^+) + \lambda_o(CF_3SO_3^-)$$

(Kohlrauschs' law of the independent migration of ions) where, for $LiClO_4$ in DMF, $\lambda_o(Li^+)$ and $\lambda_o(ClO_4^-)$ are known to be 25.0 $Scm^2\ mol^{-1}$ and 52.4 Scm^2mol^{-1} respectively[72]. For ClO_4^- the Van der Waals volume has been shown to be 0.0426 $(nm)^3$ while that for $CF_3SO_3^-$ is 0.0643 $(nm)^3$ (ref. 74). Since specific anion solvation effects are absent in systems of this sort[40], it may be assumed that anion mobility is inversely proportional to ionic volume. It follows that[75], using the DMF data:

$$\lambda_o(CF_3SO_3^-) = \lambda_o(ClO_4^-) \times (0.0426 / 0.0643)$$

$$= 34.9\ Scm^2mol^{-1} \quad \text{(in DMF)}$$

thus

$$\Lambda_o(LiCF_3SO_3) = 25.0 + 34.9$$

$$= 59.9\ Scm^2mol^{-1}$$

and, applying the Walden product rule,

$$\Lambda_o(LiCF_3SO_3) = 1.16 \times 10^{-3} \quad Scm^{-1}mol^{-1}kg$$

for PEO(400)e

The estimates for the limiting molal conductances for the two salts in PEO(400)e permits the respective K_s values to be determined from the intercepts of the plots in Fig. 2.6. i.e for $LiClO_4$:

$$\text{Intercept A} = 2.23 \times 10^{-5} \quad Scm^{-1}mol^{-\frac{1}{2}}kg^{\frac{1}{2}}$$

$$= \Lambda_o^s / K_s^{\frac{1}{2}}$$

$$\therefore \quad K_s = (1.50 \times 10^{-3} / 2.23 \times 10^{-5})^2$$

$$= 4.52 \times 10^3 \quad mol^{-1}kg$$

The same calculation for $LiCF_3SO_3$ (Intercept = 6.51 $\mu Scm^{-1}mol^{-1/2}kg^{1/2}$) yields :

$$K_s = 3.18 \times 10^4 \quad mol^{-1}kg$$

In order to obtain K_t for both salts it is necessary in addition to know Λ_o^t, or the ratio $\Lambda_o^t / \Lambda_o^s$. Fuoss[76] predicted that $\Lambda_o^t / \Lambda_o^s$ could be determined from the temperature coefficient of conductance over a wide temperature range. Unfortunately only one such system has been studied[77],

and the lack of experimental knowledge forces an estimation of the above ratio in some arbitrary way. Fuoss and Krauss[62] initially assumed that:

$$\Lambda_o^t \; / \; \Lambda_o^s \quad = \quad 1 \; / \; 3$$

but at a later stage they and other workers (e.g Boileau and Hemery[78]) recognised this as an underestimate and settled for a ratio of 2 / 3. In practice, this factor is not important in the present calculations, and the latter value is selected. As for K_s determination:

for $LiClO_4$

$$\text{Gradient B} \quad = \quad 8.18 \quad \times \quad 10^{-4} \; \text{Scm}^{-1}\text{mol}^{-3/2} \quad \text{kg}^{3/2}$$

$$= \quad \Lambda_o^t \, K_t / \, K_s^{½} \quad = \quad 2 \, \Lambda_o^s \, K_t \; / \; 3 \, K_s^{½}$$

$$\therefore \quad K_t \quad = \quad (\, 8.18 \times 10^{-4} \times 3 \times (4.52 \times 10^{3})^{½}) / (2 \times 1.50 \times \bar{10}^{3} \,)$$

$$= \quad 55 \quad \text{mol}^{-1}\text{kg}$$

for $LiCF_3SO_3$

$$\text{Gradient B} \quad = \quad 3.12 \quad \times \quad 10^{-4} \; \text{Scm}^{-1}\text{mol}^{-3/2} \; \text{kg}^{3/2}$$

$$\therefore \quad K_t \quad = \quad 72 \qquad \text{mol kg}^{-1}$$

2.3.1.3 Implications of the results with respect to polymer electrolytes.

In Table 2.2. the implications of the K_s and K_t values found in this study are illustrated by using equations (2.10) and (2.12) to calculate the percentage of the salt present as free ions, pairs, and triples over a range of concentrations, including values above and below those used in the experimental measurements. Table 2.2. certainly overemphasises the concentration of triples since higher association is not considered but the important point here is that the concentration of simple ions is small (and decreasing), and above a total salt concentration of about 0.01 mol dm^{-3}, the majority of the current is carried by triple ions.

Table 2.2. Calculated % of salt present as free ions, ion pairs, and triple ions. (Data within the area enclosed by ..... apply to the experimental conditions used in this work.)

c (mol kg^{-1})	% Ions	% Pairs	% Triples
2×10^{-4}	32	67	1
5×10^{-4}	22	76	2
1×10^{-3}	16	81	3
.....	.....	.....	.....
2×10^{-3}	12	84	4
5×10^{-3}	8	85	7
1×10^{-2}	5	85	10
2×10^{-2}	4	82	14
5×10^{-2}	2	77	21
.....	.....	.....	.....
0.1	2	71	27
0.2	1	64	35
0.5	1	54	46

(a) $LiCF_3SO_3$; $K_s = 3.18 \times 10^4$ kg mol^{-1}, $K_t = 72$ kg mol^{-1}.

Contd /.

Table 2.2. / Cont^{d}. Calculated % of salt present as free ions, ion pairs, and triple ions. (Data within the area enclosed by ..... apply to the experimental conditions used in this work.)

c (mol kg^{-1})	% Ions	% Pairs	% Triples
2×10^{-4}	63	36	1
5×10^{-4}	48	50	2
1×10^{-3}	37	59	4
.....	.....	.....	.....
2×10^{-3}	28	66	6
5×10^{-3}	19	70	11
1×10^{-2}	14	70	16
2×10^{-2}	10	68	22
5×10^{-2}	7	61	32
.....	.....	.....	.....
0.1	5	54	41
0.2	3	47	50
0.5	2	36	62

(b) $LiClO_4$; $K_s = 4.52 \times 10^3$ kg mol^{-1}, $K_t = 55$ kg mol^{-1}.

Comparison of the K_s and K_t values with those for low mol.wt. solvents of low dielectric constant is interesting, and is shown in Table 2.3. The smaller K_s and larger K_t values for PEO(400)e confirm, as one would expect, the higher stability of both the free ions and triples with respect to pairs upon changing from a monodentate ligand (i.e DMF, DXL, TMF) to the multidentate material used in this study. This is a well known phenonemon[79] where solvation by the multidentate ligand is always accompanied by restriction of translation of fewer molecules than when compared with solvation by mondentate ligands.

The most important point though, is that ionic association *does* occur in polyether electrolytes and that at the levels of salt generally incorporated in polymer electrolytes (up to about two molar), the concentration of single ions is very small, where the charged species responsible for the conductivity are triple and higher ionic aggregates.

Salt	Solvent	K_s (kg mol^{-1})	K_t (kg mol^{-1})
$LiCF_3SO_3$*	PEO(400)e	3.18×10^4	72
$LiClO_4$*	PEO(400)e	4.52×10^3	55
$LiClO_4$[63]	THF	4.8×10^7	76
$LiClO_4$[64]	DME	4.6×10^7	20
$LiClO_4$[64]	DXL	2.3×10^7	34
$LiAsF_6$[63]	DME	1.0×10^7	28

Table 2.3. K_s and K_t data for some lithium salts at 298 K.

*This work.

2.3.2 Conductance as a function of temperature.

2.3.2.1 Variation of the specific conductance, σ, with temperature.

For all polymer electrolyte systems, the temperature dependence of the conductance is one of the most useful areas of study. It has been outlined in the introduction to this thesis that for most high mol. wt. polyethylene oxide - inorganic salt systems, the behaviour of the conductance as a function of temperature may be classified according to one of three types, based upon the occurrence or co - occurrence of Arrhenius or non - Arrhenius behaviour. The latter is usually interpreted according to one of the quasi - thermodynamic theories, based upon free - volume or configurational entropy considerations.

That for either case the observed behaviour is real must be tempered by the knowledge that the amount of elastomeric material (i.e the conducting phase) and the number of charge carriers are temperature dependent properties of such systems, as noted by Berthier[23] and discussed here in chapters 4 and 5. (Certainly, with the theoretical understanding of these relatively new electrolyte materials admittedly at an early stage[35], the danger of inferring conduction mechanisms from the shapes of σ vs. T. plots with existing theories has been recognised[80].)

However, more recent work involving homogenous electrolyte materials where to a large extent the above phase / carrier problems are avoided, have in the main shown non - Arrhenius conductance behaviour, and have been interpreted in terms of free - volume or configurational entropy models. Materials used have included polypropylene oxide (PPO) - based electrolytes[18], cross - linked networks[34], and comb - branched systems[33]. In particular, the pressure dependence of conductance in PEO and PPO systems[31,32] has suggested the configurational entropy model for polymer electrolytes, and this is now favoured by several authors including Ratner[35], Cowie[33], and especially Angell[34,35]

In this study, the temperature dependence of the specific conductance, σ, was monitored on a cooling cycle, (298 - 280)K, at several concentrations in the range (0.003 - 0.055) mol kg^{-1} for the salts $LiCF_3SO_3$ and $LiClO_4$ in PEO(400)e. In each case, curvature was observed for ln σ vs. 1/T Arrhenius plots. A typical example is shown in Fig.2.7. for $LiCF_3SO_3$ (29.6×10^{-3} $molkg^{-1}$) where the dashed straight line serves only as an aid in viewing the curvature. The increasing temperature dependence of the conductance with decreasing temperature is consistent with the studies quoted above[25,33,34,81] and other media, including the fused salts[36].

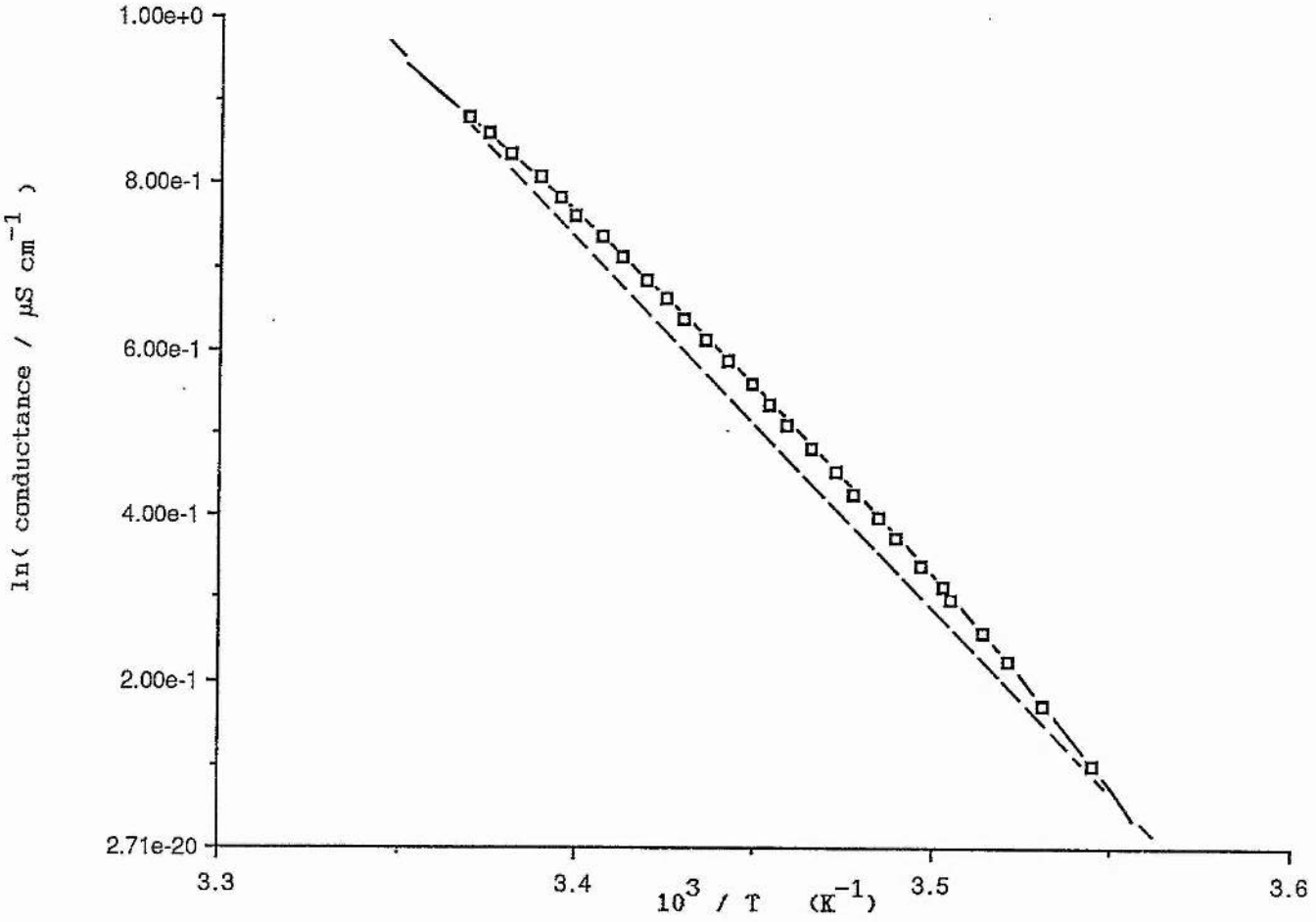

Fig. 2.7. Arrhenius plot of $\ln(\sigma)$ vs. 1/T for $LiCF_3SO_3$ in PEO(400)e (c = 0.0296 mol kg^{-1}).

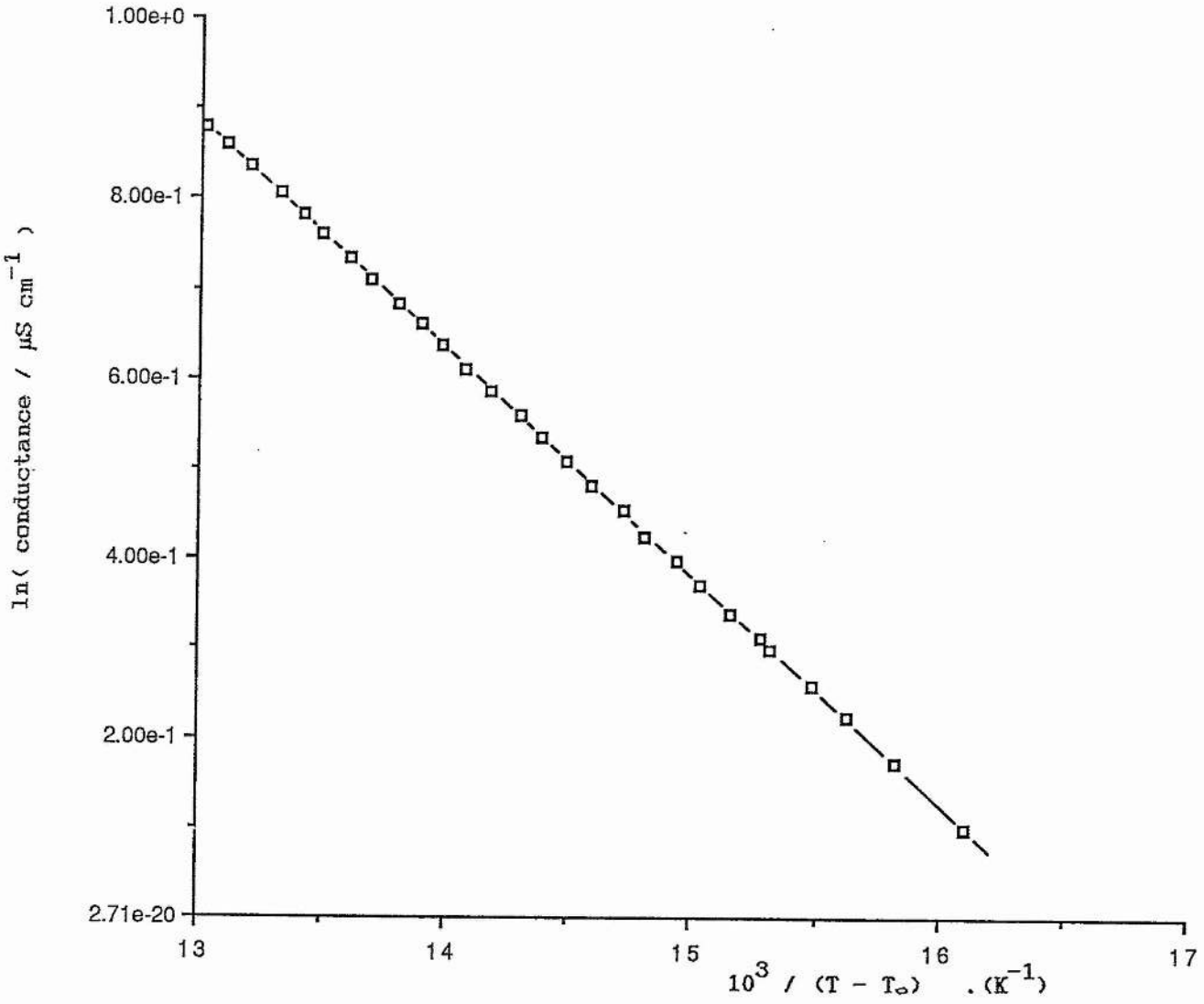

Fig. 2.8. VTF plot of $\ln(\sigma)$ vs. $1/(T - T_o)$ for $LiCF_3SO_3$ in PEO(400)e. (T_o = 220 K, c = 0.0296 mol kg^{-1}).

Data at each concentration in the range were linearised (see Fig. 2.8. for example) by application of the Vogel - Tamman - Fulcher (VTF) equation[1]:

$$\sigma T^{\frac{1}{2}} = A \exp \{ - Ea / R(T - T_o) \} \qquad (2.20)$$

where A is proportional to the number of charge carriers, Ea is a constant and to preclude arguement, T_o may be regarded either as a fitting parameter, or a physically significant term as in the case of the configurational entropy model where it represents the thermodynamic limiting glass transition temperature, as defined by Gibbs and Di Marzio[87].

Initially, the conductance vs. temperature data for the $LiCF_3SO_3$ and $LiClO_4$ solutions were analysed by two commercially available regression analysis packages, both running in the Fortran language on a Vax mainframe computer.

'Minitab', the first program, involved choosing an initial estimate for the T_o parameter (200 K say) and then incrementing this value while monitoring a statistical analysis parameter known as the 'residual sum of squares', RSS[88], for the data fit (to the VTF form) at each T_o value. When the RSS term was at a minimum value then the best - fit T_o region was located. The second regression analysis package 'Genstat' automatically gave a best - fit T_o value for the input σ vs. T data, as well as the standard error (SE) in the fit i.e $T_o = T_o \pm SE$.

Although slightly different in application, both regression analysis programs gave similar results, fitting all σ vs. T data with T_o in the region of 220 K (SE < 4 K and usually < 2 K) with no apparent trend in the resultant T_o values. (Genstat, for example, gave T_o = 220.37 K with standard error 1.69 K, for the data shown in Fig. 2.8.)

Since variance in the fitted T_o parameter would alter the obtained Ea values, it was decided to constrain T_o to 220 K for all the solutions studied, and derive Ea values by least squares analysis. (It may be argued that there is no real criterion for this procedure. It will be shown in chapter 3 however that a temperature in the region of 220 K (i.e the T_o value used in the conductance study) does mark the onset of the oligomer chain motion in these systems.) The Ea values obtained, with T_o = 220 K, are given in Table. 2.4. and show a constant Ea term of $\simeq$ 2 kJ mol^{-1} over the entire concentration range for both salts. (Variance at lower concentrations are likely to be a result of increased scatter in measured conductance values which, especially for $LiCF_3SO_3$, approached the limits of conductance bridge measurement ($\geq 10^{-8}$ S cm^{-1})).

The constant Ea term may seem surprising if it is considered that the number of charge carriers, and carrier type, are changing with concentration for both salts, as was shown in the previous section, and points to the role of the polymer as a determining factor in the ionic motion.

c / 10^3 mol kg^{-1}	Ea / kJ mol^{-1}	c / 10^3 mol kg^{-1}	Ea / kJ mol^{-1}
2.7	2.3	6.0	1.9
4.7	2.3	10.2	2.0
6.9	2.2	14.2	2.1
10.1	2.1	18.2	2.1
13.1	2.1	22.3	2.1
20.0	2.1	27.2	2.1
29.7	2.1	34.8	2.1
35.0	2.1	43.6	2.1
42.7	2.1	54	2.1
(a) PEO(400)e.$LiCF_3SO_3$		(b) PEO(400)e.$LiClO_4$	

Table 2.4. Ea terms obtained by least squares analysis of ln σ vs. $10^3/(T - T_o)$ data (i.e the VTF form above (2.20)), using T_o = 220K, for (a) $LiCF_3SO_3$ and (b) $LiClO_4$ in PEO(400)e.

2.3.2.2 Generation of $\Lambda c^{\frac{1}{2}}$ isotherms; K_t variation with temperature.

In 2.3.1, K_s and K_t data were evaluated at 298 K for $LiCF_3SO_3$ and $LiClO_4$ in PEO(400)e, where molal conductances were monitored against concentration in the range (0.002 - 0.08) mol kg^{-1} . In principle, with temperature as an added variable, the thermal dependence of the parameters K_s and K_t could also be monitored, yielding equilibrium constants for the equilibria previously identified. In a broader sense, the study of ion pair dissociation constants vs. temperature has been one of the main methods in determining the enthalpy changes in the process[89] but such studies have usually been applied only to the well characterised aqueous systems. An important study by Denison and Ramsey[90] on various perchlorates in ethylene chloride is a notable exception however.

For the systems studied here with the electrochemical technique, the evaluation of heats of association for the ion pair process would require knowledge of limiting molal conductance values (i.e Λ_o^s) with temperature, representing a major piece of work. The evaluation of K_t with temperature however, yielding information on the triple ion formation process, would require only the assumptions made in the previous section, and measurement of the conductance as a function of concentration and temperature. Then, as before, determination of slope

and intercept of $\Lambda c^{½}$ vs. c plots would yield K_t values over a range of temperatures. Such three - dimensional data ($\Lambda = f(c,T)$) were obtained for both salts in PEO(400)e in the concentration range (0.003 - 0.06) mol kg^{-1} and temperature range (298 - 283)K.

It was immediately apparent from the data that whereas no variation was observed for the $LiClO_4$ solutions, the $LiCF_3SO_3$ data exhibited a monotonic shift in the conduction minimum, to lower concentration values with decreasing temperature i.e ≃ (0.025 → 0.013) mol kg^{-1} for (298 → 283)K. If it is remembered that:

$$\Lambda = A\, c^{-1/2} + B\, c^{1/2} \qquad (2.15)$$

then the position of the conduction minimum may be obtained by differentiation with respect to c and setting $d\Lambda / dc = 0$ i.e

$$d\Lambda / dc = d(A\, c^{-1/2} + B\, c^{1/2}) / dc \qquad (2.21)$$

$$= -½\, A\, c_{min}^{-3/2} + ½\, B\, c_{min}^{-1/2} \qquad (2.22)$$

and, when $d\Lambda / dc = 0$

$$\rightarrow \quad A\, c_{min}^{-3/2} = B\, c_{min}^{-1/2} \qquad (2.23)$$

thus

$$A = B\, c_{min} \qquad (2.24)$$

predicting that if the minimum shifts then the ratio A / B (= intercept / gradient, $\Lambda c^{1/2}$ vs. c plot) and hence K_t changes. This is what was observed when, at 1K intervals, $LiCF_3SO_3$ $\Lambda c^{1/2}$ vs. c isotherms were plotted and K_t values obtained at each temperature. For clarity only some representative data are shown for both the salts studied (Fig. 2.9.); all K_t values obtained for both salts in PEO(400)e, are given in Table .2.5.

K_t for $LiCF_3SO_3$ is observed to increase monotonically with decreasing temperature, suggesting more association to triples at lower temperatures, whereas $LiClO_4$ values are invariant (no minimum shift was observed).

These values refer to the equilibrium $A + AB \rightleftharpoons A_2B$ for the formation of either triple ion type, as was outlined in 2.3.1.1. The enthalpy change for the process may be determined by application of the Van't Hoff isochore[32]:

$$d(\ln K) / dT = \Delta H^{\ominus} / RT^2 \qquad (2.25)$$

and recognising that

$$(d/dT)\ (1/T) = -1/T^2 \qquad (\text{or } dT/T^2 = -d(1/T))$$

thus

$$d \ln K / d(1/T) = -\Delta H^{\ominus} / R \qquad (2.26)$$

where R is the gas constant, 8.314 $J\,mol^{-1}\,K^{-1}$.

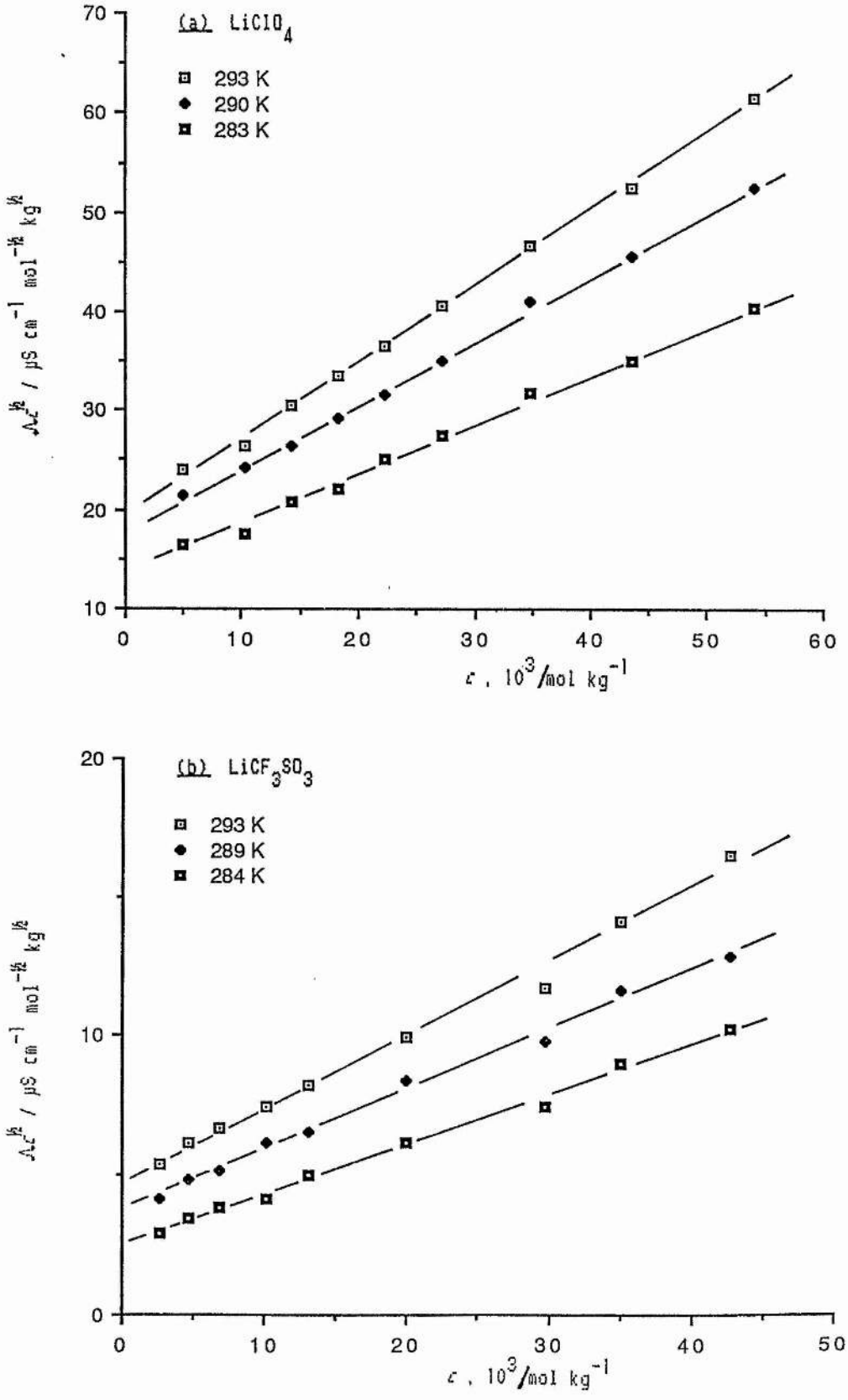

Fig. 2.9. $\Lambda c^{1/2}$ vs. c isotherms for (a) $LiClO_4$ and (b) $LiCF_3SO_3$ in PEO(400)e.

T / K.	$LiCF_3SO_3$; K_t (kg mol^{-1})	$LiClO_4$; K_t (kg mol^{-1})
298	72	55
296	75	56
295	77	57
294	79	56
293	82	56
292	84	57
291	85	57
290	89	56
289	91	55
288	94	56
287	97	56
286	99	56
285	104	57
284	107	57
283	114	58

Table 2.5. K_t data as a function of temperature for $LiCF_3SO_3$ and $LiClO_4$ in PEO(400)e.

It follows that a plot of ln K_t vs. 1/T should yield a straight line, slope $-\Delta H^{\ominus} / R$, from which $\Delta H^{\ominus}$ is obtained.

Such a plot is shown in Fig. 2.10 for the $LiCF_3SO_3$ data over the temperature range (298 - 280)K. Least squares analysis yields:

$$\text{gradient} = 2393.5\ K = -\Delta H^{\ominus} / R$$

$$\therefore \quad \Delta H^{\ominus} = -19.9\ kJ\ mol^{-1}$$

indicating that triple ion formation for $LiCF_3SO_3$ in PEO(400)e is an exthothermic process.

The $LiClO_4$ data are observed to be essentially invariant over the temperature range, implying an enthalpy change $\Delta H^{\ominus} \simeq 0$ kJ mol^{-1} for the process. Unfortunately, there is a complete lack of information available with which to compare the data obtained here. Petrucci[65] however, did determine K_t values for $LiClO_4$ in tetrahydrofuran at three temperatures i.e

$$298K, \quad K_t = 76.5\ kg\ mol^{-1}$$

$$258K, \quad = 69.5\ kg\ mol^{-1}$$

$$243K, \quad = 66.0\ kg\ mol^{-1}$$

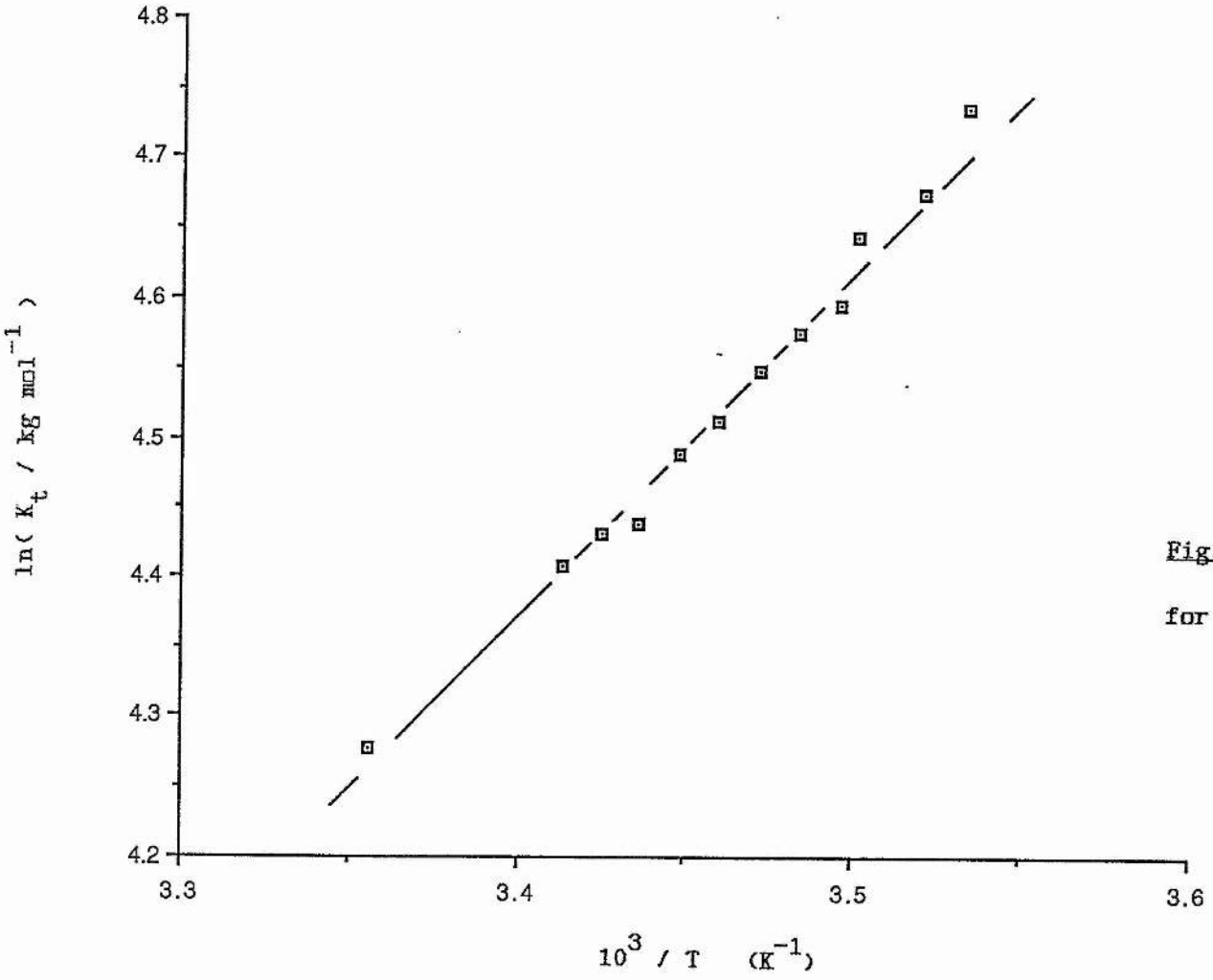

Fig. 2.10. $\ln(K_t)$ vs. 1/T for $LiCF_3SO_3$ in PEO(400)e.

A Van't Hoff plot for this limited data yields $\Delta H^{\ominus} \simeq 1.9$ kJ mol^{-1}, which is considered to be in reasonable agreement with the PEO(400)e.$LiClO_4$ value determined here. This is perhaps reassuring since it would be expected that the heats involved in bond making and breaking for ion - solvent interactions, and for ion - ion interactions (as well as those for the ion pair) to be similar for a given salt with change to a solvent of similar donor properties.

Chapter 3

3 NUCLEAR MAGNETIC RESONANCE STUDIES ON LOW MOL. WT. PEO ANALOGUE SYSTEMS.

3.1 Introduction.

Nuclear magnetic resonance spectroscopy (nmr) is a branch of radiofrequency spectroscopy concerned with transitions between the spin states of different nuclear energy levels.

As a spectroscopic tool it is a well established and powerful technique which, by suitable choice of experimental method, can be used to probe molecular structure and dynamics. A further advantage of nmr methods is that they can be employed to study a wide range of motional frequencies using one basic technique for the same sample over a wide range of temperature and pressure in a non - destructive manner. This, coupled with the multi - nuclear capability of nmr, lends itself to the study of polymer electrolytes where knowledge of phase behaviour, dynamics, and environment, is crucial in their characterisation. Polyether electrolytes of the type PEO.MX, are suitable candidates for such a study and there have been a number of investigations using nmr methods.

Berthier and co - workers[22,23,41], in an important series of papers, studied extensively the phase behaviour of several polyether electrolyte materials, concentrating on PEO.$LiCF_3SO_3$, PEO.NaI, and to a lesser extent, PEO.$LiClO_4$. In the case of PEO.$LiCF_3SO_3$, evaluation of the parameter known as T_2, the spin - spin relaxation time (described in section 3.2) for the ^1H (polymer chain) and ^{19}F ($CF_3SO_3^-$) nuclei, allowed calculation of the fractions of crystalline to elastomeric components and the relative amounts of the salt therein, as a function of temperature. Good agreement was found between nmr and differential scanning calorimetry data, and the phase diagram based on both sets of data was used to analyse the conductivity of the system above 333 K.

From the results of these studies, Berthier presented evidence that the stoichiometry of the high melting temperature crystalline phase in these materials was not EO / M^+ = 4 / 1, as had been previously proposed, based on ideas of cation location within a four co - ordinate ether oxygen cage, but 3.5 / 1 for PEO.$LiCF_3SO_3$ and 3 / 1 for PEO.$LiClO_4$ and PEO.NaI. (This was qualified at a later stage by several workers including Hibma[91] (x - ray diffraction) and Linford *et al*[92] (energy dispersive x - ray analysis)).

Cheradame and Killis[4,32] have used nmr as an integral part of a multi - disciplinary investigation of PEO - based crosslinked networks, where, as one would suppose, the movements and the 'freezing' of both anions (ClO_4^- , $CF_3SO_3^-$) and cations (Li^+) were shown to follow closely the extent of segmental motion allowed in the polyether chain at all temperatures. These observations complimented others in proposing free volume as the basic parameter governing the transport properties of the electrolyte networks.

The sodium nucleus, ^{23}Na, is suitable for nmr study and as such Warboys[33] identified two sodium environments at room temperature in PEO_8NaSCN, which he believed corresponded to crystalline and amorphous phases. At higher temperatures, where only an elastomeric phase occurs, a single sodium environment was observed.

In many respects, it was to be an nmr technique known as pulsed field gradient (pfg) nmr[34] which began a new era in the investigation and characterisation of polymer electrolytes, by measuring the bulk diffusive properties of the mobile species therein. The power of this technique was illustrated in an elegant study by Bhattacharja *et al*[31]. Here, for the system $PEO_8LiCF_3SO_3$, pfg - nmr determined anion and cation diffusion coefficients, the associated transport number numbers (t_+,t_-), and the activation barrier for the respective ions. Subsequent application

of radiotracer techniques to polyether electrolyte systems[95], determining the same parameters, has yielded data in good agreement with that of pfg nmr.

In this and the following chapters, the results of a multi - nuclear nmr study, complimented by some conductivity and differential scanning calorimetry, are presented for both low mol. wt. and high mol. wt. polyether electrolyte systems.

3.2 Theory.

3.2.1 Nuclear spin and the applied field

This section outlines the basic theories and concepts of nmr with relevance to the study of polymer electrolyte systems. It is not intended to be comprehensive or far ranging, a function of standard texts, but give sufficient detail for understanding of the following results and discussion sections.

Many elements contain nuclei which possess a nuclear spin and therefore a spin angular momentum, $I\hbar$ (where I is the spin quantum number and $\hbar = h/2\pi$, h is Plancks constant). The spinning motion of the charged nucleus acts like a circular current and so generates a magnetic field with an associated magnetic dipole moment μ. These two vector quantities are related by[96] :

$$\vec{\mu} = \gamma . I\hbar \qquad (3.1)$$

where γ is the magnetogyric ratio, a characteristic function of a given nucleus. The component of the spin angular momentum in an arbitrary direction, the z - direction for example, will be $I_z\hbar$ and will take values given by the magnetic quantum number, m, which can have (2I + 1) values from -I to I in integer steps.

In the presence of an applied magnetic field, B_o, a magnetic dipole will process around this field, in a manner similar to that of a gyroscope in the earths gravitational field, and will have a non - degenerate set of energy levels, the Zeeman levels, each with energy $\mu.B_o$ ($= -\gamma m\hbar B_o$) separated by $\gamma\hbar B_o$, i.e for protons, ^1H, $I = \frac{1}{2}$ $\therefore$ $m = +\frac{1}{2}, -\frac{1}{2}$, two Zeeman levels (see Fig. 3.1.), where the higher energy state corresponds to spins aligned against the field direction, and the lower state to those aligned with it. The nmr experiment consists of detecting transitions between these levels, induced by the absorbtion of electromagnetic radiation at a resonance frequency ω_o, known as the Larmor frequency[37], satisfying the condition:

$$\omega_o = \gamma B_o \qquad (3.2)$$

where ω_o corresponds to the frequency of precession of the magnetic dipoles. (There is usually a distribution of frequencies due to dipolar interactions on a nearest - neighbour scale (nanometres) giving Zeeman levels perturbed by dipolar effects.)

For a collection of nuclei in a sample at thermal equilibrium, the Zeeman levels will be populated according to the Boltzmann distribution and as such have more nuclei in the lower (energy) spin state than the other, giving rise to, in essence, a macroscopic magnetization aligned along the field direction (Fig. 3.2).

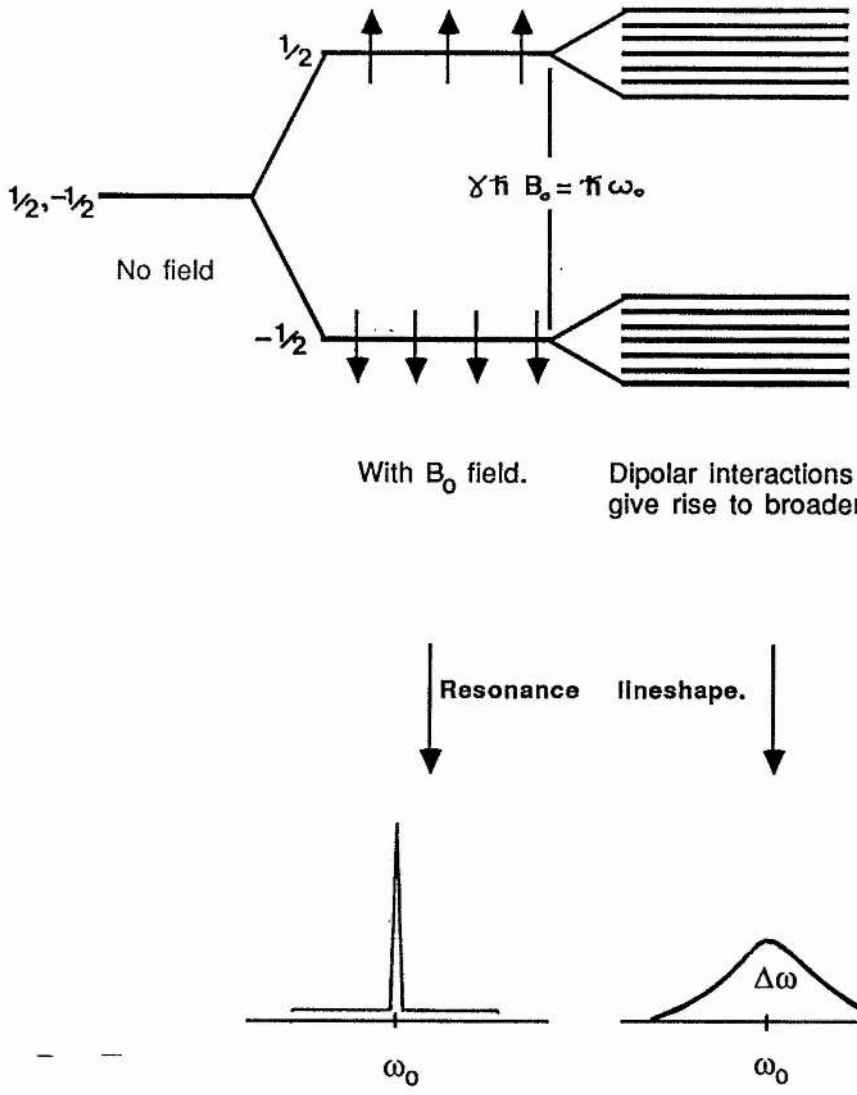

Fig. 3.1. A schematic representation of the origin of the nmr resonance line of nuclei with spin I = 1/2. The narrow line is typical of liquids while the broader line is typical of solids or viscous liquids.

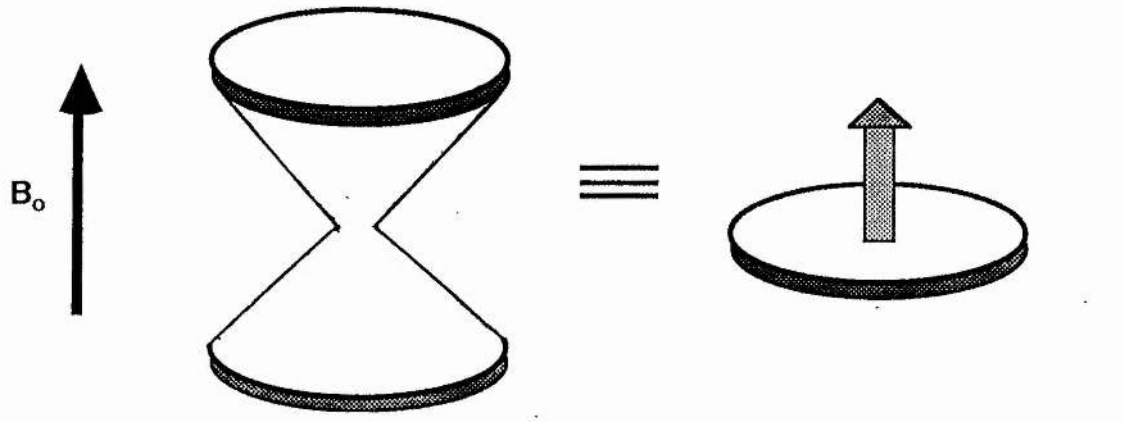

Fig. 3.2. A representation of how a collection of nuclei with the same Larmor frequency give rise to a macroscopic magnetization along the B_o direction.

3.2.2 The pulsed experiment

Most modern nmr measurements are performed in a pulsed experiment, stimulating all precessional frequencies, where the sample is subjected to short bursts of high intensity radio frequency (rf) power. Absorbtion of rf power alters the direction of the macroscopic magnetization with respect to the field and it is the resulting time - dependence of the magnetization recovery to the equilibrium value along a particular direction which is monitored.

A basic pulsed experiment is to apply an intense B_1 rf field pulse at resonance to tip the magnetization 90° from the B_o direction, this is referred to as a 90° pulse[39]. (The B_o direction is arbitrarily taken as

the z - direction in an x-y-z orthogonal axis set.) This turns the magnetization into the xy plane, where it is observable as an oscillating signal in a detector coil (Fig. 3.3.). As the magnetization returns to equilibrium in the z - direction, the coil signal will decay (usually exponentially) with time. The decaying signal, proportional to the amount of magnetization in the xy plane, $M_{xy}(t)$, is known as the free induction decay (fid), the fourier transform of which is familiar to most organic chemists. The time constant for this decay (i.e for $M_{xy}(t)$ to decay to 1/e of its original value, $M_{xy}(0)$), is termed the transverse or spin - spin relaxation time, T_2, where:

$$M_{xy}(t) \quad \alpha \quad \exp (- 1 / T_2) \qquad (3.3)$$

In Fourier transform terms πT_2 approximates to the inverse of the line width at half - height.

Following the 90° pulse the spins will return to precession about the B_o field and the equilibrium magnetization along the z - direction will be recovered. The characteristic relaxation time for this process is termed the longitudinal or spin - lattice relaxation time T_1.

3.2.3 The nature of T_1 and T_2 relaxation.

The T_1 relaxation process is envisaged as occurring by exchange of the absorbed rf energy from the perturbed nuclei to the surroundings or 'lattice' as heat, involving quanta of energy equal to the Zeeman level

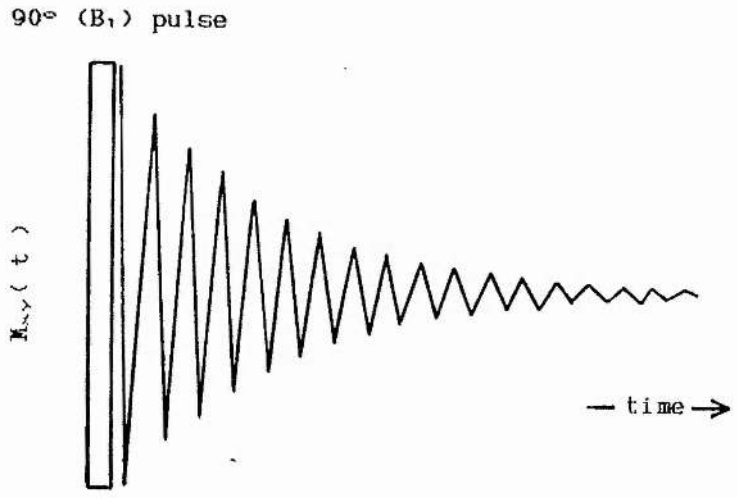

Fig. 3.3. A representative free induction decay following a 90° pulse where successive fid peaks (or troughs) define the M_{xy} decay profile.

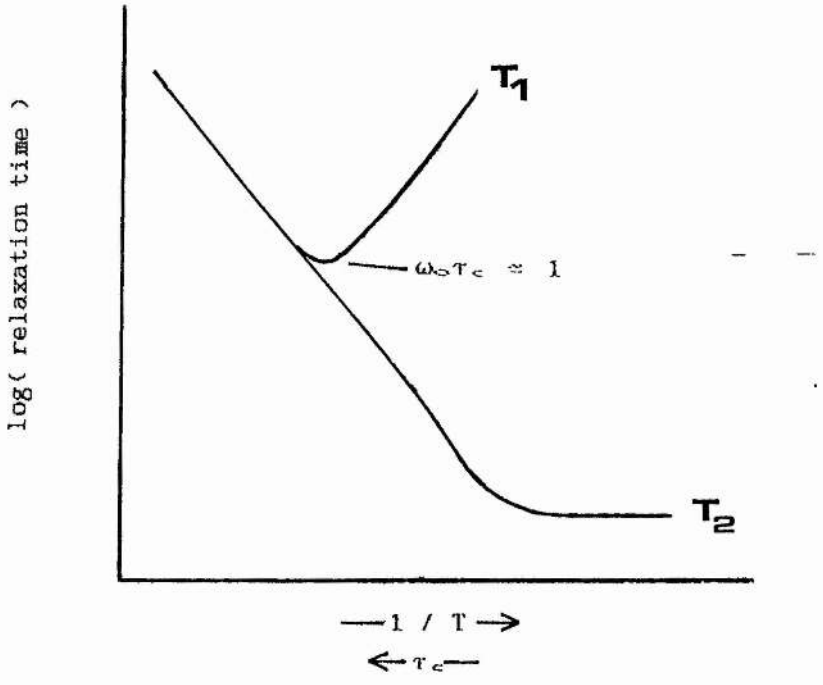

Fig. 3.4. The temperature dependences of the relaxation parameters T_1 and T_2 .

separation. It is thus an enthalpy effect. For the relaxation to occur there must be some specific interaction between the nuclei and their environment. Six types of interaction have been identified[99] and an important one, known as the dipole - dipole mechanism, involves energy exchange with nearby fluctuating magnetic fields created by other dipolar nuclei. (The interaction is the same as the magnetic dipole with the magnetic component of the B_1 field pulse.)

The T_2 relaxation process occurs usually by direct interaction of spins, which cause relaxation in the x-y plane without any energy exchange. This is in fact an entropy effect, randomizing magnetic vectors in that plane. This relaxation is important in solids where strong spin - coupling allows efficient transverse relaxation and a fast decay of M_{xy}.

3.2.4 Relation of T_1 and T_2 to molecular motion.

The relation of the relaxation parameters T_1 and T_2 to molecular motion has been subject to several treatments, the most familiar of which known as BPP theory (after its originators Bloembergen, Purcell and Pound[100]) yielding the following equations:

$$1 / T_1 \quad \alpha \quad B_{loc} \cdot \tau_c / (1 + \omega_o^2 \tau_c^2) \qquad (3.4)$$

and

$$1 / T_2 \quad \alpha \quad \tau_c \qquad (3.5)$$

where B_{loc} is that part of the local dipolar field modulated by the local motion, and τ_c is a correlation time for the motion, generally following an Arrhenius behaviour i.e

$$\tau_c = \tau_o \exp(Ea / kT) \qquad (3.6)$$

Combining equation (3.6) with with the above relationships (3.4, 3.5) leads to the temperature dependences shown in Fig. 3.4. for the transverse and spin - spin relaxation times. The minimum in the T_1 plot is important because it enables a good estimate to be made of the correlation time describing the motion at this temperature, where $\omega_o\tau_c \simeq 1$ (Greenbaum[101] undertook a study of this nature for PEO_4NaClO_4 , determining a correlation time for chain motion from the proton resonance). At lower temperatures, or in the limit of zero motion, T_2 assumes what is sometimes known as the 'rigid lattice' value, common to most solids, where spin - spin interactions are strong. With increasing temperature and molecular motion comes an increase in T_2, or narrowing of the resonance line, which can be envisaged as a progressive averaging of the dipolar interactions between spacially proximate nuclei.

3.2.5 Quadrupolar Nuclei

In addition to a magnetic dipole moment, nuclei with I > ½ possess an electric quadrupole moment, due to an uneven distribution of electric charge within the nucleus. When present, this electric moment may interact with an electric field gradient and have associated energy terms (nuclear quadrupole resonance, nqr, studies this). For our purposes we regard a quadrupolar nucleus in a magnetic field as giving rise to Zeeman levels perturbed by quadrupolar effects. The consequences are progressive as the quadrupolar interaction increases. Fig. 3.5. shows the allowed Zeeman transitions for a spin 3/2 nucleus (i.e ^{7}Li or ^{23}Na). With no quadrupolar effects the three allowed transitions all have the same energy separation thus Larmor frequency. With a first order quadrupolar interaction[102], the upper and lower Zeeman transitions are perturbed to Larmor frequencies above and below the unaffected central transition (line) to give satellite lines. In the second order case, the central line is also affected, noted as a broadening or sometimes complete disappearance, of the line. Determination of the type of interaction experienced by a quadrupolar nucleus is thus a direct comment upon its environment and may be useful in polyether electrolytes where such nuclei are found as cationic species.

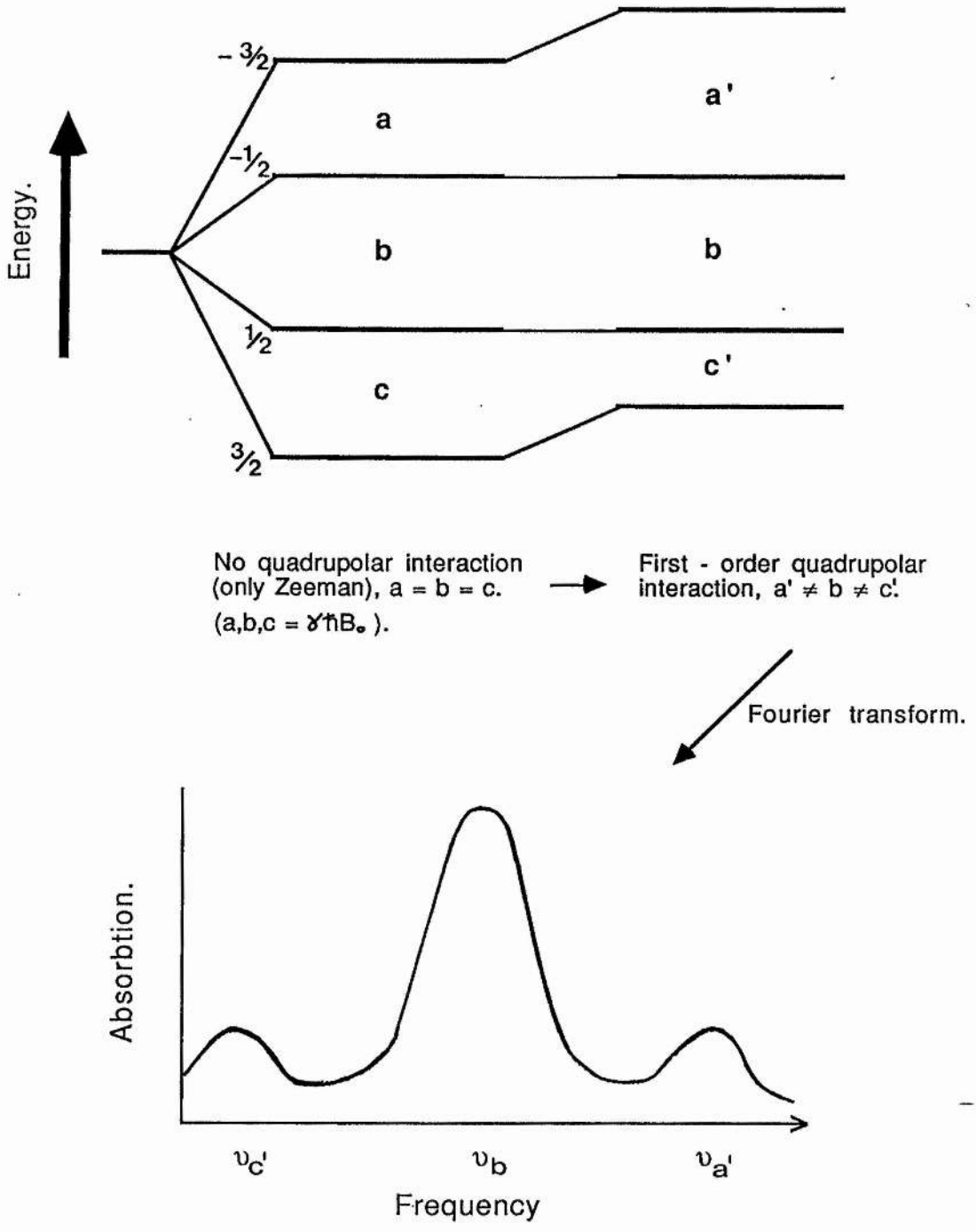

Fig. 3.5. The Zeeman energy level diagram for a spin I = 3/2 nucleus, showing how the satellite transitions a and c (-3/2 → -1/2, 1/2 → 3/2) have altered energies (a' and c'), relative to the central line b, when quadrupolar interactions occur.

3.2.6 Relevance to polyether electrolytes.

Many polymers and salt - containing polymers exhibit phase heterogeneity, where elastomeric and crystalline regions co - exist for a wide range of temperature, pressure and salt content. Fig. 3.6(a). shows the ^1H (proton) fid of a poly(ethylene oxide) sample used in this work, at 298 K. The decay shows an initial fast decrease of the transverse magnetization, M_{xy}, at short time ($\simeq$ 0 - 20 μs) and a slower decay to longer time ($\simeq$ 200 μs). It is typical of a polymer in the semi - crystalline state, where the two nmr signals observed are due to the separate contributions from both crystalline and amorphous domains[103], which decay with differing time constants i.e T_2 values. The crystalline regions are characterised by a fast decay (small T_2, of the order of the rigid lattice value) because by their nature significant chain motion is restricted, allowing static dipolar interactions between nuclei to produce efficient transverse relaxation. Amorphous regions above their Tg however, are allowed motions which may be considered to be quasi - liquid, where significant molecular motion effectively averages dipolar interactions to zero, giving less efficient relaxation and a slower decay of the transverse magnetization i.e a long T_2 signal.

This motional effect upon the time constant for the fid is obviously of value in determining the onset of motion, i.e the Tg region, for the amorphous polymer domain since quasi - liquid motions will only occur above Tg, the appearance of a long T_2 signal marking the onset of such motion.

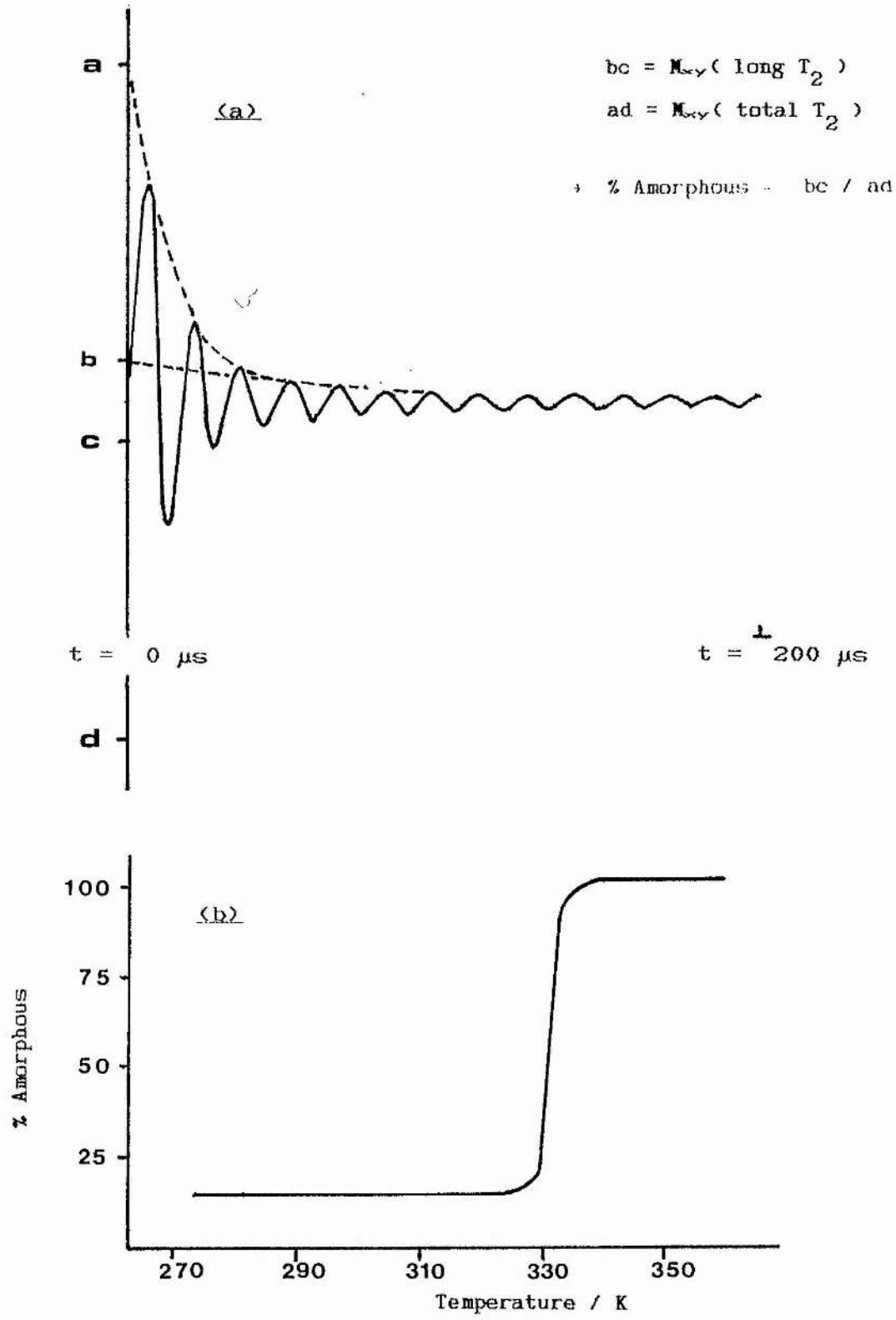

Fig. 3.6. (a) The free induction decay of Poly(ethylene oxide), mol. wt. 4 × 10^6, at 298 K and (b) The percentage amorphous content vs. temperature, as determined by the nmr method.

The contribution of each phase to the total transverse magnetization may be evaluated at zero time (usually by extrapolation) and will be in direct proportion to the number of nuclei in the respective phases, allowing calculation of the the relative amounts of each. This is shown schematically in Fig. 3.6(b). where the percentage amorphous component of poly(ethylene oxide) has been evaluated as:

(3.7) $$\% \text{ Amorphous} = M_{xy} \text{ (long } T_2 \text{)} / M_{xy} \text{ (total } T_2 \text{)}$$

over a temperature range. Below ≃ 330 K, the nmr experiment shows the sample to be 10% amorphous and 90% crystalline. At ≃ 330 K a sharp event is noted yielding a totally amorphous sample i.e a single component, long T_2 decay is observed. This behaviour is consistent with the melting of pure PEO crystallites, in excellent agreement with DSC data[13]. More interesting (and complex) situations occur where varying degrees of salt are present and the phase behaviour of both the host polymer and salt may be monitored.

3.3 Experimental.

3.3.1 Sample preparation

Salts:

$LiCF_3SO_3$ (3M's Ltd.) and NaI were dried by heating under vacuum at 423 K for forty - eight hours. Upon cooling, the salts were stored in a vacuum dessicator over phosphorous pentoxide before use.

Solvents:

The preparation of the low molecular weight PEO analogue, PEO(400)e ≡ $CH_3-CO_2-(CH_2-CH_2-O)_nCO-CH_3$, was detailed in the previous experimental section (2.2).

High molecular weight (4×10^6) PEO, BDH Chemicals Ltd., was stored in a vacuum dessicator over phosphorous pentoxide for at least two weeks before use.

Electrolyte formation

By far the most common method of producing polymer electrolytes has been by solvent casting. The method used here was that of a cold grinding / hot annealing technique developed in the St. Andrews laboratories by Gray *et al*[94]. The latter method has been shown to give PEO.$LiCF_3SO_3$ electrolytes with improved conductivities to those formed by the solvent casting technique.

In the solvent - free method used here, the high mol. wt. PEO was first milled at liquid nitrogen temperature in a stainless steel ball mill. An appropriate quantity of salt was added and the mix re - milled at the same temperature. The resultant intimate mixture was then packed into a 11 mm. glass tube of the form shown in Fig. 3.7. (The tube design was that required to fit the limited space available in the nmr probe head.)

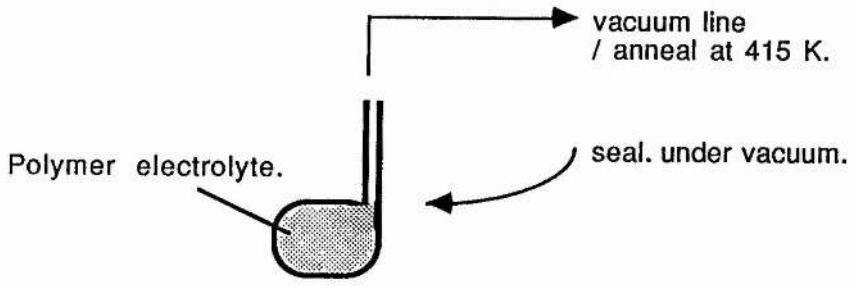

Fig. 3.7. Tube configuration for nmr probe head.

The tube was then attached to a vacuum line, annealed at 415 K for 48h under dynamic vacuum, then sealed before location in the probe coil.

3.3.2 Apparatus

The basic requirements for a nuclear magnetic resonance experiment are as follows :

(a) A magnetic field, B_o, which is locked and does not exhibit field drift.

(b) A transmitter source, capable of producing short, intense pulses of radio frequency power (the B_1 field) of the correct duration and pulse interval.

(c) A receiver system, sensitive to both the phase and amplitude of the oscillating signal produced in a reciever coil by the sample.

The apparatus used in this work fulfilled the above requirements and has been described elsewhere[105]. A diagram of the equipment involved is shown in Fig. 3.8. and the more relevant components will be described.

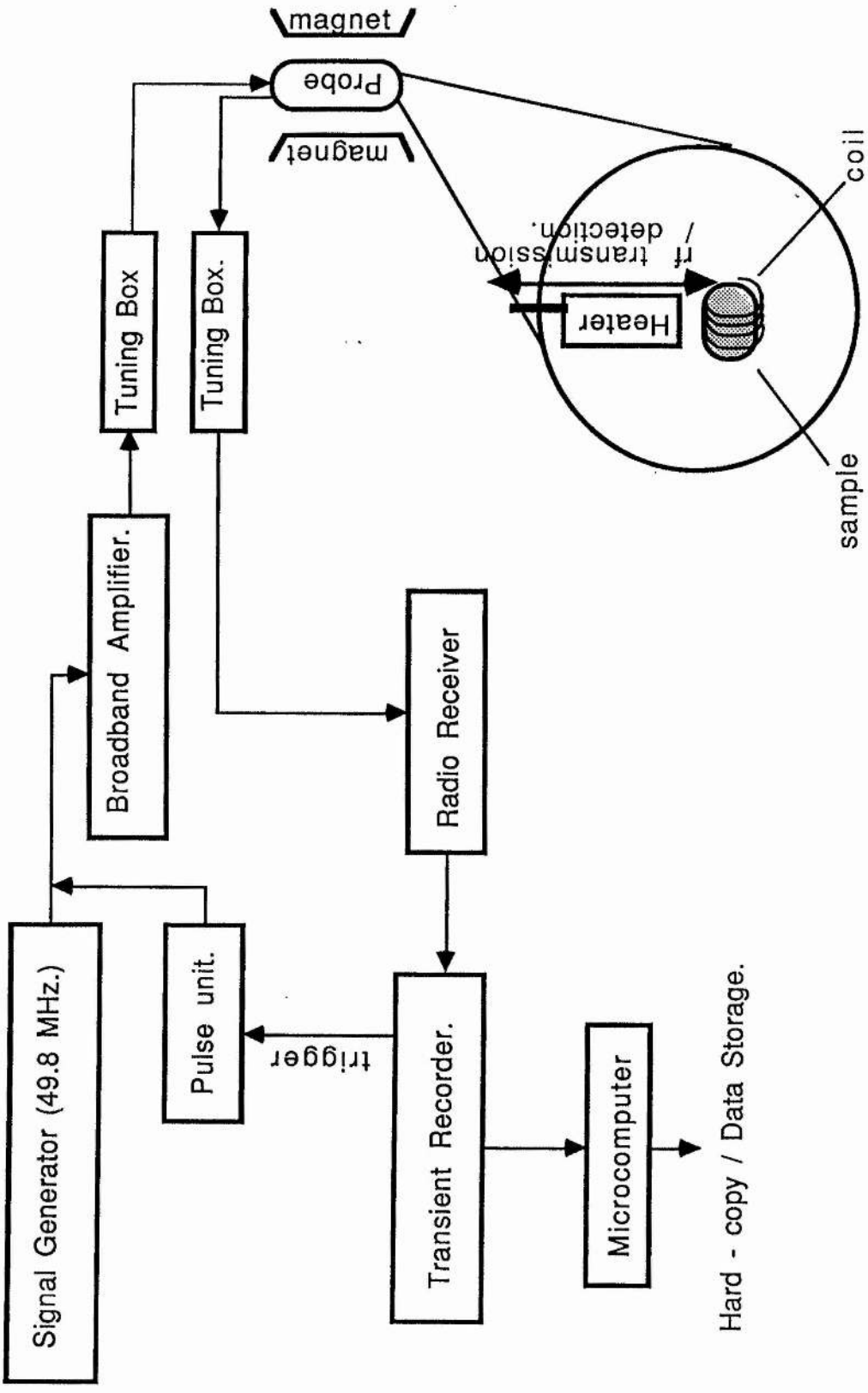

Fig. 3.8. Block diagram of the nmr apparatus.

Magnet and probe assembly

An Oxford Instruments 8T (eight Tesla) superconducting magnet was used in conjuction with a (0 - 100) amp power supply. Such magnets usually operate at very low temperatures and as such require immersion in liquid helium (boiling point 4 K) before the solenoid material conducts without energy loss. Superconducting magnets have several advantages over the older electromagnets including field stability once energized and higher possible field strengths[97].

A room temperature insert separated the magnet space (at 4 K) from the probe head. The latter contained a transmitter / receiver coil of diameter 1.3 cm. within which samples were located. Temperature variation within the insert was achieved by a thermistor controlled heater located above the sample and temperatures were measured to ± 0.5 K by a copper - constantan thermocouple linked to a calibrated digital voltmeter.

Signal generation and detection

A Farnell signal generator (model SSG 520) was used to generate a frequency locked radio frequency (rf) signal at 49.8 MHz, stablity 1 in 10^7. The signal in pulsed form was achieved using a pulse generator unit (Tektronix Inc. 2601 mainframe) amplified by two wideband rf power amplifiers (Dale electronics 325 LA, 250 kHz - 150 MHz). The nuclear free induction decay was detected as an oscillating voltage in the receiver coil by a Clark wideband receiver circuit. This was linked to a

transient recorder device (Datalab, model DL 905) which then enabled visual display of the free induction decay by oscilloscope (Hameg, model HM 705).

Data acquisition

Sweep times were displayed by the transient recorder in the range (2×10^{-4} - 50) s. The recorder acted as a multichannel device with 1024 channels where digitised decays were stored before transfer to a microcomputer (BBC Master series) via a parallel interface.

The computer operated a controlling program (stored on floppy disc) which supervised the transient recorder functions and initiated successive pulse sequences when signal averaging was employed. Signal averaging is common practice in modern spectrometer systems and is used as a method by which the noise levels inherent in most decay traces are reduced[105]. It is based on the fact that whereas the successive addition of individual data points in a free induction decay results in a n - fold increase in their value, random noise increases only as $n^{1/2}$. Typically, between 16 and 100 decays were recorded for a given signal averaging 'run' which corresponded to an enhancement in the signal to noise ratio of 4 and 10 respectively. (As a matter of interest, a noise 'filter' was written which, although simple in concept, showed good results on test data but was not used in the present work. Details of the algorithm for the noise filter are given in appendix 1.) Upon data acquisition, signal

averaged free induction decay traces were then stored to disc and/or obtained as hard copy output on a dot - matrix printer (Epson model).

3.3.3 Pulsewidth and B_1 field determination.

In nmr the 90° ($\pi/2$) pulse is the required duration of the B_1 field to tip the equilibrium macroscopic magnetization into the x-y plane[99] (where it may be monitored as an oscillating signal in a receiver coil). This is usually achieved by adjusting the pulse duration (manually in this work) to obtain a 180° pulse. For this condition no free induction decay will be observed because the magnetization has been tipped into the -z direction (signals are only detected in the x-y plane). Hence, dividing the 180° requirement by two gives the $\pi/2$ requirement.

For the samples studied the $\pi/2$ values obtained in this way for maximum B_1 field were as follows :

^1H	$\pi/2$	=	3.5 μs.
^{19}F		=	3.9 μs.
^7Li		=	9.0 μs.

The ^7Li value sometimes departed from this value due to quadrupolar effects and the reasons for this are explained where neccessary.

The B_1 field strength was calculated from the $\pi/2$ requirement for the proton signal (the strongest signal observed) via the relationship[96] :

$$t_p = 1.57 / \gamma B_1 \qquad (3.8)$$

where tp is the pulse width (duration) and γ the proton gyromagnetic ratio, 26.752×10^7 rad $T^{-1}s^{-1}$ i.e :

$$B_1 = 1.57 / (3.5 \times 10^{-6} \times 26.752 \times 10^7)$$
$$= 1.68 \text{ mT}$$
$$\simeq 71 \text{ kHz} \quad (\text{MHz} = 23.5 \text{ mT}^{[106]}).$$

One experiment involved a reduced B_1 value, obtained by reducing the output power from the final stage power amplifier. The proton $\pi/2$ requirement was then 8.0 μs. hence the B_1 field $\simeq$ 31 kHz.

3.3.4 Transverse relaxation time determination

Much of the work detailed in this and subsequent chapters was concerned with two basic signal types, short and long T_2. In homogeneous samples the transition from a short to a long T_2 fid ($\simeq$ 10 to $\gtrsim$ 700 μs for protons) marked the change from the glassy to the liquid state. In semi - crystalline samples the relative amounts the two signal types in a

two - component fid as a function of temperature gave an idea of the phase behaviour therein (chapters 4 and 5) .

For T_2 values less than about 500 μs, T_2 determination involved simply recording the free induction decay following a 90° pulse and then analysing the decay graphically as an exponential function[102,105] i.e

$$M_{xy}(t) = M_{xy}(0)\, e^{-t/T_2} \qquad (3.9)$$

where $M_{xy}(t)$ is the decay amplitude at some time, t, following the pulse, $M_{xy}(0)$ is the decay amplitude directly after the pulse, and T_2 the time for the magnetization to decay to 1/e of its initial value, $M_{xy}(0)$ i.e

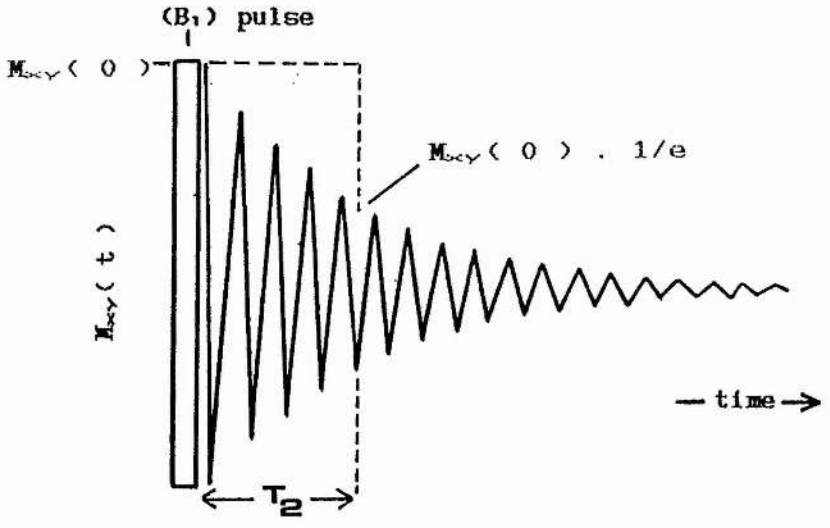

Fig. 3.9. Measurement of T_2 from the free induction decay.

Ideally, any spectrometer magnet should give the most homogeneous magnetic field possible across the sample dimension. In practise however the field is inhomogeneous and for longer free induction decays attenuates the decay length, thus giving a shorter T_2 value, in a similar manner to the dephasing of the transverse magnetization by a distibution of B_{loc} due to static dipolar interactions (3.2.4, 3.2.6).

For the magnet used in this work it was found that this *inhomogeneity limit* occurred at ≃ 700 μs; free induction decays with larger time constants were limited by inhomogeneities in B_o and would decay on a 700 μs timescale. For most experiments it sufficed that the observed T_2 values increased from a lower value (say 100 μs) to the inhomogeneity limit at 700 μs, marking the occurrence of a phase change i.e the melting of crystalline PEO at 333 K, where the ^1H T_2 was observed to increase from ≃10 μs to the inhomogeneity limit.

Certain experiments however (in 3.4.2.4) did require determination of the true transverse relaxation profile, where the real T_2 was greater than that set by inhomogeneities in B_o. This was achieved by use of a Carr - Purcell spin - echo pulse sequence[96].

The spin - echo pulse sequence is of the form $90° - \delta - 180°$ (also written $\pi/2 - \delta - \pi$) and its concept is outlined as follows (see Fig. 3.10.). The first pulse tips the equilibrium magnetization into the x-y plane where inhomogeneities in B_o dephase the magnetization at a rate faster than that governed by the true transverse relaxation process. After some time δ a second (π) pulse flips all spin vectors 180° into the -(x-y) plane and the magnetization rephases (refocuses) at 2δ giving a spin 'echo'. The amplitude of the echo at 2δ is given by :

$$M_{xy}(2\delta) = M_{xy}(0). e^{-2\delta/T_2} \qquad (3.10)$$

As the figure shows, plotting echo amplitudes at successive δ values gives the true free induction decay profile and a semilogarithmic plot of ln(echo amplitude) vs. δ will give gradient $-2/T_2$, from which T_2 may be obtained.

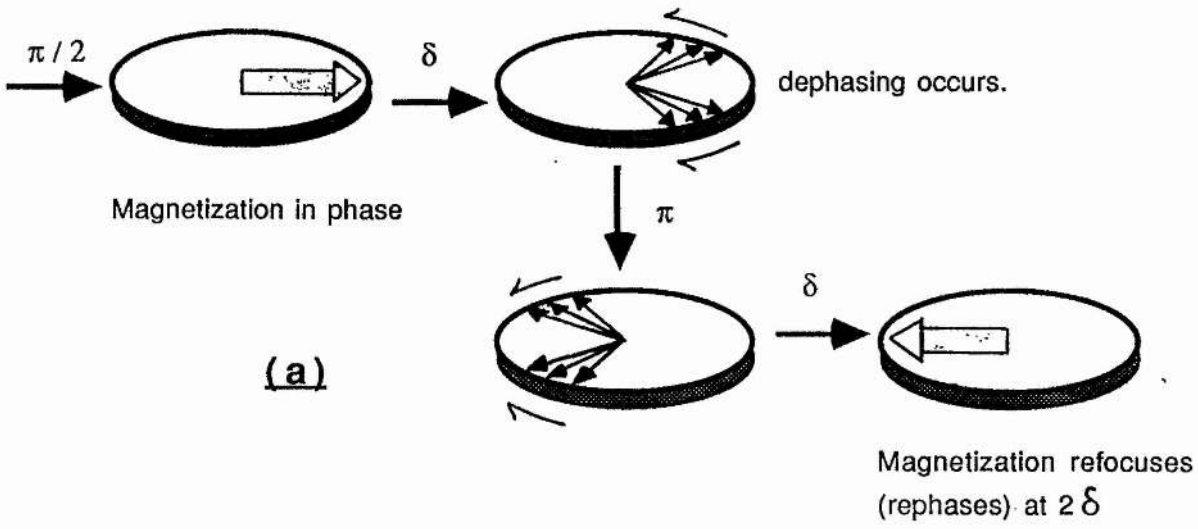

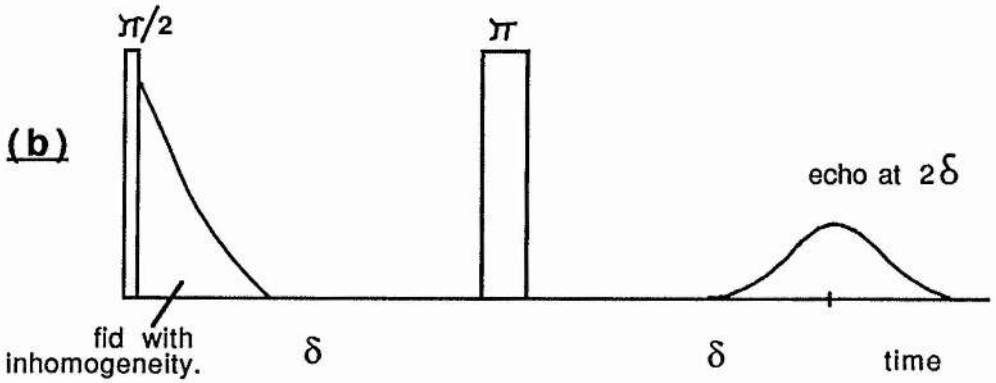

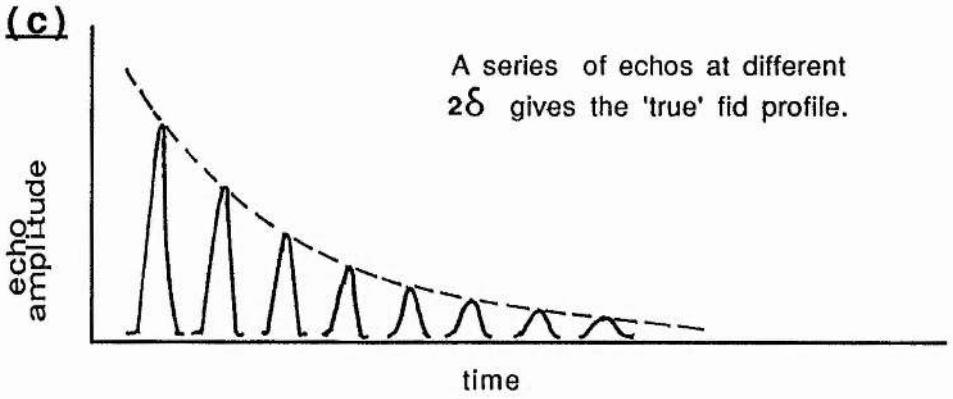

Fig. 3.10. The Carr - Purcell spin - echo pulse squence $\pi/2 - \delta - \pi$.(a) Representative diagram of the effect of the pulse sequence on the nuclear spin vectors. (b) When spin vectors rephase at 2δ an spin 'echo' forms. (c) Experiment at various δ gives the true fid profile, overcoming magnet inhomogeneity effects.

3.3.5 Measurement of the longitudonal relaxation time, T_1

Two methods were employed to measure T_1 depending on whether the studied free induction decay (fid) component was of the short or long T_2 type.

(a) Short T_2 decays.

Evaluation of T_1 relaxation times for quickly decaying fid components ($T_2 \leq 50\ \mu s$) was achieved by use of the Saturation - Recovery[106] pulse sequence, [$\pi/2$]n - δ - $\pi/2$, to ensure irradiation of all spectral frequencies occupied for a given nuclear species. The method involved an initial 'comb' of about ten 90° (i.e $\pi/2$) pulses spaced by approximately $5T_2$, which saturate[107] the spin system. 'Saturation' means that the upper and lower Zeeman levels, +½ and -½ for example, are equally populated and so the macroscopic magnetization is zero. After saturation the magnetization in the z - direction begins to return to the equilibrium value, M_z, and its magnitude at any time, δ, during this process may be monitored by a final 90° 'read' pulse which tips $M_z(\delta)$ into the M_{xy} plane where it is observed as an oscillating signal in the detector coil (Fig. 3.11.).

Then, assuming that for all times after saturation the recovery of the nuclear magnetisation follows an exponential relationship, $M_z(\delta)$ is given by the relationship[102] :

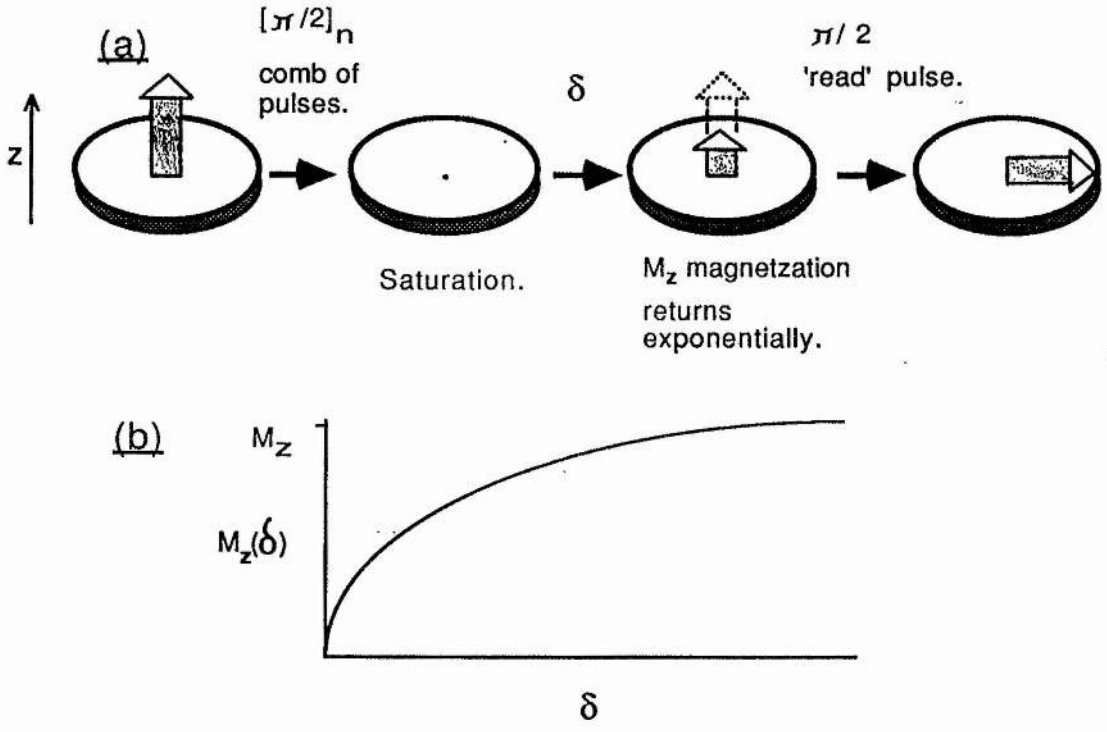

Fig. 3.11. (1) Schematic representation of the saturation - recovery pulse sequence $[\pi/2]_n$ - ∂ - π/2 and (2) a plot of how the M_z magnetization returns towards the equilibrium value following saturation.

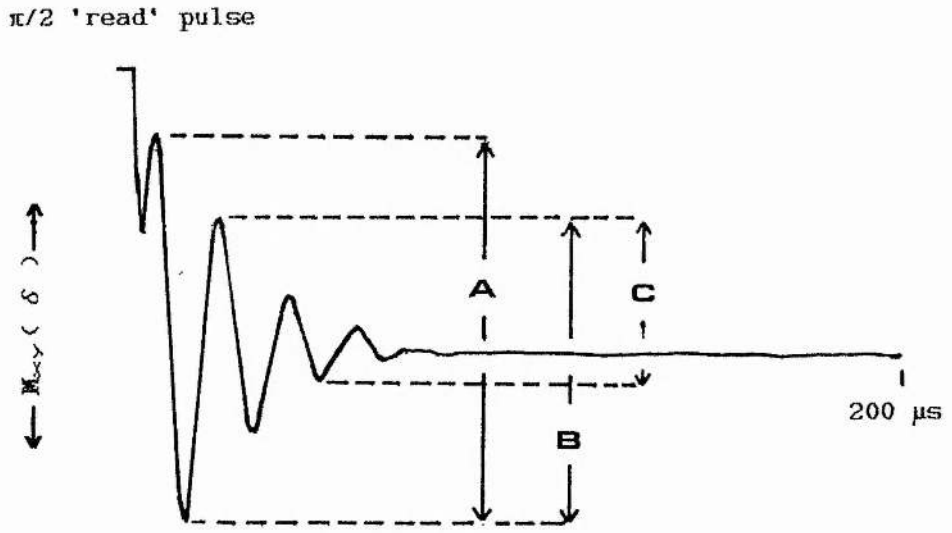

Fig. 3.12. Points on the fid beat structure which are suitable for sampling $M_z(\delta)$ for T_1 determination (^{19}F resonance in $PEO_4LiCF_3SO_3$, 330 K). A is best, where the signal to noise ratio is greatest.

$$M_z(\delta) \quad M_z \left(1 \quad e^{-\delta/T_1} \right) \qquad (3.11)$$

where δ is the separation between the initial comb, [$\pi/2$]n, and the final $\pi/2$ read pulse.

The equation therefore predicts a linear relationship for $\ln[1 - (M_z(\delta) / M_z)]$ as a function of δ, with gradient $-1/T_1$. In practice the equilibrium magnetization value, M_z, was obtained at pulse separation times times greater than $5T_1$ by measuring the peak to trough distance at a chosen point in the fid following the final pulse, as shown in Fig. 3.12 for the ^{19}F resonance in $PEO_4LiCF_3SO_3$. $M_z(\delta)$ was obtained in a similar manner, for various δ, yielding semilogarithmic plots of the type shown in Fig. 3.13. for the ^1H, ^{19}F and ^7Li signals in $PEO_9LiCF_3SO_3$.

(b) Longer T_2 decays.

Evaluation of T_1 relaxation times for fid components with $T_2 \geq 50$ μs was achieved by the Inversion - Recovery[106,107] technique (null method) using the pulse sequence $\pi - \delta - \pi/2$. This is shown schematically in Fig. 3.14. where the first pulse inverts the equilibrium magnetization into the -z direction. The magnetization then begins to return to equilibrium, passing through zero, into the +z direction. At any time δ during this process the final 90° pulse will monitor $M_z(\delta)$.

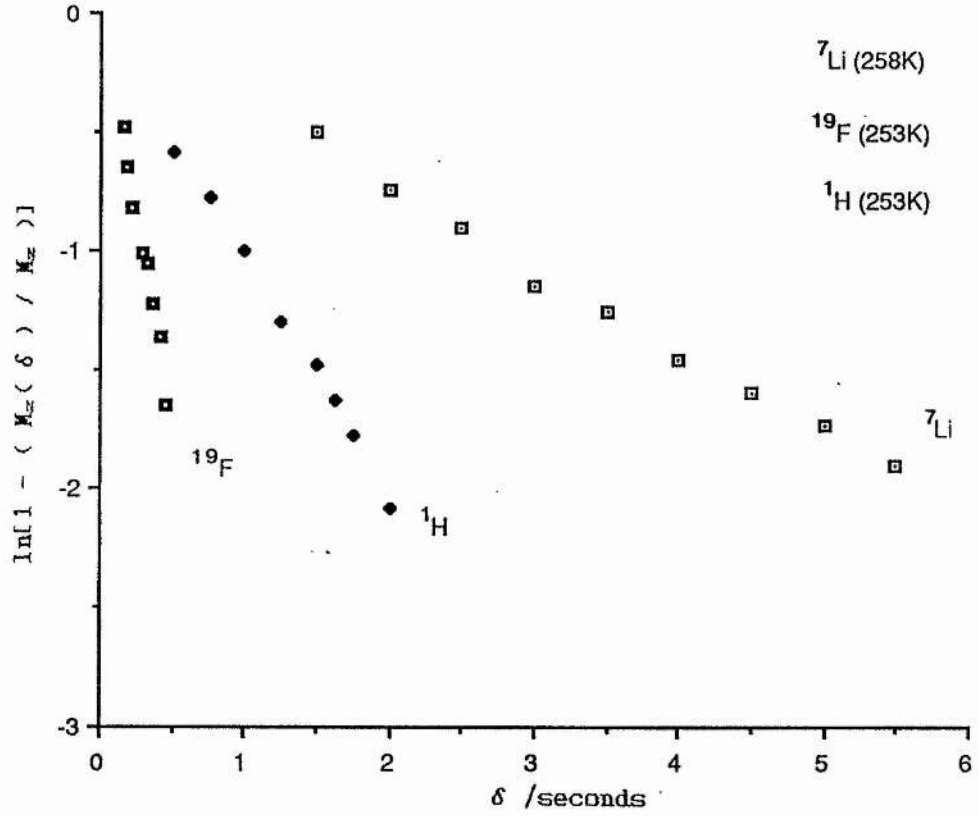

Fig. 3.13. Plots of $\ln[1 - (M_z(\delta) / M_z)]$ vs. pulse spacing, δ, for the nuclear species ^1H, ^{19}F and ^7Li in $PEO_9LiCF_3SO_3$.

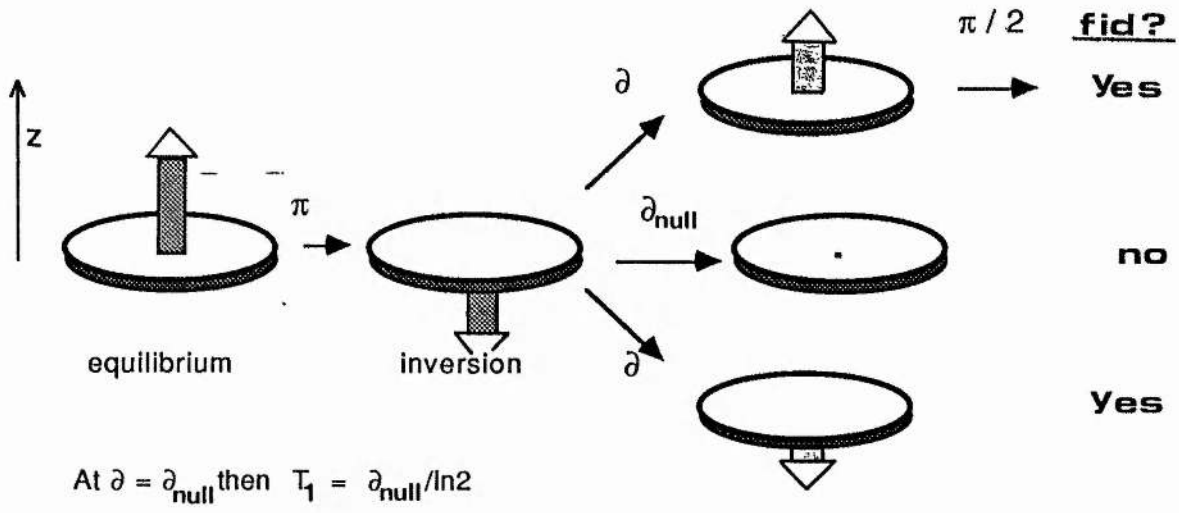

Fig. 3.14. Schematic representation of the effect of the inversion -recovery pulse sequence upon the macroscopic magnetization. Only at time ∂_{null} will no fid be observed with the read pulse and then $T_1 = \partial_{null}/\ln 2$.

As the magnetization passes through zero there is transient saturation (no net macroscopic magnetization) and the 90° pulse will give no fid in M_{xy}. At this null point for the magnetization :

$$T_1 = \delta_{null} / \ln 2 \qquad (3.12)$$

and T_1 may be computed.

Where the observed fid was more than one component i.e both short and long T_2 signals, T_1 values for the longer signal were readily obtained at times greater than $\simeq$ 50 μs where the shorter signal had decayed to zero. T_1 determination for short T_2 signals was obtained by graphical means (as outlined in 3.2.6, Fig. 3.6(a)) where the contribution to the fid from the longer signal was subtracted, leaving the only the contribution from the short T_2 decay.

Finally, both methods were referenced periodically by the use of a third pulse sequence[106,107], $\pi/2 - \delta - \pi/2$, (similar in concept to the saturation - recovery sequence where a semilogarithmic plot of $\ln[1 - (M_z(\delta) / M_z)]$ vs. δ yields T_1). For method (a) agreement for T_1 values derived by the saturation - recovery and $\pi/2 - \delta - \pi/2$ pulse sequences was usually to within 10%, which is reasonable. For method (b) agreement with the $\pi/2 - \delta - \pi/2$ sequence was better at about ± 5%.

3.4 Studies on low molecular weight PEO(400)e solutions.

3.4.1 Introduction.

The experimental work detailed here was initiated as part of a larger study concerning PEO(400)e solutions with added inorganic salt, where PEO(400)e corresponds to the endo - acetylated polyethylene glycol $CH_3CO_2(CH_2CH_2O)_8CO\,CH_3$. Three samples were studied with the nmr technique: PEO(400)e, PEO(400)e$_{20}LiCF_3SO_3$ and PEO(400)e$_8LiCF_3SO_3$. The study was multinuclear, involving measurements on the relaxation parameters of the proton (^1H), the fluorine nucleus (^{19}F), and the lithium nucleus (^7Li). This was convenient since the following assigments could be made for those nuclei as 'probes' for the physicochemical behaviour of the solution:

^1H - oligomer chain.

^{19}F - $CF_3SO_3^-$ anion.

^7Li - lithium cation.

thus those components constituting a conventional polyether electrolyte were available for study.

3.4.2 Results and Discussion.

3.4.2.1 Free Induction Decay Time Constants

For the three solutions studied, the free induction decay for each nuclear type (^1H, ^{19}F, ^7Li) showed two kinds of behaviour, based upon the magnitude of the time constant for each decay. At lower temperatures the free induction decays (fids) were found to decay rapidly yielding small T_2 values, i.e a broad linewidth, and at higher temperatures all decays were characterised by a long T_2 signal (narrow linewidth). Both fid type are shown in Fig. 3.15. for $PEO(400)e_8LiCF_3SO_3$, at 233 K and 298 K. At the lower temperature the ^1H signal shows the fastest decay with a T_2 value of $\simeq$ 10 μs, which is not uncommon for polymer protons in the solid state[103]. The ^{19}F value is longer at 30 μs and then ^7Li at 120μs. At the higher temperature the fids for all nuclear species are observed to be of the long T_2 type suggesting increased motional freedom.

With temperature as a variable, T_2 values were obtained for each nuclear type and are shown for each solution in Fig. 3.16. Initial focus is given to the two salt - containing solutions, $PEO(400)e_xLiCF_3SO_3$, where x = 8 and 20. (The solutions will now be refered to as the 8 / 1 and 20 / 1 samples respectively, indicating the ether oxygen to salt mole ratio.) In both cases an event is noted in all T_2 profiles, at ca. 253 K for the 8 / 1 sample and 249 K for the 20 / 1,

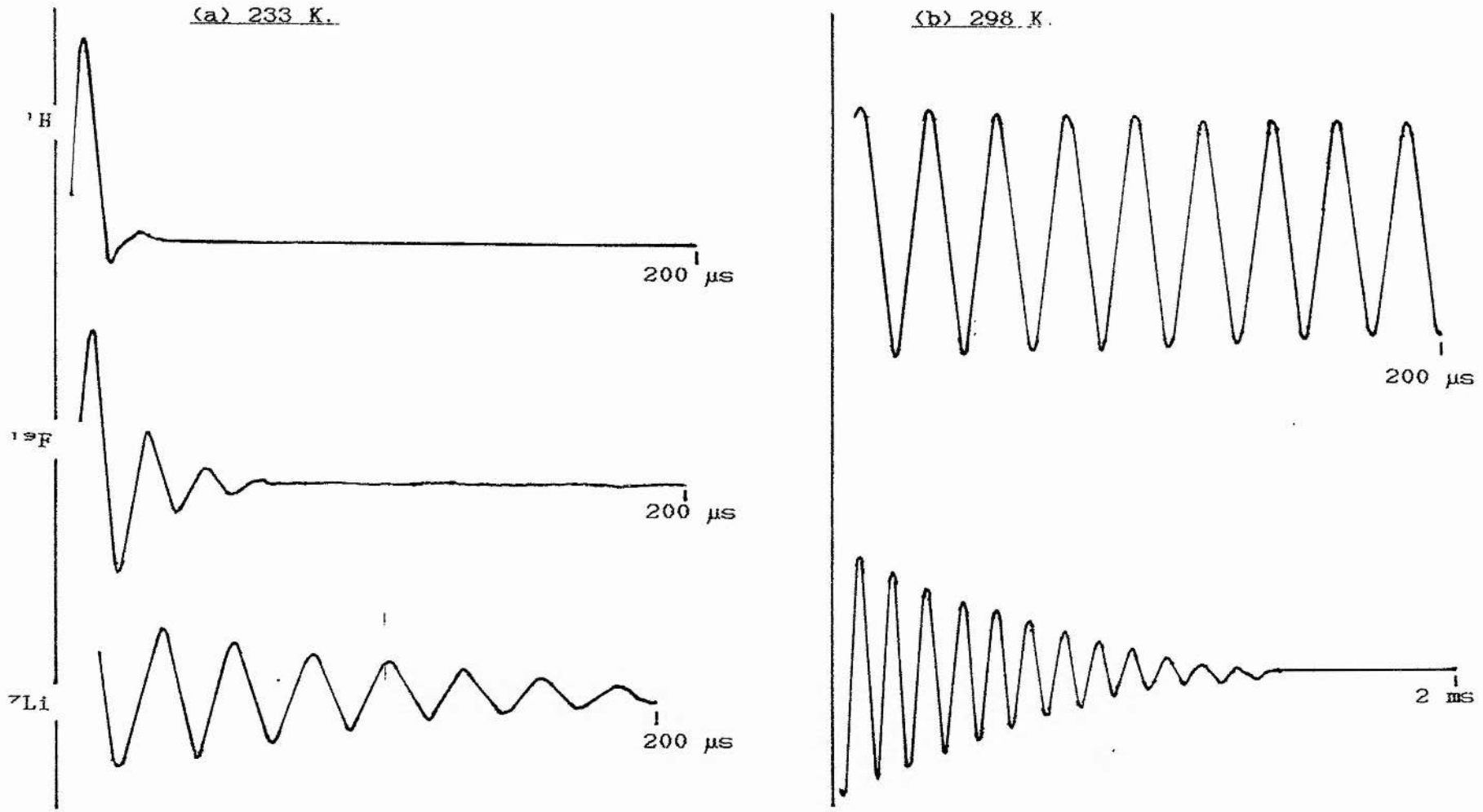

Fig. 3.15. Free induction decay (fid) traces obtained for the nuclear species ^{1}H, ^{19}F and ^{7}Li in PEO(400)$e_8LiCF_3SO_3$ at (a) ca. 233 K and (b) ca. 298 K. The fids at the higher temperature are actually for the ^{1}H signal but are also representative of those obtained for ^{19}F and ^{7}Li.

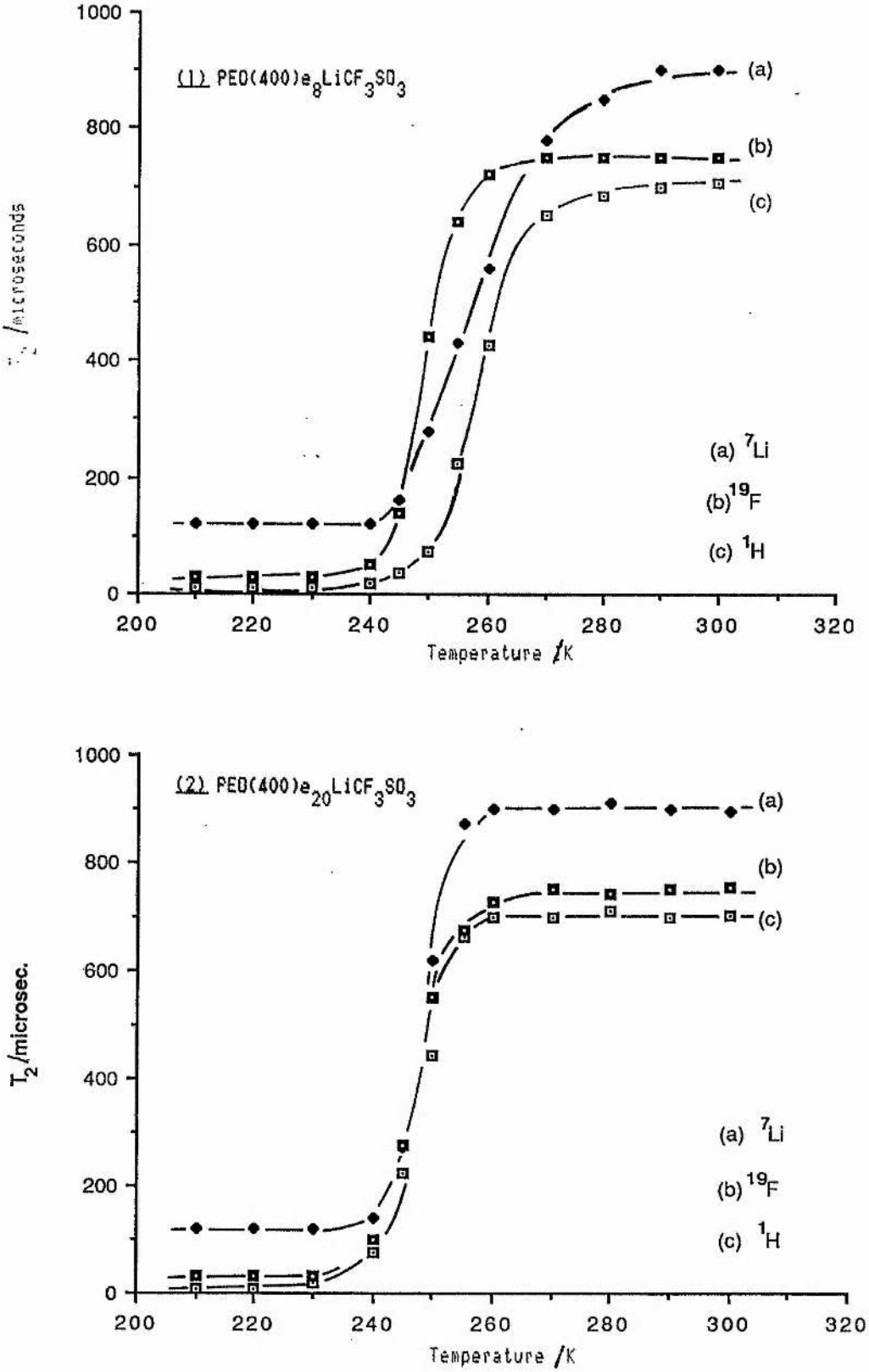

Fig 3.16. Free induction decay time constants (T_2) vs. temperature for ^1H, ^{19}F and ^7Li in (1) $PEO(400)e_8LiCF_3SO_3$ and (2) $PEO(400)e_{20}LiCF_3SO_3$.

suggesting an abrupt increase in motion for both solutions at these temperatures. This is, of course, entirely consistant with a glass to liquid transition in both cases, where the transition region is marked by the change from frozen amorphous to mobile amorphous material[1,2]. (This was verified visually by raising the temperature of the sealed samples through the above transition region in a methanol bath.) Above the transition event at about 253 K all T_2 values were observed to be at the limit set by inhomogeneities in B_o, ≈ 700 μs, as explained in the experimental section (3.3.4).

It was outlined in 3.2.4 that increased motion of a species can result in a partial or nearly complete averaging of the spin - spin interaction, giving an increased T_2 value and lengthening of the fid. Examination of the T_2 data below the event temperature shows a consistently larger T_2 value for ^7Li than either the proton or fluorine signals. This does not mean that lithiums have mobility in the glassy state relative to the polymer chain or anion, but is a consequence of the gyromagnetic ratios of the studied nuclei. i.e for an essentially frozen system, T_2 is governed entirely by the distribution of local fields[107], B_{loc}, and the dephasing of spins, the transverse relaxation process, will occur in a time of the order of $(\gamma.B_{loc})^{-1}$.

Now the gyromagnetic ratios of the respective nuclei are[107]:

nucleus	γ / 10^7 rad Tesla^{-1} sec^{-1}
^1H	26.752
^{19}F	25.167
^7Li	10.397

predicting a longer T_2 decay for ^7Li for similar local fields. It is also noted that :

$$\gamma(^{19}F) \simeq \gamma(^1H) \qquad \text{but} \qquad T_2(^{19}F) \simeq 3 \times T_2(^1H)$$

and

$$\gamma(^{19}F) \simeq 2.4 \times \gamma(^7Li) \qquad \text{and} \qquad T_2(^7Li) \simeq 4 \times T_2(^{19}F)$$

suggesting a different strength of B_{loc} for protons and fluorines but a similar one for lithiums and fluorines.

The T_2 behaviour of pure PEO(400)e, with zero salt content, contrasted that of the 8 / 1 and 20 / 1 samples in several ways. Whereas the latter exhibited a sharp change from 100% short to 100% long T_2 decays at a reasonably well defined temperature, PEO(400)e showed two component behaviour, short and long T_2, over a 40K range. The relative amount of long T_2 signal (or mobile component) was determined as a function of temperature, as described in 3.2.6, and is shown in Fig. 3.17. with the T_2 data for that component.

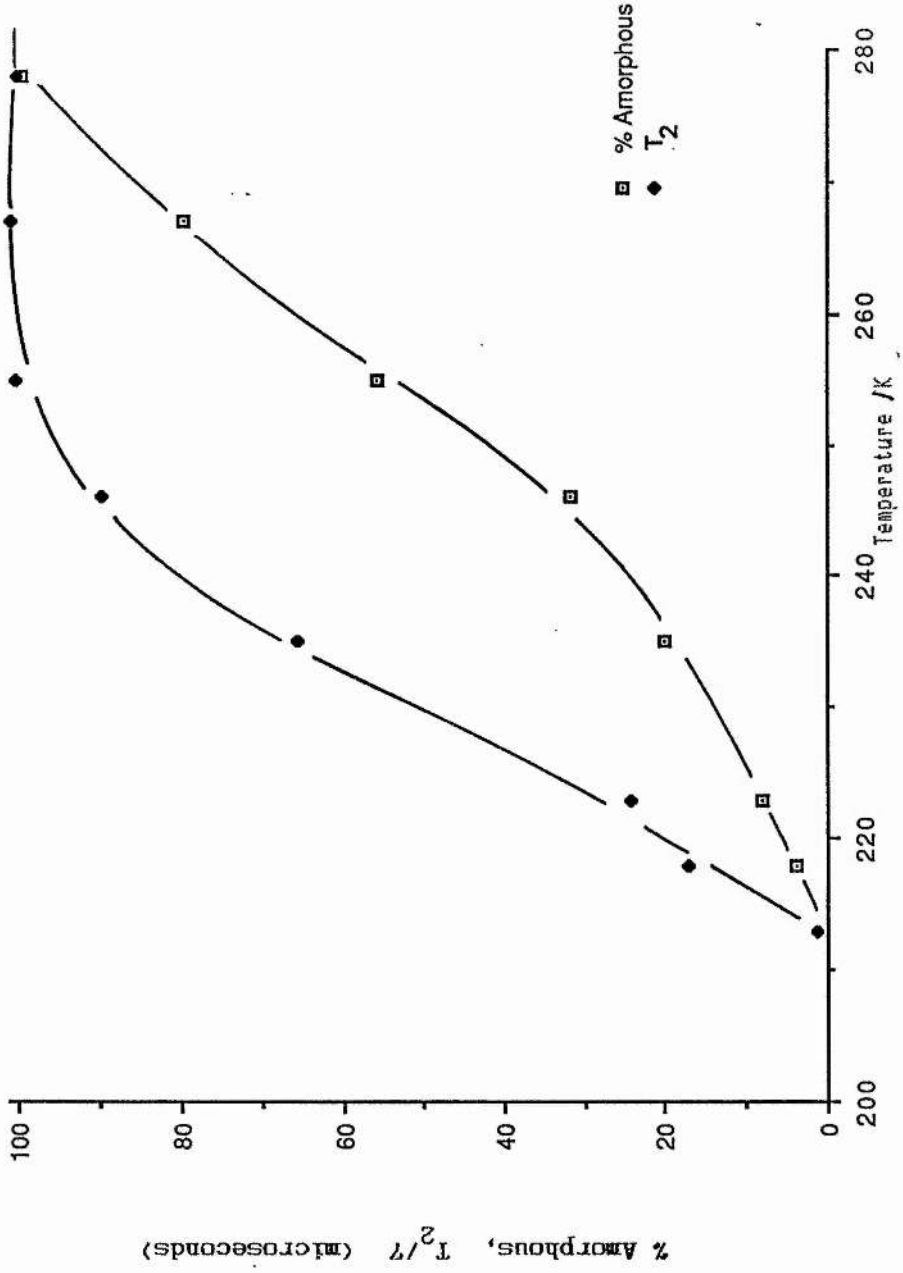

Fig. 3.17. Percentage long T_2 component ('% Amorphous') and long T_2 values for PEO(400)e.

Perhaps the most interesting point to note is that the onset of motion in the sample is evidenced at 218 K. This is very close to the T_o value of 220 K used in fitting conductivity data to the Vogel - Tamman - Fulcher (VTF) equation in 2.3.2 for $LiClO_4$ and $LiCF_3SO_3$ at low concentrations in PEO(400)e. Whether or not the presence of salt at the concentrations (0.002 - 0.08 mol kg^{-1}) used in the conductivity experiment would alter this nmr temperature for onset of motion was not investigated but it is interesting to note that the conductivity data for the 8 / 1 and 20 / 1 samples could also be fitted to the VTF form with T_o = 220 K. (The data are shown and discussed in section 3.4.2.4.)

3.4.2.2 Fid amplitude measurements and quadrupolar effects.

In 3.2.6 the concept of amplitude measurements as a means of evaluating the relative amounts of one component to another in a semi - crystalline polymer was introduced. This technique is based upon the amplitude of a given signal at zero time (i.e following a 90° pulse) being in direct proportion to the number of absorbing nuclei and is well known in polymer nmr[103]. The example given was for a homonuclear system, all protons, but can be applied to the heteronuclear case. An example of its use is shown here where the stoichiometry of the 8 / 1 and 20 / 1 samples were calculated by the nmr technique.

Following Bhattacharja *et al*[31], the relative numbers of one nuclear type to another in a homogenous solution may be calculated as :

$$n_i / n_j = A_i / (A_j \times \theta) \qquad (3.13)$$

where n_i and n_j are the numbers of the differing nuclear types, A_i and A_j the respective fid amplitudes at zero time, and θ a constant dependent on the natural abundances of i and j, and a sensitivity factor. Table 3.1. shows amplitude data for the ^1H and ^{19}F signals of the 20 / 1 sample at several temperatures. Using the above relation as :

$$n_{^1H} / n_{^{19}F} = A_{^1H} / (A_{^{19}F} \times \theta) \qquad (3.14)$$

where $\theta = 1.0625$[31], the ratio of protons to fluorines in the sample was calculated. With knowledge of the structural formula for PEO(400)e and that there are three fluorines per anion, it is an easy matter to calculate the ether oxygen to salt ratio. The actual ratio, 20 / 1, is known from the amount of PEO(400)e and $LiCF_3SO_3$ used in solution preparation.

Table 3.1. shows that the nmr method agrees well with this stoichiometry :

	Amplitude (Arbitrary)			
T / K.	^1H	^{19}F	n_H / n_F	EO / $LiCF_3SO_3$
228	100.4	3.0	31.5	20.1
272	89.5	2.7	31.2	19.9
318	83.1	2.5	31.3	20.0

Table. 3.1. ^1H and ^{19}F amplitude data at zero time for 20 / 1 PEO(400)e sample.

A more significant set of data are shown graphically in Fig. 3.18. for the ^7Li signal in the 8 /1 and 20 / 1 samples. The parameter plotted here is that of the experimentally determined n(Li) / n(F) to the theoretical ratio, 1/3, based on there being three fluorines per lithium in $LiCF_3SO_3$. The term '%Li(observed)' therefore means the percentage of the actual lithiums in the sample that are observed in the nmr experiment.

According to the data, about 60% of the theoretical lithium intensity appears to be missing in both samples at lower temperatures. The full intensity is observed however upon going from the glass to liquid states, as identified above (3.4.2.1). It was also noted that the $\pi/2$ pulse requirement for the ^7Li resonance differed in the two temperature regimes i.e $\pi/2 \simeq 5$ μs (< 250 K) and $\pi/2 \simeq 9$ μs (> 250 K).

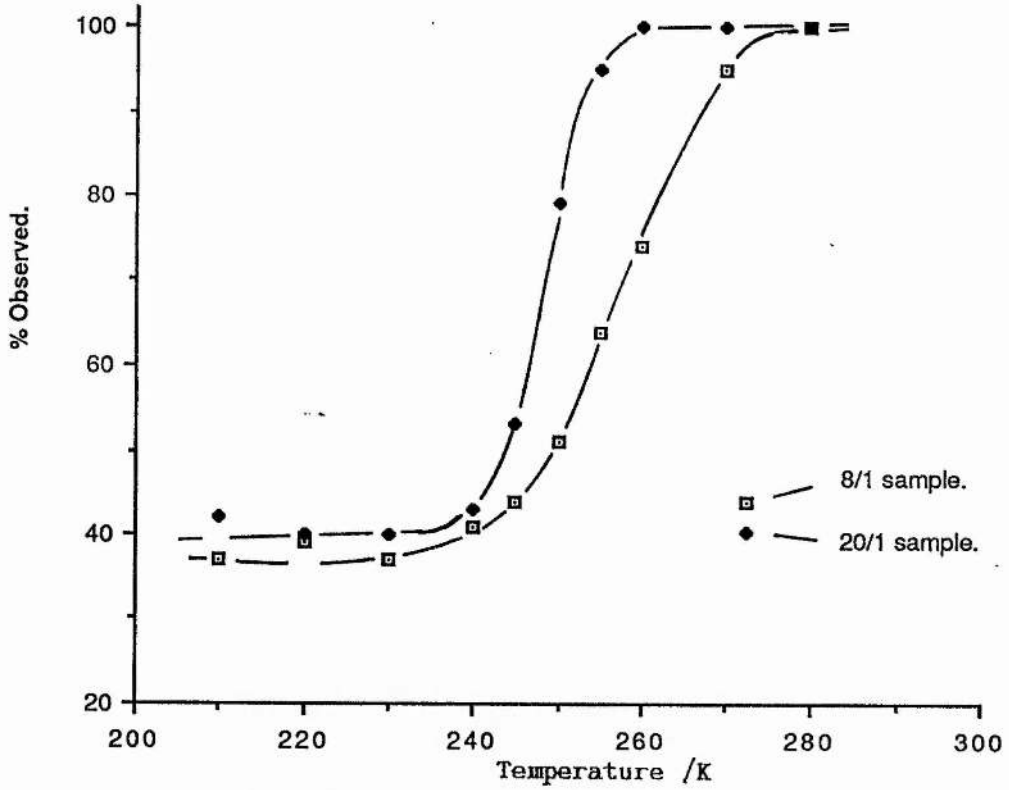

Fig. 3.18. The percentage of lithiums observed (relative to ^{19}F) with temperature in PEO(400)e,$LiCF_3SO_3$ 8/1 and 20/1 samples.

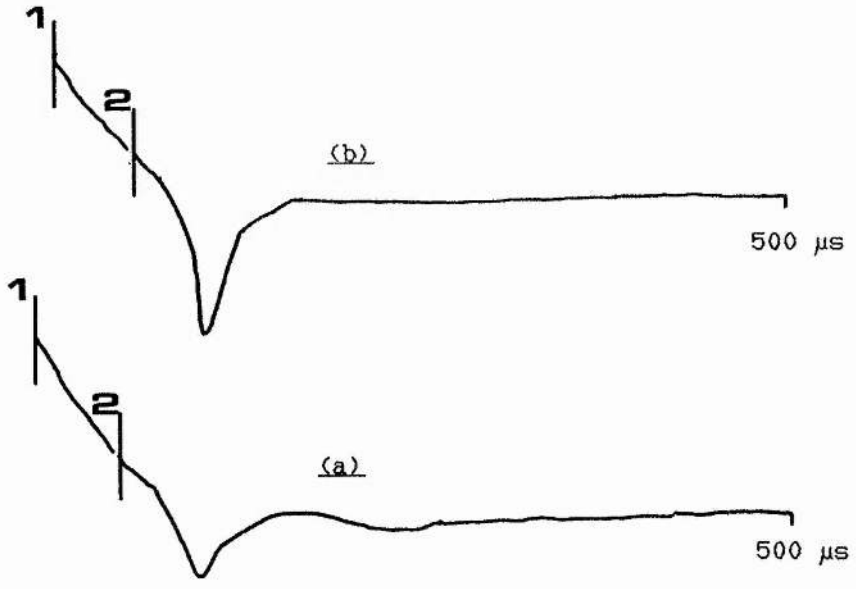

Fig. 3.19. Typical quadrupolar echo traces obtained below ca. 250K for the ^7Li resonance in (a) PEO(400)e$_8LiCF_3SO_3$ and (b) PEO(400)$_{20}LiCF_3SO_3$. Echos were obtained using a [90° - δ - 35°] pulse sequence with 90° = 9 μs, δ (pulse spacing) ≈ 50 μs and a 500 μs sweep. 1 = 90° pulse and 2 = 35° pulse.

The reason for this effect lies in the quadrupolar nature of the ^{7}Li nucleus (I = 3/2), where quadrupolar interaction between it and an electric field gradient can remove the contribution of the satellite transitions (-3/2 → -1/2, 1/2 → 3/2) to the nmr line, leaving the unperturbed central transition -1/2 → 1/2 (3.2.5, Fig. 3.5.). If the satellite lines are missing then theory[102] indicates that a first order quadrupolar interaction will manifest itself as a loss in fid intensity, 60% in the I = 3/2 case, and 'fictitious' spin = 1/2 behaviour, where the required $\pi/2$ pulsewidth is one half of that where all Zeeman transitions are observed. This appears to be the case here, the recovery of full signal intensity occurring when relative motion in the 8 / 1 and 20 / 1 samples averaged out electric field gradient effects.

Usually, $\pi/2$ considerations are adequate in determining whether or not satellite transitions are contributing to the observed signal. Further verification was achieved by use of the quadrupolar echo technique, which gives an echo if the satellite transition intensity is *not* included in the observed fid but *is* in the region of those spectral frequencies stimulated by the B_1 field[102] (see Figs. 3.5. and 3.10.). The method is similar in concept to the Carr - Purcell spin - echo method outlined previously (3.3.4) but uses the pulse sequence :

$$90^{\circ} - \delta - 35^{\circ}$$

to refocus the 'missing' satellite intensity at 2δ. Fig. 3.19. shows typical quadrupolar echo traces obtained for both the ^{7}Li 8 / 1 and 20 / 1 samples below ca. 250 K. In both cases an echo was observed, indicating that satellite intensity was in the

region of B_1. This, coupled with $\pi/2$ requirements at a given temperature, confirms that the lithium nuclei in the 8 / 1 and 20 / 1 samples experience a first order quadrupolar interaction below ca. 250 K.

In chemical terms the nmr observations mean that the lithium cation occupies a non - symmetric environment in the glassy state. As will be shown, measurements of this type assume greater importance when probing environment in the high mol. wt. heterogenous samples.

3.4.2.3 Longitudinal Relaxation.

Fig. 3.20. shows transverse relaxation time data, for all nuclear species studied, as a function of temperature for the PEO(400)e, 20 / 1 and 8 / 1 solutions. Some general features of the results are worth emphasizing :

(1) T_1 minima are associated with all components in the figures.

(2) For ^1H and ^7Li the respective minima move to higher temperatures with increasing salt content.

(3). The minima are broad and broaden with increasing salt content.

(4) Fluorine profiles are markedly asymmetric, with a smaller T_1 dependence on temperature below the minimum.

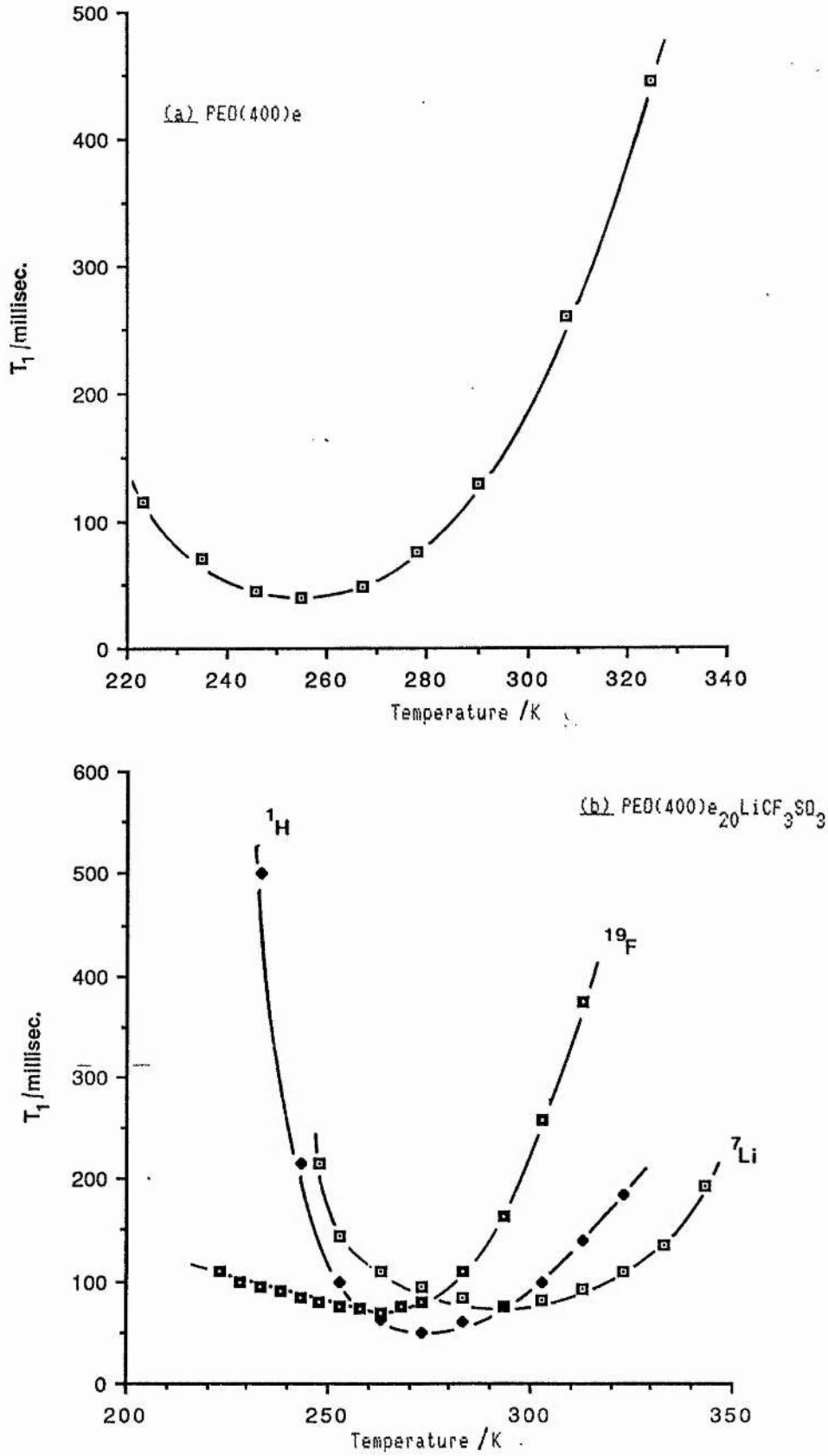

Fig. 3.20. T_1 vs. temperature for the studied nuclear species (^{1}H, ^{19}F and ^{7}Li) in (a) PEO(400)e, (b) PEO(400)e$_{20}$LiCF$_3$SO$_3$ and (c) PEO(400)e$_8$LiCF$_3$SO$_3$ (next page).

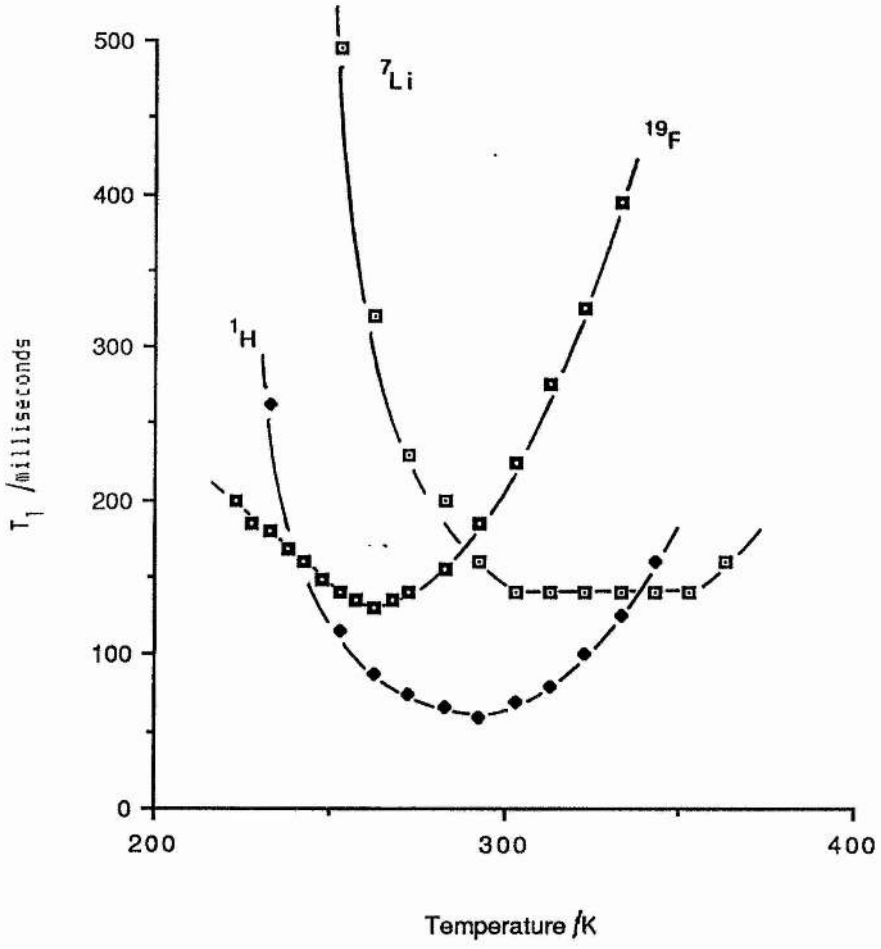

Fig. 3.20. (c) T_1 vs. temperature for the studied nuclear species in $PEO(400)_8LiCF_3SO_3$.

The presence of minima (Table 3.2.) for each nuclear type allows the statement that the relaxation process (or processes) giving rise to the minima have a correlation time τ_c :

$$\tau_c = 1 / \omega_0 \qquad (3.15)$$

where $\omega_0 = 2\pi f$ (f is the operating frequency of the spectrometer, 49.8 MHz in this work).

Table 3.2. Temperatures (Kelvin) at which T_1 minima occur in PEO(400)e and PEO(400)e.$LiCF_3SO_3$ samples.

Nucleus	Sample : PEO(400)e	20 / 1	8 / 1
^1H	255	273	293
^7Li	-	293	333†
^{19}F	-	263	263

(† estimated value, ± 5 K.)

In many viscous solutions, it is well known that the relative diffusional motion of molecules usually determines the ^1H longitudonal relaxation rate[102]. More specifically, Kimmich and Schmauder[109] proposed that for polyethylene *glycol* melts, of mol. wt. < 1000, τ_c was directly proportional to viscosity. This appears to be the case here,

where the shift to higher temperatures for the ^1H and ^7Li T_1 minima with increasing salt content probably reflects increased solution viscosity. Hence, as the solutions become more viscous, a higher temperature must be accessed to achieve the same correlation time for the motion.

The data also suggest that although both are susceptible to a viscosity effect, the relaxation mechanism for ^1H and ^7Li differ since respective minima occur at different temperatures in a given sample. If it is accepted that at their T_1 minimum, the protons in PEO(400)e relax by interaction with fluctuating dipole fields, which is probable, then at the minimum[107] :

$$(T_1 \text{min.})^{-1} = \gamma^2 (B_{loc})^2 / \omega_o \qquad (3.16)$$

where B_{loc} represents the strength of the fluctuating field. It follows that if the ^7Li is relaxed by the same field then :

$$\frac{T_1 \text{min.}(^1H)}{T_1 \text{min.}(^7Li)} = \frac{\gamma^2(^7Li)}{\gamma^2(^1H)}$$

This does not appear to hold here since $\gamma^2(^7Li) / \gamma^2(^1H) = 0.15$ but the ratios of the T_1 values

at the minima are 0.43 for the 20 / 1 sample and 0.62 for the 8 / 1. (If magnetic dipolar relaxation were to occur then the relation predicts $T_1 \simeq 350$ millisec. for ^7Li.) Abragam[114] has remarked that for spins $I > \frac{1}{2}$ the coupling of the nuclear quadrupole moment with fluctuating electric fields is almost always the main relaxation mechanism in the liquid state. This would appear to be the case here, where the lithiums are relaxed by fluctuating electric fields caused by the relative motion of ions.

According to the BPP theory (3.2.4) an Arrhenius plot of T_1 vs. temperature yields an activation energy for the process describing the relaxation. This holds well for smaller liquid molecules and superionic conductors but fails in media of the type used here, giving lower Ea terms than those derived by other techniques based on conductivity or dielectric measurements[110]. The theoretical aspects of the effect were addresed by Connor[111] and reinforced by experimental data. The reasons for this are well known and are due to a distribution of correlation times describing the motion and not a discrete τ_c. This leads to a broadening of the T_1 distribution around the minimum, which is observed here, and is consistent with Connor's studies on polyethylene glycol (200), glycerol and poly(methylene oxide). For this reason the T_1 profiles for ^1H and ^7Li were not used to evaluate Ea terms.

It was suspected however that the low temperature side of the ^{19}F T_1 minima in the salt containing samples would follow Arrhenius behaviour. There were several reasons for the assumption:

(a) The fluorine minima occurred at the same temperature in both samples (263 K).

(b) The short T_2 value at low temperature for ^{19}F of 30 μs suggested some averaging of the spin - spin interaction.

(c) It is well known that CH_3^- methyl group rotation is facile down to very low temperatures (77 K) and is as such a dominant relaxation source[11,12].

It follows that if CF_3^- internal rotation about the carbon - sulphur bond was facile in the $CF_3SO_3^-$ anion then it would persist when translational modes were frozen. The internal rotation process would not be expected to have dependence on *inter* - molecular environments hence no correlation time distribution would be envisaged and the BPP theory should apply.

Fig. 3.21. shows Arrhenius plots of the ^{19}F T_1 vs. temperature data for the 20 / 1 and 8 / 1 samples. The data appear linear with least squares analysis giving Ea = 5.8 and 5.4 kJ mol^{-1} for the 20 / 1 and 8 / 1 samples respectively. This does not confirm the hypothesis entirely as the Ea values are only an enthalpy and give no information on the type of motion involved. This was pursued by calculating the theoretical

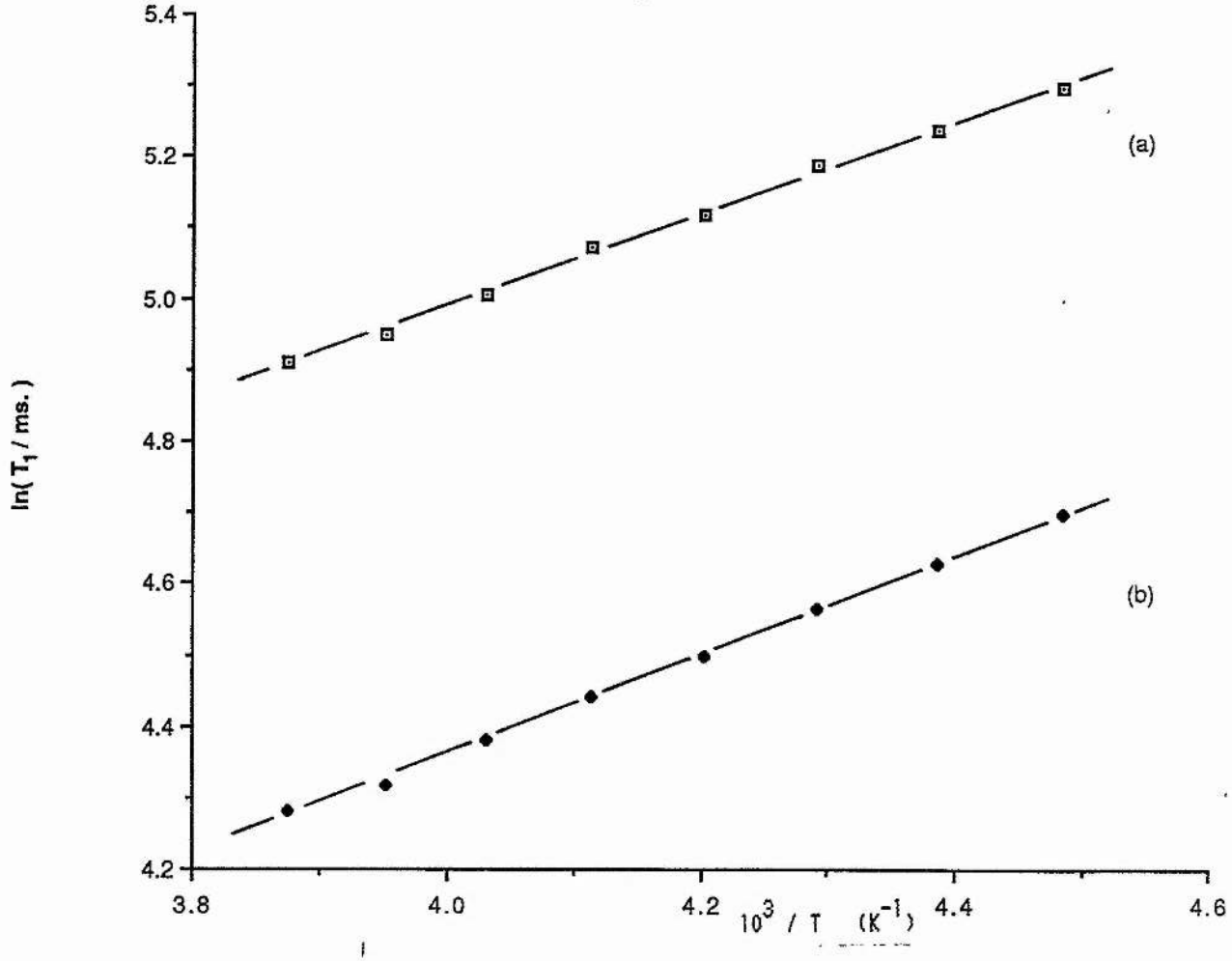

Fig. 3.21. Arrhenius plots of T_1 vs. temperature for ^{19}F in (a) $PEO(400)e_8LiCF_3SO_3$ (b) $PEO(400)e_{20}LiCF_3SO_3$.

rotational barrier in $CF_3SO_3^-$ by quantum mechanical means. (Only the result is given here, details of the calculation are located in Appendix 2.) This was found to be 6.3 kJ mol^{-1}, which is in good agreement with the nmr - calculated values and supports the hypothesis.

The optimised bondlength parameters obtained from the quantum mechanical calculation also allowed an estimate for the theoretical value at the T_1 minimum for the three - spin CF_3 rotor. This followed the method of Pajak[113], who showed that the relaxation time of an axially rotating three spin system (i.e F_3) could be expressed as :

$$(T_1)^{-1} = \frac{9}{20}\frac{C^2}{r^6}\left[\frac{\tau_c}{1 + \omega_o^2\tau_c^2} + \frac{4\tau_c}{1 + 4\omega_o^2\tau_c^2}\right] \quad (3.18)$$

where C is a constant (= 7.5×10^{-25} m^3s^{-1} for ^1H[102,113] and 6.64×10^{-25} m^3s^{-1} for ^{19}F), r = 2.17 Å is the inter fluorine distance in the CF_3 rotor, obtained from the quantum mechanical calculation. $\omega_o\tau_c$ = 0.616 in this case hence at 49.8 MHz the term in square brackets in (3.18) is equal to 4.54×10^{-9} s. Hence :

$$(T_1)^{-1} = \frac{9 \times (6.64 \times 10^{-25})^2 \times 4.54 \times 10^{-9}}{20 \times (2.17 \times 10^{-10})^6}$$

$$= 8.62 \ s.^{-1}$$

and

$$T_1 = 116 \ ms.$$

which is in good agreement with the experimentally obtained results for ^{19}F at the T_1 minimum ($T_1 \simeq 130$ ms. for the 8 / 1 sample and $\simeq 80$ ms. for the 20 / 1).

3.4.2.4 Diffusion coefficient measurement using spin - echo methods.

The nmr technique lends itself to the study of bulk diffusion in solids and liquids by the use of one of several spin - echo methods[30,31]. Indeed, as a means of probing diffusive motion in polymers, pulsed field gradient nmr finds common use[31,34]. With this in mind, it was decided to study diffusive behaviour in the PEO(400)e, 20 / 1 and 8 / 1 samples by the spin - echo method.

The Carr - Purcell spin - echo experiment was outlined in the experimental section (3.3.4) as a method for overcoming the inhomogeneities in B_o which limit the observed transverse relaxation for T_2 values $\geq$ 700 μs. It was shown that for a $\pi/2 - \delta - \pi$ pulse sequence, the initial 90° pulse tips the equilibrium magnetization into the xy plane where the spins begin to defocus (dephase). The spins could then be refocused by the application of a 180° pulse, giving an echo at 2δ. In the absence of translational motion the amplitude of the spin - echo as a function of the pulse separation, $A(\delta)$, would be given by[102] :

$$A(2\delta) \quad \alpha \quad \exp. \ (-2 \ \delta \ / \ T_2) \qquad (3.19)$$

hence a plot of ln (echo amplitude) vs. δ allows determination of the true T_2 value, overcoming inhomogeneity problems.

Whereas many nmr studies need a homogeneous B_o, the observation of bulk diffusive effects in the experiments detailed here *require* an inhomogeneous field. This is because the precise refocusing of the magnetization at 2δ is dependent upon each nucleus remaining in a constant magnetic field during the time of the experiment. If diffusion causes nuclei to move from one part of an inhomogeneous field to another, then the refocusing of $M_{x,y}$ will be incomplete and the echo amplitude reduced. Theory shows[102] that where diffusion occurs the echo amplitude will now be given by:

$$A(2\delta) \quad \alpha \quad \exp.\ [-(2\delta / T_2) - {}^{2}/_{3}\,\gamma^2 G^2 D \delta^3] \qquad (3.20)$$

where the new term describes the echo attenuation due to diffusion. G is the magnetic field gradient and D the diffusion term. A typical example of diffusive attenuation is shown in Fig. 3.22. for the proton signal in PEO(400)e at 321 K. At short times the behaviour is linear but the δ^3 dependence of the new term predicts correctly that diffusive attenuation of the echo increases at longer times, allowing evaluation of the diffusion coefficient if other terms are known.

The effect of temperature upon this diffusive attenuation is shown in Fig. 3.23. for the 20 / 1 sample, where, as one would expect, a greater effect is observed with increasing temperature, intimating a larger diffusion coefficient term in equation (3.20).

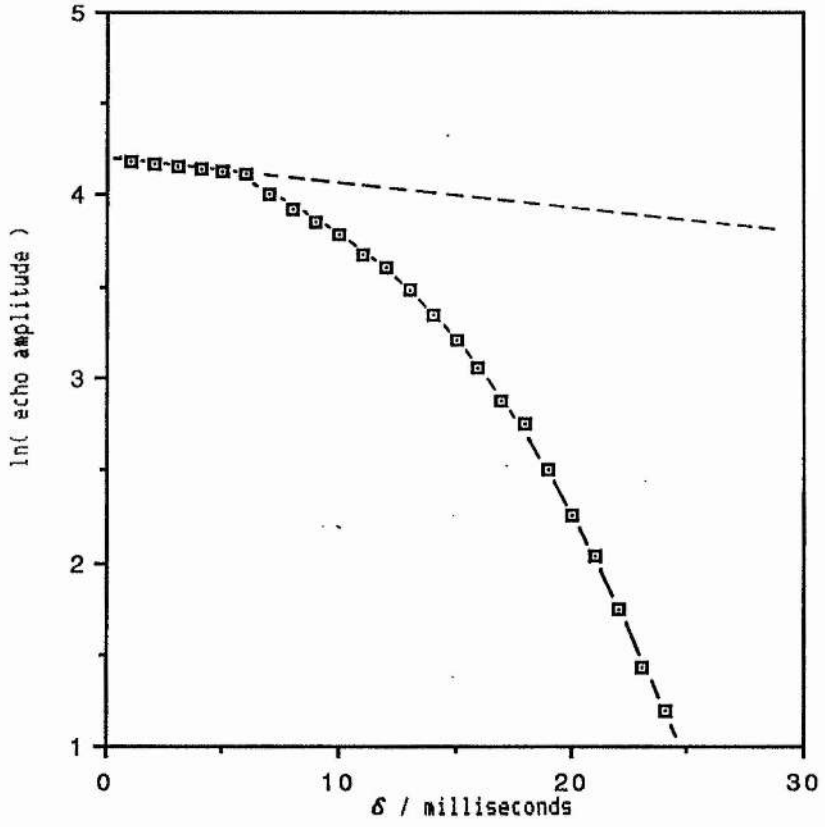

Fig. 3.22. Spin - echo amplitude (^{1}H signal) vs. pulse spacing, δ, following a Carr - Purcell pulse sequence [$\pi/2$ - δ - π] in PEO(400)e at 321K.

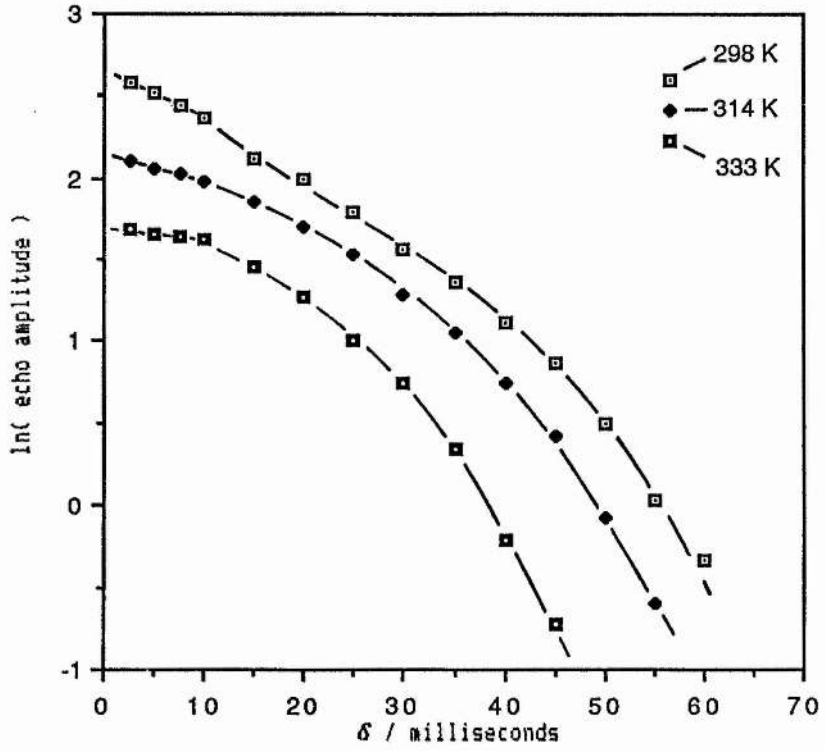

Fig. 3.23. The effect of temperature upon the diffusive attenuation of the spin - echo amplitude (^{1}H signal) in PEO(400)e_{20} $LiCF_3SO_3$.

In practice, the G term was maximised by locating the sample in an inhomogeneous part of the magnetic field. The effect on the fid was immediate, with the observed T_2 of $\approx$ 700 μs in the most homogeneous field reduced to about 15 μs. From this value the field gradient may be calculated as[114] :

$$G = 2\pi / (4 \times 10^{7} T_2 \times d) \qquad (3.21)$$

Where d is the sample diameter (metres) across which the field gradient acts, and T_2^{-1} (Hertz) is expressed in Tesla units. The sample diameter was 1 cm. and with T_2 = 15.5 μs,the field gradient was calculated to be G = 1.01 Tm^{-1}.

Knowledge of the field gradient term now allows the calculation of diffusion coefficient data if echo amplitudes are monitored as a function of pulse spacing, δ. In practice this was achieved by plotting ln (echo amplitude) against δ and extrapolating the linear portion at short times across the δ range. Inspection of equation 3.20. and Fig. 3.22. shows that the difference between the extrapolated line and the actual data, Δln A(2δ), corresponds to the diffusive attenuation term :

$$\Delta \ln A(2\delta) = {}^{2}/_{3} \gamma^2 G^2 D \delta^3 \qquad (3.22)$$

thus

$$D = 3 \Delta \ln A(2\delta) / 2 \gamma^2 G^2 \delta^3 \qquad (3.23)$$

The diffusion coefficient data could then be determined from the gradient of a further plot of $\Delta \ln A(2\delta)$ against δ^3, as shown in Fig. 3.24. for PEO(400)e at 321 K. In this data the gradient was found to be 19.15×10^4 s^{-3}. γ is $\gamma({}^1H)$, the proton gyromagnetic ratio hence :

$$\text{gradient} = {}^2/_3 \gamma^2 G^2 D$$

$$\therefore \quad D = \frac{3 \times 19.15 \times 10^4}{2 \times (42.577 \times 10^6 \times 1.01)^2} :$$

$$= 15.5 \times 10^{-11} \ m^2 \ s^{-1}$$

$$= 1.54 \times 10^{-6} \ cm^2 \ s^{-1}$$

Data obtained in this way are shown in Table 3.3. As expected, the self - diffusion coefficients for a given sample increase with temperature, obviously a viscosity effect, as well as a there being a strong effect of salt addition upon chain diffusion i.e at 314 K ;

PEO(400)e ;	D =	128 $\times 10^{-8}$	$cm^2 \ s^{-1}$
20 / 1 ;	=	9.7	"
8 / 1 ;	<	2.0	"

showing that an approximately 1 mol kg^{-1} solution (20 / 1 sample) gives rise to about a ten - fold increase in the diffusion coefficient compared to the pure solvent while the 8 / 1 sample imparts more than a fifty - fold increase. (This is why the temperature ranges of study were different for the three samples, diffusive attenuation could only be observed at higher temperatures for the most concentrated solution.)

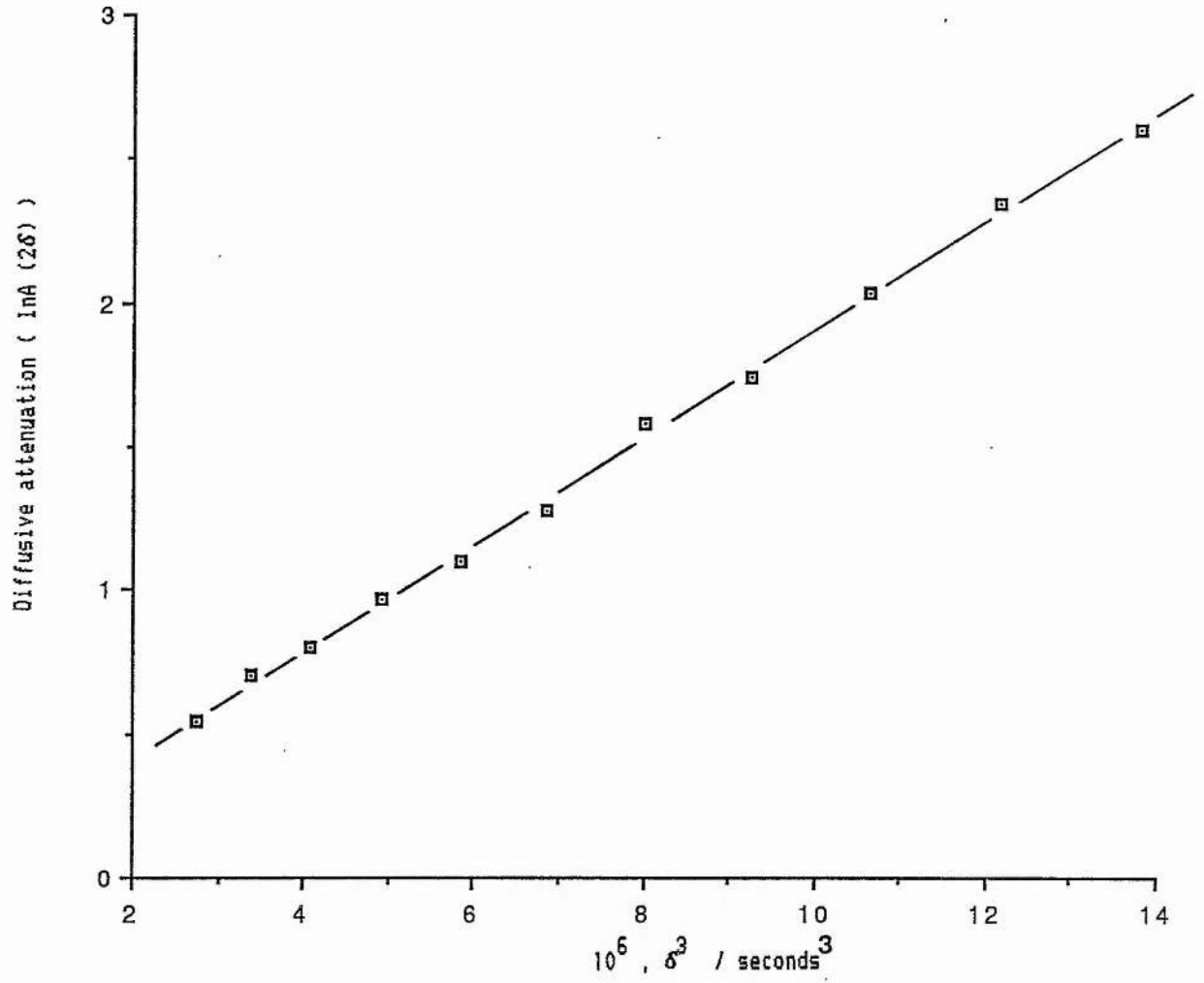

Fig. 3.24. Plot of diffusive attenuation ($\Delta \ln A(2\delta)$) vs. δ^3 for the ^1H signal in PEO(400)e at 321 K.

PEO(400)e		$PEO(400)e_{20}LiCF_3SO_3$		$PEO(400)e_8LiCF_3SO_3$	
Temp. /K.	D	Temp. /K.	D	Temp. /K	D
283	46.5				
289	54.6				
293	68.1				
299	85.7	298	4.8		
305	91.9	306	6.7		
314	127.8	314	9.7	318	2.3
321	155.0	322	14.5	325	3.1
329	198.4	333	18.8	332	4.1
				340	5.7
				352	7.6

(Diffusion coefficient = D . 10^{-8} cm^2 s^{-1})

Table 3.3. Spin - echo diffusion data for PEO(400)e systems.

$PEO(400)e_{20}LiCF_3SO_3$		$PEO(400)e_8LiCF_3SO_3$	
Temp. /K.	D_s	Temp. /K.	D_s
313	4.9	316	1.9
318	6.1	318	2.1
323	7.5	321	2.5
328	9.1	324	3.0
332	10.6	327	3.4
338	12.5	332	4.2
343	14.6	335	5.0
349	17.2	338	5.7
		343	7.1
		348	8.1

(Diffusion coefficient = D_s . 10^{-8} cm^2 s^{-1})

Table 3.4. Salt diffusion data for PEO(400)e systems obtained from conductance data via the Nernst - Einstein equation.

The behaviour can perhaps be contrasted with aqueous solution, where a 4 mol kg^{-1} NaCl solution at 298 K shows only a 1.5 - fold viscosity increase relative to pure water[115].

It is perhaps unfortunate that the diffusive characteristics of the salt (the lithium cation and $CF_3SO_3^-$ anion) could not be studied here with the spin - echo technique; transport data as a function of temperature would immediately follow[31]. This was principally due the lower relative ^7Li and ^{19}F concentration than ^1H in the samples giving smaller echo amplitudes which were soon lost in noise levels of the spectrometer. Table 3.4 . however, shows salt diffusion coefficient data as a function of temperature for the 20 / 1 and 8 / 1 samples, calculated from the relevant conductance data and the Nernst - Einstein relation[32]:

$$\sigma/c = z^2 F^2 D_s / RT \qquad (3.24)$$

where

$$D_s = 2t_{Li^+} \cdot D_{CF_3SO_3^-} = 2t_{CF_3SO_3^-} \cdot D_{Li^+} \qquad (3.25)$$

F is the Faraday, z the ionic charge, c the salt concentration and the other terms have the usual meanings. This equation finds standard use in media such as superionic conductors[116], describing the conductance of Na^+ in β - alumina for example, but its application to polymer electrolyte systems where a jump - distance distribution probably occurs, and not a discreet jump distance as the Nernst - Einstein eqn. postulates, has been questioned[116]. Nevertheless, this has not stopped several authors using it;

Berthier[22] for example, found good agreement between the actual conductance and the number of charge carriers predicted by nmr, via the Landau correction and Nernst - Einstein relation for PEO.$LiCF_3SO_3$.

Reasonable agreement is found here, especially for the 8 / 1 sample, a correlation between the salt and polymer chain diffusion coefficients indicating simply that viscosity determines the ionic motion, which is a free - volume concept[35]. It must be noted that the *total* salt concentration was used as the charge carrier concentration in the above Nernst - Einstein calculation, whereas it has been proposed that a much smaller concentration of conducting species than the actual salt content exists in dilute PEO(400)e solution. This does not necessarily invalidate the proposed behaviour in either regime however; Chadwick[117] has evaluated the salt diffusion coefficient in low mol. wt. (tetraglyme) PEO.NaSCN solutions by both conductance and radiotracer techniques. If we consider that the conductance monitors only the motion of the charged species, D(σ), and radiotracer techniques the translational motion of all species, D(tot.), then :

$$D(\sigma) / D(\text{tot.}) \ll 1$$

would mean extensive formation of neutral mobile clusters. This was found at lower concentrations, supporting the low concentration conductance results presented here (2.3.1). Chadwick found though that the D(σ) / D(tot.) ratio was unity at higher salt concentrations, supporting currents views[116] that at higher

concentrations in polyether electrolytes a quasi fused - salt situation exists, where all the salt contributes to the conductance.

It is also recognised that the nmr and the conductance diffusion coefficients determined here can have error sources; in the field gradient term for the former where the short T_2 value used may be $T_2 \pm 3\mu s$, and the use of molal concentration and not molar values in the latter. The problems are negated however if the temperature dependence of both the diffusion coefficient for the polymer and the conductance for the salt are monitored. This is shown in Fig. 3.25. for the three samples studied where the relevant transport properties are plotted against reduced temperature i.e the VTF form described earlier, with T_o = 220K. The conductances were found to show the usual non - linear Arrhenius behaviour and it is certain that the data fit to linearity in the region of T_o = 220 K. The nmr diffusion data however are subject to more scatter so linearity with T_o in the region of 220 K is more uncertain but comparison of the Ea terms resultant from such plots are interesting, and are shown below in Table 3.5. :

Sample:	PEO(400)e	20 / 1	8 / 1
Ea(σ). kJ mol^{-1}.	(2.0)	3.2	4.3
Ea(D). "	≃ 1.9	≃ 3.0	≃ 4.0

Table. 3.5. Comparison of nmr and conductivity Ea terms for PEO(400)e solutions.

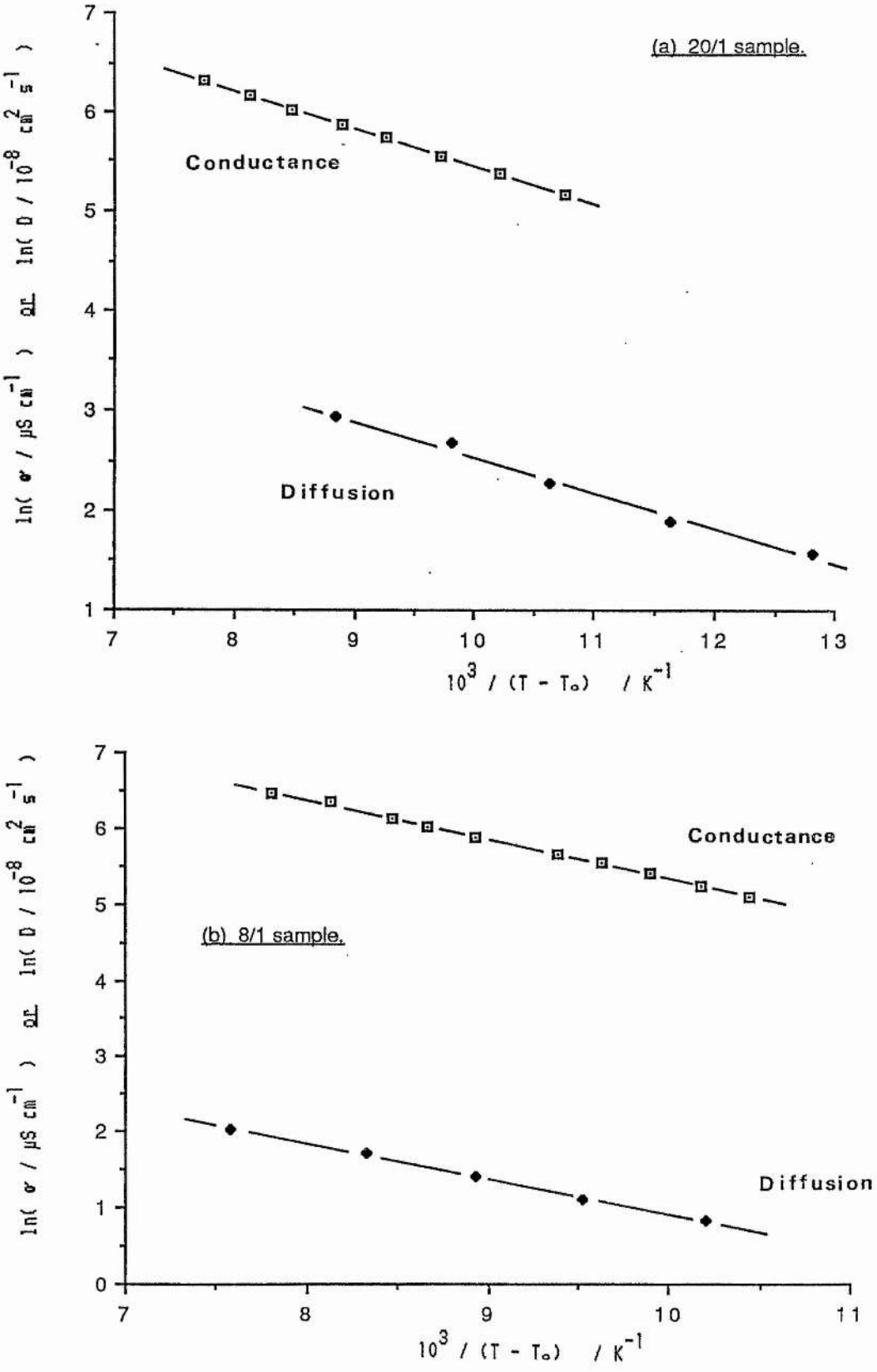

Fig. 3.25. Semilogarithmic plots of conductance and diffusion (^1H) data against reduced temperature, $T - T_o$ (T_o = 220 K), for (a) PEO(400)$e_{20}LiCF_3SO_3$, (b) PEO(400)$e_8LiCF_3SO_3$ and PEO(400)e (next page).

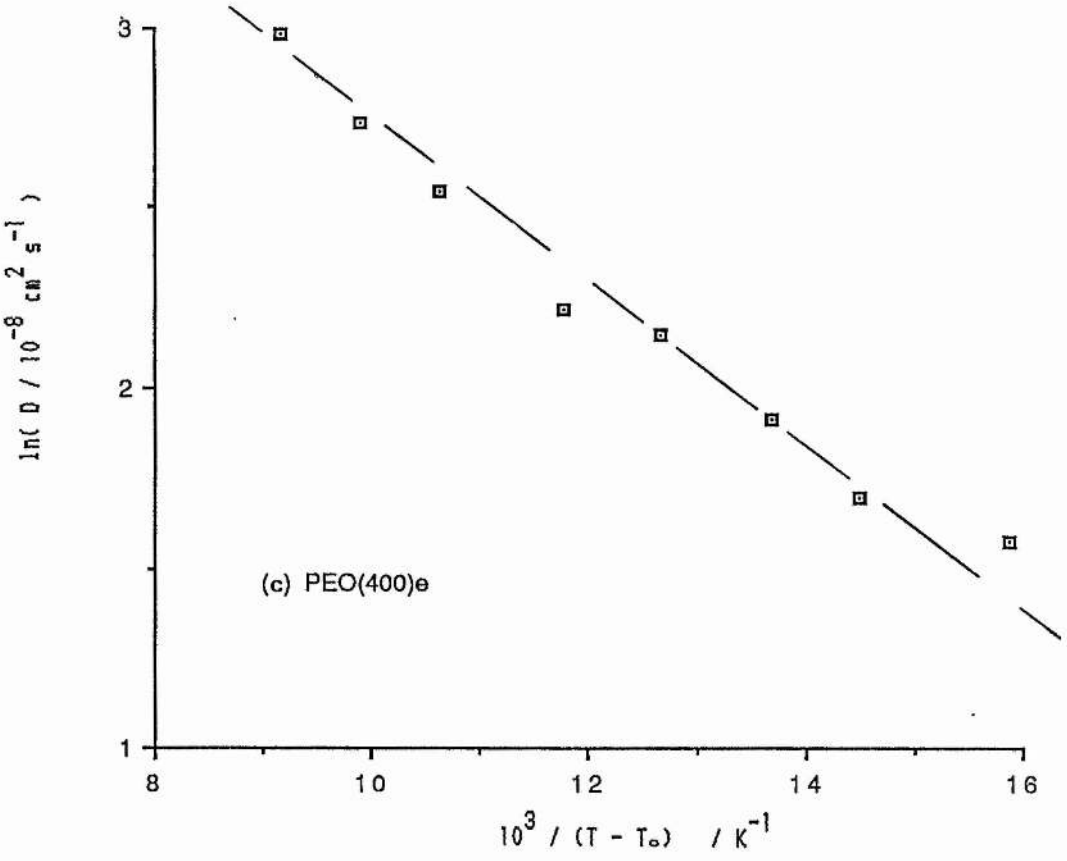

Fig. 3.25. (c) Semilogarithmic plot of diffusion data against reduced temperature, $T - T_o$ (T_o = 220 K), for PEO(400)e.

Ea(σ) represents the apparent activation term for the conductance data and Ea(D) that term for the nmr data. The bracketed value is the activation term obtained for low salt concentrations (0.003 - 0.06 mol kg^{-1}) in PEO(400)e. There would appear to be a correlation here, explainable as the viscosity of the solution, proportional to D^{-1}, determining ionic transport. The data finds qualitative agreement with that of Hall *et al*[25], who found an increased temperature dependence of conductance with increased viscosity for higher salt concentrations of $LiClO_4$ in tetraglyme, $CH_3O \leftarrow CH_2CH_2O \rightarrow_4 CH_3$.

Chapter 4

4. NMR STUDIES ON HIGH MOLECULAR WEIGHT POLY(ETHYLENE OXIDE) - BASED SYSTEMS

4.1 Introduction.

Nuclear magnetic resonance results will now be presented for materials which comprise the conventional polyether electrolyte; a solution of high molecular weight poly(ethylene oxide) containing an inorganic salt.

The concepts applicable to the nmr study of such systems are essentially the same as those detailed for lower mol. wt. polyether solutions but are complicated by several factors;

(1) Phase heterogeneity i.e the co - existence of crystalline and amorphous domains, occurs over a wide range of temperature.

(2) The distribution of salt within such systems is uneven, with differing amounts in the respective crystalline and amorphous phases.

(3) The relative proportions of the various phases and hence the amount of salt in the amorphous (conducting) phase, is temperature dependent.

The reasons for a nmr study of such systems is that, in principle, all the above factors can be addressed, provided the technique can monitor and assign phase behaviour to both the polymer and the salt.

Much of the groundwork for this study has been presented by Berthier and co - workers[22,23,41] who investigated the phase behaviour of both polymer and salt in several systems; PEO.$LiCF_3SO_3$, PEO.$LiClO_4$ and PEO.NaI. Conclusions drawn from such studies were that the ether oxygen to salt stoichiometry of the so - called crystalline salt rich phase was less than the 4 / 1 previously proposed[1], and that the amorphous phase, not the crystalline, was responsible for the conductance.

In this chapter a more detailed nmr examination of the PEO.$LiCF_3SO_3$ system is presented, coupled with and reinforced by results for the pure polymer and pure salt.

4.2 Results and discussion.

4.2.1 Poly(ethylene oxide)

By way of an introduction to the heterogeneous case, initial focus is given to poly(ethylene oxide), PEO, molecular weight 4×10^6. The polymer is semi - crystalline at room temperature containing only about 10% amorphous material. Differential scanning calorimetry (DSC) indicates[13] the occurrence of two thermal events, consistent with a glass transition at ca. 225 K (amorphous phase) and a melt transition at ca. 333 K (crystalline phase). Above the melt transition the polymer is single phase, totally amorphous.

4.2.1.1 Transverse relaxation time data.

The nmr data shown in Fig. 4.1. for the sample used here are in good agreement with the DSC results, where the amorphous content has been calculated as the ratio of the amplitude of the long T_2 signal to the total fid amplitude, as outlined in 3.2.6. At temperatures below about 223 K the observed fid was found to be single component, short T_2. Above this value the fid was two - component, with the appearance of a longer T_2 signal identifying motion within the amorphous phase i.e the

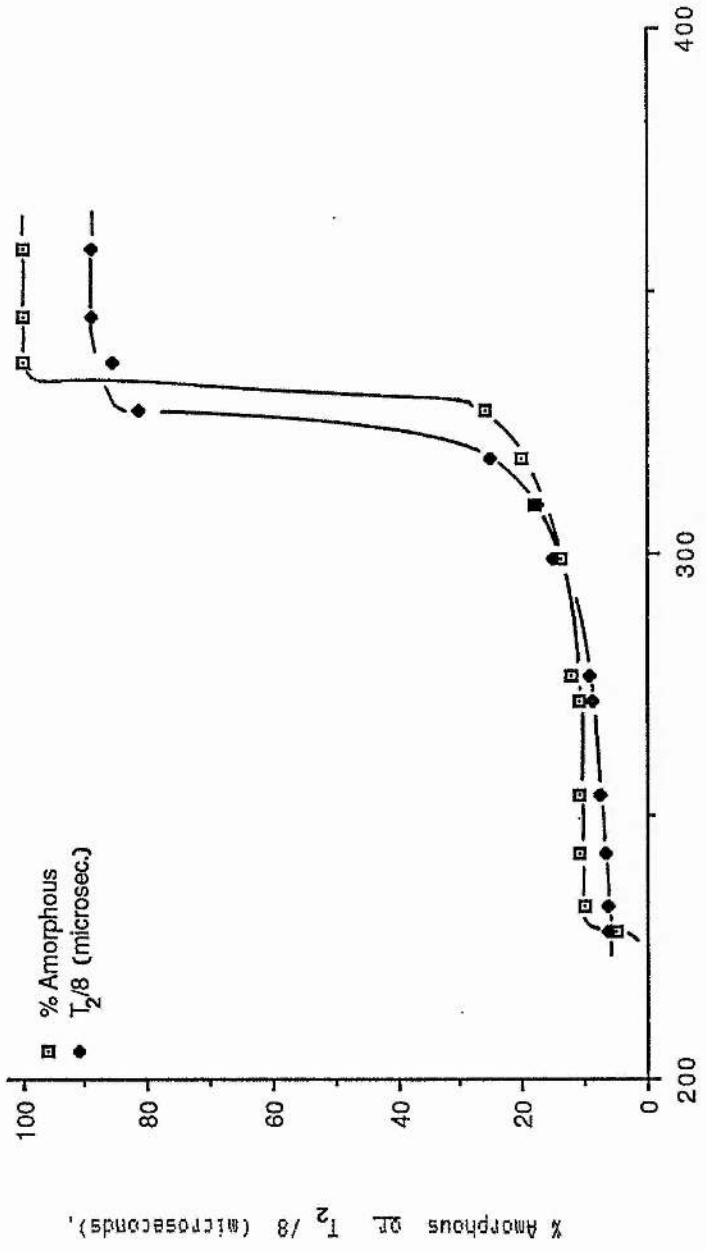

Fig. 4.1. Plots of the percentage amorphous content (i,e the amount of long T_2 component) and the actual T_2 values for that component, vs, temperature, for the ^1H signal in poly(ethylene oxide), molecular weight 4×10^6.

glass transition region. This fraction of amorphous component remained constant at 12% until a major event was noted at (328 - 333) K, signifying the melting of PEO crystallites, to give a single component long T_2 signal, representative of the amorphous phase.

Also included in the figure are the actual long T_2 signal values, which are observed to follow closely the actual amount of amorphous material in the sample. The data are essentially constant until a progressive lengthening was noted in the fid with temperature from about 293 K and then a surge to the homogeneity limit from (323 - 333) K i.e the crystalline PEO melting region. The fact that such a large change occurs in the T_2 values ($\simeq$ 150 μs to > 700 μs) upon going from an amorphous component at 313 K to the same material at 338 K is a comment upon polymer physics and has been observed in several semi - crystalline polymers[11e]. For many polymeric materials below the crystalline melting temperature, amorphous components can be envisaged as comprising only short, hindered motion, links between the crystallites. With the melting transition and removal of motional constraints will come a considerable mobility gain and averaging of spin - spin interactions, giving a much longer T_2 fid.

4.2.1.2 Longitudinal relaxation time data.

In a similar manner to T_2 evaluation, analysis of the two component free induction decay also permitted determination of spin - lattice relaxation times for the crystalline and amorphous phases, which are shown in Fig. 4.2. (Pulse sequences and T_1 calculation have been described fully in 3.3.5.)

Inspection of Fig. 4.2. shows that at most temperatures T_1 values for the crystalline phase are about an order of magnitude larger than the corresponding amorphous values. For crystalline polymer components the longitudinal relaxation mechanism is usually envisaged as due to restricted amplitude oscillations of all chains about main chain axes[1,9], which is not as efficient a dipolar relaxation mechanism (and hence gives longer T_1 values) as the larger amplitude motions occuring in amorphous components above the glass transition temperature. This allows the statement that the respective spin systems (i.e crystalline and amorphous) are for the most part isolated from each other. What this means is that the processes by which the crystalline and amorphous domains lose absorbed rf energy as heat in returning to the equilibrium state are different, and that the exchange of energy between the two spin systems is not a dominant feature.

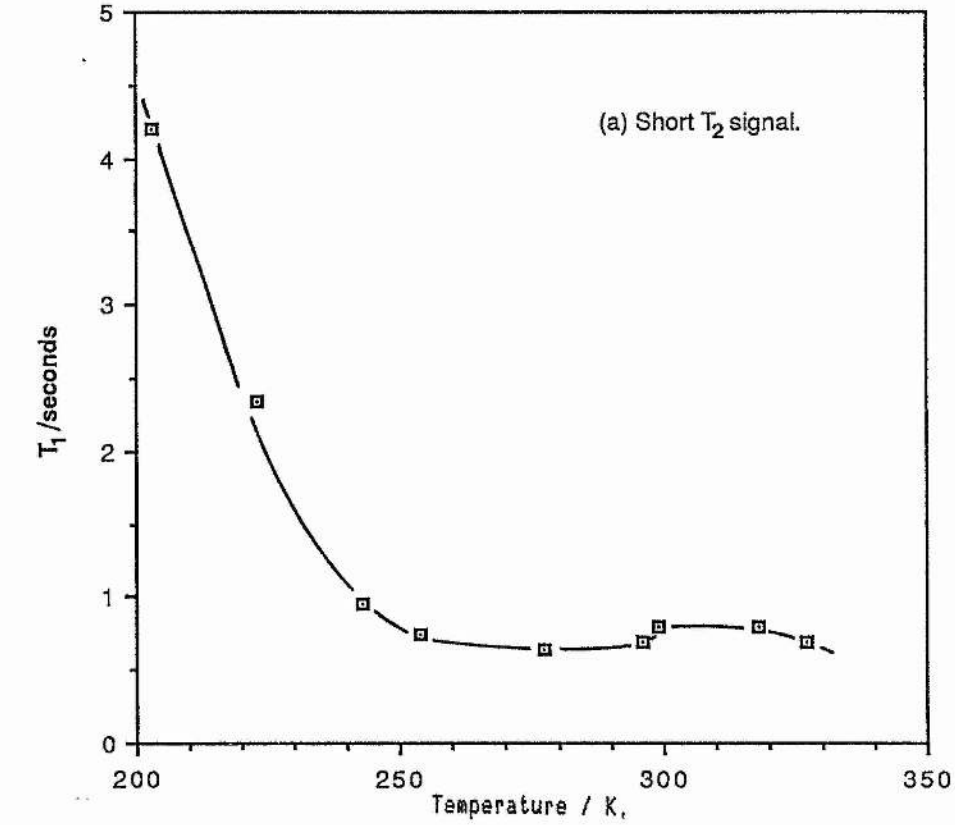

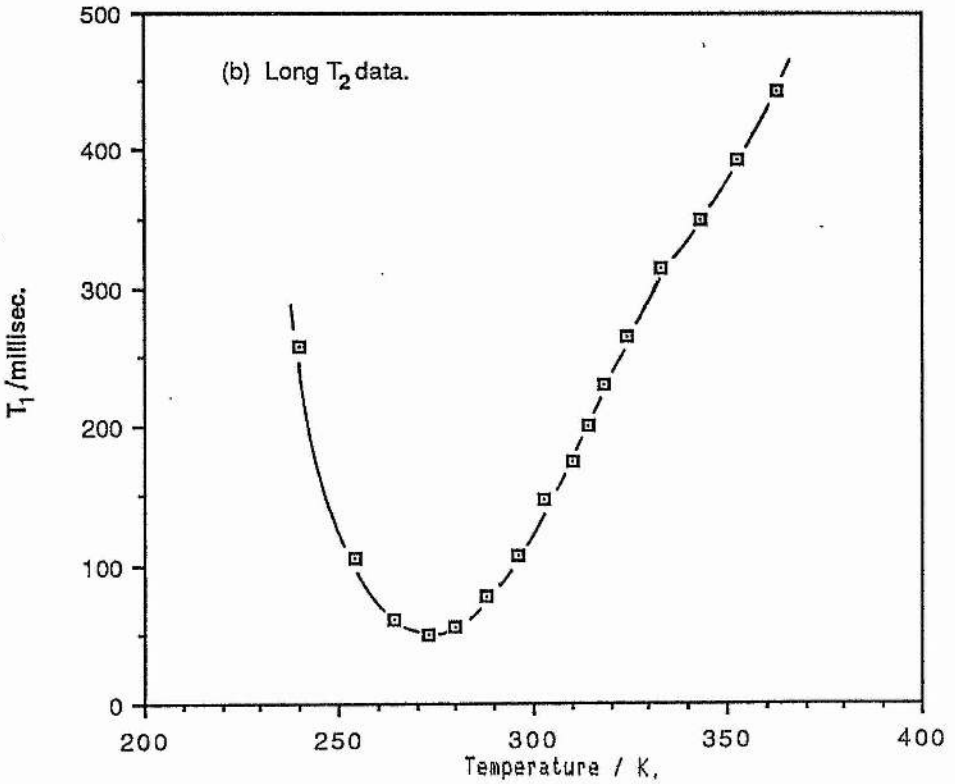

Fig. 4.2. Longitudonal relaxation time (T_1) data for (a) the short T_2 signal (crystalline material) and (b) the long T_2 signal (amorphous material) in poly(ethylene oxide), molecular weight 4×10^6.

The T_1 data for the amorphous component were found to show a minimum value of 50 ms. at 273 K and a distinct change of slope at about 333 K. There are two possible explanations for the reduced temperature dependence of T_1 above the latter temperature:

(a) The melting of PEO crystallites yields an amorphous phase with a wider distribution of correlation times for the motion(s) responsible for the relaxation than in the amorphous component below 333 K.

(b) Reduced motional constraints above 333 K mean a lower activation barrier for the motion. (BPP theory[100] predicts that $T_1 \alpha \exp(-Ea / RT)$.)

Given that the observed T_1 changes occur where T_2 considerations imply increased motional freedom in the amorphous phase, it is suggested that the latter case is responsible for the observed behaviour.

4.2.2 The nmr response of PEO.$LiCF_3SO_3$ systems.

Lithium Trifluoromethanesulphonate, $LiCF_3SO_3$, is one of the most popular salts used in the formation of polymer electrolyte materials. It dissolves in poly(ethylene oxide) to high molar concentration, giving a heterophase material where the salt exists in two forms:

(1) As a component of a crystalline phase, melting at temperatures greater than about 445 K, which contains 3.5 moles of ether oxygen units per mole of salt (i.e EO / Li $\simeq$ 3.5 / 1).

(2) In solid solution in the amorphous phase, which is considered to be responsible for the high ionic conductivity of the electrolyte.

Various studies, based mainly on nmr, DSC, optical microscopy and conductivity[22,120,121], have led to the elucidation of the phase diagram for the electrolyte, which is shown in Fig. 4.3. The diagram shows the occurrence of the above phases as well as pure crystalline PEO, the relative amounts of which depending on the total salt content and temperature. (Certain authors[18] have suggested a eutectic polymer - salt composition at very low salt concentrations but this does not concern us for the molar ratios used here.)

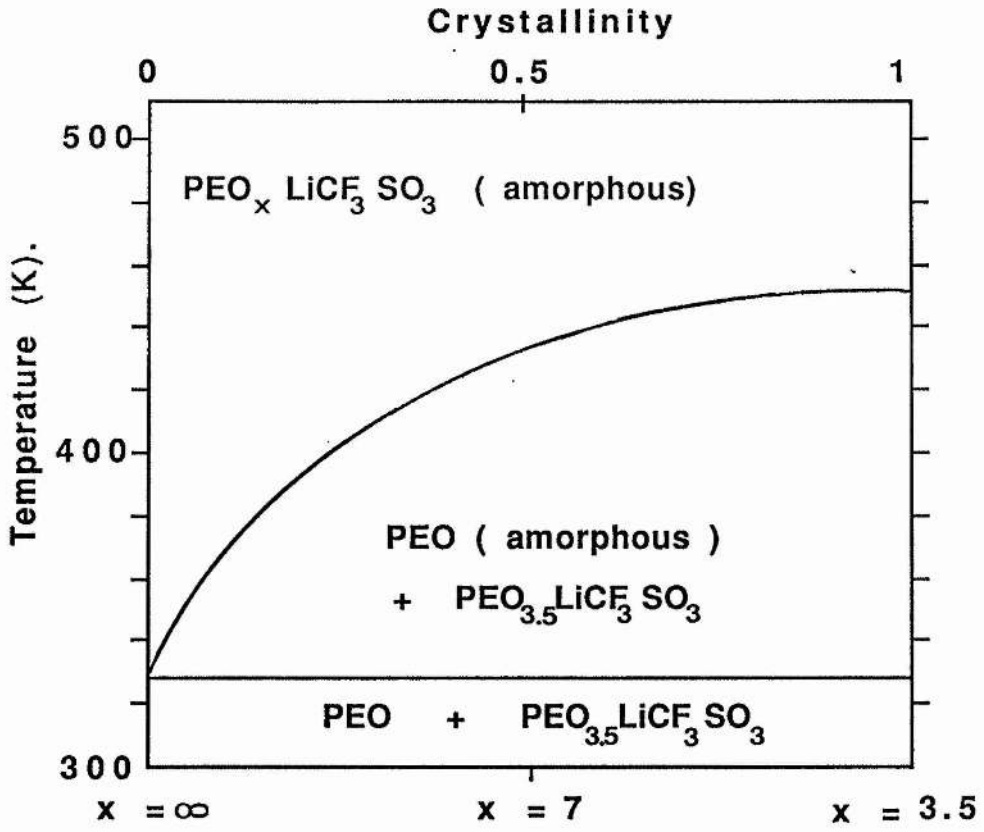

Fig. 4.3. PEO$_x$ LiCF$_3$ SO$_3$ phase diagram.

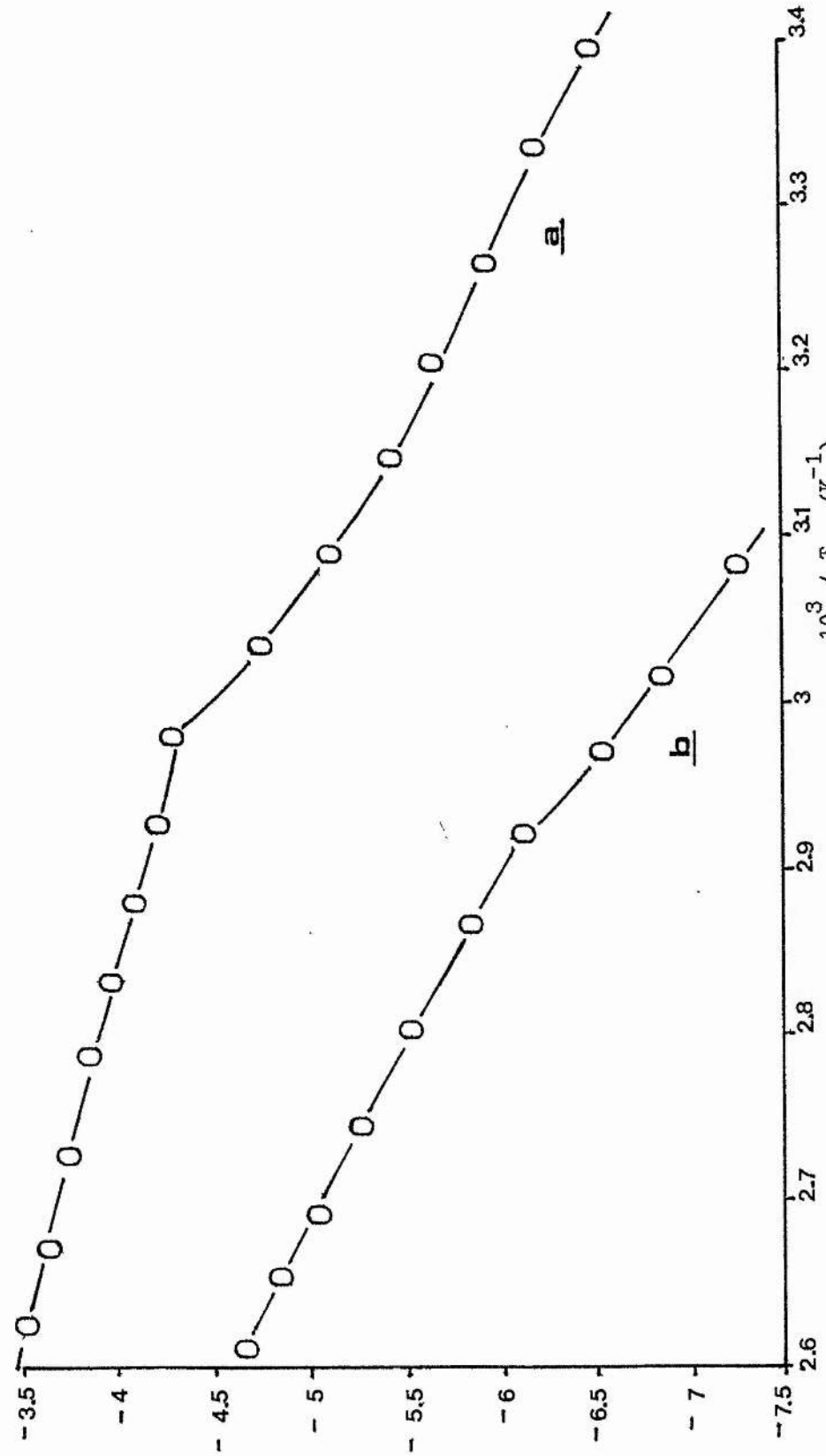

Fig. 4.4. Semilogarithmic plots of conductance vs. temperature for (a) $PEO_8LiCF_3SO_3$ and (b) $PEO_4LiCF_3SO_3$. (Data from reference [122]).

Two $PEO.LiCF_3SO_3$ samples were investigated in this study, with EO / Li mole ratio equal to 4 / 1 and 9 / 1. The following assignments are made :

$PEO_4LiCF_3SO_3$ → 4 / 1 sample.

$PEO_9LiCF_3SO_3$ → 9 / 1 sample.

The available conductance data[18,22,122] for electrolytes with similar overall stoichiometries are shown in Fig. 4.4. The data show the well known result that those electrolytes of the order of 4 / 1 composition are poor conductors compared to what is regarded as the optimum stoichiometry of EO / Li = (8 - 10) / 1.

4.2.2.1 Measurements based upon free induction decay amplitudes.

(a) ^1H and ^{19}F data.

The free induction decays of ^1H and ^{19}F nuclei in the 4 / 1 and 9 / 1 samples were found to be characterised by two - component behaviour over a range of temperatures. In a similar manner to earlier results the decay components for a given nuclear type were resolvable into crystalline or low mobility fractions (short T_2 values) and amorphous or mobile fractions, with long T_2 values. This in turn allowed evaluation of the phase behaviour of the polymer (^1H) and $CF_3SO_3^-$ anion (^{19}F) as a function of temperature for both samples (Fig. 4.5.).

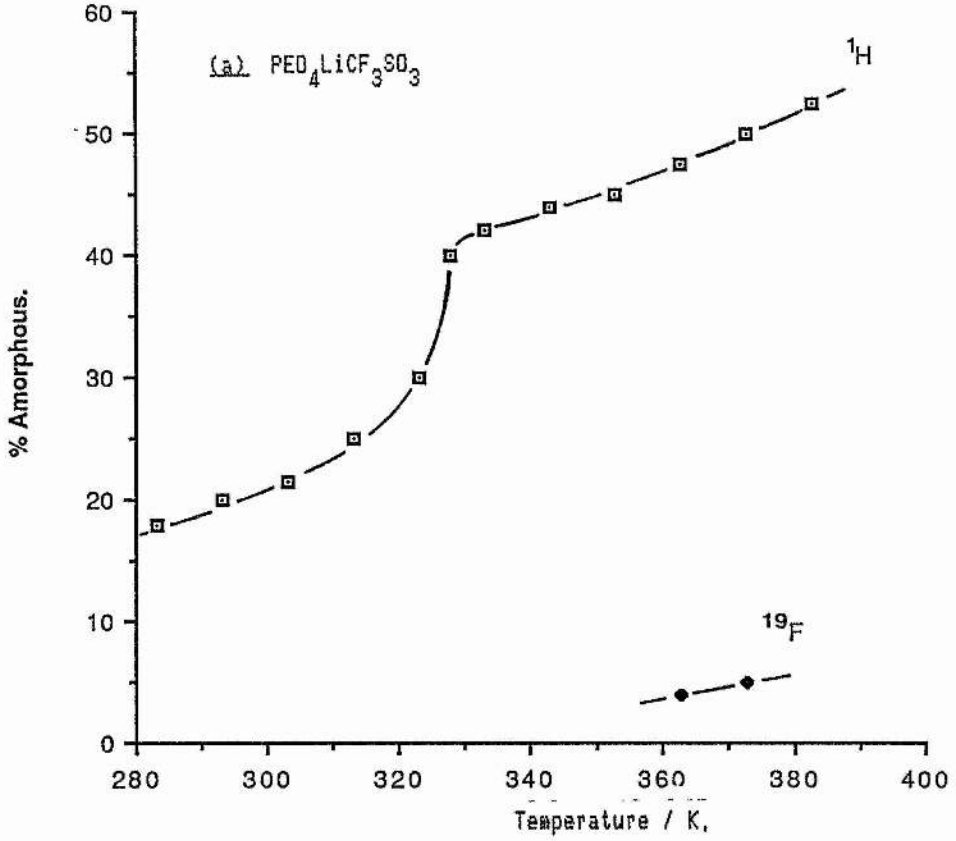

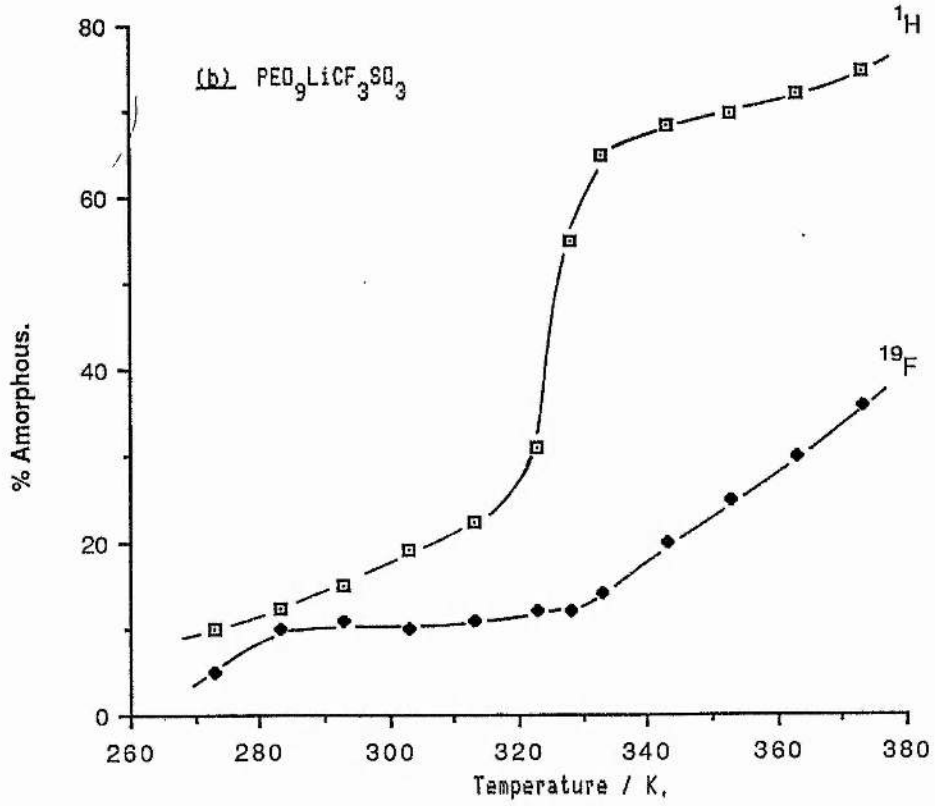

Fig. 4.5. The percentage amorphous (long T_2 component) vs. temperature for the ^1H and ^{19}F signals in (a) $PEO_4LiCF_3SO_3$ and (b) $PEO_9LiCF_3SO_3$.

The phase diagram for PEO.$LiCF_3SO_3$ predicts that the 9 / 1 sample contains 60% pure PEO and 40% crystalline complex (EO / Li ≃ 3.5 / 1) at room temperature. Obviously no provision is made in it for estimation of the equilibrium amorphous content at this temperature. The nmr data show that the amorphous polymer content in the 9 / 1 sample remains below 25% at temperatures less than 313 K but increases sharply to about 68% between 328 K and 333 K, and is concurrent with the onset of the region of reduced apparent activation energy in the conductance plot. The same analysis for the ^{19}F data shows the absence of a sharp event at ≃ 330 K, clearly demonstrating that the increased amorphous fraction for the proton (polymer) signal comes from the melting of uncomplexed poly(ethylene oxide) giving a more extensive amorphous polymer phase and more facile ionic transport within it. This is perhaps reinforced in Fig. 4.6. where ^1H long T_2 values are shown for both samples. In the 9 / 1 case the T_2 profile is observed to follow closely that of the percentage amorphous component (Fig. 4.5.). At ≃ 330 K the fast rise to the homogeneity limit suggests an increased motional freedom for the amorphous component which again translates as a lower energy barrier to conduction. Above 333 K the remaining crystalline fraction is therefore that of the complex.

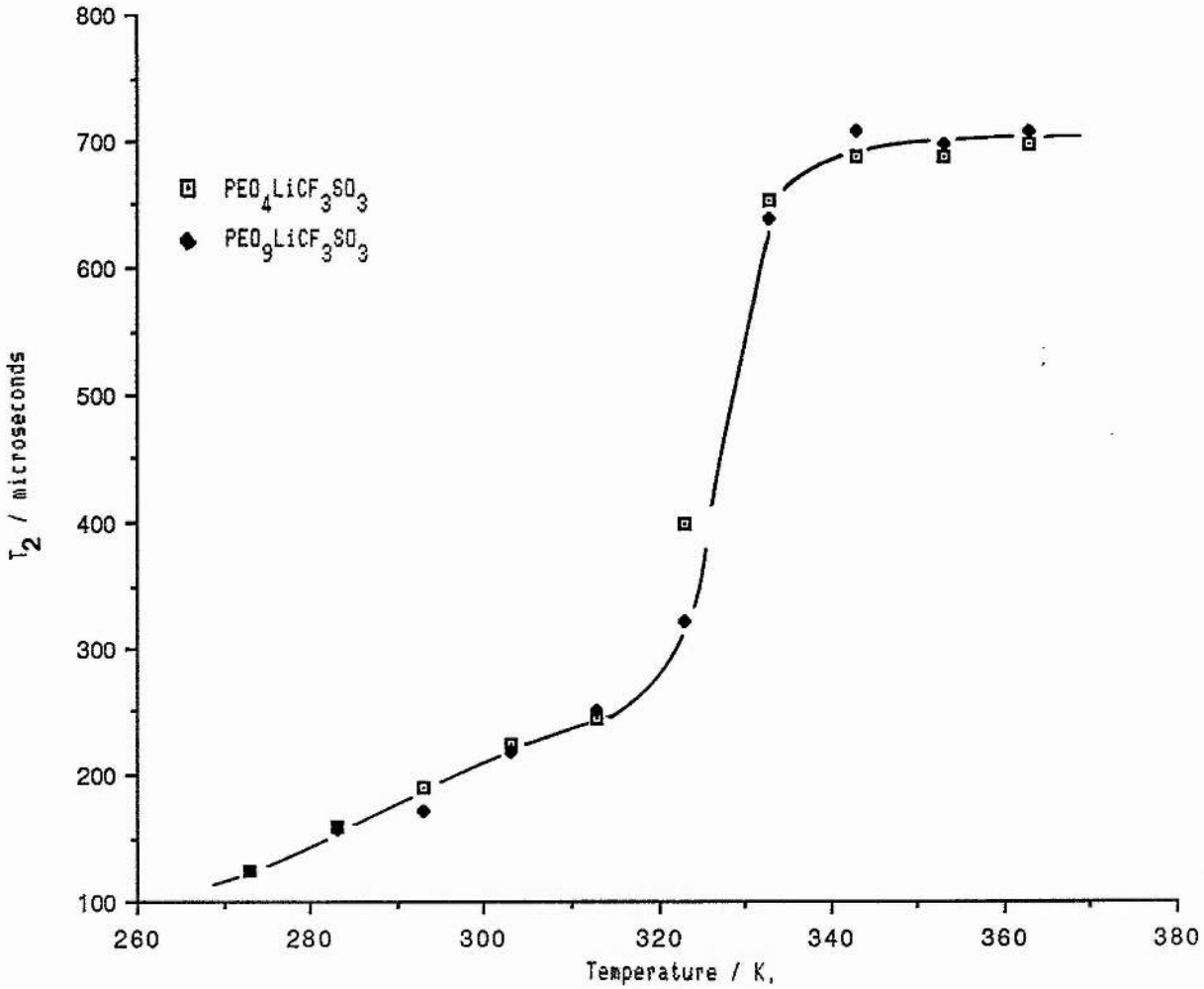

Fig. 4.6. T_2 vs. temperature for the ^1H long T_2 signal (polymer chain) in $PEO_4LiCF_3SO_3$ and $PEO_9LiCF_3SO_3$ samples.

Following Berthier[22], the nmr data above the pure PEO melt transition at 333 K can be used to estimate the stoichiometry of the complex in this particular sample, where the following relationship is applicable :

$$X_c = (X(^1H) \times n) / X(^{19}F) \qquad (4.1)$$

Here, X_c is the stoichiometry of the crystalline complex, $X(^1H)$ the remaining crystalline component above 333 K, n the overall stoichiometry of the sample i.e 9 / 1, and $X(^{19}F)$ the remaining crystalline fluorine component above 333 K. Hence, at 338 K :

$$X_c \simeq (0.325 \times 9) / 0.825$$

$$\simeq 3.5 \text{ EO / Li.}$$

The ^1H data for the 4 / 1 sample confirmed, as would be expected from the phase diagram, that this sample contained a larger crystalline complex fraction than the 9 / 1. Here, the percentage amorphous content showed only a small (≃ 12%) increase at (323 - 328) K, suggesting a smaller initial pure PEO content. Inspection of Figs. 4.6. and 4.4. show that this small melting event is important however, allowing increased motional freedom for the amorphous chains (evidenced by the T_2 data) and easier ionic transport, observed as a knee in the conductance plot.

In the 4 / 1 sample the surprising result was that the fluorine signal was found to be single component, short T_2 (≈ 30 μs) over most of the temperature range until above 360 K where a small amount ((5%) of long T_2 component was observed. This immediately infers that the number of mobile anionic species i.e charge carriers, is small in this sample and is entirely consistent with the 4 / 1 sample being a much poorer conductor than in similar electrolytes of somewhat lower overall salt content. (Indeed, this is a general feature of many PEO - based electrolytes.)

There is however a discontinuity in the predicted phase behaviour of the 4 / 1 material; the same calculation as for the 9 / 1 sample (equation 4.1) gives EO / Li ≈ 2.3 as the stoichiometry of the salt rich crystalline phase. This is an improbable value and an explanation will be presented at a later stage.

One of the most interesting features of the proton data for both samples in Fig. 4.5. is the *increasing* amorphous polymer fraction below 333K for both samples, rising by about 20% in a 40 K range from about 280 K. This behaviour seems to have received scant attention from other workers[13] who took few data points in this temperature range, concentrating their analyses above ≈ 333 K.

The behaviour contrasts that of the pure poly(ethylene oxide) sample, Fig. 4.1., which showed a smaller (≈ 12%) and temperature independent amorphous fraction below 333 K. If the pure PEO content of the salt containing samples shows a similar temperature independent amorphous fraction then attention focuses on the supposed crystalline complex as the source of the increasing amorphous component. Two possible scenarios are suggested, based upon previous characterisation of the crystalline domains in electrolyte materials of this type :

(1) The structure of the crystalline complex may well be of the type proposed by Hibma[91] , following x - ray analysis of PEO.NaI and PEO.KSCN, in which the salt was shown to occupy a gross three - dimensional array with polymer chains situated in channels delimited by the array. To quote Hibma, " the given chain conformation in the complex is just one of several conformations which can be written, all having similar energy". In chemical terms, this equates to the possibility of thermally stimulated transitions between conformer states. In nmr terms this would mean a motional process which could give rise to averaging of spin - spin interactions and thus a longer T_2 'amorphous' signal. The amplitude of this response would be expected to increase as temperature is increased, accessing more and more polymer conformations and so give rise to an increased 'amorphous' component.

(2) The crystalline complex has been shown to be spherulitic in nature[2] and as such a long T_2 component could originate from the outer regions of the spherulites[5], where increased disorder would permit motion of polymer chains at lower temperatures than in the crystalline , ordered, inner regions. As temperature increases the motional averaging giving rise to the longer T_2 signal would occur progressively towards the spherulite centre, giving an increased 'amorphous' component.

Either situation explains the observation that the 4 / 1 sample shows a larger amorphous content than the 9 / 1 at temperatures below 333 K; the origins of the long T_2 signal has some of its base in the crystalline complex. There is more of this material in the 4 / 1 sample hence a larger contribution to the long T_2 signal than in the 9 / 1 sample. (The data presented here in fact goes against what would perhaps be a conventional view. This would expect a larger amorphous contribution from the 9 / 1 sample based upon there being a greater PEO fraction with associated amorphous content, and more PEO - crystalline complex boundaries.) The discontinuity observed above, based on the calculation of complex stoichiometry from the observed nmr crystalline fractions, would also be explained if it is acknowledged that motion in complex domains reduces the short T_2 signal contribution.

Which model is operative here may be a matter for discussion but the spherulitic case is more attractive on the grounds that such entities have been visually identified (scanning electron microscopy[121]) and that the Hibma x - ray study was on drawn PEO.MX fibres which showed relatively diffuse diffraction lines, suggesting at least some disorder of structure. In either case there is an obvious warning about assuming the partition of the short and long T_2 nmr data into crystalline and amorphous components, which has been assumed by other workers. It is suggested that the technique is valid on a gross scale, but may not be so accurate in explaining trends in the data such as those observed here.

Final consideration is given to the ^{19}F data for the 4 / 1 and 9 / 1 samples. It has been mentioned that the absence of a long T_2 fluorine signal in the 4 / 1 sample was consistent with a small number of mobile ions (charge carriers) and the poorer conductivity for the sample. Fig. 4.5. on the other hand shows that the 9 / 1 sample possessed a 'mobile' signal over the entire temperature range, consistent with more charge carrying species and the much better conductivity shown by the sample. Above 333 K the onset of an increasing amorphous fluorine component in the 9/1 sample (and latterly the appearance of a long T_2 signal in the 4 / 1 data) is well established[22,35] as being due to the progressive dissolution of the so - called crystalline complex into the newly acquired amorphous phase.

(b) ^{7}Li data.

Mention has not yet been given to the nmr response for the lithium nucleus, ^{7}Li. The reasons for this include clarity of presentation of results but are mainly due to the quadrupolar nature of the nucleus (I = 3/2) and the consequence of this property on the interpretation of the data.

Fig. 4.7. shows T_2 values for the observed lithium free induction decays in the 4 / 1 and 9 / 1 samples as a function of temperature. In the case of the 4 / 1 sample, the ^{7}Li fid was found to be single component, short T_2 ($\simeq$ 120 μs) over the entire temperature range, with no long T_2 (or mobile) component observable. This is consistent with the ^{19}F result which implied that only a small fraction of the total salt content contributed to the conductance, explaining the relatively poor electrolytic performance of the material.

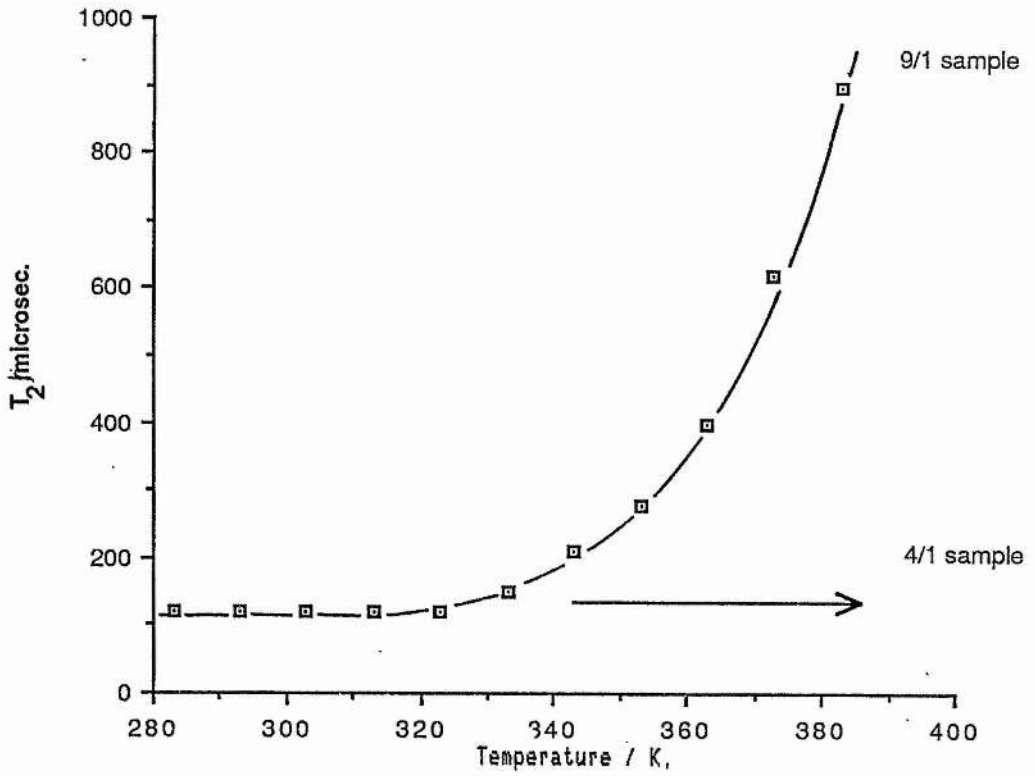

Fig. 4.7. Transverse relaxation times (T_2) vs. temperature in $PEO_4LiCF_3SO_3$ (4/1 sample) and $PEO_9LiCF_3SO_3$ (9/1 sample).

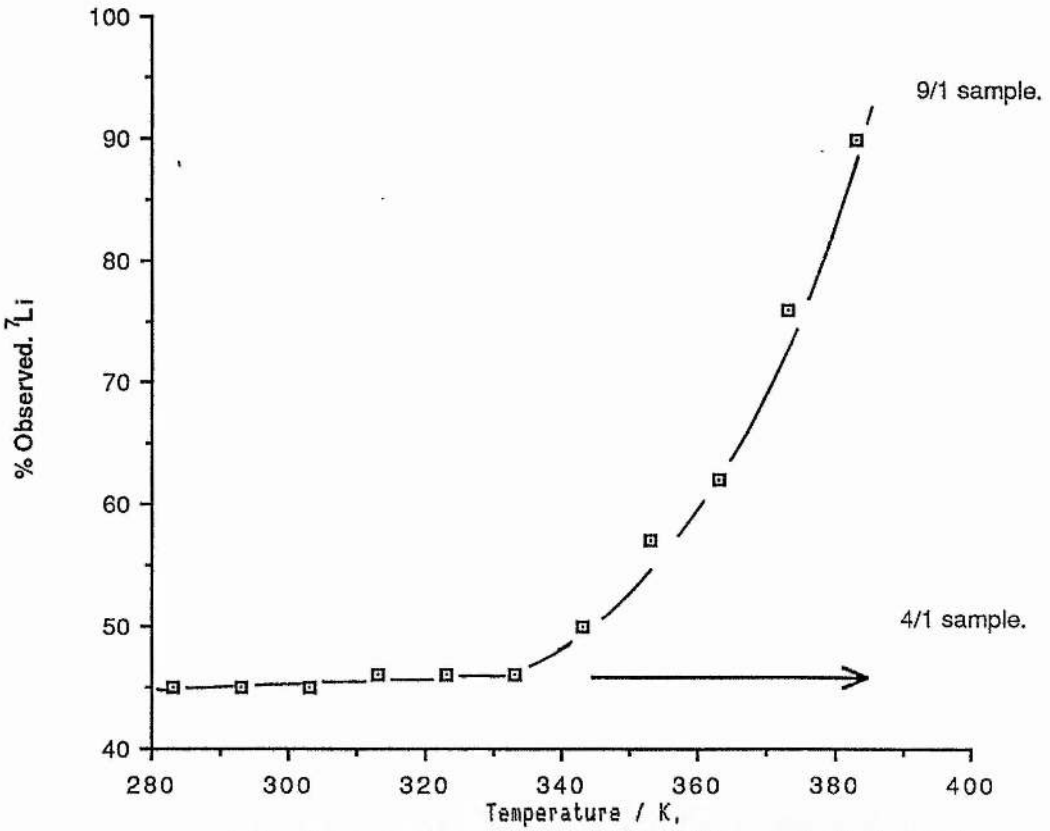

Fig. 4.8. The percentage of the actual lithium content observed in the nmr experiment for $PEO_4LiCF_3SO_3$ and $PEO_9LiCF_3SO_3$ samples.

In the 9 / 1 sample the ^7Li fid was also observed to be of short T_2 (again, ~ 120 μs) at all temperatures below 333 K but at this point began to lengthen progressively with increasing temperature up to the highest temperature recorded, 383 K. The onset of this process is obviously concurrent with the melting of the pure PEO crystallites and the onset of an increasing amorphous fluorine (anion) content as the crystalline complex begins to dissolve into the new amorphous polymer fraction. Unlike fluorine, two - component behaviour was not observed for the ^7Li nucleus, only a monotonic increase in the length of the fid with temperature above 333 K. This suggests that increased motional freedom for all the observed lithium species, hence averaging of the spin - spin interactions, is dependent upon the dissolution process.

The term 'observed lithium species' has been used above because a similar experiment to that detailed in 3.4.2.2 suggested that not all lithiums in the sample were observable in the nmr experiment. In the previous section, lithium and fluorine free induction decay amplitudes were compared as a function of temperature in PEO(400)e.$LiCF_3SO_3$ solutions. It was concluded that in the glassy state (≤ 250 K) the loss of lithium signal intensity, about 60%, was due to static quadrupolar interactions removing the contribution to the nmr signal of the satellite transitions $-3/2 \rightarrow -1/2$ and $1/2 \rightarrow 3/2$, leaving only the central line intensity $-1/2 \rightarrow 1/2$. The conclusion was reinforced by pulsewidth considerations, the presence of a quadrupolar echo, and the inclusion of satellite intensity above the glass - liquid transition region.

Fig. 4.8. shows a similar plot to that presented in 3.4.2.2. where '% Li Observed' means the ratio of the fraction of lithiums in the sample calculated by nmr means, to the actual content, based upon there being one lithium per three fluorines in $LiCF_3SO_3$. In the 4 / 1 sample the percentage was observed to remain close to 45% at all temperatures. In the 9 / 1 sample at lower temperatures, the percentage observed remained close to 45% but above 333 K began a monotonic increase to 90% at the highest temperature recorded, 383 K. If this behaviour was based upon that observed for the lithium resonance in the low mol. wt. PEO(400)e solutions, then it would be assumed that satellite intensity is not included for those lithium nuclei in the crystalline complex but there is a gradual inclusion as the crystalline complex dissolves into the amorphous material. However, further experiment and other observations demonstrated clearly that this was not the case :

(1) The pulsewidth for the observed signal was readily observed to be that of the dipolar value, ≈ 10 μs, and not the ficticious spin value of 10 / 2 = 5 μs.

(2) At no temperature was a quadrupolar echo observed, even down to 77 K.

(3) Variation of the B_1 field i.e the strength of the 90° pulse showed that the observed lithiums occupied a very symmetric environment.

The first point (1) establishes quite clearly that the satellites of the observed spins are contributing to the intensity of the resonance line. (If satellite intensity is missing then theory indicates[102] that the required pulse width for a 90° pulse is reduced to one half of its normal value for an I = 3/2 nucleus like ^{7}Li.) This immediately suggests that the percentage lithiums observed, as calculated, is a direct comment on the actual number of lithiums in the sample which are seen in the nmr experiment; the remaining amount ((100 - 45) = 55% below 333 K) experience a 'wipe - out' effect, removing their contribution to the nmr signal.

The final two points verify this proposal, and Fig. 3.5. (from chapter 3) should be consulted as a qualitative aid. (2) In the quadrupolar echo experiment, the pulse sequence described in 3.4.2.2, $90^\circ - \delta - 35^\circ$, gave no quadrupolar echo at any temperature, for a variety of pulse spacings. This showed that there was no, or very little, resonance intensity in the region of those frequencies stimulated by the B_1 field (i.e the 90° pulse). Coupled with (1) this confirms that the satellite intensity is included in the observed signal.

(3) The strength of the B_1 field pulse determines the range of spectral frequencies stimulated at, and in the region of, the Larmor frequency[106,107]. Inspection of Fig. 3.5. shows that reduction of B_1 may lose satellite intensity, which will move out of the range stimulated by the pulse, and will not be detected. In practice, the B_1 field was reduced from 71 kHz. to 31 kHz. by reducing the power output from the power

amplifier giving the output pulse. (B_1 calculation is detailed in the experimental section, 3.3.3.) Over the temperature of study (213 - 373)K the reduced B_1 value was found to have no effect upon the amplitude of the ^7Li fid. What this means is that any spread of satellite intensity must be less than 31 kHz., quadrupolar interactions small, and the observed lithium ions must sit in an electrically symmetric environment. This result finds agreement with several other studies: Greenbaum[101] for example, concluded from linewidth and 90° pulse-width considerations on the ^{23}Na resonance in $PEO_{4.5}LiClO_4$, that there were no appreciable quadrupolar interactions in this electrolyte and so a highly symmetric enviroment for the sodium ions. Worboys[93] found a similar 'symmetric' environment for the ^{23}Na signal in PEO_8NaSCN. Only a study by Gorecki[13], again for the ^{23}Na resonance, noted the presence of quadrupolar interactions. In this case the sodium resonance in PEO.NaI samples was found to be of very short T_1 and T_2 (of the order of microseconds) which suggested to the author a resonance line broadened by quadrupolar effects.

What the ^7Li nmr results obtained in this work mean on a gross scale is that significant numbers of lithium nuclei are not observed by the nmr technique (i.e are experiencing a second order quadrupolar interaction, 3.2.5) hence there must be inequivalence of lithium sites. The available nmr studies[4,13,22,93,101] on poly(ethylene oxide) - based electrolytes do not seem to mention intensity loss but it appears that amplitude measurements of the type detailed here were not performed, and it was assumed that the entire lithium (or sodium) content was monitored.

The nature of the 'wipe - out' effect, removing the contribution to the nmr signal of significant numbers of nuclei, must be due to environments of low symmetry, possibly of the ion - pair type, for the missing lithium ions. The effect is not uncommon ; semiconducting materials such as the tungsten bronzes, $(Na)_xWO_3$, show a wipe - out effect of the ^{23}Na resonance under certain conditions[105] and the alloying of copper metal with zinc or silver gives rise to an all or nothing effect where only those ^{63}Cu nuclei near the added Zn or Ag nuclei experience a second order perturbation[102].

The results now pose the question as to the location of both the observable and 'missing' lithium nuclei. It would seem perhaps that the conventional view of one phase, one ionic environment, may be inadequate in describing the materials studied here. The 4 / 1 sample gives some indication of this in that the phase diagram predicts the electrolyte should be predominantly (≃ 85%) crystalline complex, the remaining amount poly(ethylene oxide). Fig. 4.8. therefore predicts that the salt within the 'crystalline complex' occupies two environments, only one observable with the nmr technique. Does this fit with a spherulite model for the morphology of the crystalline complex, where the outer regions are more disordered than the inner ?

Certainly, the 9 / 1 data show that the percentage observable lithiums increases as the crystalline complex dissolves into the amorphous phase, showing that the missing lithium content is in the complex. (If the data in Fig. 4.8. are extrapolated to where 100% lithiums are observed, the temperature where this occurs is ≈ 398 K, in good agreement with the point of total dissolution of the complex according to the phase diagram (≈ 405 K), above which the electrolyte is single phase amorphous.

4.2.2.2 Longitudinal relaxation behaviour.

T_1 data are now presented for the relevant nuclear species (^1H, ^{19}F and ^7Li) in the PEO.$LiCF_3SO_3$ 4 / 1 and 9 / 1 samples, and also the pure salt, $LiCF_3SO_3$. The data are shown in Fig. 4.9. as stacked plots, where for clarity the proton data are displaced vertically from the corresponding ^7Li and ^{19}F data for a given sample.

Some general features of the data are worth emphasising :

(1) A T_1 minimum is associated with nearly all components of the figures.

(2) The short T_2 ^1H data have substantially longer T_1 values at the minimum than for the long T_2 ^1H data.

(3) For the 4 / 1 and 9 / 1 samples the ^{19}F and ^7Li T_1 minima occur at temperatures below the ^1H minima.

A summary of the temperatures at which T_1 minima occur for the relevant nuclear species in the three samples studied is given in Table 4.1.

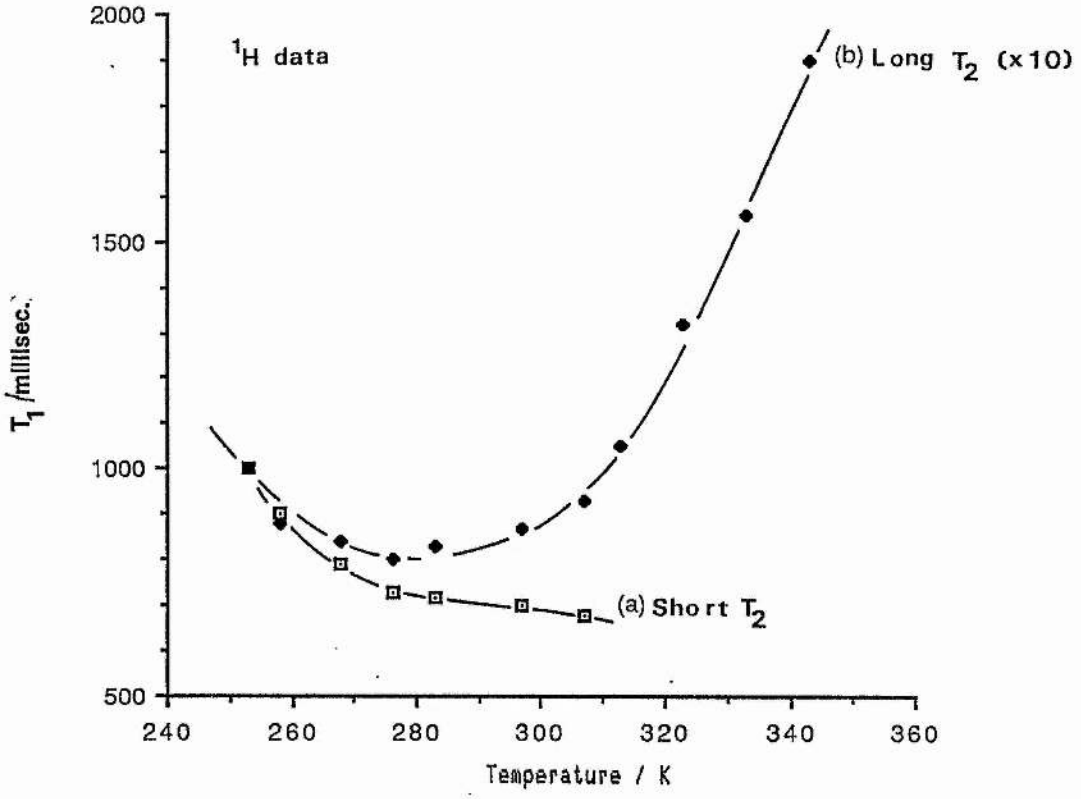

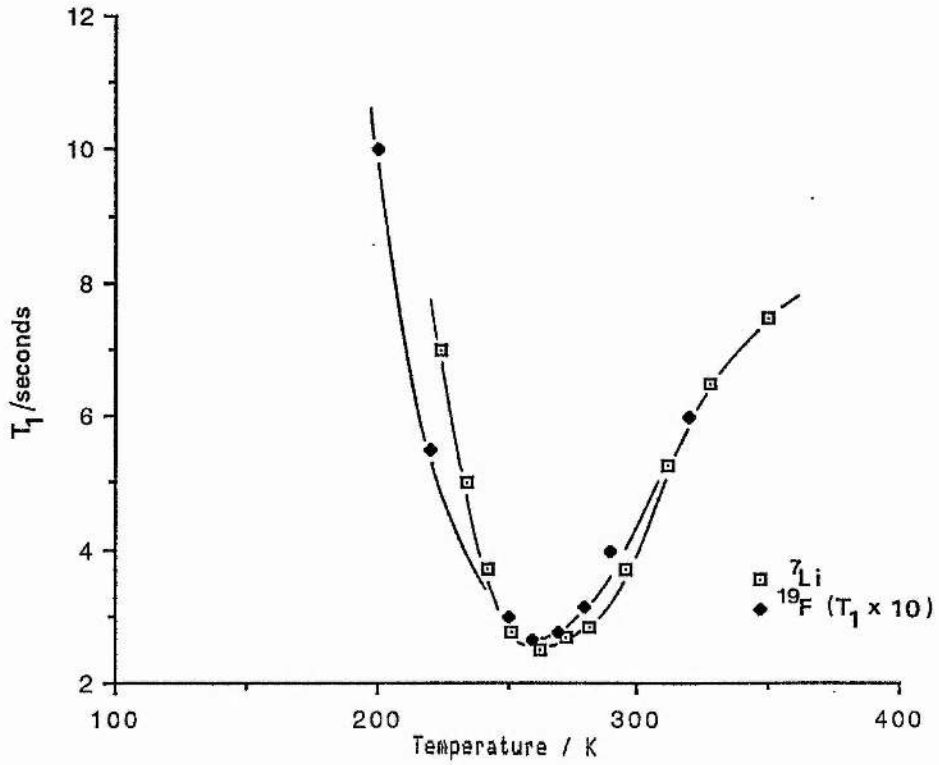

Fig. 4.9. (1) Longitudonal relaxation time data for the studied nuclear species (^{1}H, ^{19}F and ^{7}Li) in $PEO_9LiCF_3SO_3$.

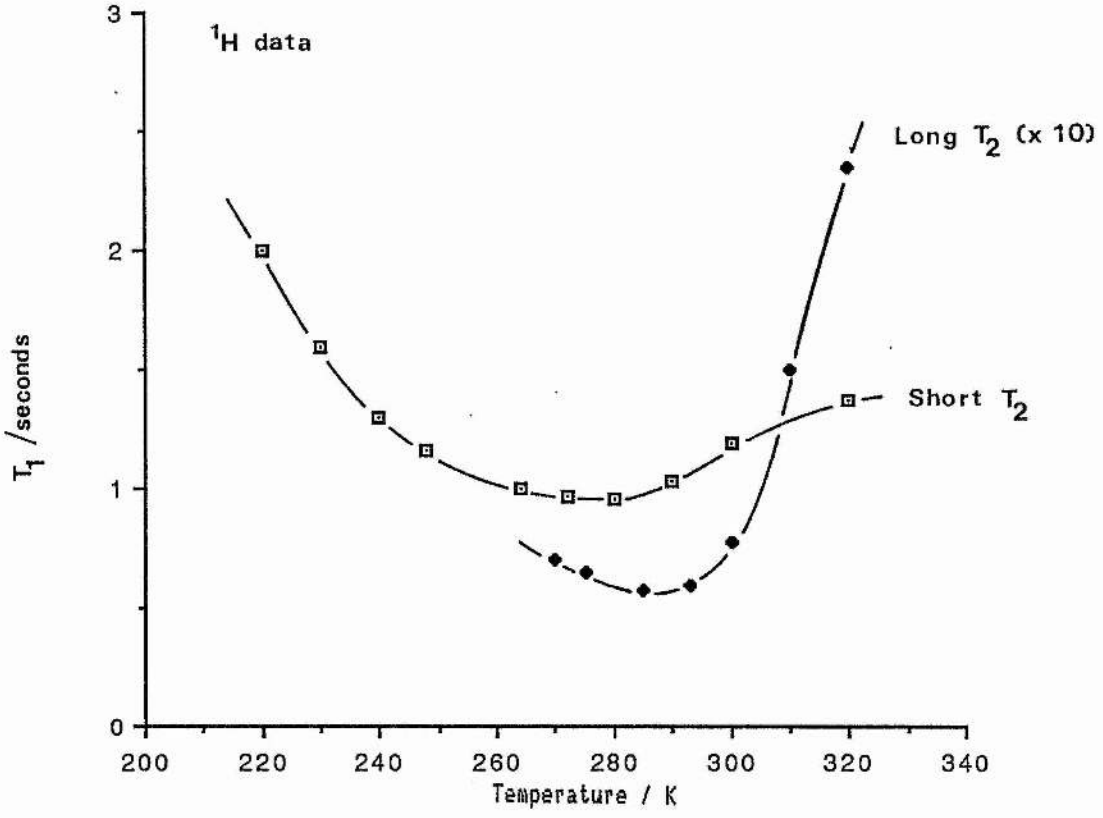

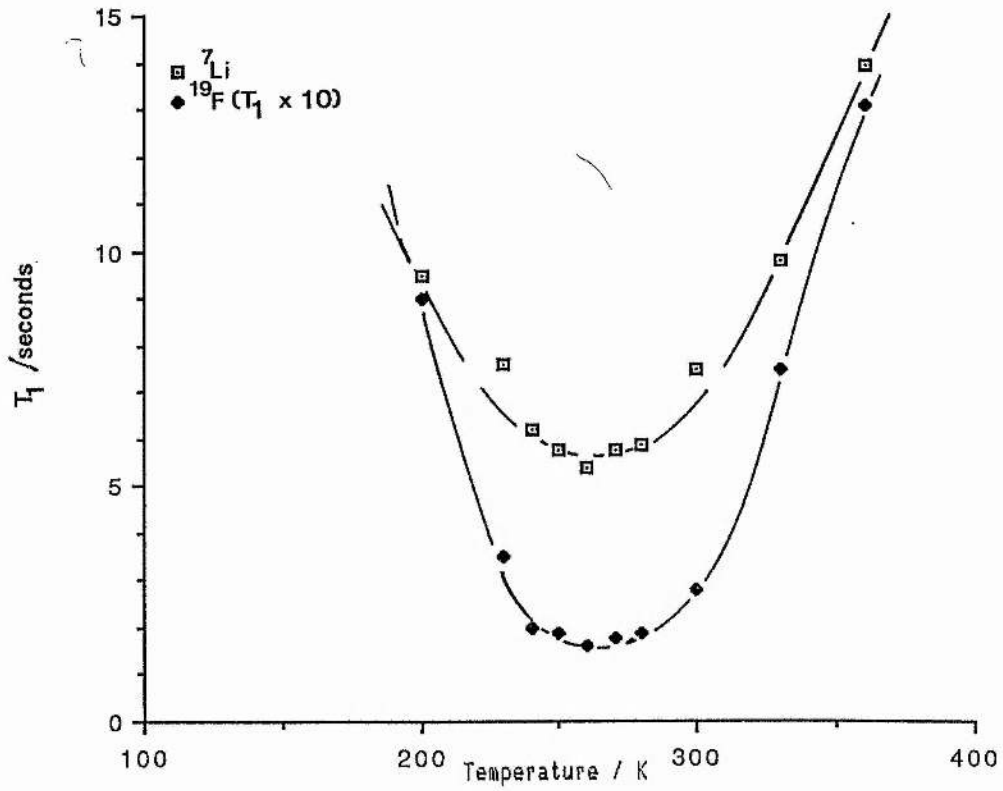

Fig. 4.9. (2) Longitudonal relaxation time data for the studied nuclear species (^{1}H, ^{19}F and ^{7}Li) in $PEO_4LiCF_3SO_3$.

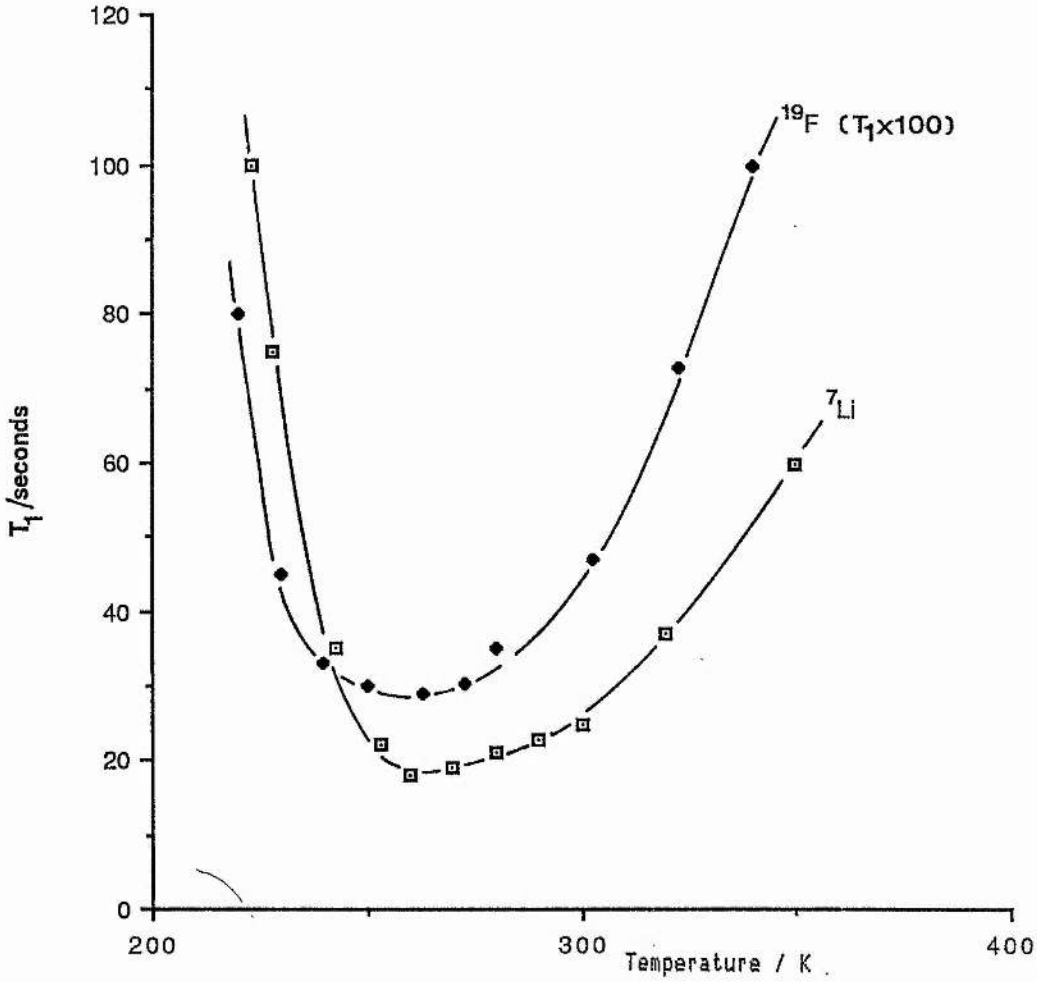

Fig. 4.9. (3) Longitudonal relaxation time data for the studied nuclear species (^{19}F and ^{7}Li) in $LiCF_3SO_3$.

Sample	^1H(long T_2)	^1H(short T_2)	^7Li	^{19}F(short T_2)
$PEO_9LiCF_3SO_3$	280	-	260	265
$PEO_4LiCF_3SO_3$	285	270	260	263
$LiCF_3SO_3$	-	-	263	263

Table 4.1. Temperatures (Kelvin) at which T_1 minima occur for ^1H, ^{19}F and ^7Li in $PEO.LiCF_3SO_3$ electrolytes and $LiCF_3SO_3$

In 3.2.4 it was mentioned that where a T_1 minimum occurs BPP theory gives $\omega_o.\tau_c \simeq 1$, where $\omega_o = 2\pi f$, from which an estimate can be made for the correlation time describing the motion, τ_c. It follows that for any T_1 minimum in the figures where f = 49.8 MHz, the spectrometer operating frequency :

$$\tau_c \simeq 1 / (2 \times \pi \times 49.8 \times 10^6)$$

$$\simeq 3.2 \times 10^{-9} \text{ s.}$$

which, according to Ratner[35], may find relevance as the renewal rate, λ, in the DBP (Dynamic Bond Percolation) theory, mentioned in chapter 1. Ratner remarked that the high temperature (> 333 K) T_1 minimum found for the long T_2 ^1H signal found by Greenbaum[101] in $PEO_{4.5}LiClO_4$ may have value in obtaining a λ parameter for use in describing the tranport processes occuring in that electrolyte. It is suggested that the minima observed in this study may not have such relevance since most are associated with the crystalline adduct at the temperatures where the

minima occur. (This comment includes the long T_2 ^1H signal which, as has been proposed in 4.2.2.1. may find a significant contribution from the adduct.)

In pure PEO it was remarked that the differing magnitudes of the spin - lattice relaxation times for the short and long T_2 components of the ^1H free induction decay allowed the statement that the spin systems responsible for the two signal types were isolated from each other. This behaviour appears to be retained in the 4 / 1 and 9 / 1 electrolyte samples where the short T_2 'crystalline' signals have T_1 > 700 ms and the amorphous signals T_1 < 100 ms at ca. 280 K. There is some evidence of thermal mixing of spin systems in the 9 / 1 sample however, manifest as a monotonic decrease in the short T_2 signal T_1 data with increasing temperature and a slightly elevated T_1 minimum value (in comparison to the other samples) for the longer signal.

It is clear from the figures, and the data in Table 4.1., that in the 4 / 1 and 9 / 1 samples the temperature at which the T_1 minima occur for the ^{19}F and ^7Li nuclei are coincident at ca. 260 K, some (10 - 15)K below the relevant proton data. The pure salt data is also interesting in that minima occur at all in the temperature regime studied; for many salts a T_1 minimum for either the cation or anion would only be expected at or near the fusion temperature (≈ 620 K for $LiCF_3SO_3$) where the relative motion of ions at the Larmor frequency in the molten state would give rise to the most efficient longitudonal relaxation. In 3.4.2.3 it was

shown that spin - internal rotation was the dominant relaxation mechanism for ^{19}F in the $CF_3SO_3^-$ anion in the glassy (frozen) state of PEO(400)eLiCF_3SO_3 solutions. This would appear to be the case in the solid state phenonemon observed here for the pure salt where the CF_3 group, spinning about the principal axis of the anion at ≃ 50 MHz, is responsible for the ^{19}F relaxation. Certainly, T_1 at the minimum is of the correct order, ≃ 300 ms (although the calculation used in 3.4.2.3 suggested a value nearer 100 ms) which is to be contrasted with ^{19}F in LiF, where $T_1(^{19}F)$ = 120 s at room temperature[123] i.e an efficient relaxation mechanism, such as spin - internal rotation in $CF_3SO_3^-$, is not available for ^{19}F in LiF.

More significantly, for the ^7Li resonance in the pure salt, the T_1 profile follows very closely that of ^{19}F, showing quite clearly that the fluctuating magnetic fields creating by the spinning CF_3 group exert a major influence upon the ^7Li relaxation, resultant in the temperature coincidence of the T_1 minima (≃ 260 K) where the the ^{19}F relaxation is strongest. (T_1 at the minimun for ^7Li in $LiCF_3SO_3$ is also much shorter, at ≃ 19 s, than in LiF, ≃ 300 s at room temperature.)

The above result is interesting enough but assumes more importance in the 4 / 1 and 9 / 1 electrolyte samples in that the ^7Li data still 'track' the ^{19}F data, the temperature at which the T_1 minima occur identical (within error) to that of the pure salt and some (10 - 15)K below the positions of the ^1H minima. The implication here is that anions ($CF_3SO_3^-$) and cations (Li^+) are spacially proximate in the crystalline

phase, allowing the relaxation effects caused by ^{19}F on ^{7}Li in the pure salt to occur in the 4 / 1 and 9 / 1 samples.

This certainly agrees with the proposal given in the previous section; that significant numbers of lithium nuclei in the crystalline adduct were not observed in the nmr experiment because they occupied environments of low symmetry. Therefore, spacial association between anions and cations in the crystalline phase would :

(a) Produce electric field gradient (efg) effects, observable in ^{7}Li fid amplitude measurements.

(b) Give rise to relaxation effects, where the dominant relaxation mechanism for one nucleus (^{19}F) is imposed on another (^{7}Li).

To state that the enviroments giving rise to the observed relaxation effects are due to ion - pair formation, for example, would be unwise without further evidence (i.e Papke[44] determined $LiNO_3$ contact ion pairs in $PEO_{4.5}LiNO_3$ by infra - red and Raman spectroscopy). It can be said though that the 'observable' ^{7}Li fraction are influenced strongly by spacially proximate anions, the non - observable fraction (which experience a wipe - out effect) probably more so.

Chapter 5

5. MIXED SALT POLYMER ELECTROLYTE SYSTEMS.

5.1 Introduction.

A study by Moryoussef[124] on the conductivity of PEO / alkaline - earth salt complexes revealed the interesting result that the mixing of salts had a noticeable enhancement on conductivity i.e a $PEO_{15}[CaBr_2]_{0.5}[CaI_2]_{0.5}$ complex had a greater conductivity than either of the pure $PEO_{15}[CaX_2]_1$ X = Br / I, complexes. Although not verified experimentally, it was suggested that this was due to a plasticising effect which favoured the formation of an amorphous phase at the expense of the crystalline phase. To contrast this, Armand[6], at an early stage in the study of PEO - based electrolytes, reported a reduction in conductance when salts were mixed (for a $PEO_{4.5}[LiSCN]_{0.5}[KSCN]_{0.5}$ electrolyte) which was explained as an example of the mixed alkali effect observed in organic glasses.

Intuitively, if the addition of a salt to PEO forms ordered, crystalline domains, which have been shown to occupy a secondary role in the conduction process[22], then mixing of salts may create topological disorder in such phases due to the presence of ion types of differing size and shape. The immediate implication would be more amorphous character, a larger mobile ion concentration and so an improved conductivity for the mixed salt in comparison to the single salt system.

With the above points in mind it was decided to pursue the mixed salt theme and study the nmr, conductance and DSC behaviour of the mixed salt electrolyte PEO.[$LiCF_3SO_3$].[NaI]. Two nominal EO / salt concentrations were studied :

(a) $PEO_4[LiCF_3SO_3]_{0.5}[NaI]_{0.5}$ where the respective salt concentrations were equal at EO / M^+ = 8 / 1 and the overall salt concentration was EO / (Li^+ + Na^+) = 4 / 1.

(b) $PEO_8[LiCF_3SO_3]_{0.5}[NaI]_{0.5}$ EO / M^+ = 16 / 1, EO / (Li^+ + Na^+) = 8 / 1.

$LiCF_3SO_3$ was chosen as one solute component because its PEO complexes had previously been studied by the nmr technique. NaI was chosen because its PEO complexes have a similar (simple) phase diagram to that of $LiCF_3SO_3$, and mixing of both anion and cation types was desired.

5.2 Experimental.

5.2.1 Formation of electrolyte films.

Salt(s) and polymer, in the correct proportions, were ground together to form an intimate mixture, as outlined in 3.3.1, Films were then prepared using a two - stage hot pressing process, developed in the St. Andrews laboratories by Gray *et al*[104], all operations performed within an argon atmosphere dry box. 5mm. diameter pellets of the polymer / salt mixture were formed by means of a hydraulic press (Specac, model P/N 1500). The pellet was then transferred to a 10mm. die and heated to ca. 390 K for two hours, allowed to cool to 345 K, then re - pressed with a pressure of (7.6 MPa). The method was found to give homogeneous films of (150 - 300)μm thickness which were then annealed at (390 - 420)K for 48h before cooling and subsequent use.

The films, as prepared, were suitable for location between the electrodes of the conductance cell. For DSC, portions of a pressed film were cut into small segments (approximately 0.2 × 1 × 5 mm.) and about 5mg. of material sealed into aluminium DSC pans (≈ 7 mm. diameter).

5.2.2 Conductance measurement by a.c impedance methods.

Batteries, to which polymer electrolytes have relevance, are direct current (d.c) devices. Conventional two - probe techniques for measuring d.c conductances in polymer electrolytes are usually difficult to apply because of electrode - electrolyte contact problems. Although four - probe methods have recently been developed which overcome this[126], alternating current (a.c) methods still represent the most popular approach to the determination of the electrical properties of polymer electrolytes[27,127,128].

Apparatus.

A block diagram of the experimental set - up for conductance determination, which has been described in detail elsewhere[129], is shown in Fig. 5.1. The essential component was a frequency response analyser (Solartron, model 1170) comprising a variable frequency source sensitive to both the phase and amplitude of an a.c voltage. The analyser was subject to computer control (Tektronix, model 4052), which initiated and supervised all analyser functions.

The experimental cell consisted of a former containing two stainless steel (blocking) electrodes of 10mm. diameter, between which electrolyte films were located. The former sat within a glass container which in turn was located in an oven. Sample temperatures were measured to ± 0.5 K by

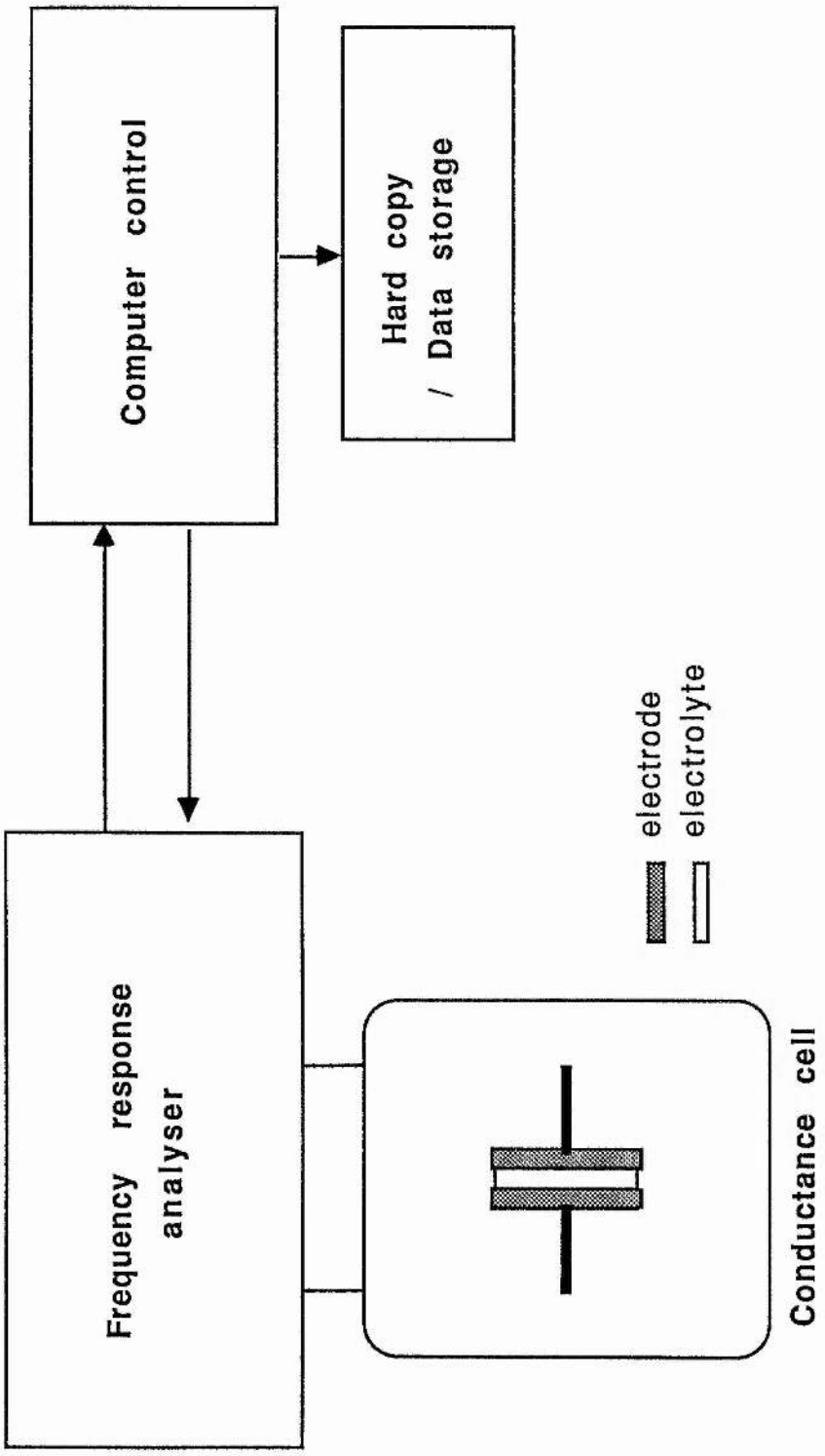

Fig. 5.1. Schematic of the experimental set - up for conductance measurement by the a.c impedance method.

a calibrated thermocouple device located next to the sample and an argon atmosphere was maintained at a slight overpressure to exclude atmospheric moisture. Measurements were taken on a heating cycle of the form :

(a) Heat to desired temperature.
(b) Allow at least ½hr. for thermal and phase equilibrium.
(c) Frequency response measurement.

usually in the range (290 - 385) K.

The a.c measurement.

In an alternating current experiment a sinusoidal voltage of known frequency is applied to the conductance cell and the sinusoidal current flowing as a result of this perturbation determined[130] (Fig. 5.2.). Two parameters are required to relate this current to the applied potential. One is the opposition to the flow of charge and is equal to the ratio of the voltage and current maxima, V_m / I_m, analagous to d.c resistance. The other parameter, θ, is the phase difference between the voltage and current. Combination of V_m / I_m and θ gives the impedance, Z, of the cell, which is a vector quantity[131]. For an electrochemical cell, $|Z|$ (= V_m / I_m) and θ are functions of the sinusoidal frequency and give information on the electrical properties of the cell.

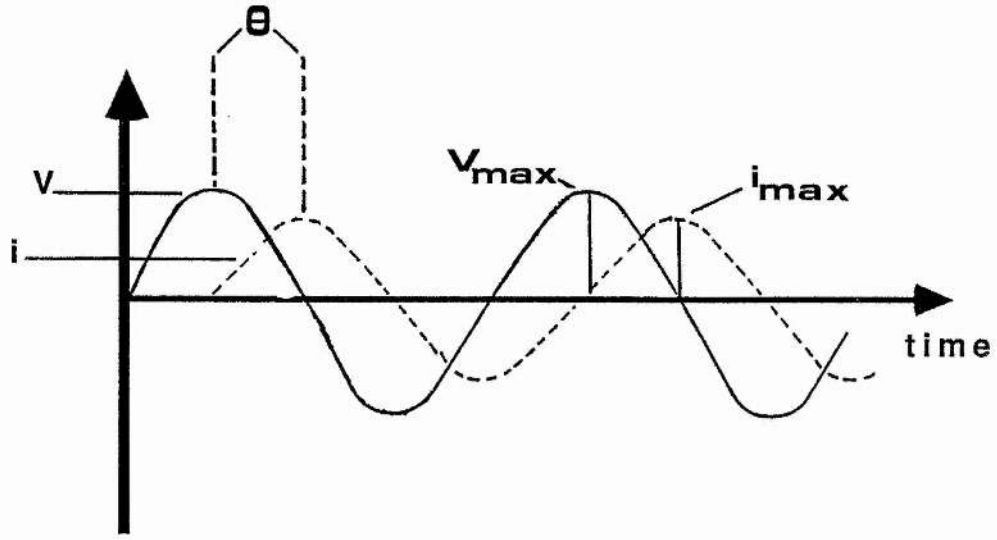

Fig. 5.2. The sinusoidal voltage (V) and current (i) at a single frequency for a cell. θ is the phase difference between the applied voltage and resultant current.

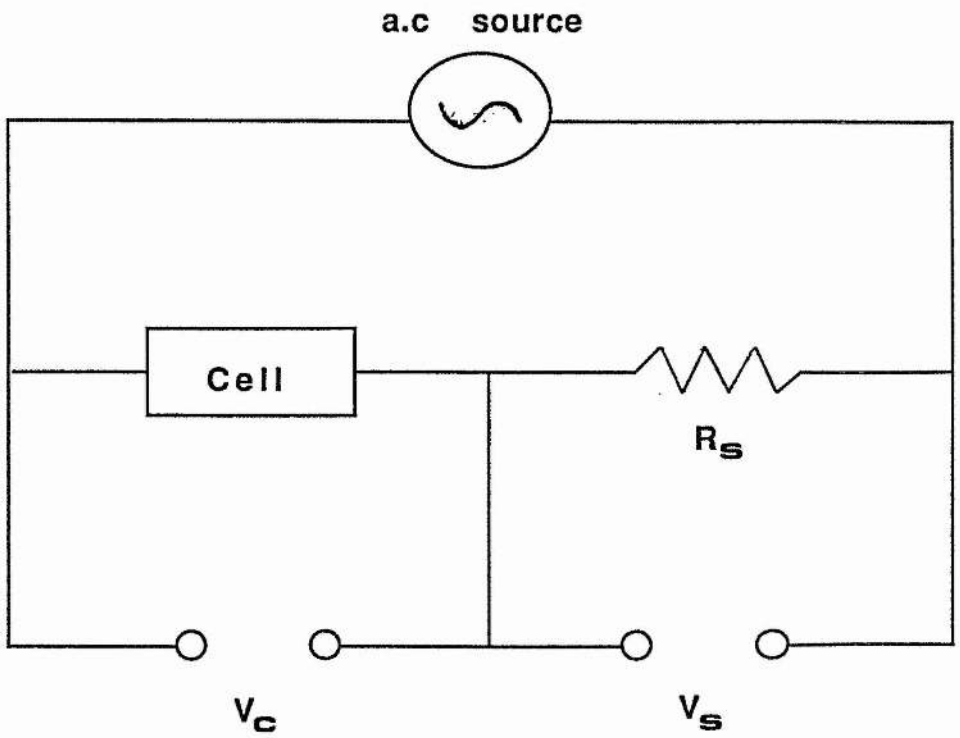

Fig. 5.3. Schematic representation of the circuit used to determine the a.c impedance of a two terminal cell.

The function of the frequency response analyser (FRA) is to generate a sinusoidal voltage across the conductance cell, and a standard resistance, R_s, in series (the magnitude of which is similar to that of the cell, $|Z|$), Fig. 5.3. The analyser then steps sequentially through the frequency spectrum (1MHz → 1Hz in this work) measuring the voltage across the cell V_c and across the the standard resistor V_s. The current through the standard resistor is in phase with V_s and is given by $I_s = V_s / R_s$. For each frequency the analyser obtains the ratio V_s / V_c and when divided by R_s gives the magnitude of the cell impedance $|Z|$. The phase difference between V_s and V_c is also the phase difference θ between the cell voltage and the current and allows the determination of the vector quantity Z at each frequency in the spectrum. Z is usually represented on a complex impedance diagram, which is analagous to the representation of a complex number in the complex plane, where $Z = |Z|\cos\theta - i|Z|\sin\theta$. ($|Z|\cos\theta$ is usually symbolized Z' and $|Z|\sin\theta$ symbolized Z''. i is $(-1)^{1/2}$.)

In polymer electrolyte study, the electrolyte / electrode system with ionically blocking electrodes (stainless steel in this work) is usually modelled to a circuit of the type shown in Fig. 5.4.[130] R_b represents the electrolyte resistance i.e

$$1 / R_b = \sigma^+ + \sigma^- \qquad (5.1)$$

as the ions move back and forth with the applied sinusoidal voltage.

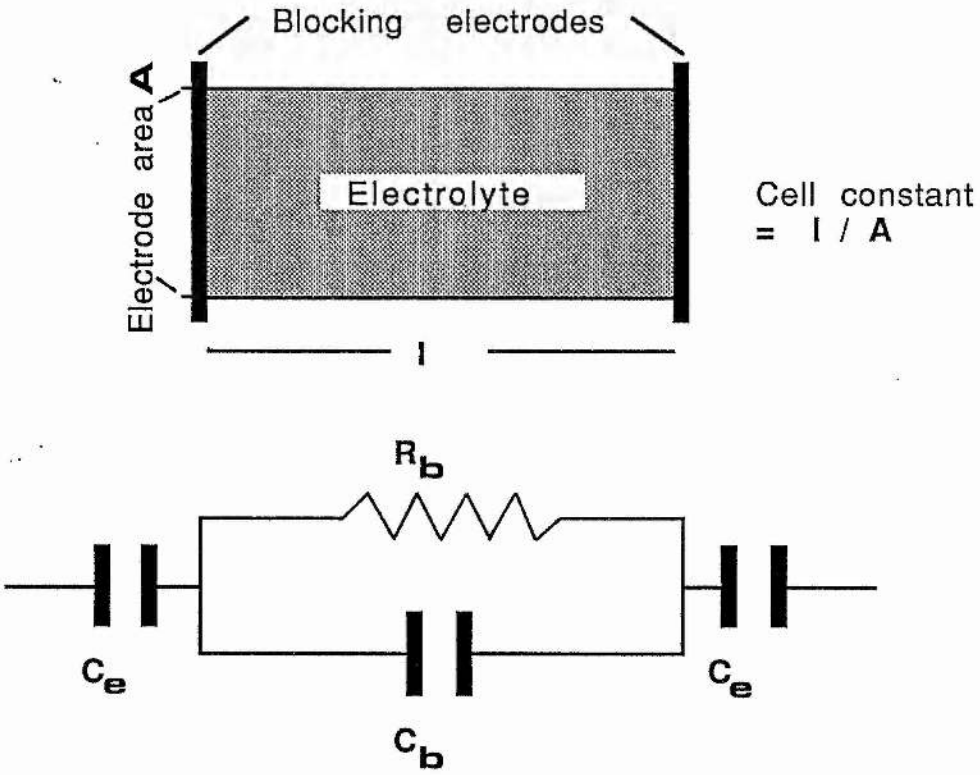

Fig. 5.4. Schematic of a polymer electrolyte - blocking electrodes cell and the equivalent circuit used to model it. (Symbols are defined in the text.)

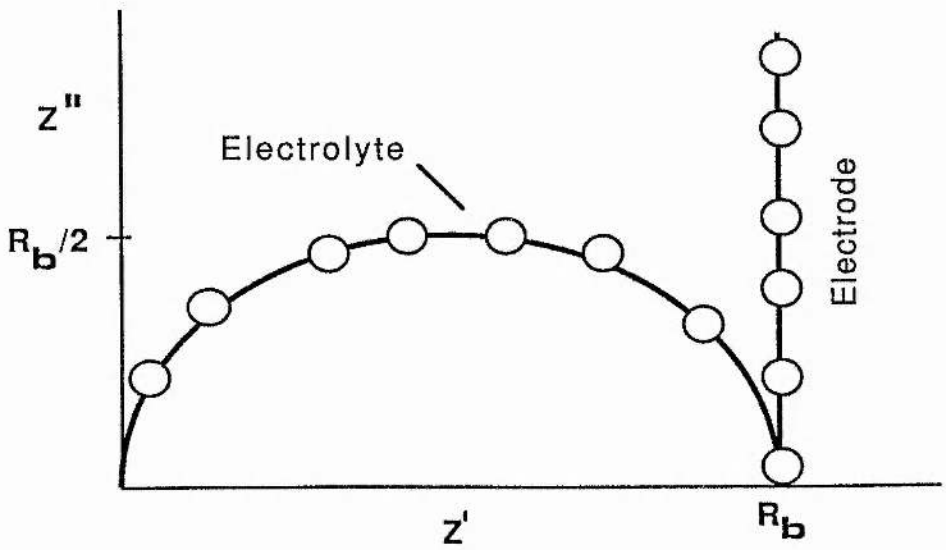

Fig. 5.5. The ideal complex impedance plot for the equivalent circuit shown in Fig. 5.4.

C_b represents the dielectric polarisation of the polymer chain in the alternating field, and C_e a capacitance due to accumulation of charge at the polymer / electrode interface during each half - cycle. The impedance of the circuit at each frequency may be calculated with estimates for R_b, C_b and C_e, leading to a complex impedance plot of the type shown in Fig. 5.5. Here the higher frequency semicircle is described by the parallel combination of R_b and C_b, the lower frequency 'spike' describes the linear combination of R_b and C_e ($C_e \simeq 10^5 C_b$). The most important point in the diagram in relation to conductance determination is where the semicircle and spike meet on the Z' axis, which corresponds to R_b, the zero frequency (d.c) resistance of the electrolyte. Hence :

$$\sigma_{d.c} = \text{cell constant} \; / \; R_b \qquad (5.2)$$

In general, the equivalent circuit (Fig. 5.4.) does reproduce the gross features of the a.c response of real cells and the R_b obtained is used in determining the electrolytic conductance.

A typical complex impedance plot, representative of the type obtained in this work, is shown in Fig. 5.6. and is in accord with those found by other workers using the impedance technique[31,132]. In comparison to the response for the equivalent circuit the semicircle is broadened and the spike no longer vertical. Such behaviour is common and has been explained as due to ion - trapping to pairs, ionic atmosphere effects, and the inhomogeneous nature of the polymer electrolyte[130].

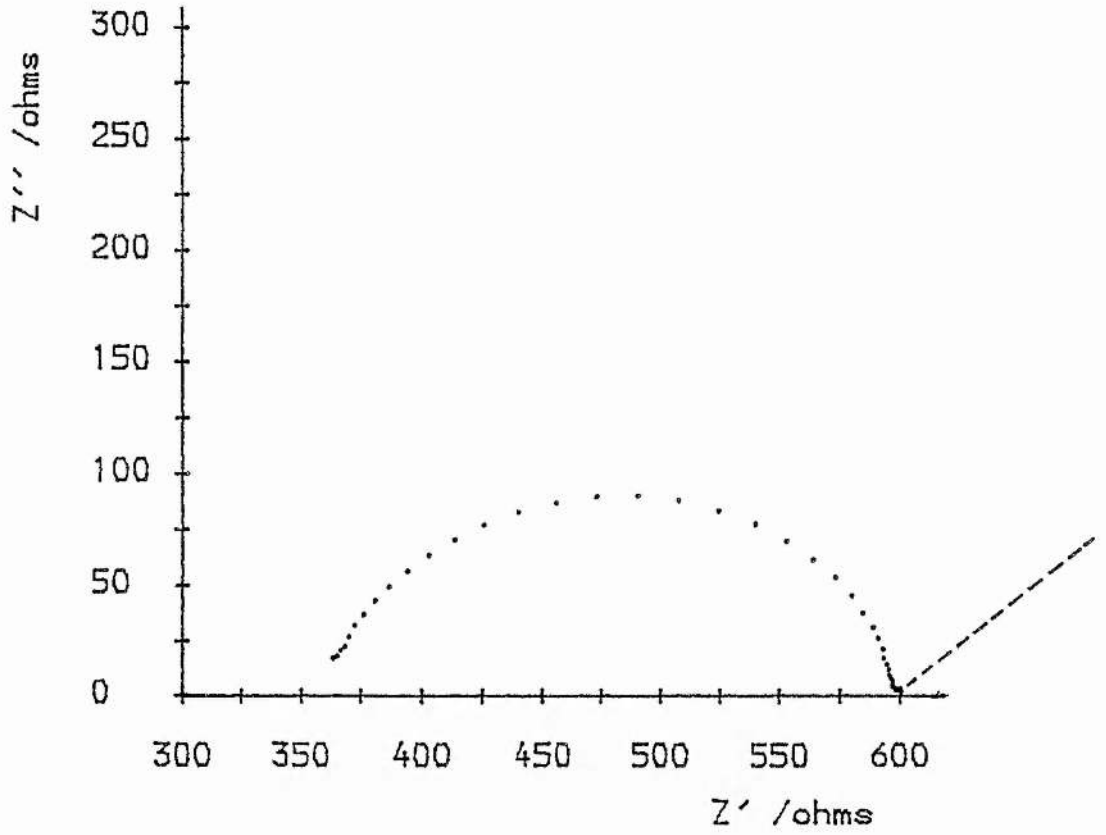

Fig. 5.6. A complex impedance plot, obtained in the frequency range 65kHz to 1Hz and using non - blocking electrodes, for $PEO_9LiCF_3SO_3$ at 363 K (from reference 30). The lower frequency spike (see text) was not observed because the lower frequencies required (< 1Hz) were not used. The dashed line however represents the usual spike orientation for a real polymer electrolyte system.

5.2.3 Differential Scanning Calorimetry.

Differential scanning calorimetry has occupied an important role in polymer electrolyte studies, where thermogram analysis has yielded information on the glass transition, recrystallisation behaviour, crystallite fusion / dissolution and ultimately, the phase diagram for some electrolytes[13]. In this work however the technique occupied a subsidiary role and so only a limited description is given.

Principle:

DSC is a technique which records the energy necessary to establish zero temperature difference between a sample and a reference material, against either time or temperature, as the two specimens are subjected to identical temperature conditions in an environment heated or cooled at a controlled rate[106].

Apparatus and method.

DSC thermograms were obtained using a Perkin Elmer apparatus (model DSC-1B), the essential elements of which are shown schematically in Fig. 5.7. In operation the sample and reference are heated separately by individually controlled heater elements. The power to these heaters is

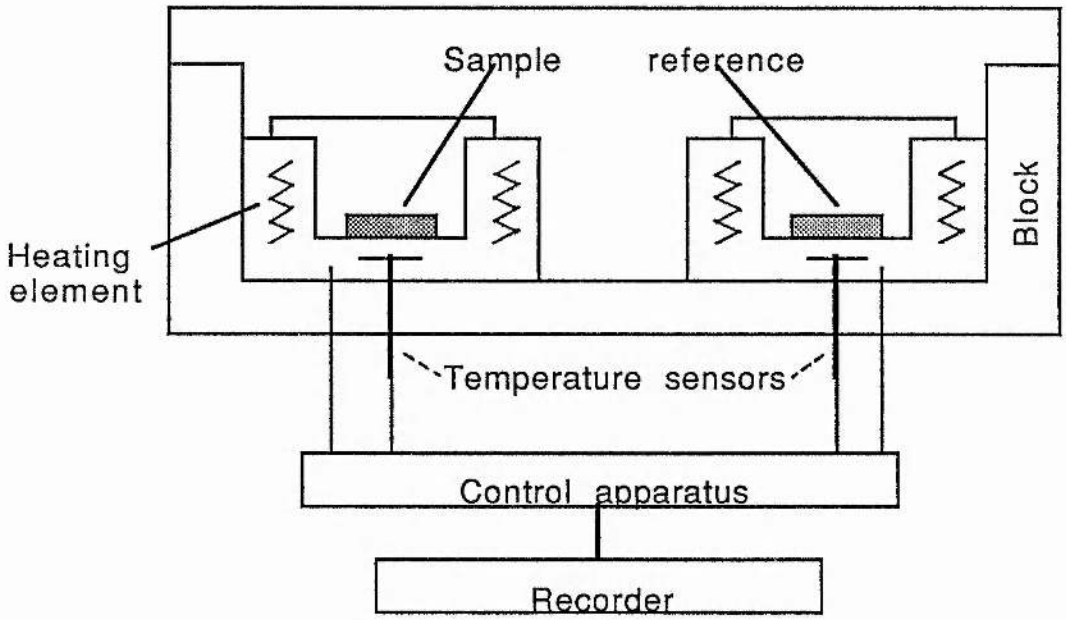

Fig. 5.7. Schematic of differential scanning calorimetry apparatus.

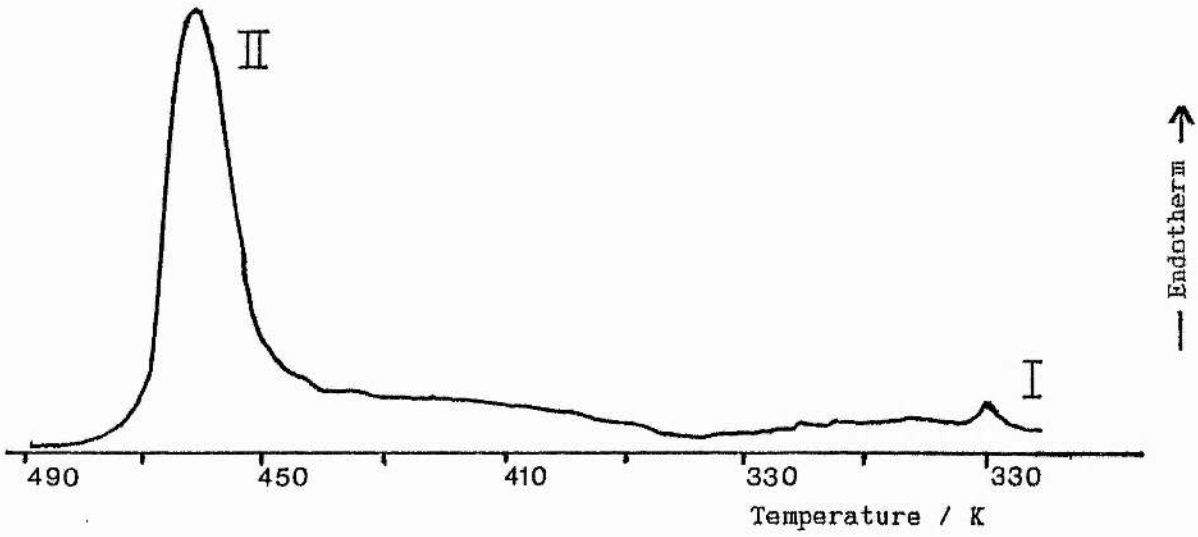

Fig. 5.8. The DSC thermogram for PEO_4NaI, obtained on a heating cycle (8 K min^{-1}).

adjusted continuously in response to any thermal effects in the sample, such as a glass transition or fusion event, and in this way the sample and reference are kept at identical temperatures. The differential in power supplied to the heaters to achieve this condition is then recorded, usually as a function of temperature.

The DSC thermogram.

A thermogram typical of many polymer electrolyte materials is shown in Fig. 5.8. for PEO_4NaI. Two endothermic events are observed. The first at ca. 333 K is usually attributed to the fusion of PEO crystallites whilst the second at somewhat higher temperature ca. 470 K describes the heat of dissolution of the salt - rich crystalline phase into the amorphous phase. (The temperature of total dissolution of the crystalline complex is dependent on the overall salt content and the study of this effect forms the basis for evaluation of the phase diagram, Fig. 1.2, chapter 1.) Both events are consistent with changes noted at similar temperatures using other techniques including optical microscopy and conductance measurements[18] (endotherm I), and nmr[13] (endotherms I and II).

5.3 Results and discussion.

5.3.1 Conductance behaviour

For clarity the conductance results for those electrolytes of 4 / 1 overall salt concentration will be given first (EO / (Li^+ + Na^+) = 4 / 1), followed by the results for the 8 / 1 samples.

(a) Samples with 4 / 1 nominal salt concentration.

Fig. 5.9. shows $\log_{10}\sigma$ versus 1/T for $PEO_4LiCF_3SO_3$, PEO_4NaI and the mixed salt system $PEO_4[LiCF_3SO_3]_{0.5}[NaI]_{0.5}$ The conductivity versus temperature behaviour observed here is typical of most semi - crystalline polyether electrolytes i.e a low temperature regime (< ca. 322 K) with a larger apparent activation term, Ea, for conduction in comparison to a higher temperaure regime (> ca. 333 K) of notably lower apparent Ea. (The term 'apparent Ea' is used here to describe the overall temperature dependence of the conductance, which is less here for the higher than the lower temperature regime. As was outlined in chapter 1, whether or not the Ea term describes the ionic transport has still to be determined.)

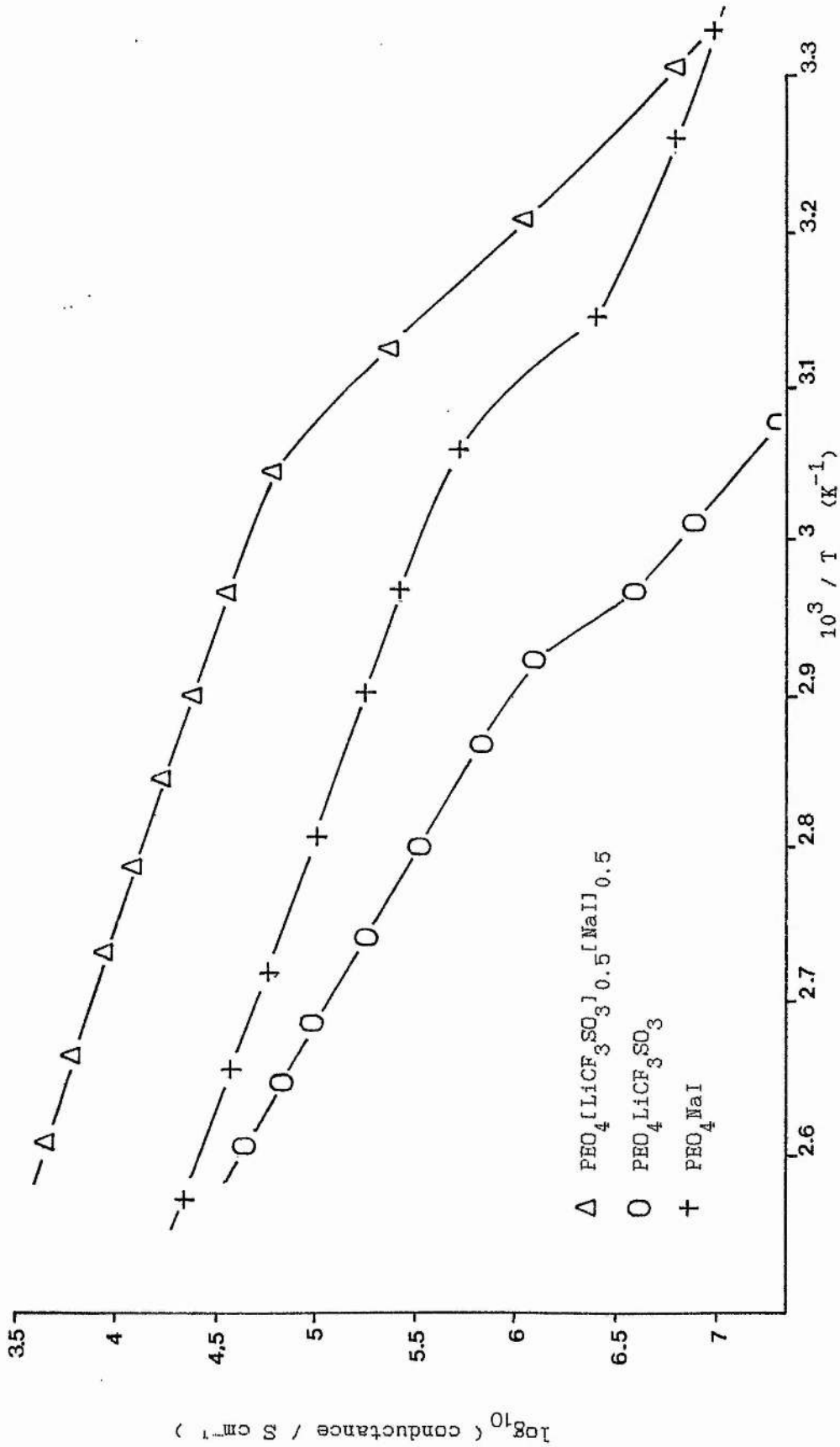

Fig. 5.9. Semilogarithmic plots of conductance vs. temperature for $PEO_4[LiCF_3SO_3]_{0.5}[NaI]_{0.5}$, $PEO_4LiCF_3SO_3$ and PEO_4NaI. ($PEO_4LiCF_3SO_3$ data from reference [122]).

Comparison of the conductance data in Fig. 5.9. shows that the mixed salt system gives a marked improvement on both of the single salt systems $PEO_4LiCF_3SO_3$ and PEO_4NaI. Table 5.1. gives some representative conductance data for the three electrolyte materials at two arbitrary temperatures, 345 K and 383 K.

Sample	σ(345K) /10^6 Scm^{-1}	σ(383K) /10^5 Scm^{-1}
$PEO_4LiCF_3SO_3$	1.0	2.5
PEO_4NaI	5.6	3.3
$PEO_4[LiCF_3SO_3]_{.5}[NaI]_{.5}$	42.0	23.0

Table 5.1. Conductance data at (345, 383)K for single and mixed salt electrolyte materials.

Comparison of the data in Fig. 5.9. and Table. 5.1. shows that the mixed salt system is a better conductor by about an order of magnitude than either of the single salt materials. (In the temperature regime of interest, which is the region of lower apparent Ea for semi - crystalline polymer electrolytes.) It would appear therefore, that for the chosen salts at nominal 4 / 1 overall concentration, the mixing of salt types produces an improved electrolytic conductance in comparison to either single salt system, which is in qualitative agreement with the Moryoussef data.

(b) Samples with 8 / 1 nominal salt concentration.

The relevant conductance data for $PEO_8LiCF_3SO_3$, PEO_8NaI and $PEO_8[LiCF_3SO_3]_{0.5}[NaI]_{0.5}$ are shown in Fig. 5.10. It is apparent that the dramatic effects noted when salts were mixed for the 4 / 1 samples are somewhat attenuated for the 8 / 1 concentrations but the mixed salt system is still the best conductor (a repeatable result) with conductance values above ca. 340 K about twice that of the single salt materials. Again, a comparative table is given (Table 5.2) :

Sample	σ(345K) /10^5 Scm^{-1}	σ(383K) /10^4 Scm^{-1}
$PEO_8LiCF_3SO_3$	7.0	4.3
PEO_8NaI	4.8	4.3
$PEO_8[LiCF_3SO_3]_{.5}[NaI]_{.5}$	19.0	8.3

Table 5.2. Conductance data at (345, 383)K for single and mixed salt electrolyte materials.

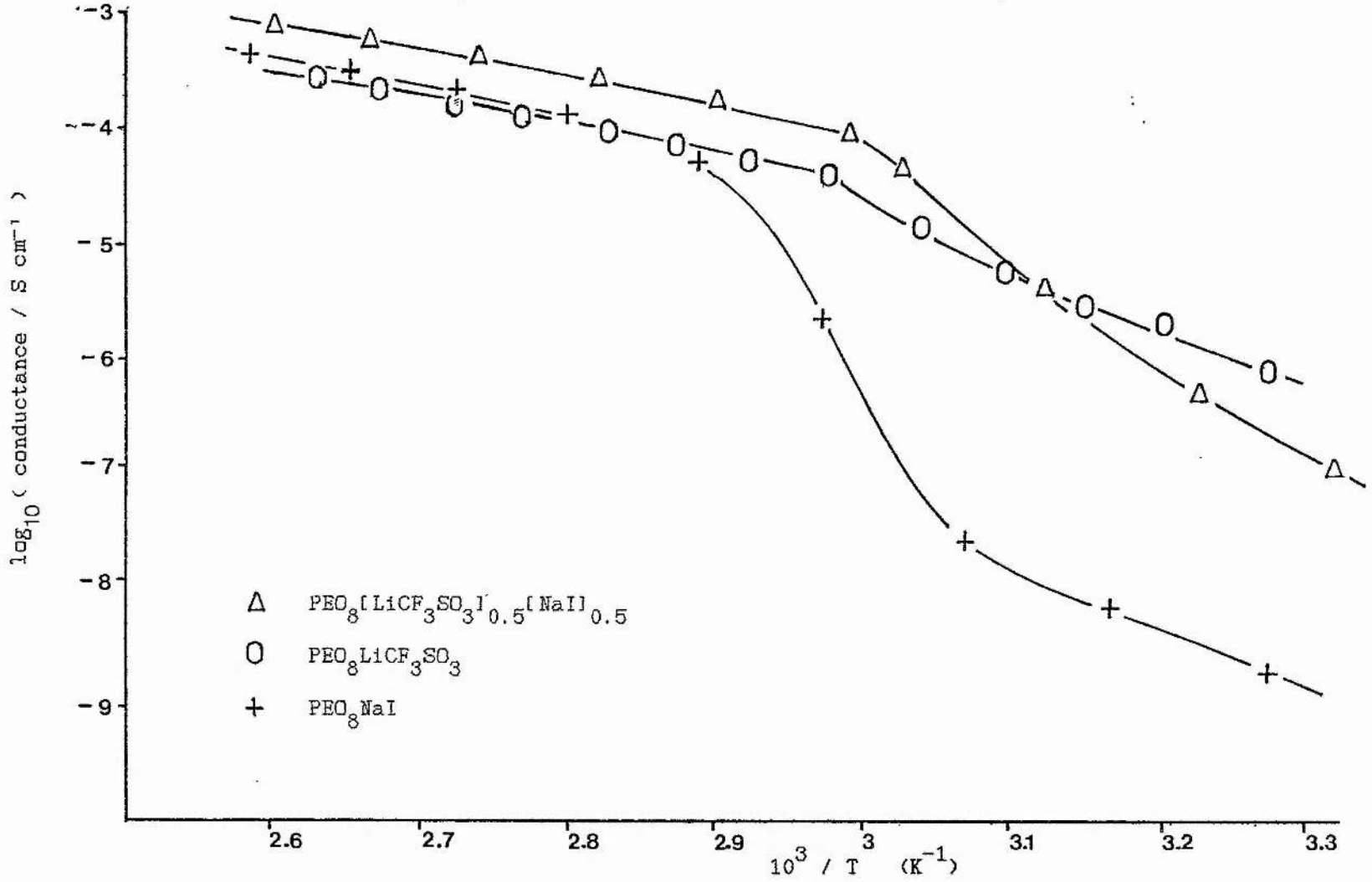

Fig. 5.10. Semilogarithmic plots of conductance vs. temperature for $PEO_8[LiCF_3SO_3]_{0.5}[NaI]_{0.5}$, $PEO_8LiCF_3SO_3$ and PEO_8NaI. ($PEO_8LiCF_3SO_3$ data from reference [122]).

5.3.2 Differential scanning calorimetry (DSC).

DSC thermograms obtained for the 4 / 1 and 8 / 1 mixed and single salt samples are shown in Fig. 5.11. The heating rate for the data was 8 K min^{-1} but in practice there were no major differences for heating rates between 1 K min^{-1} and 16 K min^{-1}.

DSC thermograms for $PEO.LiCF_3SO_3$ and PEO.NaI electrolytes have regularly appeared in the literature[22,125] and their behaviour is well known; for 4 / 1 concentrations a small event at ca. 330 K is ascribed to the fusion of pure PEO crystallites whilst endotherms at much higher temperatures, ca. 460 K for $PEO_4LiCF_3SO_3$ and 465 K for PEO_4NaI, are assigned to the melting of the salt - rich crystalline complex (EO / M^+ < 4 / 1). Similarly, for the 8 / 1 concentrations at ca. 330 K there is a larger endotherm than in the 4 / 1 materials (because there is a larger PEO - type fraction), then endotherms at ca. 420 K for $PEO_8LiCF_3SO_3$ and ca. 460 K for PEO_8NaI, attributable to the melting of the crystalline complex. The relevant data here are in agreement with these results.

The mixed salt materials however showed somewhat atypical thermograms. The 4 / 1 mixed salt sample featured a slightly larger event at ≃ 325 K (than for the single salt systems) and then a very broad endotherm from ≃ 360 K to 450 K. This process appeared to finish before either of the single salt systems began a high temperature endothermic event. The latter point, and the broadness of the mixed salt endotherm, would suggest that any crystalline complex existing in the mixed salt

material is less stable than either of the single salt moieties and melts, presumably releasing charge carriers into an amorphous phase, over a range of temperatures. Thus, the mixing of salts would seem to perturb the crystalline domain, probably by the introduction of topological disorder which inhibts the more efficient crystallisation (i.e long range order) to be expected in the single salt systems.

This mixed salt effect was also noted in in the 8 / 1 sample, which showed similar behaviour to the 4 / 1 mixed salt sample but over a narrower temperature range. At ≈ 333 K a large endotherm occured at a typical temperature for the melting of PEO crystallites, which was concurrent with the knee in the conductance plot for this sample (Fig. 5.10.). Following this sharp endotherm it is apparent that the crystalline complex began to dissolve into the newly acquired amorphous phase immediately, realised as a broad endothermic event finishing by ≈ 405 K, before either 8 / 1 PEO.NaI or PEO.$LiCF_3SO_3$ event had began.

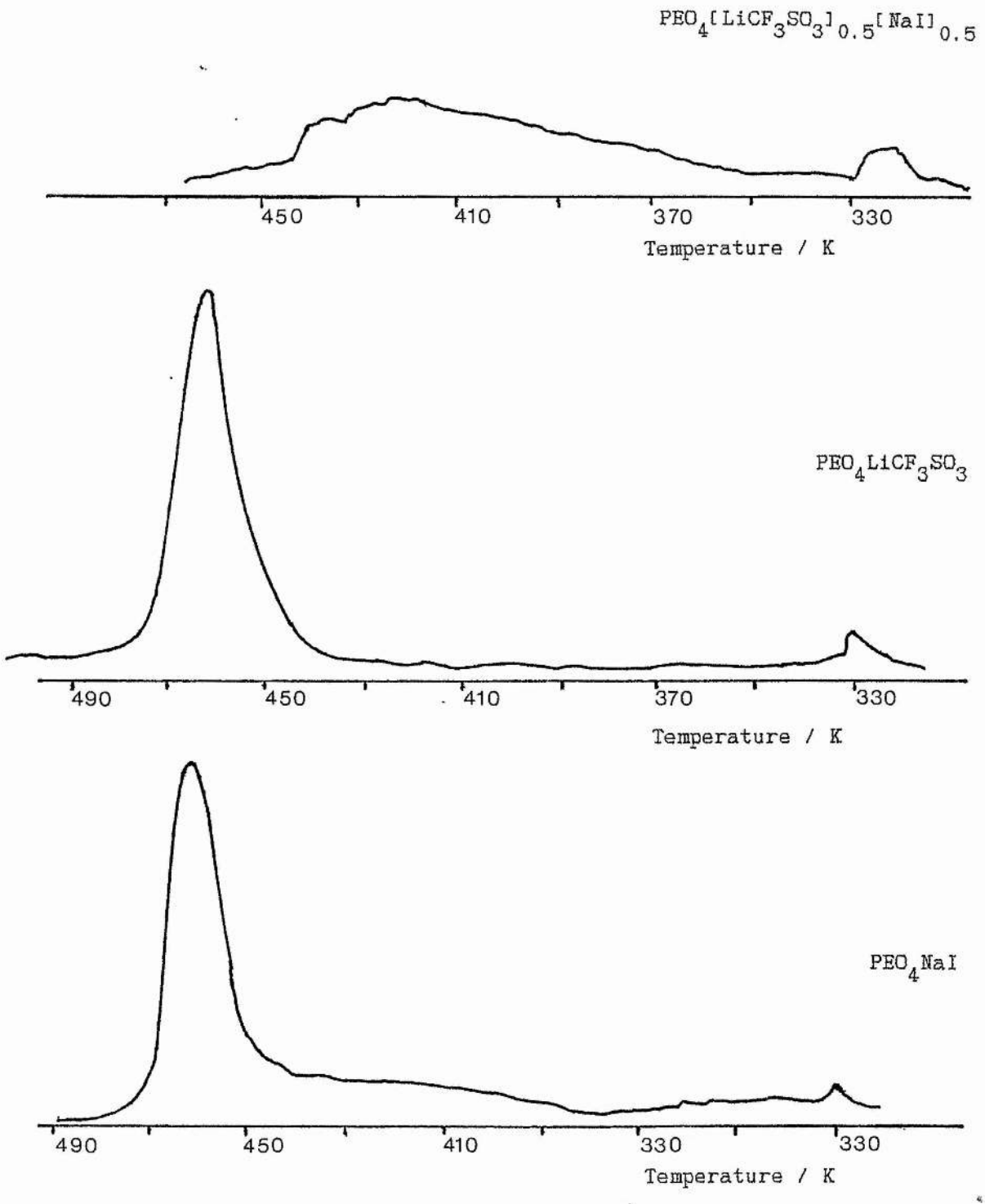

Fig. 5.11. DSC thermograms for (1) $PEO_4[LiCF_3SO_3]_{0.5}[NaI]_{0.5}$, $PEO_4LiCF_3SO_3$ and PEO_4NaI. (2) $PEO_8[LiCF_3SO_3]_{0.5}[NaI]_{0.5}$, $PEO_8LiCF_3SO_3$ and PEO_8NaI (next page).

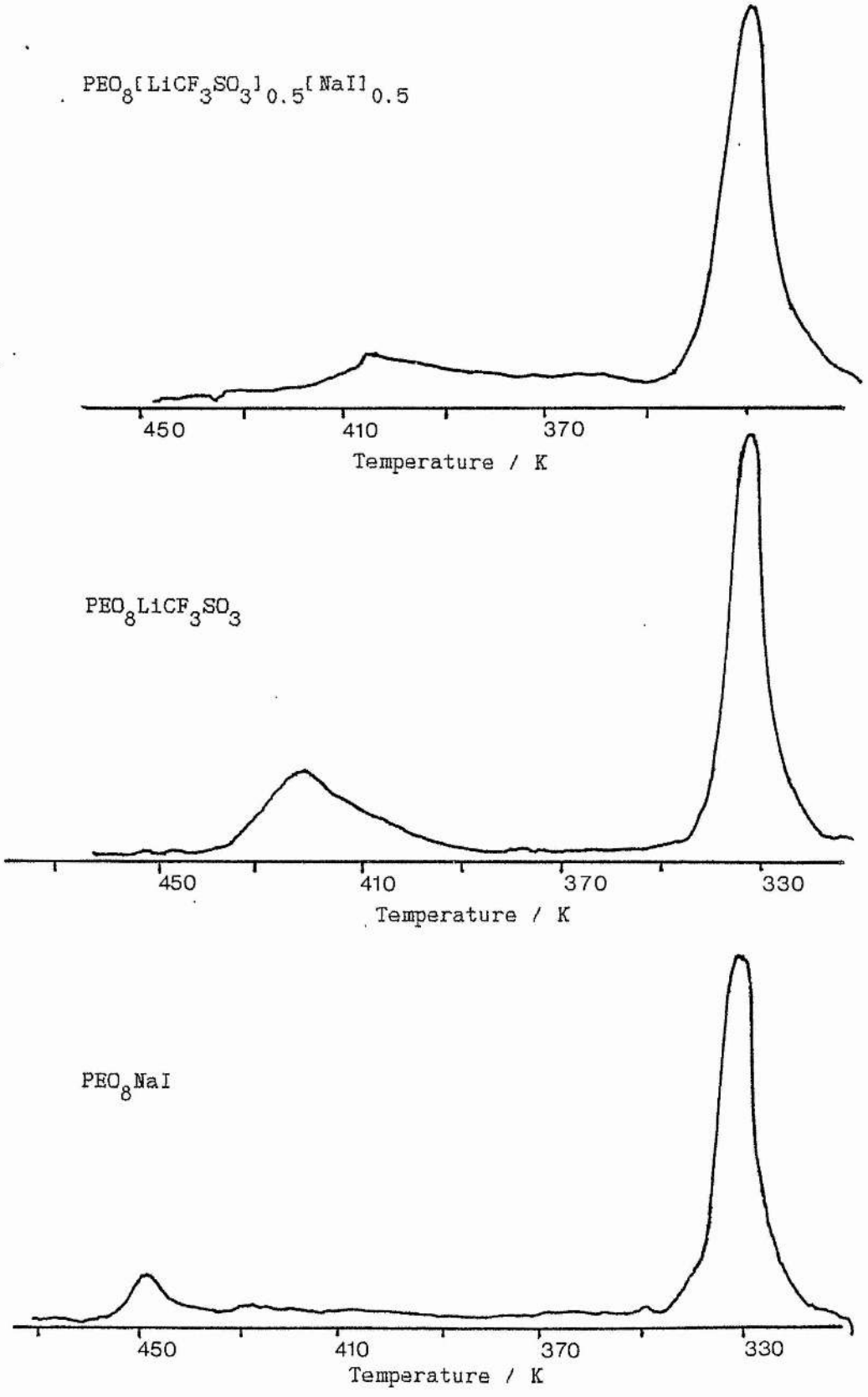

Fig. 5.11. /Cont^{d} (2) DSC thermograms for $PEO_8[LiCF_3SO_3]_{0.5}[NaI]_{0.5}$, $PEO_8LiCF_3SO_3$ and PEO_8NaI.

5.3.3 Nuclear magnetic resonance

The Moryoussef work mentioned above (and Armand's for that matter) was only a conductance study and no other characterisation of the $CaBr_2$ / CaI_2 mixed salt system was undertaken; in this work further characterisation was given to the $LiCF_3SO_3$ / NaI mixed salt electrolyte by the nmr technique.

5.3.3.1 ^1H (proton) data.

(a) 4 / 1 Samples.

Fig. 5.12(a) shows familiar plots of the percentage amorphous ^1H content (polymer chain) vs. temperature for the mixed - salt, NaI and $LiCF_3SO_3$ electrolytes, as determined by the nmr technique. The single salt profiles are essentially consistent with those of other workers[22,41], where the remaining short T_2 fraction above ca. 333 K was assigned to that of a high melting temperature crystalline complex. As was noted and discussed in chapter 4 for the PEO.$LiCF_3SO_3$ systems, both the mixed salt and NaI systems show a monotonically increasing amorphous fraction below ca. 333 K.

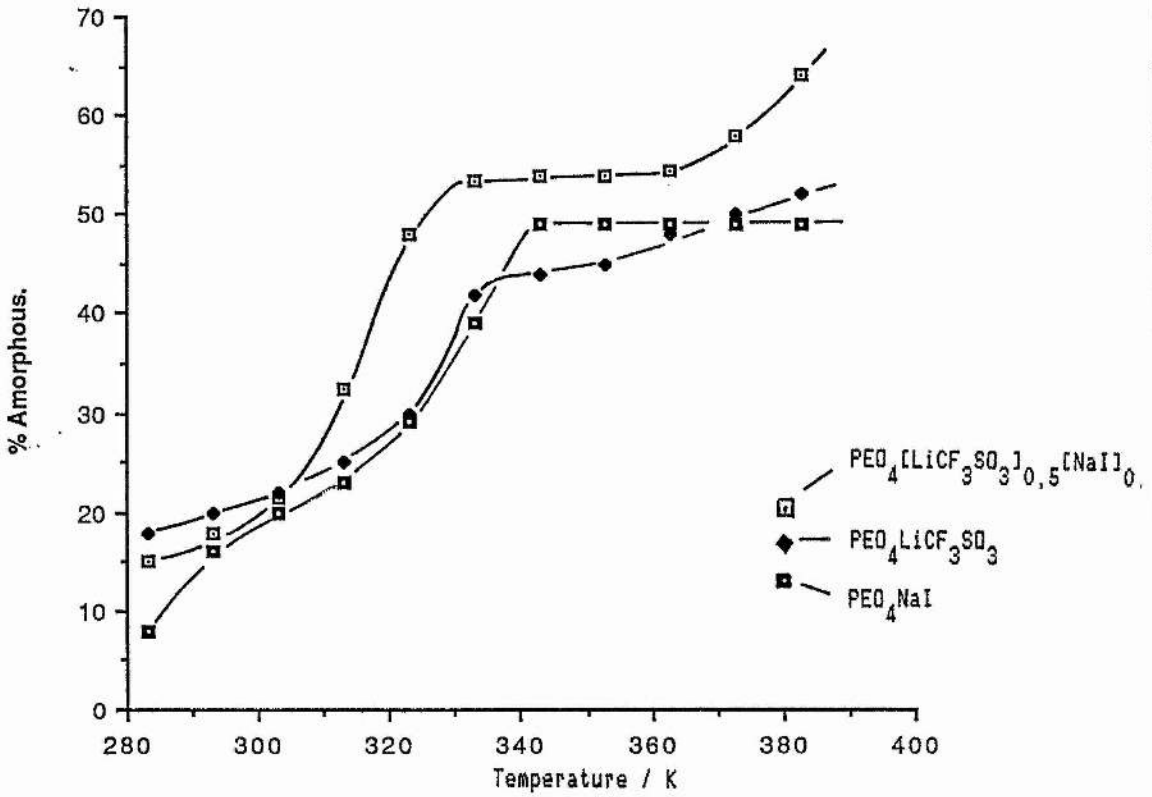

Fig. 5.12(a). The percentage amorphous polymer content vs. temperature (determined by nmr) for $PEO_4[LiCF_3SO_3]_{0,5}[NaI]_{0,5}$, $PEO_4LiCF_3SO_3$ and PEO_4NaI.

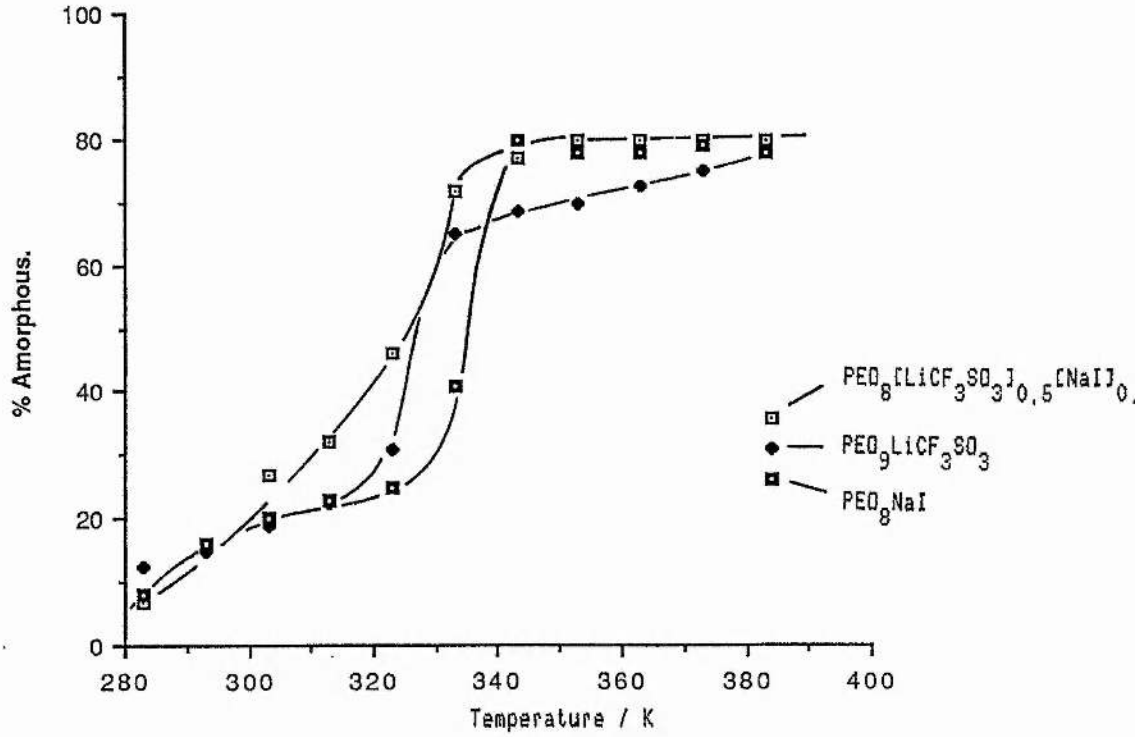

Fig. 5.12(b). The percentage amorphous polymer content vs. temperature (nmr) for $PEO_8[LiCF_3SO_3]_{0,5}[NaI]_{0,5}$, $PEO_9LiCF_3SO_3$ and PEO_8NaI.

It is apparent from the figure that Moryoussefs' somewhat intuitive contention of an increased amorphous (conducting) phase when salts are mixed is vindicated in comparing the mixed salt with the $LiCF_3SO_3$ material, the mixed salt system showing 7-10% more amorphous character at most temperatures. A similar conclusion can be reached in comparing the mixed salt with the NaI material except in the (340 - 360)K temperature range where the estimated errors (< 10%) associated with analysis of the bi - component fid may permit data overlap. (It should be noted however, that repeated measurements consistently gave a larger percentage amorphous value to the mixed system in this temperature range.)

The temperature dependence of the mixed salt amorphous fraction is also interesting and finds accord with the DSC data: (1) The onset of an event in the nmr data at ≃ 300 K, finishing at ≃ 330K, occurs in a similar temperature range as the small endotherm in the DSC data (Both occur at slightly lower temperatures than similar events for the single salt systems). (2) At ≃ 370 K the mixed salt amorphous fraction begins to increase from a plateau value of ≃ 54%, matching to within 10 K the onset of the broad high temperature DSC endotherm. This is consistent with a melting phenonemon where the short T_2 crystalline material becomes amorphous and so long T_2 in the nmr experiment. (Unfortunately, higher temperatures were not available to the nmr experiment due to unacceptable helium boil off in the superconducting magnet liquid helium jacket.)

(b) 8 / 1 Samples.

The ^1H nmr data detailed for the PEO.$LiCF_3SO_3$ sample in the following comparison concerns an EO / Li ratio of 9 / 1, not 8 / 1 as for the conductance and DSC data. It is considered that this has no deleterious bearing on the interpretations given.

The general trends for the mixed salt and single salt samples, shown in Fig. 5.12(b), are consistent with the accepted picture for many polyether - based electrolytes of roughly EO / M^+ = 8 / 1 concentration, where a pure PEO - type fraction melts at ca. 330 K to yield a larger amorphous fraction (70 - 80)%, the remaining crystalline fraction above this temperature due to the salt - polymer crystalline adduct. Unlike the percentage amorphous data for the 4 / 1 samples, no clear conclusions can be drawn as to an increased amorphous fraction where salts are mixed here (i.e above ≃ 330 K). This is because the estimated errors in the fid (graphical) analyses were larger at < 15%, due to the remaining short T_2 (crystalline signal) being small, hence permitted data overlap.

5.3.3.2 ^{19}F and ^{7}Li data.

Given that analysis of the relevant fids can yield similar information for the ^{7}Li (cation) and ^{19}F (anion) nuclei as it does for ^{1}H, data were also taken for those nuclei and their percentage amorphous (or mobile) component calculated vs. temperature for both the mixed salt and pure $LiCF_3SO_3$ systems (Fig. 5.13.). For clarity, the nmr results for the 4 / 1 samples will be discussed first (Fig. 5.13(a)).

(a) ^{19}F Signal:

In chapter 4 it was found that the $PEO_4LiCF_3SO_3$ fluorine signal was single - component, short T_2 ($\simeq$ 30μs) until above $\simeq$ 360 K where a small amount ($\leq$ 5%) of long T_2 component was observed. This was taken as evidence of only a small overall concentration of mobile species (i.e charge carriers) in the electrolyte and was consistent with the poor conductance behaviour of the material. In contrast, the mixed salt system showed a much larger mobile fraction over the entire temperature range, rising monotonically to $\simeq$ 24% of the total signal at 380 K.

(b) ^{7}Li Signal:

In the $PEO_4LiCF_3SO_3$ sample the ^{7}Li fid was found to be single - component short T_2 ($\simeq$ 120μs) over the entire temperature range, with no long T_2 (or mobile) component observable. In the mixed salt system the striking observation was two - component behaviour (both short and long

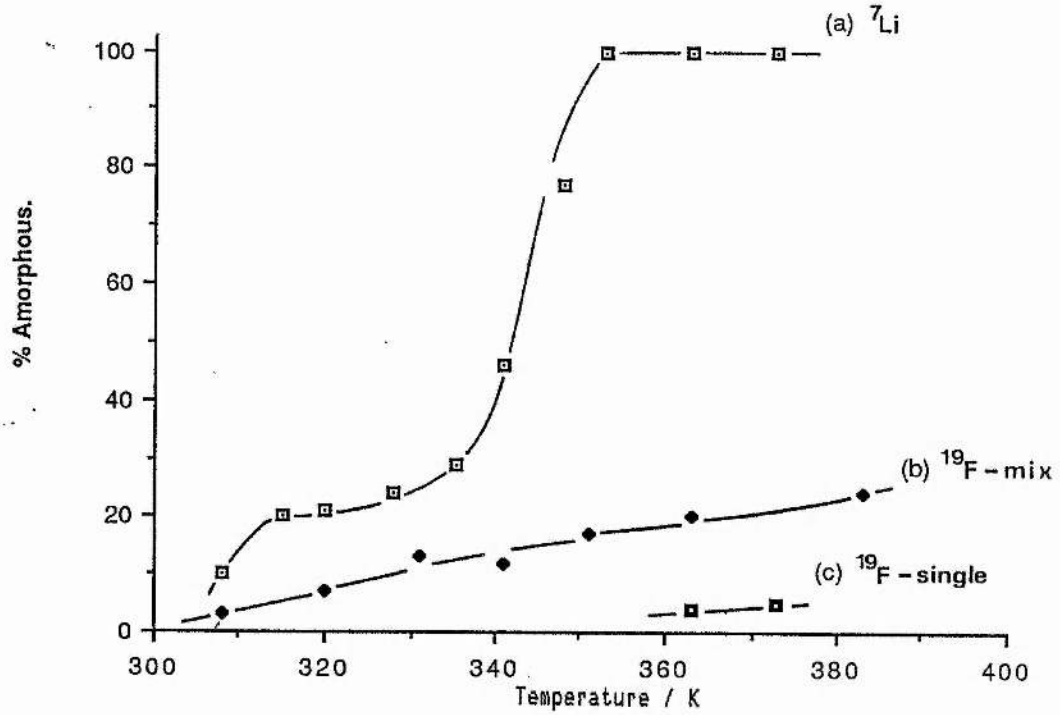

Fig. 5.13(a). The percentage amorphous content (a) ^{7}Li and (b) ^{19}F (^{19}F - mix) in $PEO_4[LiCF_3SO_3]_{0,5}[NaI]_{0,5}$. Included for comparison is the relevant ^{19}F data (^{19}F - single) for $PEO_4LiCF_3SO_3$.

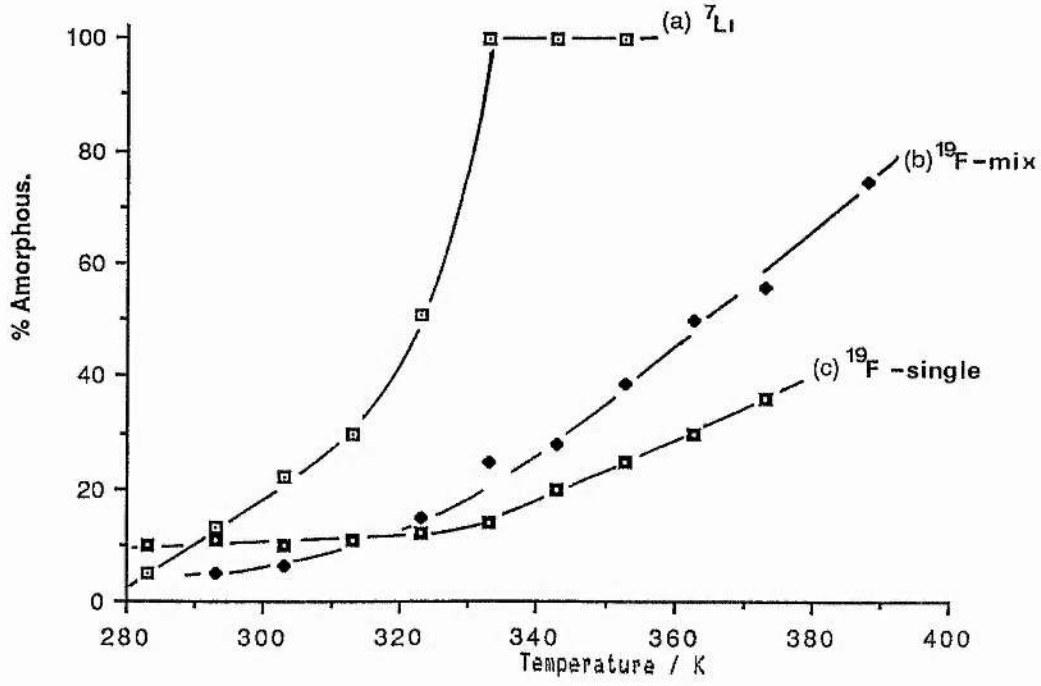

Fig. 5.13(b). The percentage amorphous content (a) ^{7}Li and (b) ^{19}F (^{19}F - mix) in $PEO_8[LiCF_3SO_3]_{0,5}[NaI]_{0,5}$. Included for comparison is the relevant ^{19}F data (^{19}F - single) for $PEO_9LiCF_3SO_3$.

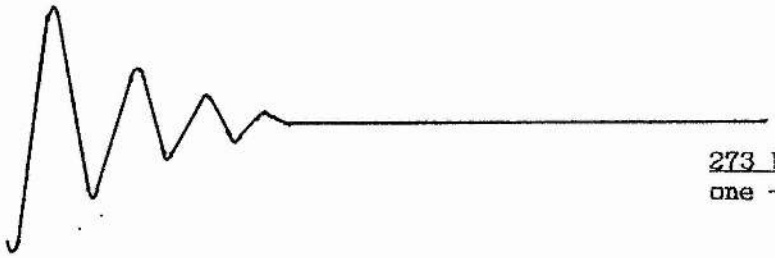

273 K. 500 μs. sweep
one - component fid, short T_2.

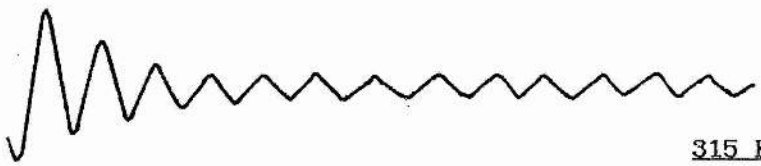

315 K. 1 ms. sweep
two - component fid
short and long T_2.

353 K. 1 ms. sweep
one - component fid, long T_2.

Fig. 5.14. The free induction decay of ^7Li in $PEO_4[LiCF_3SO_3]_{0.5}[NaI]_{0.5}$ at 273 K, 315 K and 353 K.

T_2) with the appearance and growth of a long T_2 signal *near the onset of the region of reduced apparent activation energy* in the σ vs. temperature plot and the endotherm at ca. 320 K in the DSC data. This mobile component was found to grow rapidly with temperature and by 350 K (where all the $PEO_4LiCF_3SO_3$ signal was still short T_2) the ^7Li fid was observed to be one - component long T_2, suggesting that all nmr - observable lithium cations were now mobile in the system. Examples of the ^7Li fid at three representative temperatures are given in Fig. 5.14. to illustrate this process.

Similar results were noted in comparing the 8 / 1 mixed salt with the $PEO_9LiCF_3SO_3$ sample (Fig. 5.13(b)).

^{19}F Signal:

In the $PEO_9LiCF_3SO_3$ sample the ^{19}F amorphous component remained invariant at ca. 10% up to ≃ 333 K and therafter began a slow monotonic increase to ca. 35% by 373 K, consistent with the progressive dissolution of the crystalline complex into the amorphous PEO phase (see chapter 4, 4.2.2.1). The ^{19}F long T_2 signal in the mixed salt 8 / 1 sample showed similar behaviour except the increase in the amorphous fraction was montonic over the entire temperature range, with no apparent influence from the event at ≃ 330 K noted for the ^1H signal, suggesting a different phase location for the $CF_3SO_3^-$ anion to that of the Li^+ cation. Although smaller in value below 320 K, the mixed salt amorphous ^{19}F fraction soon passed the corresponding $PEO_9LiCF_3SO_3$ fraction and by

390 K was found to be about 75% of the total two - component signal, suggesting that percentage of $CF_3SO_3^-$ to be mobile in the system.

^7Li Signal:

Whereas the ^7Li signal in $PEO_9LiCF_3SO_3$ only began a lengthening in T_2 value (i.e the line narrowed) at ≃ 333 K and did not show two - component behaviour, the ^7Li resonance showed the appearance of a long T_2 (mobile) lithium fraction at only 283 K, growing rapidly then surging, in conjunction with the ^1H event for that sample, to 100% long T_2 (amorphous) by 330 K.

It is realised that, in effect, six samples are being discussed here and the salient features of the study may lose their emphasis. With this in mind the more important points resultant from the mixed salt study are outlined:

(1) The mixed salt materials $PEO.[LiCF_3SO_3]_{0.5}[NaI]_{0.5}$ gave a superior conductivity to either of the single salt systems.

(2) DSC showed the mixed salt crystalline phase to melt over a range of temperatures below the sharper events noted for the single salt systems.

(3) ^{1}H nmr showed that the 4 / 1 mixed salt system had a larger amorphous content (i.e a more extensive conducting phase) than the relevant single salt materials.

(4) ^{7}Li and ^{19}F nmr intimated more charge carrying species in the amorphous phase for the mixed salt materials.

(5) A dramatic effect on the lithium motion was noted at ≃ 330 K for the mixed salt systems, consistent with the release of motional constraints implied by the ^{1}H nmr and DSC data and the onset of the region of reduced apparent activation energy in the conductance plots.

The points can conveniently be explained as due to topological effects conferred on the electrolyte system by the mixing of salts. Stereoregularity and thus ion - ion and ion - solvent interactions neccessary in forming the crystalline adduct are modulated and give a more disordered (and thermally more labile) crystalline phase than for a typical single salt system. If the crystalline domains are spherulitic in nature[121,133] (which are inherently more disordered towards the extremities[108]) then the mixed salt effect would seem to be general, where polymer chain motional thresholds between the extremes of static crystalline and liquid - like amorphous are lowered across the temperature range. In turn this would imply more potential charge carriers in a more extensive amorphous phase, giving a larger conductivity than for the relevant single salt systems.

5.3.3.3 The ^{23}Na resonance.

Mention has not yet been given to the free induction decay characteristics of the sodium nuclear species, ^{23}Na, in the relevant samples (i.e the PEO.NaI and mixed salt samples). For this nucleus it was found that fid time constants were essentially invariant at ≃ 180 μs at all temperatures for the 4 / 1 and 8 / 1 stoichiometries used, and long T_2 signals were not evident. This does not necessarily mean that the sodium species were not mobile in these systems but is again a consequence of quadrupolar interactions.

^{7}Li and ^{23}Na are both I = 3/2 nuclei and as such possess an electric quadrupole moment, Q. Now for ^{7}Li $Q = -4 \times 10^{-30}$ m^2 and for ^{23}Na $Q = 0.1 \times 10^{-28}$ m^2 and it is differences in the magnitude of this term which can confer differing nmr behaviour for these nuclei[107]. For quadrupolar nuclei the T_2 parameter can be written as[102,106,107] :

$$(T_2)^{-1} \quad \alpha \quad \chi^2 \qquad (5.3)$$

where

$$\chi^2 \quad = \quad e^2 Q \; q_{zz} / h \qquad (5.4)$$

χ is known as the nuclear quadrupolar coupling constant, $e.q_{zz}$ is an electric field gradient term, e the charge on the proton and h is Plancks constant.

Inspection shows that the χ^2 parameter is six times larger for ^{23}Na than ^{7}Li hence T_2 for the former may be shorter by that amount for similar local electric field gradients. It follows that whereas partition of the ^{7}Li fid into short and long T_2 components representing immobile and mobile cationic species is a straightforward process, a similar analysis for the ^{23}Na fid may not be possible because quadrupolar interactions keep the fid T_2 of even a 'mobile' sodium nucleus of the short T_2 type. This would appear to be the case in this work, where ^{23}Na linewidths were never narrower than about 2 kHz (for certain quadrupolar nuclei in solution the linewidth may be tens of kHz or more[107]) and short / long T_2 assignments were not possible.

This behaviour for the ^{23}Na resonance in polymer electrolyte materials finds accord with that noted other workers[33,101], where, although a line narrowing was observed with temperature in PEO.NaSCN and PEO.$LiClO_4$ systems, the linewidth was never less than about 1 kHz ($T_2 \simeq 320\ \mu s$).

5.3.3.4 Attenuation of the ^{7}Li and ^{23}Na fid intensity.

As in previous sections, the term 'observed species' has been used in discussing the nmr response of the quadrupolar nuclei present in the mixed salt samples. The reasons for this terminology again concerns a 'wipe - out' effect, mentioned in 4.2.2.1 to explain the intensity anomaly in ^{7}Li fid amplitude data, whereby the contribution of significant numbers of the quadrupolar nuclei are not observed in the nmr experiment, in this case ^{7}Li and ^{23}Na nuclei.

This conclusion was reached from similar observations to those noted in 4.2.2.1 :

The $\pi/2$ (90^{o}) pulse width for ^{7}Li and ^{23}Na was of the dipolar value for both nuclei, ca. 9 μs and 14 μs respectively, suggesting that satellite intensity was included in the observed signal. (The ^{7}Li resonance in the 8 / 1 mixed salt system was an exception below $\simeq$ 210 K where $\pi/2$ was $\simeq$ 4μs, suggesting only the $-\frac{1}{2} \rightarrow \frac{1}{2}$ central line transition was observed.)

A quadrupolar echo was not observed for either quadrupolar nucleus in the 4 / 1 or 8 / 1 mixed salt samples at any temperature.

A summary of the ratio of the number of nmr - observed quadrupolar nuclei to the actual concentration in a given sample, i.e the 'percentage observed', is given in Table 5.3. for the six samples studied by the nmr technique :

Sample.	% Observed (±10%):	^{7}Li	^{23}Na
$PEO_4LICF_3SO_3$		45	
PEO_4NaI			65
$PEO_4[LiCF_3SO_3]_{0.5}[NaI]_{0.5}$		47	55
$PEO_9LiCF_3SO_3$	< 333K,	45	
	> 333K	(45 - 90)	
PEO_8NaI	< 333K		75
	> 333K		(80 → 100)
$PEO_8[LiCF_3SO_3]_{0.5}[NaI]_{0.5}$	< 333K	50	55
	< 375K	(50 - 60)	
	385K	70	

Table 5.3. Percentage observed quadrupolar species in PEO - based electrolyte samples.

For the 8 / 1 PEO.NaI sample below ≃ 333K, about 75% of the theoretical sodium content was observed and full ^{23}Na fid intensity was obtained by 380 K, consistent with the release of 'lost' nuclei from the crystalline adduct as it dissolved into the amorphous phase. This result reinforces the assumption that a residual quadrupolar interaction kept the ^{23}Na fid short T_2 at ≃ 180μs (linewidth broad, ≃ 2 kHz), even though significant numbers of those nuclei must be mobile in the amorphous phase at ca. 380 K ($\sigma > 4 \times 10^{-4}$ Scm^{-1}). Upon the mixing of salts the

fraction of ^{23}Na observed in the nmr experiment decreased from the values found in the corresponding PEO.NaI 4 / 1 and 8 / 1 samples, reflecting an increase in the number of nuclei affected by a second order quadrupolar interaction (hence not observed). The values obtained for ^{23}Na in the mixed salt samples, ca. 55% in both, appeared temperature invariant up to 388 K.

Of perhaps more immediate interest in this work is the nmr response of the ^{7}Li nucleus. For the 4 / 1 mixed salt sample the ^{7}Li fid went from all short T_2 (120 μs) at 310 K, to all long T_2 by 350 K (at the inhomogeneity limit, ≃ 900 μs), the signal remaining at ≃ 45% of the theoretical intensity over this and the entire temperature range of study. Since the lithium signal intensity does not change it is concluded that the short to long T_2 transition for that nucleus concerns one sample enviroment, with no added intensity from, for example, the appearance of 'lost' lithiums.

This immediately suggests a deviation from the accepted view for single salt 4 / 1 materials, such as those used in this work, where about 90% of the sample is composed of 'crystalline complex', the remaining fraction pure PEO, which in the mixed salt case would have to solvate the nmr - observable Li^+ in the ratio EO / Li = 1.6 / 1. Instead the data fit the disordered spherulite model (mentioned in 4.2.2.1) where the distinction between the mixed salt and the $PEO_4LiCF_3SO_3$ samples is that the outer (disordered) regions of the former permit lithium cations to become mobile above ≃ 310 K, noted as a long T_2 signal, but the latter

single salt material does not. The effect is thus noted as an improved conductivity resultant from more charge carriers in the mixed salt 4 / 1 sample in comparison with the $PEO_4LiCF_3SO_3$ sample.

A similar model may be envisaged in comparing the mixed salt electrolyte $PEO_8[LiCF_3SO_3]_{0.5}[NaI]_{0.5}$ with that of $PEO_9LiCF_3SO_3$, with the addition that non - observable lithiums may add to the ^7Li signal intensity above ≃ 333 K as material with true crystalline character dissolves into the newly aquired amorphous PEO fraction. (Analysis of Fig. 4.8. in chapter 4 and Table. 5.3, this chapter, shows in fact that the increase in number of observable lithiums occurs at a slightly faster rate in the $PEO_9LiCF_3SO_3$ sample below ≃ 380 K. The difference however is that the mixed salt ^7Li signal is at the inhomogeneity limit (≃ 900 μs) by 333 K but the single salt fid only lengthens in T_2 slowly from 120μs at 333 K to the inhomogeneity limit by ≃ 385 K. This suggests that that the mixed salt lithiums become mobile quickly compared to the same nuclear species in the $PEO_9LiCF_3SO_3$ sample.)

5.3.3.5 Recrystallisation behaviour

Final consideration is given to the recrystallisation behaviour of the mixed salt systems, as studied by the nmr technique. This involved the heating of samples in an oven to ≃ 475 K (i.e above the liquidus temperature as determined by DSC, to give a homogeneous amorphous phase), then quenching to 77 K in liquid nitrogen to 'freeze' the amorphous state, giving a short T_2 ^1H (≃ 10 μs) or ^{19}F (≃ 30 μs) signal. Upon rapid heating to 313 K the amorphous state passed through Tg to give a longer T_2 signal, whereupon the growth of the crystalline fraction (i.e the growth of a short T_2 signal) was monitored as a function of time. (The heating rate was ca. 10 K min^{-1}. Tg for the mixed salt samples, detected as a lengthening of the short T_2 fids, was found to be ca. 298 K for the 4 / 1 and ca. 283 K for the 8 / 1 sample, showing the expected viscosity effect on Tg of salt content.)

Fig. 5.15. shows the relevant plots for the ^1H and ^{19}F nuclei in the respective mixed salt samples. Here '% Crystallinity' indicates the amount of crystalline fraction obtained from the usual two - component fid analysis. (^7Li was not studied because its T_1 was long, of the order of seconds, and noise levels required signal averaging (≃ 36 fids) during which time the observed fid would be changing due to the recrystallisation process.)

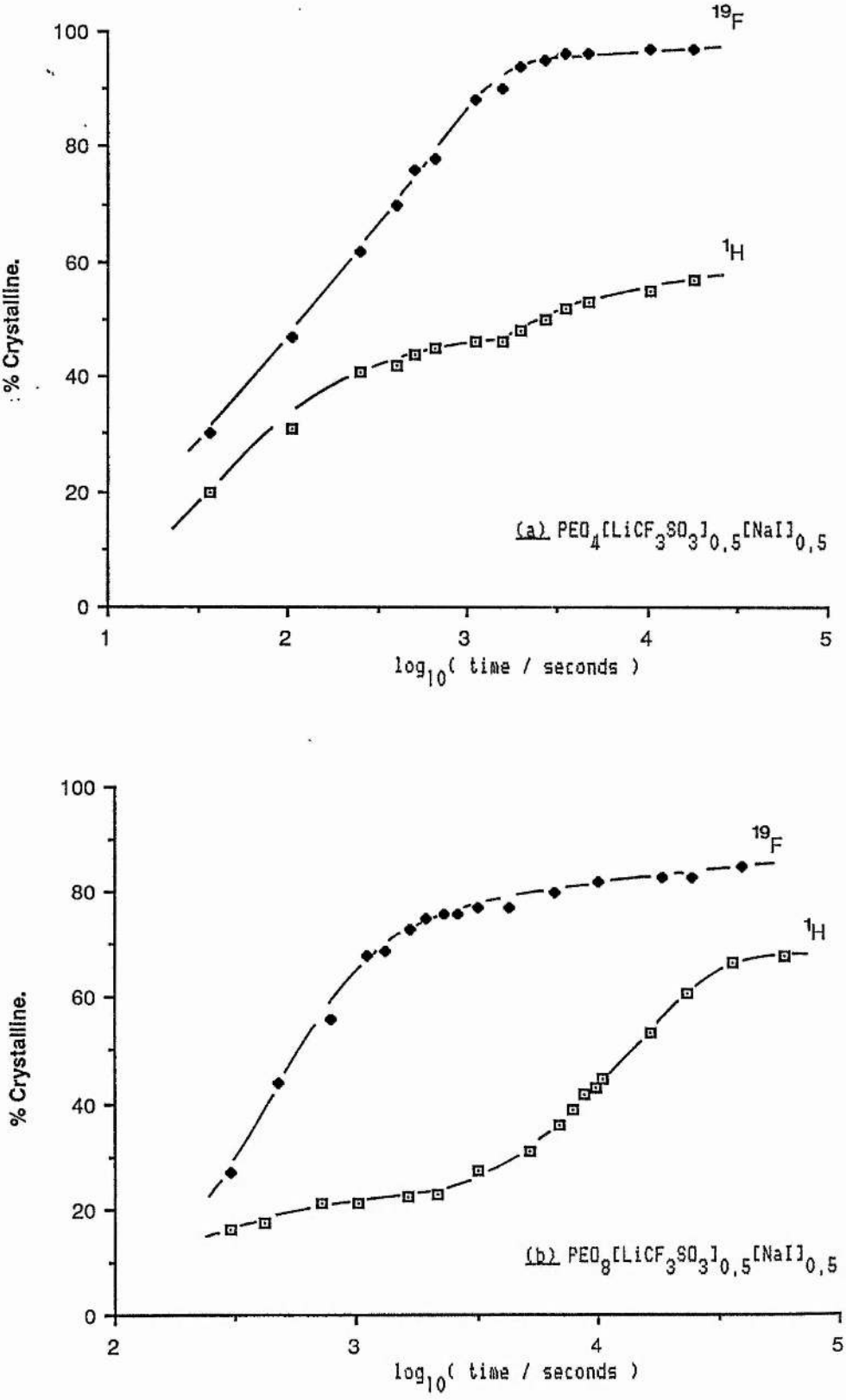

Fig. 5.15. Isothermal recrystallisation data (313 K), as determined by nmr, for the polymer host (^1H signal) and the $CF_3SO_3^-$ anion (^{19}F signal) in (a) $PEO_4[LiCF_3SO_3]_{0,5}[NaI]_{0,5}$ and (b) $PEO_8[LiCF_3SO_3]_{0,5}[NaI]_{0,5}$.

4 / 1 Sample.

The ^1H data shows that at 313 K there was a rapid initial recrystallisation, taking roughly six minutes, with about 46% of the protons losing their motion in the process. This value remained constant for ≃ 3/4 hr. until a second, slow loss of proton motion was noted, taking ≃ 5 hr. to reach the equilibrium fraction at 313 K of the heating cycle experiment (Fig. 5.12.). It is also interesting to note that the 46% of the electrolyte which initially recrystallised under isothermal conditions corresponds to the 46% of the electrolyte remaining above 333 K in the heating cycle, which was assigned to the high melting temperature crystalline complex. It is not unreasonable therefore, to assume that the initial recrystallisation observed here is that of the high melting temperature phase.

The ^{19}F data shows that the $CF_3SO_3^-$ anion continually lost motion until at ≃ 3/4 hr. it, like the ^1H, slowly headed off towards the equilibrium value obtained on the heating cycle (≃ 95%). If the initial processes (0 - 3/4 hr.) for the polymer chain and $CF_3SO_3^-$ anion occurred in the same phase, then it can be concluded (from simple arithmetic) that nearly all the anion is in the crystalline complex phase with the approximate stoichiometry EO / $CF_3SO_3^-$ ≃ 4 / 1. (Interestingly, the reverse arguement implies that the predominant anionic species in the mixed salt amorphous (conducting) phase is iodide.) The ^{19}F recrystallisation data immediately show why the percentage amorphous ^{19}F

data in Fig. 5.13. is not as sensitive to the event noted at ≃ 333 K for the ^{7}Li percentage amorphous data; the $CF_3SO_3^-$ anions are in a salt - rich crystalline phase which only dissolves progressively into the available amorphous fraction.

8 / 1 Sample.

The 8 / 1 sample was found to show recrystallisation profiles and timescales similar to that of the 4 / 1 but, as would be expected for the electrolyte of lower overall salt content, the fraction of crystalline complex was less. The ^{1}H data again showed what could be described as a two - stage process; a faster initial recrystallisation period taking about 3/4 hr., with about 24% of the protons losing their motion, followed by a slow loss of proton motion to the equilibrium value noted in the heating cycle experiment (≃ 70%). That there is a slower second process is probably in qualitative in agreement with the accepted view that following the initial recrystallisation of the crystalline complex the remaining material is still too concentrated in salt to allow immediate formation of crystalline PEO - type material. Hence, time is required for the diffusion of remaining ionic species and the reorganisation of PEO chains. (For intermediate salt concentrations (EO / M^+ ≥ 10 / 1) the effect is particularly evident; $PEO_{10}NaI$ remains totally amorphous for several hours before recrystallisation of any type occurs and $PEO_{10}LiClO_4$ may be maintained in an amorphous state for several days[13,129].)

Similarly, the ^{19}F data was two - stage, with change of recrystallisation rate occurring at the same time as for the protons (≃ 3/4 hr.). Again, if the initial processes occur in the same phase then most of the $CF_3SO_3^-$ content is in that phase with the approximate stoichiometry EO / $CF_3SO_3^-$ ≃ 5 / 1. This is not neccessarily a heretical statement (it is currently accepted that the EO / salt concentration is ≤ 4 / 1 in the crystalline complex) but allows for a small amount of iodide anion to be present in the high melting temperature complex, the remaining iodide fraction again the predominant anionic species in the mixed salt amorphous phase. (An interesting experiment would perhaps be to look at competitive effects in a system of the type :

$$PEO.M^+(CF_3SO_3^- / I^-)$$

where only one cationic species is present, and deduce if there is a preferred phase for either anion type.)

Appendices

APPENDIX 1

The addition filter

Throughout the nmr work use was made of signal averaging to improve signal to noise ratios thus giving a 'cleaner' fid signal for subsequent analysis. There were times however when signal averaging was somewhat time - consuming i.e for ^{7}Li with $T_1 \simeq 30$ s, waiting $5T_1$ between pulse repetitions and averaging 36 free induction decays, meant at least 1½ hrs for that data point at that temperature.

Apart from reducing noise levels by operating at higher field strengths (Zeeman levels are pushed further apart, giving a stronger rf absorbtion) or improving receiver electronics, the noise must be accepted and signal averaging used to reduce it.

In this work, the free induction decay was detected as an oscillating voltage (in the receiver coil), digitized, and then transferred to computer as 1024 data points. As an excercise, a noise 'filter' was written to manipulate the data, involving the simplest of algorithms i.e in the basic computer dialect :

```
FOR  Y = 1 TO 1024
X(Y) = ( X(Y) + X(Y + 1) ) / 2          One filter cycle.
NEXT Y
```

where successive fid data points in the origonal array (X(Y)) are averaged to generate a new array i.e :

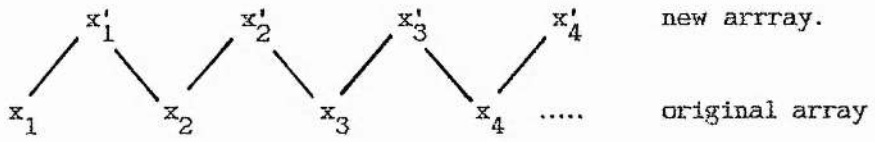

The filter was tested by synthesising a free induction decay of known peak to trough amplitudes (using a scaled function of the form sin(x).exp(-x)), shown in Fig. A.1., then adding noise to it via the basic 'RANDOM' command. The data was then 'filtered' according to the above algorithm. Each cycle took ≈ 5s. to run using BBC basic and the observed effect was to pull the noise in towards the pure fid profile. With two filter cycles the fid was observed to be notably 'cleaner' and by the 5th. cycle (i.e 5th. generation data) fid peak - trough amplitudes were essentially those of the parent fid.

Similar effects were noted upon real data, as shown in Fig. A.2. but it was considered that the use of such a simple algorithm without further characterisation would be unwise in determining fid amplitudes.

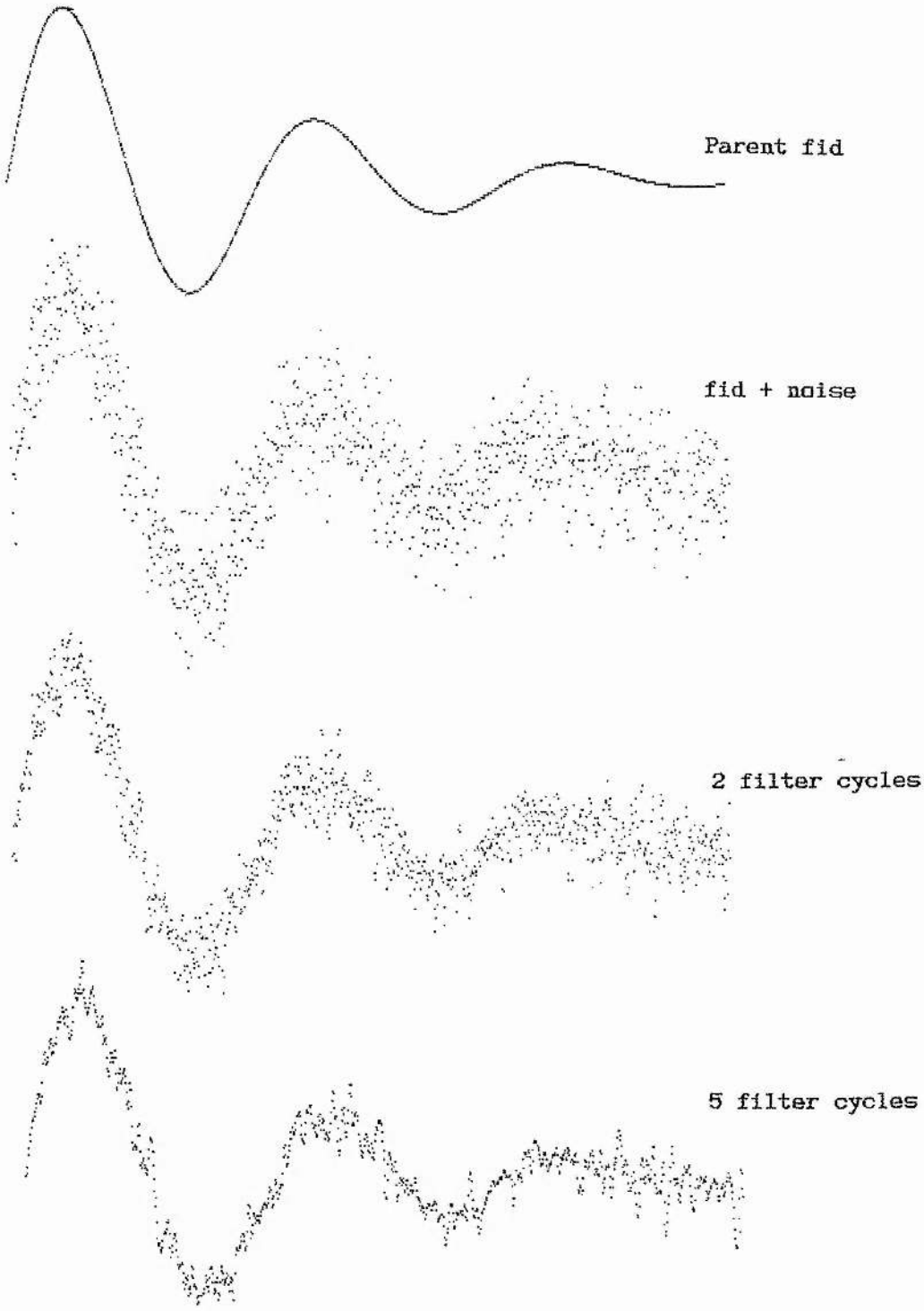

Fig. A.1. The effect of the addition filter upon a computer - generated 'noisy' free induction decay. The parent fid (no added noise) is included for comparison.

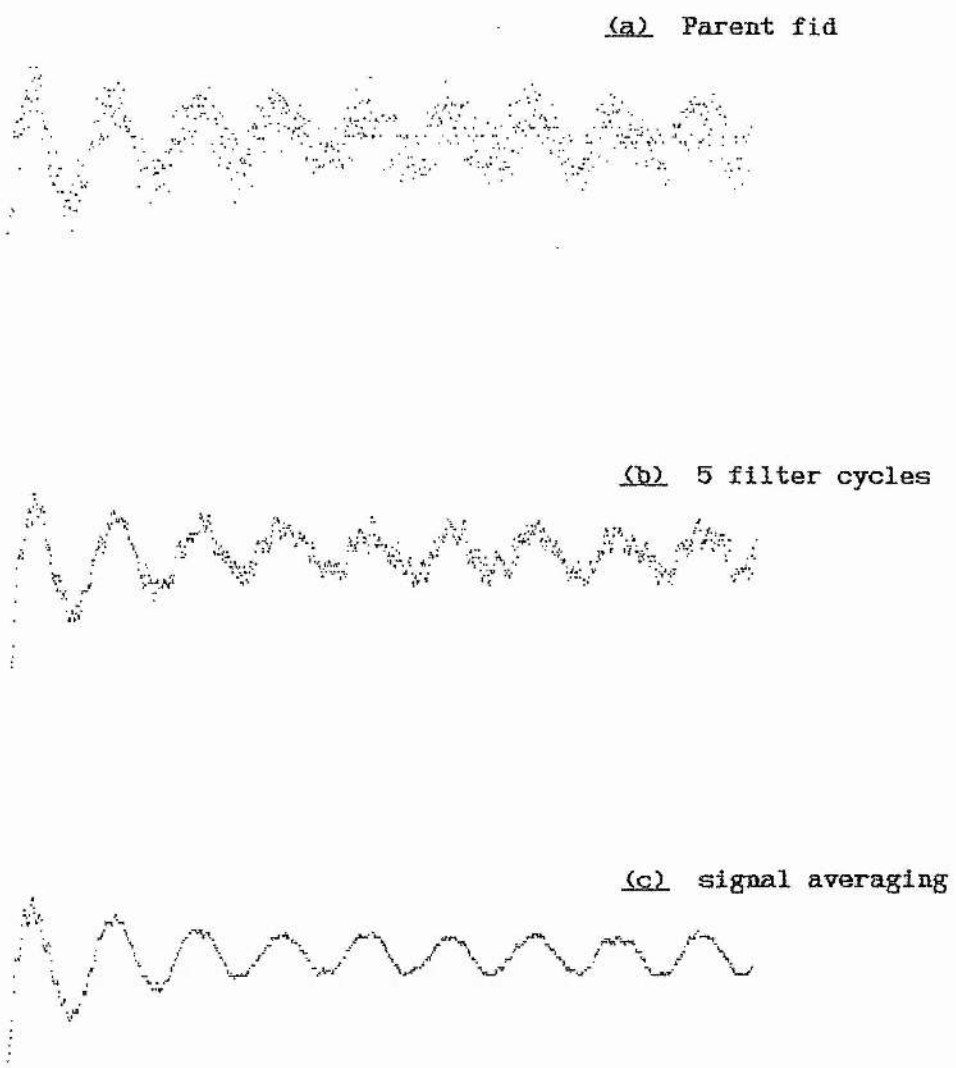

Fig. A.2. The ^{19}F fid in $PEO_8[LiCF_3SO_3]_{0.5}[NaI]_{0.5}$ at elevated temperature. (a) The fid following a single $\pi/2$ pulse (parent fid). (b) The effect of the addition filter (5 cycles) upon the parent fid. (c) The signal averaged fid (49 parent fids).

Appendix 2

The rotation barrier in the $CF_3SO_3^-$ anion by MNDO calculation.

Modified Neglect of Differential Overlap (MNDO) calculations, based upon molecular orbital theory, are semiempirical methods particularly suited to structural and heat of formation calculations for known (and hypothetical) molecular species[134]. As mainframe computer time has become more available (and less expensive) the use of such calculations has found increasing use in chemistry as a corroborative tool for experimental data. With this in mind the CF_3 rotation barrier in the trifluoromethanesulphonate anion ($CF_3SO_3^-$) was calculated by the MNDO method.

Calculations of the MNDO type involve the use of a set of predetermined parameters to define the forms and energies of the atomic orbitals of the constituent atoms in the studied molecule. The calculation then involves finding the combinations of these atomic orbitals which give rise to sets of molecular orbitals with the correct symmetries and the lowest (most negative) electronic energy for the chosen molecular and / or electronic constraints. This is known as the linear combination of atomic orbitals (LCAO) formalism[134]. Core (non - bonding) electrons are not considered but electron - electron interactions are taken into account (with the self - consistent field (SCF) method).

The computer program (from the Quantum Chemistry Program Exchange library, number 455) was run on a Vax mainframe computer by D. Higgins. Initial constraints involved an estimate of interatomic bondlengths, a formal charge of [-1] on the molecule, and that the F_3 system formed an equilateral triangle in a plane perpendicular to the principal axis of the anion. (A similar geometry was adopted for the oxygens in the SO_3 group.) The following bondlengths were chosen from reference tables[134] as initial estimates for those in the anion (Table A.1):

Bond	Bondlength / Angstroms.
carbon - fluorine	1.36
carbon - sulphur	1.79
sulphur - oxygen	1.75

Table A.1. Estimated bondlengths in the $CF_3SO_3^-$ anion before the optimisation procedure.

A sub - program then optimised these values (and the three - dimensional geometry of the atoms in the molecule) before proceding to the main operation of calculating the heat of formation of the anion as a function of the dihedral angle i.e the angle between the fluorines in the CF_3 group, and the oxygen atoms in the SO_3 group when the molecule is viewed along its Newman projection. (For each dihedral angle increment the molecular geometry was again optimised before the heat of formation calculation.)

This enthalpy information is shown in Fig. A.3., where the 'reaction co - ordinate' sampled the increment in the dihedral angle as the CF_3 group was rotated relative to the SO_3 group. It is apparent from the figure that the lowest energy configuration for the anion was calculated for a staggered conformation (dihedral angle = 60°) whilst the least favourable geometry was with an eclipsed configuration (dihedral angle = 0°). This is entirely reasonable and is consistent with other studies, such as those for ethane[136] or the aminophosphines[136], where the staggered conformations were shown to be of lower energy than the eclipsed, the difference between the two extremes representing the rotation barrier in those molecules.

Inspection of the figure shows therefore that the internal rotation barrier for the molecule studied here ($CF_3SO_3^-$ anion) corresponds to the heat of formation of the anion in the eclipsed conformation minus the corresponding value for the staggered i.e :

$$[\ -508.87\ -\ (\ -515.20\ )\ ]\ \times\ 10^3\ J\ =\ 6.3\ kJ\ mol^{-1}$$

In addition, the MNDO package yielded the interatomic distance data shown in Table A.2. from which the inter - fluorine distance was taken as 2.17 Angstroms.

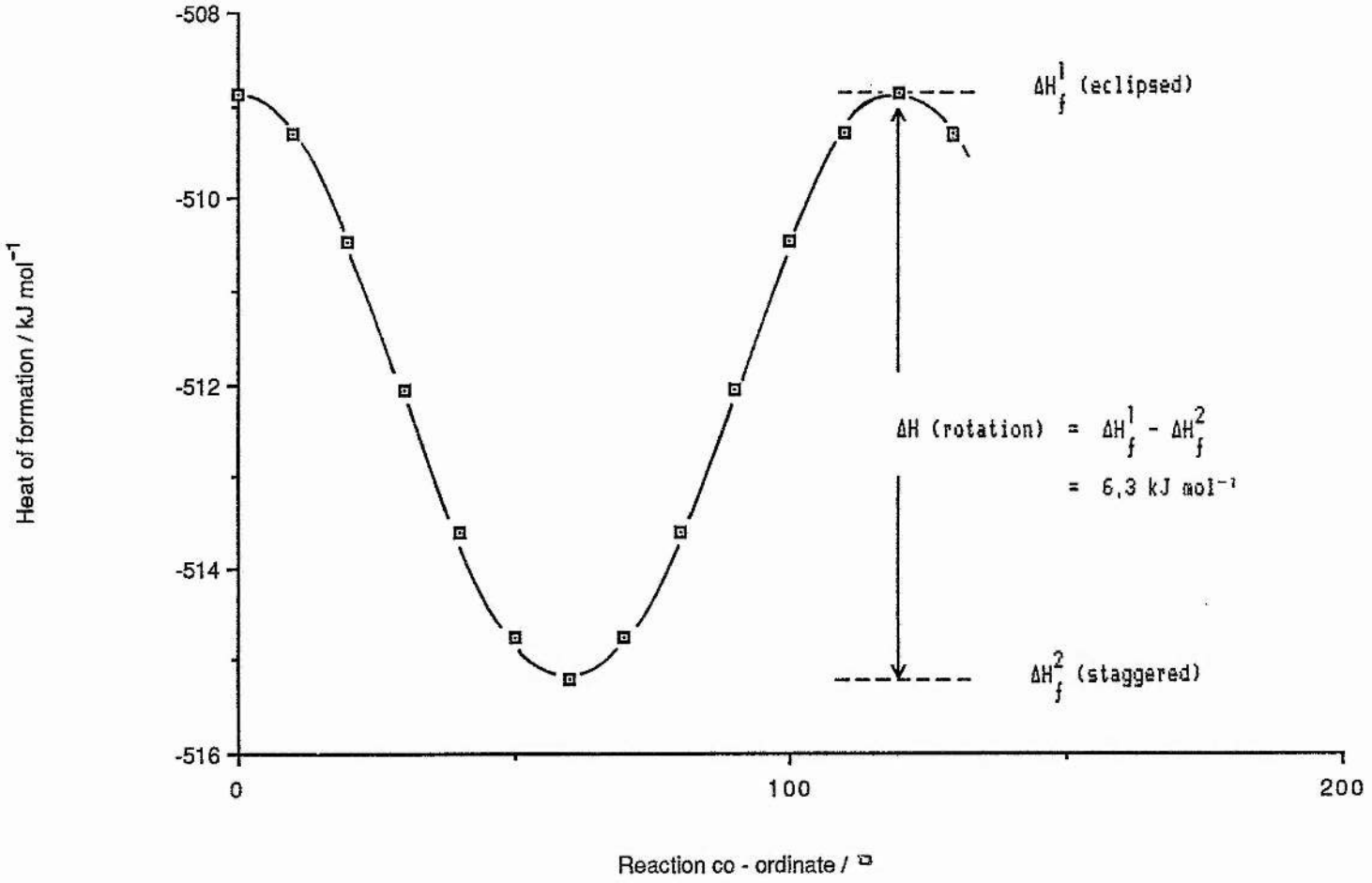

Fig, A,3, Plot of heat of formation (ΔH_f) vs, reaction co - ordinate (i,e the dihedral angle) for the $CF_3SO_3^-$ anion, as evaluated by MNDO calculation,

	C(1)	S(2)	O(3)	O(4)	O(5)	F(6)	F(7)	F(8)
C(1)	0.000							
S(2)	2.020	0.000						
O(3)	2.840	1.528	0.000					
O(4)	2.840	1.528	2.551	0.000				
O(5)	2.840	1.528	2.551	2.551	0.000			
F(6)	1.351	2.823	3.246	4.007	3.426	0.000		
F(7)	1.351	2.823	4.007	3.246	3.426	2.166	0.000	
F(8)	1.351	2.823	3.246	3.246	4.007	2.166	2.166	0.000

Table A.2. Interatomic distance data (in Angstroms) obtained from MNDO calculation for the $CF_3SO_3^-$ anion.

(X(n) represents the atomic symbol, X i.e C = carbon, and the number assigned to a given atom in the MNDO calculation, n.)

References

[1] M.B. Armand, J.M. Chabagno and M. Duclot in 'Fast Ion Transport in Solid Electrolytes', Eds. P. Vashista, J.N. Mundy and M.J. Duclot, North Holland, New York (1979).

[2] M. Gauthier, International Symposium on Polymer Electrolytes 1, St. Andrews, Scotland (1987).

[3] B. Scrosati in 'Polymer Electrolyte Reviews 1', Eds. J.R. MacCallum and C.A. Vincent, Elsevier, London (1987).

[4] H. Cheradame and J.F. LeNest in 'Polymer Electrolyte Reviews 1', Eds. J.R. MacCallum and C.A. Vincent, Elsevier, England (1987).

[5] D.E. Fenton, J.M. Parker and P.V. Wright, Polymer, 14, 589 (1973).

[6] M.B. Armand, J.M. Chabagno and M. Duclot, Second International Meeting on Solid Electrolytes, St. Andrews, Scotland (1978).

[7] M. Watanabe and N. Ogata in 'Polymer Electrolyte Reviews 1', Eds. J.R. MacCallum and C.A. Vincent, Elsevier, London (1987).

[8] S. Clancy, D.F. Shriver and L.A. Ochrymowycz, Macromolecules, 19, 606 (1986).

[9] C.S. Harris, D.F. Shriver and M.A. Ratner, Macromolecules, 19, 987 (1986).

[10] M. B. Armand in 'Polymer Electrolyte Reviews 1', Eds. J.R. MacCallum and C.A. Vincent, Elsevier, London (1987).

[11] 'Poly(ethylene oxide)', F.E. Bailey Jnr and J.V. Koleske, Academic Press, New York (1976).

[12] Y. Takahashi and H. Takadoro, Macromolecules, 6, 672 (1973).

[13] W. Gorecki, Ph. D. Thesis, Grenoble, France (1984).

[14] J.R. MacCallum and C.A. Vincent in 'Polymer Electrolyte Reviews 1', Eds. J.R. MacCallum and C.A. Vincent, Elsevier, London (1987).

[15] D.L. Papke, M.A. Ratner and D.F. Shriver, J. Electrochem. Soc., 129, 1694 (1982).

[16] J.M. Chabagno, Ph. D. Thesis, Grenoble, France (1980).

[17] 'Ion Solvation', Y. Marcus, Wiley, Chichester (1985).

[18] C.D. Robitaille and D. Fateaux, J. Electrochem. Soc., 133, 307 (1986).

[19] M. Stainer, L.C. Hardy, D.H. Whitmore and D.F. Shriver, J. Electrochem. Soc., 131, 784 (1984).

[20] H. Sato and R. Kikuchi, J. Chem. Phys., 65, 677 (1971).

[21] J.M. Parker, P.V. Wright and C.C. Lee, Polymer, 22, 1305 (1981).

[22] M. Minier, C. Berthier and W. Gorecki, J. Physique, 45, 739 (1984).

[23] C. Berthier, W. Gorecki, M. Minier, M.B. Armand, J.M. Chabagno and P. Rigaud, Solid St. Ionics, 11, 91 (1983).

[24] R.G. Linford and S. Hackwood, Chem. Rev., 81, 327 (1981).

[25] P.G. Hall, G.R. Davies, I.M. Ward and J.E. McIntyre, Polymer Comm., 27, 100 (1986).

[26] A. Bouridah, F. Dalard, D. Deroo and M.B. Armand, Solid St. Ionics, 18 + 19, 287 (1986).

[27] P. Ferloni, G. Chiodelli, A. Magistris and M. Sanesi, Solid St. Ionics, 18 + 19, 265 (1986).

[28] J.E. Weston and B.C. H. Steele, Solis St. Ionics, 7, 81 (1982).

[29] M. Leveque, J.F. LeNest, H. Cheradame and A. Gandini, Makromol. Chem. Rapid. Comm., 4, 497 (1983).

[30] J. Evans, Ph. D. Thesis, Univ. of St. Andrews.

[31] S. Bhattacharja, S.W. Smoot and D.H. Whitmore, Solid St. Ionics, 18 + 19, 306 (1986).

[32] 'Physical Chemistry', P.W. Atkins, Oxford Univ. Press (1982).

[33] J.M.G. Cowie and Agnes C. Martin, Polymer Comm., 26, 298 (1986).

[34] A. Killis, J.F. Le Nest, A. Gandini and H. Cheredame, Macromolecules, 17, 63 (1984).

[35] M. Ratner in 'Polymer Electrolyte Reviews 1', Eds. J.R. MacCallum and C.A. Vincent, Elsevier, England (1987).

[36] M.H. Cohen and D. Turnbull, J. Chem. Phys., 31, 1164 (1959).

[37] G. Adam and J.H. Gibbs, J. Chem. Phys., 43, 139 (1965).

[38] 'The Physics of Amorphous Solids', R. Zallen, Wiley, New York (1983).

[39] A.J. Shatenstein, E.S. Petrov, M.I Belousova, K.G. Yanova and E.A. Yakoleva, Dokl. Akad. Nauk. SSSR., 15, 353 (1965).

[40] A.J. Parker, Q. Rev., 16, 163 (1962).

[41] W. Gorecki, R. Andriani, C. Berthier, M.B. Armand, M. Mali, J. Roos and D. Brinkman, Solid St. Ionics, 18 + 19, 295 (1986).

[42] H. Cheradame, A. Gandini and J.F. Le Nest, 5th. International Conference on Solid State Ionics, Lake Tahoe, (1985).

[43] R. Dupon, B.L. Papke, M.A. Ratner, D.H. Whitmore and D.F. Shriver, J. Am. Chem. Soc., 104, 6247 (1982).

[44] B.L. Papke, M.A. Ratner and D.F. Shriver, J. Electrochem. Soc., 129, 1434 (1982).

[45] D. Teeters and R. Frech, Solid St. Ionics, 18 + 19, 271 (1986).

[46] C.R.A. Catlow, A.V. Chadwick, G.N. Greaves, L.M. Moroney and M.R. Worboys, Solid St. Ionics, 9 + 10, 1107 (1983).

[47] R.M. Fuoss, J. Solution Chem., 7, 771 (1978).

[48] 'Advanced Inorganic Chemistry', P.J. Durrant and B. Durrant, Longman, London (1970).

[49] S. Yanagida, K. Takahashi and M. Okahara, Bull. Chem. Soc. Jpn., 51, 3111 (1978).

[50] K. Shigehara, N. Koboyashi and E. Tsuchida, Solid St. Ionics, 14, 85 (1984)

[51] J. Maxfield and I.W. Shepherd, Polymer, 16, 505 (1975).

[52] E.A. Bekturov, S.E. Kudailbergonav, Z.Kh. Bakanova, V.Zh. Ushanov and G.S. Kanapynanova, Polymer Comm., 26, 81 (1985).

[53] C. Detellier and P. Lazlo, Helv. Chim. Acta., 59, 1333 (1976).

[54] 'Natural and Synthetic High Polymers', K.H. Meyer, Interscience, New York (1950).

[55] 'Practical Biochemistry', D.T. Plummer, McGraw - Hill (1978).

[56] L.E. Craig and W. Konisberg, J. Phys. Chem., 65, 166 (1961).

[57] 'Electrochemistry', C.W. Davies, George Newnes Ltd., London (1967).

[58] 'Philips PW9509 User Guide', Pye Unicam Ltd. (1980).

[59] 'Modern Batteries', C.A. Vincent, Edward Arnold Publishers, London (1984).

[60] G.A. Sorrie, personal communication.

[61] M.B. Reynolds and C.A. Kraus, J. Am. Chem. Soc., 70, 1709 (1948).

[62] R.M. Fuoss and C.A. Kraus, J. Am. Chem. Soc., 55, 2387 (1933).

[63] P. Jagodzinski and S. Petrucci, J. Phys. Chem., 78, 917 (1974).

[64] S. Onishi, H. Farber and S. Petrucci, J. Phys. Chem., 84, 2922 (1980).

[65] H. Farber, D. Irish and S. Petrucci, J. Phys. Chem., 87, 3515 (1983).

[66] 'Electrolytic Conductance', R.M. Fuoss and F. Accascina, Interscience, New York (1959).

[67] W.F. Luder, P.B. Kraus, C.A. Kraus and R.M. Kraus, J. Am. Chem. Soc., 58, 255 (1936).

[68] M.A. Elliot and R.M. Fuoss, J. Am. Chem. Soc., 61, 294 (1939).

[69] G.I. Cathers and R.M. Fuoss, J. Polymer Sci., 2, 12 (1947).

[70] M. Nicolas and R. Reich, J. Phys. Chem., 83, 749 (1979).

[71] D. Saar, J. Branner, H. Farber and S. Petrucci, Adv. Molec. Relaxation Processes, 16, 262 (1980).

[72] J.E. Prue and P.J. Sherrington, Trans. Far. Soc., 57, 1795 (1961).

[73] J.R. MacCallum, personal commnunication.

[74] A. Cuthbertson, personal communication.

[75] D.S. Reid and C.A. Vincent, J. Electroanal. Chem., 18, 427 (1968).

[76] R.M. Fuoss, J. Am. Chem. Soc., 56, 1857 (1934).

[77] G.S. Bien, C. A. Kraus and R.M. Fuoss, J. Am. Chem. Soc., 56, 1860 (1934).

[78] S. Boileau and P. Hemery, Electrochim. Acta, 21, 647 (1976).

[79] C. Detellier and P. Lazlo, Helv. Chim. Acta., 59, 1333 (1976).

[80] P.G. Hall, G.R. Davies, J.E. McIntyre, I.M. Ward, D.J. Bannister and K.M.F Le Brocq, Polymer Comm., 27, 98 (1986).

[81] J.J. Fontanella, M.C. Wintersgill, J.P. Calame, M.K. Smith and C.G. Andeen, Solid St. Ionics, 18 + 19, 253 (1986).

[82] J.J. Fontanella, M.C. Wintersgill, J.P. Calame, F.P. Pursel, D.R. Figueroa and C.G. Andeen, Solid St. Ionics, 9 + 10, 1139 (1983).

[83] J.M.G. Cowie, International Symposium on Polymer Electrolytes 1, St. Andrews, June 1987. (Proceedings to be published in the British Polymer Journal.)

[84] C.A. Angell, Solid St. Ionics, 9 + 10, 3 (1983).

[85] E. Williams and C.A. Angell, J. Polym. Sci., Polym. Lett. Ed., 11, 383 (1973).

[87] J.H. Gibbs and E.A. DiMarzio, J. Chem. Phys., 28, 373 (1958).

[88] 'Applied Regression Analysis', N.R. Draper and H. Smith, Wiley, New York (1981).

[89] 'Ion Association', C.W. Davies, Butterworths, London (1962).

[90] J.T. Denison and J.B. Ramsey, J. Am. Chem. Soc., 77, 2615 (1955).

[91] T. Hibma, Solid St. Ionics, 9 + 10, 1101 (1983).

[92] J.F. Le Nest, Thesis, INP Grenoble (1985).

[93] M.R. Worboys, Ph. D. Thesis, Univ. of Kent at Canterbury (1985).

[94] E.O. Stejskal and J.E. Tanner, J. Chem. Phys., 42, 288 (1965).

[95] A.V. Chadwick, J.H. Strange and M.R. Worboys, Solid St. Ionics, 9 + 10, 1155 (1983).

[96] 'Relaxation in Magnetic Resonance', C.P. Poole and H.A. Farach, Academic Press, New York (1971).

[97] 'Spectroscopy', Eds. B.P. Straugham and S. Walker, Halsted Press, London (1976).

[98] 'Pulse and Fourier Transform NMR', T.C. Farrar and E.D. Becker, Academic Press, New York (1971).

[99] 'High Resolution NMR', E.D. Becker, Academic Press, New York (1980).

[100] N. Bloembergen, E.M. Purcell and R.V. Pound, Phys. Rev., 73, 679 (1948).

[101] S.G. Greenbaum, Solid St. Ionics, 15, 259 (1985).

[102] 'The Principles of Nuclear Magnetism', A. Abragam, Clarendon Press (1961).

[103] V.J. McBrierty and D.C. Douglass, J. Polym. Sci. Macromol. Rev., 16, 295 (1981).

[104] F.M. Gray, J.R. MacCallum and C.A. Vincent, Solid St. Ionics, 18 + 19, 282 (1986).

[105] W. Ramage, Ph. D. Thesis, St. Andrews (1975).

[106] 'Nuclear Magnetic Resonance', F.A. Rushworth and D.P. Tunstall, Gordon and Breach, London (1973).

[107] 'Nuclear Magnetic Resonance Spectroscopy', R.K. Harris, Pitman, London (1983).

[108] 'Experimental Methods in Polymer Chemistry', J. F. Rabek, Wiley - Interscience, London (1980).

[109] R. Kimmich and Kh. Schmauder, Polymer, 18, 225 (1977).

[110] M. Villa, Mag. Res. Rev., 6 (1980).

[111] T.M. Connor, Trans. Far. Soc., 60, 1574 (1964).

[112] 'Nuclear Magnetic Resonance. Chemical Society Specialist Periodical Reports. Volume 1', Ed. R.K. Harris, Alden and Mowbray Ltd., Oxford (1972).

[113] S. Pajak, First Specialised 'Colloque Ampere', Institute of Nuclear Physics, Poland (1973).

[114] D.P. Tunstall, personal communication.

[115] 'Electrolyte Solutions', R.A. Robinson and R.H. Stokes, Butterworths, London (1959).

[116] Proceedings of the International Symposium on Polymer Electrolytes 1, St. Andrews (1987). (To be published in the British Polymer Journal.)

[117] A.V. Chadwick, personal communication.

[118] D.W. McCall and D.R. Falcone, Trans. Far. Soc., 66, 262 (1970).

[119] V.J. McBrierty, D.C. Douglass and T.A. Weber, J. Polym. Sci. Polym. Phys. Ed., 14, 1271 (1976).

[120] J.E. Weston and B.C.H. Steele, Solid St. Ionics, 2, 347 (1981).

[121] R. Neat, M. Glasse, R. Linford and A. Hooper, Solid St. Ionics, 18 + 19, 1088 (1986).

[122] F.M. Gray, personal communication.

[123] R.V. Pound, J. Phys. Chem., 57, 743 (1953).

[124] A. Moryoussef, M. Bonnat, M. Fouletier and P. Hichter, Proceedings of the 6th. RISO International Symposium on Metallurgy and Materials Science, Roskilde (1985).

[125] C.K. Chiang, G.T. Davies, C.A. Harding and J. Aarons, Solid St. Ionics, 9 + 10, 1121 (1983).

[126] L.J. Van der Pauw, Philips Research Reports, 13, 1 (1958).

[127] M.C. Wintersgill, J.J. Fontanella, J.P. Calame, M.K. Smith, T.B. Jones, S. Greenbaum, K.J. Adami, A.N. Shetty and C.G. Andeen. Solid St. Ionics, 18 + 19, 326 (1986).

[128] P.G. Bruce, F. Krok, J. Evans and C.A. Vincent, International Symposium on Polymer Electrolytes 1, St. Andrews, Scotland (1987).

[129] J.R. MacCallum, M.J. Smith and C.A. Vincent, Solid. St. Ionics, 11, 307 (1984).

[130] P.G. Bruce in 'Polymer Electrolyte Reviews 1', Eds. J.R. MacCallum and C.A. Vincent, Elsevier, London (1987).

[131] 'College Physics', F.W. Sears, M.W. Zemansky and H.D. Young, Addison - Wesley, New York (1974).

[132] K. West, B. Zachan - Christiansen and T. Jacobsen, International Symposium on Polymer Electrolytes 1, St. Andrews, Scotland (1987).

[133] R.J. Neat, A. Hooper, M.D. Glasse and R.G. Linford, Proceedings of the 6th. RISO International Symposium on Metallurgy and Materials Science, Roskilde (1985).

[134] 'A Handbook of Computational Chemistry', T. Clark, Wiley - Interscience, London (1985).

[135] P.K. Mehrota and R. Hoffman, Theoret. Chim. Acta., 48, 301 (1978).

[136] W.B. Jennings, J.H. Hardy and S. Worely, J. Chem. Soc. Chem. Comm., 30 (1980).